

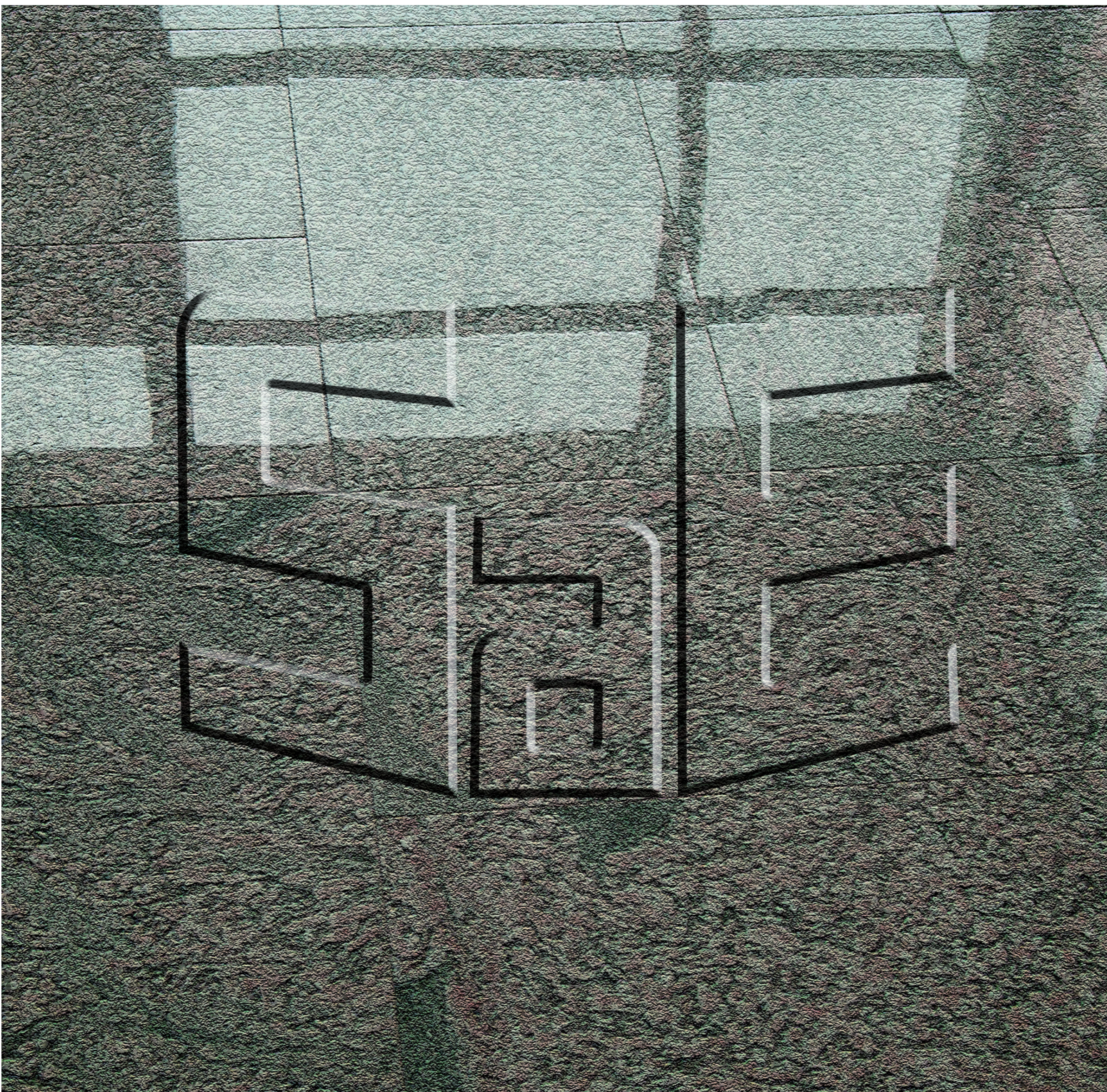
STRUCTURE AND ENVIRONMENT

KIELCE UNIVERSITY OF TECHNOLOGY

Quarterly
Vol. 15, No. 4, 2023

ISSN 2081-1500
e-ISSN 2657-6902

• Architecture and urban planning • Civil engineering and transport • Environmental engineering, mining and energy



Available online at: <https://sae.tu.kielce.pl>

Contents

structure

MACIEJ KRASOWSKI, PRZEMYSŁAW BUCZYŃSKI, JURAJ MUŚUTA

INFLUENCE OF THE BINDER ON THE PROPERTIES OF COLD MIXTURES WPLYW ŚRODKA WIAZĄCEGO NA WŁAŚCIWOŚCI MIESZANEK NA ZIMNIO	185
---	------------

MICHAŁ SZCZECINA

NUMERICAL ANALYSIS OF STRESS AND TEMPERATURE IN THE FRICTION STIR WELDING (FSW) PROCESS OF STEE NUMERYCZNA ANALIZA ROZKŁADU NAPRĘŻEŃ I TEMPERATURY W PROCESIE ZGRZEWANIA TARCIOWEGO Z PRZEMIESZANIEM DLA STALI	196
---	------------

RAMJAN ALI, IFTEKHAR ANAM, SHIGEO YOSHIDA

CFD AND EXPERIMENTAL INVESTIGATION OF THE IMPACT OF DIMENSIONAL MODIFICATIONS ON WIND PRESSURE COEFFICIENT DISTRIBUTION ANALIZA CFD ORAZ METODY EKSPERYMENTALNE W BADANIACH WPLYWU MODYFIKACJI WYMIARÓW NA ROZKŁAD WSPÓŁCZYNNIKA PARCIA WIATRU	208
---	------------

EDYTA SPYCHAŁ, MARTIN VYŠVAŘIL

RHEOLOGICAL PROPERTIES OF CEMENT PASTES MODIFIED WITH PUMICE, TRASS AND CHALCEDONITE POWDER WŁAŚCIWOŚCI REOLOGICZNE ZACZYNÓW CEMENTOWYCH MODYFIKOWANYCH PUMEKSEM, TRASEM I MAĆZKĄ CHALCEDONITOWĄ	217
---	------------

JUSTYNA STĘPIEŃ, MATEUSZ M. IWAŃSKI, EVA REMIŠOVÁ, MARTIN DECKÝ, DUŠAN BRILIAK

THE COMPARATIVE STUDIES OF THE PROPERTIES OF JOINT SEALANTS PRODUCED BY MANUFACTURERS AND IN LABORATORY CONDITIONS WITH THE USE OF HIGHLY MODIFIED BITUMEN BADANIA PORÓWNAWCZE WŁAŚCIWOŚCI MAS ZALEWOWYCH WYTWARZANYCH PRZEZ PRODUCENTÓW I W WARUNKACH LABORATORYJNYCH Z WYKORZYSTANIEM ASFALTU WYSOKOMODYFIKOWANEGO	227
---	------------

ANDRZEJ SZYCHOWSKI

LOCAL BUCKLING OF ONE-SIDE ELASTICALLY RESTRAINED THIN-WALLED CROSS-SECTION WALL UNDER LONGITUDINAL STRESS VARIATION WYBOCZENIE LOKALNE JEDNOSTRONNIE SPRĘŻYŚCIE ZAMOCOWANEJ ŚCIANKI PRZEKROJU CIENKOŚCIENNEGO PRZY WZDŁUŻNEJ ZMIENNOŚCI NAPRĘŻEŃ	244
--	------------

environment

SZYMON SYLWESTER SOBURA

ASSESSMENT OF THE SUITABILITY OF SPECTRAL INDICES FOR DETECTING AREAS OF INCREASED STRESS AMONG PLANTS - A CASE STUDY OF THE BOTANICAL GARDEN IN KIELCE OCENA PRZYDATNOŚCI WSKAŹNIKÓW SPEKTRALNYCH DO WYKRYWANIA OBSZARÓW WZMOŻONEGO STRESU WŚRÓD ROŚLIN - STUDIUM PRZYPADKU OGRODU BOTANICZNEGO W KIELCACH	253
--	------------

EDYTA NARTOWSKA

GROUNDWATER CONTAMINATION RISK ASSESSMENT IN THE FIRST EXPLOITABLE AQUIFER STRATUM WITHIN BODZENTYN MUNICIPALITY, ŚWIĘTOKRZYSKIE VOIVODESHIP OCENA RYZYKA ZANIECZYSZCZENIA WÓD PODZIEMNYCH W PIERWSZEJ EKSPLOATOWANEJ WARSTWIE WODONOŚNEJ NA TERENIE GMINY BODZENTYN, WOJEWÓDZTWO ŚWIĘTOKRZYSKIE	269
---	------------

ABSTRACTS	279
------------------------	------------

GUIDELINES FOR AUTHORS	287
-------------------------------------	------------

Editor-in-Chief:

Zdzisława OWSIAK, Kielce University of Technology, Poland

Managing Editor:

Justyna ZAPĄŁA-SŁAWETA, Kielce University of Technology, Poland

Editorial Advisory Board:

Joanna GIL-MASTALERCZYK, Kielce University of Technology, Poland

Agata LUDYNIA, Kielce University of Technology, Poland

Grzegorz MAZUREK, Kielce University of Technology, Poland

Editors:

Vadim ABIZOW, Kyiv National University of Technologies and Design, Ukraine

Satoshi AKAGAWA, Hokkaido University, Sapporo, Japan

Tomasz ARCISZEWSKI, George Mason University, USA

Łukasz BAŁ, Kielce University of Technology, Poland

Mark BOMBERG, McMaster University, Canada

Jan BUJNAK, University of Žilina, Slovakia

Lidia DĄBEK, Kielce University of Technology, Poland

Jarosław GAWDZIK, Kielce University of Technology, Poland

Barbara GOSZCZYŃSKA, Kielce University of Technology, Poland

Jerzy HOŁA, Wrocław University of Science and Technology, Poland

Go IWAHANA, University of Alaska Fairbanks, USA

Marek IWAŃSKI, Kielce University of Technology, Poland

Andrej KAPJOR, University of Žilina, Slovakia

Tomasz KOZŁOWSKI, Kielce University of Technology, Poland

Andrzej KULICZKOWSKI, Kielce University of Technology, Poland

Jozef MELCER, University of Žilina, Slovakia

Mikhail NEMCHINOV, Moscow State Automobile and Road

Technical University MADI, Russia

Andrzej S. NOWAK, Auburn University, USA

Wojciech G. PIASTA, Kielce University of Technology, Poland

Jerzy Z. PIOTROWSKI, Kielce University of Technology, Poland

Karel POSPÍŠIL, The Transport Research Centre CDV, Czech Republic

Claude VAN ROOTEN, Belgian Road Research Centre, Belgium

Grzegorz ŚWIT, Kielce University of Technology, Poland

Wiesław TRĄMPCZYŃSKI, Kielce University of Technology, Poland

Jerzy WAWRZEŃCZYK, Kielce University of Technology, Poland

Janusz WOJTKOWIAK, Poznań University of Technology, Poland

Piotr WOYCIECHOWSKI, Warsaw University of Technology, Poland

Language Editors:

Łukasz ORMAN, Kielce University of Technology, Poland

Technical Editors:

Marek BIAŁEK, Kielce University of Technology, Poland

Tadeusz UBERMAN, Kielce University of Technology, Poland

Cover design:

Waldemar KOZUB, Kielce University of Technology, Poland

General data:

Format of the journal – electronic form

Frequency of publication – quarterly

The quarterly issues of Structure and Environment are their original versions

e-ISSN 2657-6902

ISSN 2081-1500

DOI: 10.30540/sae/0000

The journal published by:

Kielce University of Technology Tysiąclecia Państwa Polskiego 7 Str. 25-314 Kielce, Poland

T.: + 48 41 342 45 41

De Gruyter Poland:

Bogumiła Zuga 32A Str. 01 – 811 Warsaw, Poland

T.: +48 22 701 50 15

Journal Metrics:

Index Copernicus Value (IVC) 2021 = 100

The Polish Ministry of Education and Science 2023 = 70 pkt



Kielce University of Technology
2023

INDEX  COPERNICUS
I N T E R N A T I O N A L



structure
structure



INFLUENCE OF THE BINDER ON THE PROPERTIES OF COLD MIXTURES

WPŁYW ŚRODKA WIĄZĄCEGO NA WŁAŚCIWOŚCI MIESZANEK NA ZIMNO

MACIEJ KRASOWSKI*, PRZEMYSŁAW BUCZYŃSKI
Kielce University of Technology, Poland
JURAJ MUŠUTA
University of Zilina, Slovakia

Abstract

The paper aims to present the basic properties of cold mixes in terms of the type of binding agent. In the theoretical part of the article, a description of the technology for producing cold recycled mixtures and the types of road binders used in cold mixtures was presented. The research part presents the experimental design, and gives an overview of the research methodology used to assess the impact of the type of binding agent. Mixes differing in type and binder content were designed. During the laboratory work, mixtures were prepared with cement binder (CBGM), cement-modified polymer binder (CBGM+P), mineral-cement-emulsion modified with polymer binder (BE-RCM+P), and mineral-cement mixtures with foamed bitumen modified with polymer binder (FB-RCM+P). The project aimed to produce cold mixtures with variations in the type and amount of binder used. The mixtures were prepared using cold mix technology. The effect of the binder on the cold mix properties was studied. During the research, the following properties were examined: void content (V_m), indirect tensile strength (ITS), resistance to water damage (TSR), stiffness modulus using the IT-CY method and an axial compressive strength. On the basis of the research carried out, an analysis was made. Among other things, the polymer modification was found to have a positive effect on the void content of the mix. The research carried out in this way made it possible to show the influence of the binder on the properties of cold mixes.

Keywords: cold mixture, recycling, substructure, foamed asphalt, asphalt emulsion, hydraulic binder, modification

Streszczenie

Praca miała na celu przedstawienie podstawowych właściwości mieszanek na zimno w aspekcie rodzaju środka wiążącego. W części teoretycznej artykułu przedstawiono opis technologii wykonywania mieszanek metodą recyklingu głębokiego na zimno oraz rodzaje spoiw drogowych wykorzystywanych w mieszankach na zimno. W części badawczej przedstawiono plan eksperymentu oraz przybliżono metodykę badawczą wykorzystaną w ocenie wpływu rodzaju środka wiążącego. Zaprojektowano mieszanki związane cementem (CBGM), mieszanki związane cementem modyfikowane polimerem (CBGM+P), mieszanki mineralno-cementowo-emulsyjne modyfikowane polimerem (MCE+P) oraz mieszanki mineralno-cementowe z asfaltem spienionym modyfikowane polimerem (MCAS+P). Projekt zakładał wykonanie mieszanek w technologii na zimno, zróżnicowanych pod względem rodzaju oraz ilości zastosowanego spoiwa. W ramach badań sprawdzono zawartość wolnych przestrzeni V_m , wytrzymałość na rozciąganie pośrednie ITS, odporność na szkodliwe działanie wody TSR, moduł sztywności według metody IT-CY oraz przeprowadzono badanie wytrzymałości na ścislenie osiowe po 28 dniach pielęgnacji. Na podstawie wykonanych badań dokonano analizy. Tak przeprowadzone badania pozwoliły na ukazanie wpływu spoiwa na właściwości mieszanek na zimno.

Słowa kluczowe: mieszanka na zimno, recykling, podbudowa, asfalt spieniony, emulsja asfaltowa, spoiwo hydrauliczne, modyfikacja

*Corresponding Author: e-mail: mkrasowski@tu.kielce.pl

1. INTRODUCTION

Continued growth in the number of road users directly translates into increased loads transferred to road surface structures [1]. This causes degradation of the traffic sections in use, which consequently require increased maintenance. When the fatigue life of a structure is lost [2], which occurs most often in the substructure layers, costly reconstruction of the damaged road section is necessary. The start of a remodelling or refurbishment project usually involves the use of new materials. This translates into increased lead times, increased costs and increased environmental degradation. The use of recycling technology enables the reuse of materials from the deteriorated structure, allowing for intervention in the degraded subbase layer and improving the parameters of the subsoil. One of the most common technologies used for road reconstruction is cold recycling technology. Cold mixtures also use binders in the form of asphalt bonding agents [3] and hydraulic binders. The continuous development of technology is leading to a search for modifying agents [4-7]. Recycling technology can also become a place for the disposal of materials, while exploiting their technological potential [8, 9].

The concept of “cold” deep recycling encompasses two types of mixtures. Mineral-cement-emulsion (BE-RCM) and mineral-cement mixtures with foamed bitumen (FB-RCM). Both technologies involve reusing material from the demolition of damaged structures. In addition, a hydraulic binder, bonding agent, water and possible graded aggregate are added during the manufacturing process [10]. The use of BE-RCM or FB-RCM technology allows for the re-building of layers containing tar components, which are only possible using the “cold” methods, i.e. without heating, at ambient temperature [11]. This fact makes BE-RCM and FB-RCM extremely economical and environmentally friendly technologies.

A wide variety of binding agents are used in the cold-mix technology around the world, and their main purpose is to improve the properties of the materials to be incorporated. In many places there is a lack of availability of high-quality raw materials. The method of using binding agents can be used for the construction of new roads but also for the renovations of old sections. The local material is enriched by various binding agents and is then built in again, so that no new material has to be supplied, resulting in high financial, time and environmental savings [14]. There are many binding agents available on the market. Hydraulic binders, special road binders and asphalt bonding agents are

used. In addition, there is ongoing research into new binders [15] additives [8] or modifiers [16]. Each of the measures has the same task, to improve the performance of the material, increasing strength and resistance. Depending on the chosen technology, appropriate binding agents are selected. Important considerations are availability, price and method of building in.

One of the characteristic features of material recycled with the use of asphalt bonding agents is the characteristic distribution of the bonding agent between the fine particles of the mineral skeleton. In the case of foamed asphalt, it is combined with a fine fraction. When asphalt emulsion is used, the coarser fractions (above 2 mm) play a more important role in the mix. When the layer is compacted, we obtain a mixture with a void content of less than 12%. This value was obtained, among others, in publications by Buczyński [15] and Dołżycki [17]. The produced recycled mix therefore behaves partly like an unbound mix, using friction between the grains to transfer loads. In addition, it works as a visco-elastic material that transmits tensile stresses without causing damage. The produced component is therefore treated as a hybrid layer combining the properties of unbound mixes and partly the properties of susceptible mixes [10].

Mineral binders are among the most widely used binding agents in the world. These include cement, lime, and their mixtures with the addition of fly ash, blast furnace slag [18]. The main function of these binders is to increase load-bearing capacity. In the case of lime binders, a reduction in soil plasticity is observed [12]. The strength achieved with mineral binders will depend mainly on the amount of agent used and the type of material being processed. However, this does not mean that applying a large amount of binder will have a positive effect. As demonstrated by Buczyński and Iwański [19], improperly designed cold recycled mixes can become excessively stiff, leading to shrinkage cracks in the substructure. In contrast, as Jaworska has shown [20], an insufficient amount of cement can reduce the indirect tensile strength and thus shorten fatigue life.

Today’s technologies make it possible to improve the properties of traditional materials. This process involves the introduction of a new ingredient that improves the properties of the starting material. This method is called modification and the most commonly used substances in this technology are polymers, used in various forms [20]. Polymer modification has been used successfully in cement concrete mixtures. When cement and a polymer modifier are mixed together, a new type of bonding agent called a polymer-

cement binder is obtained. Bonding in a concrete mix produced with such a bonding material is as follows:

- fine particles of the modifier are dispersed in the liquid phase of the cement slurry. As the setting process begins, unbound cement particles and mineral grains accumulate on the surface;
- free grains of polymer powder are encapsulated in the air voids of the mixture. During the drying process, the polymer particles are densely packed and coalescence occurs, resulting in the formation of a continuous polymer film.

Polymer-modified cement concretes have better watertightness and workability. Aggregate adhesion is improved and the mix is more susceptible, thus increasing bending strength. In addition, the adhesion of the concrete mix to the substrate is improved, as described by Łukowski [22]. The use of polymer modification also has a beneficial effect on the performance of mineral mixtures bound with hydraulic binders (CBGM). Research carried out by Buczyński, Iwański, Mazurek, Krasowski J., Krasowski M. [16] give positive results on fracture resistance. Bound mixtures carry the risk of cracking, transferring to the surface layers of the road structure. Repairing this type of damage is labour-intensive and expensive.

Modification technology can lead to a reduced risk of cracking. Research conducted by Krasowski J. [23] show a positive effect of polymer modification. Moreover, a study by Buczyński [6] also found no effect on the value of axial compressive strength [24] which is the main factor analysed in this type of mixture. Positive results of polymer modification were presented by Buczyński and Iwański in their publication [4] also presented in the case of studies on mineral-cement mixtures with foamed bitumen (FB-RCM). The use of redispersible polymer powders (RPPs) was found to have a beneficial effect on the densification process. A comparison of physical and mechanical properties, as well as water and frost sensitivity, confirmed that the RPP modifier increased waterproofing. The use of RPPs had a positive effect on the mechanical properties. The modification contributed to an increase in cohesion and elasticity without stiffening the base layer, i.e., no increase in elastic modulus was observed. The application of the modification extends the visco-elastic range of the FB-RCM mixture. The obtained results paint a positive picture of polymer modification in the case of deep cold recycled mixes and may be indicative of the formation of a mineral-cement-polymer composite microstructure [25]. Such an effect can have a positive impact on the other parameters of the mixtures.

Numerous research papers focusing on cold mixtures do not provide answers to the topic related to the influence of individual components on the properties of the mixture. Because of this, it is necessary to present the influence of the binding agent on the properties of cold mixtures. This publication therefore focuses on this issue. The scope of the tests, the type and composition of the mixes were chosen to fully show the impact of the binding agent on the properties of the cold mixes.

2. PURPOSE AND SCOPE OF RESEARCH

The aim of the study was to show the influence of the binding agent on the properties of cold mixtures. An assessment of the influence of the type of binding agent on properties of the cold mixture was carried out by evaluating the following mixtures:

- two mixtures bound by a hydraulic binder (CBGM);
- three mixtures bound by a polymer modified hydraulic binder (CBGM+P);
- three polymer modified mineral-cement-emulsion mixtures (BE-RCM+P);
- three mineral-cement mixtures with polymer-modified foamed bitumen (FB-RCM+P);
- asphalt concrete for the base course (AC 22 P).

All mixes, with the exception of the asphalt concrete, were made using a common mineral skeleton. This made it possible to eliminate the influence of the mineral mix composition on their properties.

The test methods used to assess the influence of the type of binder on the cold mix properties are presented in Table 1.

Table 1. Research methods used to evaluate mixtures

Properties	Test standard
Void content (V_m)	PN-EN 12697-8 [26]
Indirect tensile strength (ITS) – cohesion	PN-EN 12697-23 [27]
Water resistance (TSR)	Wirtgen [10, 12]
Stiffness modulus S_m	PN-EN 12697-26 [28] (in the ITC-CY system)
Axial compressive strength (R_c)	PN-EN 13286-41 [24]

2.1. Design of mixtures produced through deep cold recycling

The premise of the design was to produce a universal mineral mixture, meeting the grain size requirements for CBGM, BE-RCM and FB-RCM mixtures [29, 30]. The mineral skeleton was based on aggregates commonly used in road construction and material

from road surface demolition. Natural aggregates of continuous grain size, asphalt waste, cement, road asphalt and asphalt emulsion were used. Some of the mixtures have undergone polymer modification.

Figure 1 shows the grain size curve of the mineral mixture, which was the same for all the cold mixtures analysed.

By adopting a uniform mineral skeleton, it will be possible to assess the effect of individual binding agents on the properties of the mixtures. Table 2 shows the composition of the mixtures analysed. All mixtures, have been divided and assigned to the appropriate

analytical group, depending on their composition. The starting mixture was a cement-bound mixture (CBGM), which was then polymer-modified to produce a polymer modified cement-bound mixture (CBGM+P). Based on the modified mixture (CBGM+P), BE-RCM and FB-RCM mixtures were made. The content of foamed bitumen and asphalt emulsion in the mixtures was chosen so that the mixtures had the same amount of dosed asphalt. Therefore, the amount of asphalt in the mixtures was equal. The mixtures designed in this way demonstrate the influence of the bonding agent dosing method on the properties of the final mixture.

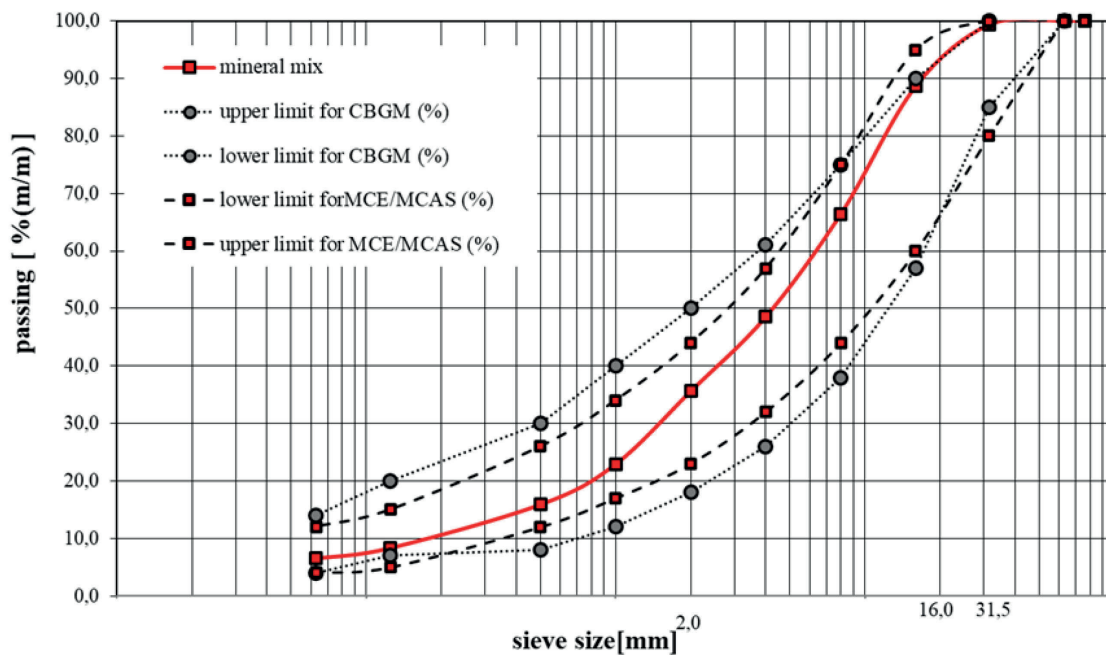


Fig. 1. Grain size curve of the universal mineral mixture

Table 2. Composition of the analysed test mixtures based on a universal mineral mixture

Mixture type	Mixture code	CEM I 42.5R Cement	Polymer (RPP)	Asphalt emulsion C60B10ZM/R	Foamed asphalt 70/100
		[%]	[%]	[%]	[%]
CBGM	C2	2.0	0.0	0.0	0.0
CBGM+P	C2+P0.5	2.0	0.5	0.0	0.0
BE-RCM+P	C2+P0.5+E5	2.0	0.5	5.0	0.0
FB-RCM+P+P	C2+P0.5+AS3	2.0	0.5	0.0	3.0
CBGM+P	C2+P3.5	2.0	3.5	0.0	0.0
BE-RCM+P	C2+P3.5+E5	2.0	3.5	5.0	0.0
FB-RCM+P+P	C2+P3.5+AS3	2.0	3.5	0.0	3.0
CBGM	C3.5	3.5	0.0	0.0	0.0
CBGM+P	C3.5+P2	3.5	2.0	0.0	0.0
BE-RCM+P	C3.5+P2+E5	3.5	2.0	5.0	0.0
FB-RCM+P+P	C3.5+P2+AS3	3.5	2.0	0.0	3.0

2.2. Design of the asphalt concrete mix

For comparison purposes, the test plan used asphalt concrete designed for sub-base layers with a grain size of up to 22.4 mm. A mix recipe was made for (AC 22P) KR 3-4 traffic intensity. The mineral skeleton consisted of the local aggregates summarised in Table 3.

Table 3. Mineral materials used to produce the AC 22P KR 3-4 mix

No.	Grain size	Rock name	Density ρ_a
1	16/22.4	dolomite	2.71
2	8/16	dolomite	2.70
3	2/8	dolomite	2.70
4	0/4	dolomite	2.68
5	Filler added	limestone	2.70

Mineral mixture, subjected to dust extraction during the production process. The share of dust decreased by 25%. This resulted in a slightly altered grain size. The final shape of the mineral mixture is shown in Figure 2.

For the project, 35/50 penetration road asphalt was also used. Table 4 shows the basic properties of asphalt.

An asphalt content of 3.9 per cent was used for the mix, which meets the minimum bonding agent content of the mix [32].

The mixture also includes an amine-based adhesion agent. This material is characterised by its high stability at mix production temperatures. The manufacturer recommends using an additive of 0.3% in relation to the asphalt content.

Table 5 provides a summary the mixture design.

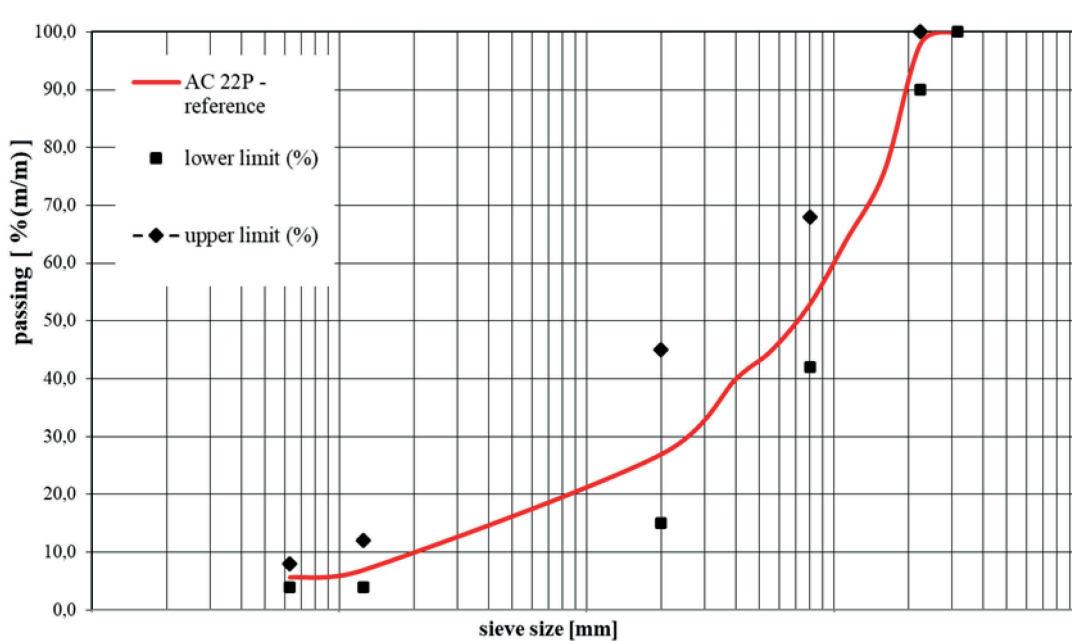


Fig. 2. Mineral mixture grain size curve

Table 4. Basic properties of 35/50 road asphalt [31]

Property	Research method	Unit	Parameter value
Penetration at 25°C	PN-EN 1426	0.1 mm	35–50
Softening temperature	PN-EN 1427	°C	50–58
Fracture temperature According to Fraass	PN-EN 12593	°C	(-14.1) – (-11.1)
Density at 15°C	PN-EN 15326	kg/m ³	1026

Table 5. Summary of the mixture design

No.	Material	Share in % (m/m)	
		mm	mma
1	16/22.4	24.0	23.1
2	8/16	23.0	22.1
3	2/8	18.0	17.3
4	0/4	33.0	31.7
5	Mineral filler – limestone	2.0	1.9
6	Road asphalt 35/50	–	3.9
7	Adhesive agent	–	0.1
Total		100	100

3. TEST RESULTS FOR COLD RECYCLED MIXTURES

An assessment of the influence of the type of binding agent on the properties of the cold mixture was carried out according to the adopted scope of the study presented in Table 1. The scope covers the basic properties of cold-produced mixtures. The scope of the work, the testing methodology and the execution of the samples were carried out in accordance with the norms and guidelines used in Poland.

3.1. Void content - V_m

A determination of the void content V_m was carried out for the mixtures analysed. This parameter plays a very important role and determines, among other things, resistance to the damaging effects of water, frost or the formation of permanent deformations. The void content is a fundamental parameter defining a given mixture. The test was performed on Marshall samples with a diameter of 101.6 mm and a height of 63.5 ± 2 mm. The samples were compacted with a Marshall tamper 2x75 strokes. Figure 3 shows the results obtained during the study.

Analysing the presented graph of void content V_m in the mixture, it can be clearly seen that the asphalt concrete mixture has the lowest values. The V_m factor of the AC 22P mix is 5.6%. Another group of mixtures are CBGM mixtures that have undergone polymer modification. The results obtained are significantly

lower than those of traditional hydraulic binder-bound mixtures. Classic CBGM mixtures have a significantly higher ratio than polymer-modified bound mixtures. The C3.5 mix contains 12.4% voids, while the C3.5+P2 mix contains 8.6% voids. This may be due to the improved workability of the material as a result of the polymer modification. This phenomenon was observed in traditional cement concrete [22]. The use of an asphalt bonding agent affects the V_m factor. Adding foamed bitumen sequentially increases the voids in the mixture compared to the bound mixture undergoing modification. In comparison, the C3.5+P2+AS3 mixture contains 12.7% voids. The foamed bitumen combines with the fines to close the voids in the mix. The use of asphalt emulsion changes the void values. Mixtures made using BE-RCM technology have the highest void content of all those analysed. The twin mixture to the previously mentioned C3.5+P2+E5 has a void content of 13.9%. The influence of the bonding agent dosing method is therefore apparent. Each of the mixtures made with BE-RCM and FB-RCM technology has identical asphalt content. This means that the use of foamed bitumen technology results in a reduction in the void content and therefore a tighter seal of the mixture and more precise filling of the voids.

Like modified CBGM mixtures, mixtures containing FB-RCM foamed bitumen have a low V_m factor. This

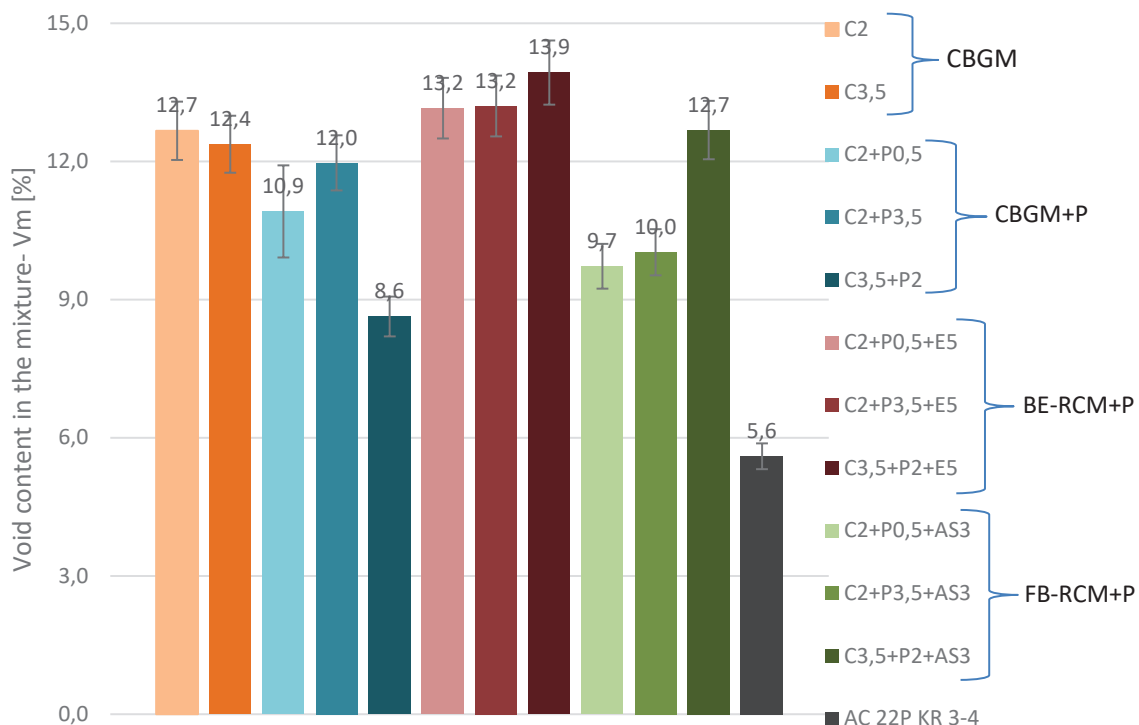


Fig. 3. Void content V_m in the mixtures

means that the mixtures are well workable, well compactible, and that the bonding agent and fine particles of the mineral material fill the voids formed between the coarse grains of the mineral skeleton.

3.2. Indirect tensile strength – ITS_{dry}

An indirect tensile strength ITS_{dry} determination of mixtures was performed. This parameter is extremely important for mixtures in road pavement construction, in the context of predicting fatigue life. Road subbase work in the tensile range, therefore the analysis of the ITS parameter is extremely important. The test was carried out at a temperature of 25°C. Figure 4 shows the results obtained for the mixtures.

Considering the results shown in Figure 4, it should be noted that mixes containing 3.5% cement binder have the highest ITS_{dry} value. The initial C3.5 mixture is characterised by an ITS dry coefficient of 1537.5 kPa. The addition of polymer powder at 2% leads to a decrease in the coefficient, and the C3.5+P2 mixture has an indirect tensile strength of 1370.2 kPa. A decrease in the coefficient value is also seen when asphalt bonding agent is added to the mixture. The use of 5% asphalt emulsion leads to a decrease in the ITS_{dry} value, and the mixture with a C3.5+P2+E5 designation has a strength of 1163.3 kPa. In comparison, the use of foamed bitumen at 3% causes a greater drop in strength than asphalt

emulsion. The C3.5+P2+AS3 mixture has a strength of 930.7 kPa. The mix of asphalt concrete has an indirect tensile strength of 1440.8 kPa. Summarising the results obtained for the mixes produced by the deep cold recycling process, it can be seen that the highest values in each group were characterised by mixes bound with CBGM cement (C2 and C3.5). On each occasion, a decrease in the parameter was noted following the addition of redispersible polymer powder, and the loss of strength was proportional to the amount of additive used in the form of RPP. A decrease in the parameter with the use of an asphalt bonding agent can be seen further down. The BE-RCM and FB-RCM mixtures had inferior strength parameters, compared to pure cement and cement-polymer mixes. The ITS_{dry} values obtained for the mixtures using foamed bitumen and asphalt emulsion were convergent, but the mixtures with foamed bitumen had the lowest value of the analysed parameter. The smallest ITS_{dry} parameter value of 345.1 kPa corresponded to the C2+P3.5+AS3 mixture. The main reason for this low result was the use of 3.5% redispersible polymer powder in the mixture’s formulation. The highest ITS_{dry} value was achieved by a C3.5 mix bound only by cement at 3.5%. 1537.5 kPa was recorded. This is approximately 4.5 times higher, compared to the C2+P3.5+AS3 mixture.

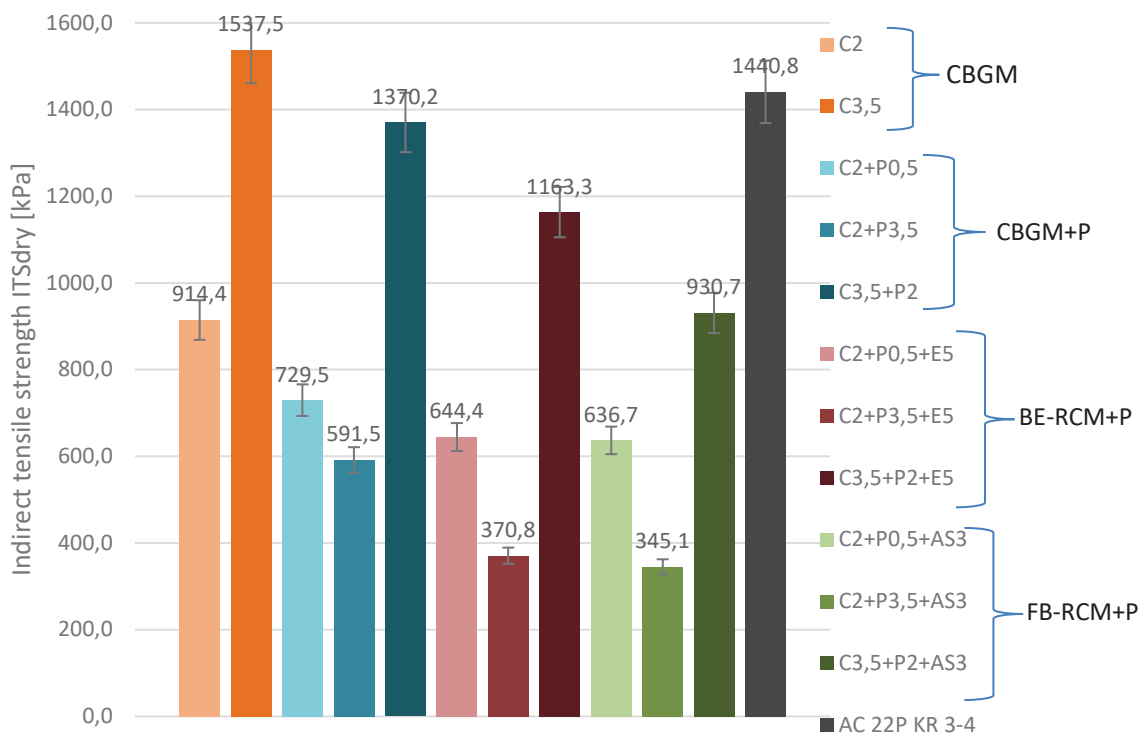


Fig. 4. Indirect tensile strength ITS_{dry}

3.3. Water resistance – TSR

A water resistance determination was carried out for the mixtures analysed. This is a test of the water resistance of the mixture in indirect tension. Road pavement construction layers are exposed to moisture, so for mixtures subjected to harmful effects of water, the parameter of resistance in indirect tension is a very important factor in determining the mixture. Figure 5 shows the results obtained during the study.

Analysing Figure 5, it should be noted that the mixtures containing asphalt bonding agent and an increased content of polymer powder have the highest resistance to water. Mixtures containing only 0.5% polymer have lower water resistance. This is evident in the C2+P0.5+E5 and C2+P3.5+E5 mixes. The former mixture has a resistance of 85%, while the twin mixture with increased polymer content has

a resistance of 97%. This implies a strong effect of the polymer modification on the water resistance of BE-RCM mixtures. This is identical for FB-RCM mixtures. The slight effect of the asphalt bonding agent dosing method on the resistance of the TSR mixtures is also apparent, as shown [5]. Mixtures made with asphalt emulsion achieved higher resistance compared to mixtures with foamed asphalt. In comparison, the asphalt concrete mix has a water resistance of 95%. In the case of mixtures bound only by cement, the influence of the cement binder content is apparent. A C3.5 mix containing 3.5% cement in its composition has a resistance of 86%. In comparison, the C2 mix achieved a resistance of 83%. Adding polymer powder to the mix bound only by cement had a positive effect in each case. A slight increase in resistance was achieved.

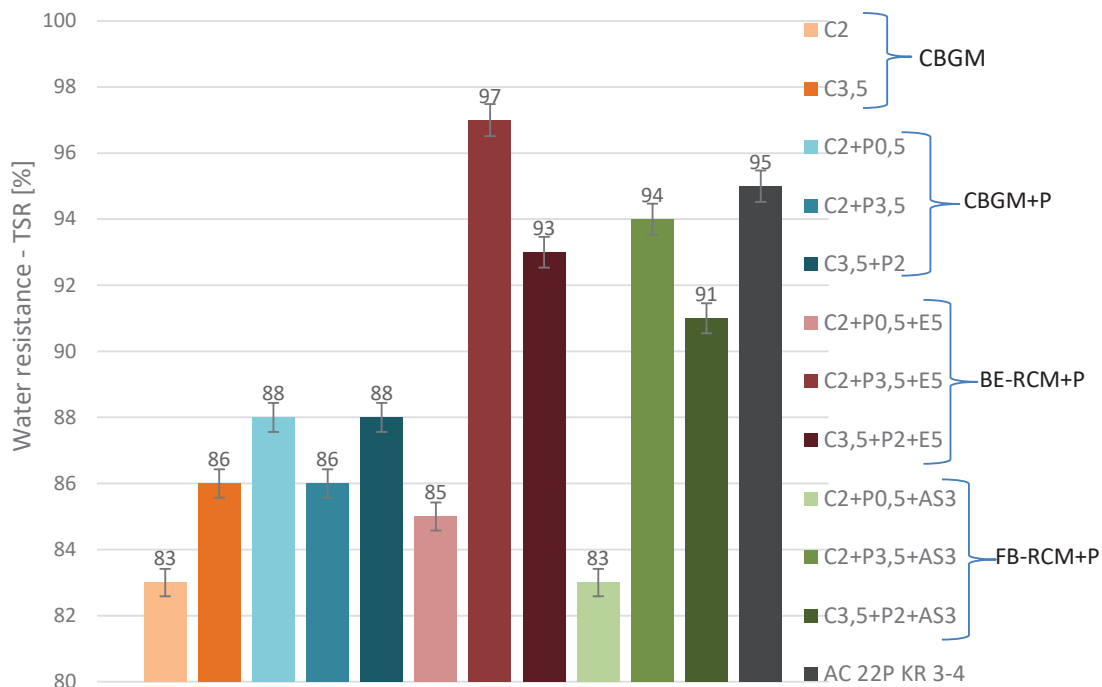


Fig. 5. TSR water resistance of the analysed mixtures

3.4. Elastic stiffness modulus – IT-CY

The results of the determination of the stiffness modulus S_m of the mixtures will be discussed below. An IT-CY test was performed at temperatures (-10°C, 5°C, 13°C, 25°C, 50°C). This makes it possible to evaluate the performance of the mixture under varying environmental conditions, depending on the season. This means that it is possible to observe the performance of the mixture in winter conditions, the gradual thawing and the exposure of the mixture to permanent deformations created at high temperatures. The results obtained are shown in Table 6.

It can be seen from Table 6 that the highest value of the stiffness modulus among the mixtures analysed was recorded for AC 22P at -10°C. The next highest recorded was the C3.5+P2 mixture. It is a substructure bound with 3.5% cement and 2% redispersible polymer powder. When analysing the other polymer-modified CBGM mixtures, it should be noted that they have the highest stiffness modulus values over the entire temperature range. Importantly, the effect of the bonding agent dosing method on the stiffness modulus value was also observed. Mixtures containing foamed bitumen in their composition have a higher stiffness

Table 6. Values of the stiffness modulus S_m of the analysed mixtures

Mixture type	Code of the mixture	Mixture stiffness modulus S_m [MPa], at the temperature of determination				
		-10°C	5°C	13°C	25°C	50°C
CBGM	C2	15674.0	12167.5	6543.3	3579.0	–
	C3.5	23915.3	21053.8	17884.8	14635.5	4771.0
CBGM+P	C2+P0.5	19378.5	19205.0	17014.5	12276.5	6062.3
	C2+P3.5	21596.0	20158.7	17772.7	11449.7	4905.7
	C3.5+P2	29892.5	30048.3	27032.0	23361.5	16330.3
BE-RCM +P	C2+P0.5+E5	11500.0	8963.0	4754.3	2737.7	2141.3
	C2+P3.5+E5	12084.8	7170.5	5965.3	2972.8	1855.3
	C3.5+P2+E5	16214.3	15795.8	12065.0	8076.5	2487.0
FB-RCM +P	C2+P0.5+AS3	14785.3	12241.5	8622.5	4435.5	753.3
	C2+P3.5+AS3	16129.5	15389.5	12681.5	7591.3	2083.3
	C3.5+P2+AS3	20870.8	18569.3	18017.3	13892.3	7537.0
AC	AC 22P KR 3-4	28863.0	19677.0	14440.0	6608.0	752.0

modulus. It should be noted that at high temperatures the asphalt concrete mixture has low stiffness. For comparison, at 50°C the AC22P mixture has a stiffness modulus of 752.0 MPa, while the C3.5+P2 cement-polymer mixture has a stiffness modulus of 16330.3 MPa. Importantly, the initial C3.5 mixture had a stiffness modulus of 4771.0 MPa. The significant impact of the polymer MIXTURE modification is therefore apparent. This phenomenon is apparent even at the smallest polymer contribution. The C2 mixture HAD a stiffness modulus of 3579.0 MPa at 25°C. After adding a 0.5% polymer powder and creating

a C2+P0.5 mixture, 12276.5 MPa was recorded. A significant effect of the bonding agent dosing method on the recorded stiffness modulus values can also be deduced from Table 6. The C3.5+P2+E5 mix recorded a stiffness modulus in the range 16214.3 – 2487.0 MPa. The twin mix with C3.5+P2+AS3 foamed bitumen achieved a stiffness modulus of 20870.8 – 7537.0 MPa.

3.5. Axial compressive strength – R_{m28}

Another parameter considered was the axial compressive strength after 28 days of conditioning. The results obtained are shown Figure 6.

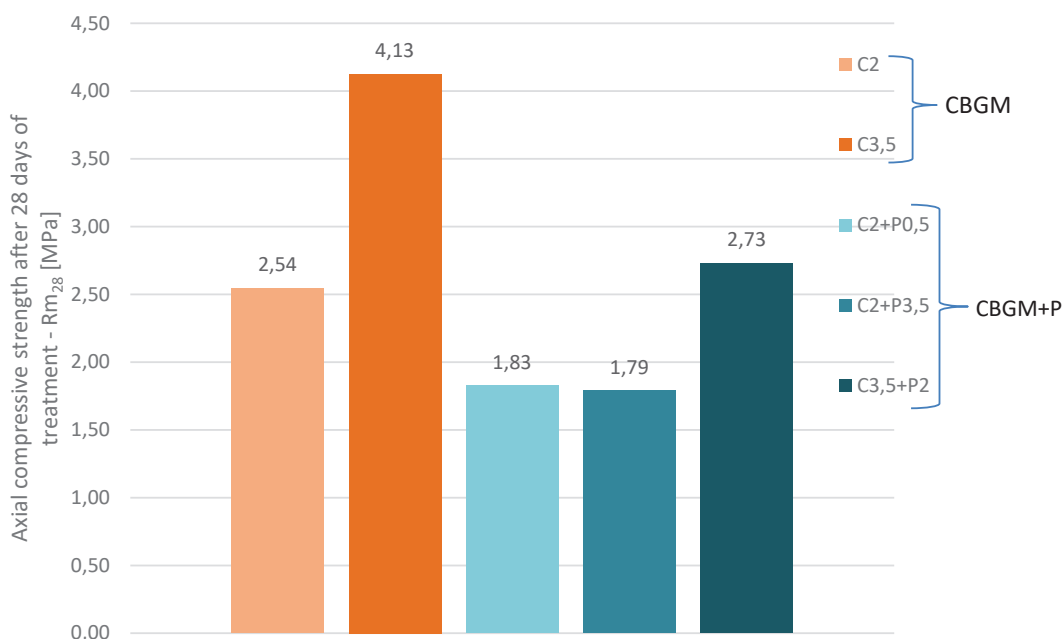


Fig. 6. Axial compressive strength after 28 days of treatment – R_{m28}

Analysing Figure 6, it is clear that the classic hydraulically bound mixtures have the highest axial compressive strength of those shown. The substructure designated C2, bound with 2% cement, has a strength of 2.5 MPa. The C2+P0.5 mixture presented next, containing 2% cement and 0.5% redispersible polymer powder, achieved a lower compressive strength value. A decrease in the analysed parameter of 0.6 MPa was recorded. After increasing the RPP content of the mix, a C2+P3.5 mix with a strength of 1.7 MPa was obtained. The highest ranked mixture turned out to be C3.5. As a result of the test, its strength was determined at 4.1 MPa. After adding a 2% modifier and creating a C3.5+P2 mixture, 2.7 MPa was recorded.

After reviewing the results presented, it is important to note the significant effect of the cement content of the mix on the axial compressive strength. Increasing the binder content improves the analysed parameter. In the case of the polymer modifier, a reduction in the strength of the mixture is achieved. The addition of 0.5% powder resulted in a loss of strength of 24% of the initial value. However, with the addition of 3.5%, there was a 32% decrease in strength. As can be seen from this example alone, the decrease is significant, but it is not possible to demonstrate a linear relationship of strength decrease with increasing modifying agent content. In comparison, in a mixture bound with 3.5% cement, there was a 34% drop in strength when 2% RPP was added.

4. CONCLUSIONS

Summing up the analysis of the research results:

1. The BE-RCM mixtures presented are characterised by a higher void content than the modified CBGM mixtures. This represents an increase in the parameter as a result of the use of asphalt emulsion. In addition, a difference in the coefficient
2. The void content of the CBGM mix decreases as a result of polymer modification. The initial C3.5 bound mix has a void content of 12.4%. The addition of 2% polymer powder resulted in a decrease in voids. For the C3.5+P2 mix, the parameter was 8.6%. The polymer powder leads to better workability and better filling of voids.
3. The smallest ITS_{dry} parameter value of 345.1 kPa corresponded to the C2+P3.5+AS3 mixture. The main reason for this low result was the use of 3.5% cent redispersible polymer powder in the mixture's formulation. The highest ITS_{dry} value was achieved by a C3.5 mix bound only by cement at 3.5%. 1537.5 kPa was recorded. This is approximately 4.5 times higher, compared to the C2+P3.5+AS3 mixture.
4. The FB-RCM mixture with the C2+P3.5+E5 designation achieved a better TSR value than the asphalt concrete mixture. This is due to the sealing of the mix by the asphalt foam and the resulting polymer film.
5. It should be noted that hydraulic binder-bound mixtures subjected to the polymer modification process achieve different values to the classic CBGM mixture. The modification alters the values obtained, and the mix itself is characterised by intermediate performance, sitting between traditional cement-bound mixtures and mineral-cement mixtures with FB-RCM foamed asphalt.
6. The influence of the method of dosing the bonding agent into the mix is also important. This is evident in the case of the BE-RCM and FB-RCM mixtures under consideration. It should be noted that in both cases the final bonding agent content was identical.

References

- [1] Bańkowski W.: *Evaluation of fatigue life of asphalt concrete mixtures with reclaimed asphalt pavement*. Appl Sci 2018;8:469. <https://doi.org/10.3390/app8030469>.
- [2] Buczyński P.: *Charakterystyka trwałości zmęczeniowej recyklowanej podbudowy*. J Civ Eng Environ Archit 2016. <https://doi.org/10.7862/rb.2016.70>.
- [3] Iwański M., Chomicz-Kowalska A., Buczyński P., Mazurek G., Cholewińska M., Iwański M., et al.: *Procedury projektowania oraz wytyczne stosowania materiałów odpadowych i z recyklingu do technologii wytwarzania mieszanek metodą na zimno z asfaltem spienionym (MCAS)*. 2018.
- [4] Buczyński P., Iwański M.: *The influence of a polymer powder on the properties of a cold-recycled mixture with foamed bitumen*. Materials 2019;12:4244. <https://doi.org/10.3390/ma12244244>.
- [5] Krasowski J., Iwański M., Buczyński P.: *Analysis of the Impact of Redispersible Polymer Powder on the Water and Frost Resistance of Cold-Recycled Mixture with Bitumen Emulsion*. IOP Conf Ser Mater Sci Eng 2021;1203:022006. <https://doi.org/10.1088/1757-899X/1203/2/022006>.

- [6] Buczyński P., Iwański M., Mazurek G., Krasowski J., Krasowski M.: *Effects of Portland Cement and Polymer Powder on the Properties of Cement-Bound Road Base Mixtures*. Materials 2020;13:4253. <https://doi.org/10.3390/ma13194253>.
- [7] Iwański M., Chomicz-Kowalska A., Maciejewski K.: *Application of synthetic wax for improvement of foamed bitumen parameters*. Constr Build Mater 2015;83:62–9. <https://doi.org/10.1016/j.conbuildmat.2015.02.060>.
- [8] Kukielka J., Bańkowski W.: *The experimental study of mineral-cement-emulsion mixtures with rubber powder addition*. Constr Build Mater 2019;226:759–66. <https://doi.org/10.1016/j.conbuildmat.2019.07.276>.
- [9] Wpływ pyłów powstałych w procesie odpalania kruszywa na właściwości podbudowy z asfaltem spienionym 2012.
- [10] Wirtgen. Cold Recycling Technology. 2012.
- [11] Piłat J., Radziszewski P.: *Nawierzchnie asfaltowe: podręcznik akademicki*. Wydawnictwa Komunikacji i Łączności, Warszawa 2010.
- [12] Wirtgen Group. *Podręcznik recyklingu na zimno*. Wirtgen GmbH; 2006.
- [13] Asphalt Academy. Technical Guideline: Bitumen Stabilised Materials. A Guideline for the Design and Construction of Bitumen Emulsion and Foamed Bitumen Stabilised Materials 2009.
- [14] Iwański M., Chomicz-Kowalska A.: *Właściwości recyklowanej podbudowy z asfaltem spienionym*. Drogownictwo 2011:271–7.
- [15] Buczyński P., Iwański M., Krasowski J.: *Assessment of the Impact of Hydraulic Binder on the Properties of the Cold Recycled Mixture with Foamed Bitumen and Bitumen Emulsion: Field Tests*. Buildings 2020;10:223. <https://doi.org/10.3390/buildings10120223>.
- [16] Buczyński P., Iwański M., Mazurek G., Krasowski J., Krasowski M.: *Effects of Portland Cement and Polymer Powder on the Properties of Cement-Bound Road Base Mixtures*. Materials 2020;13:4253. <https://doi.org/10.3390/ma13194253>.
- [17] Dołżycki B., Jaczewski M., Szydłowski C.: *Analysis of selected mechanical properties of mineral-cement-emulsion mixtures (MCE)*. Drogi Mosty 2023;22:41–61. <https://doi.org/10.7409/rabdim.023.003>.
- [18] Czapik P., Zapała-Sławeta J., Owsiak Z., Stępień P.: *Hydration of cement by-pass dust*. Constr Build Mater 2020;231:117139. <https://doi.org/10.1016/j.conbuildmat.2019.117139>.
- [19] Dołżycki B., Jaskała P.: *Review and evaluation of cold recycling with bitumen emulsion and cement for rehabilitation of old pavements*. J Traffic Transp Eng Engl Ed 2019;6:311–23. <https://doi.org/10.1016/j.jtte.2019.02.002>.
- [20] Jaworska B., Łukowski P., Jaworski J.: *Influence of cement substitution by calcareous fly ash on the mechanical properties of polymer-cement composites*. MATEC Web Conf 2018;163:03005. <https://doi.org/10.1051/mateconf/201816303005>.
- [21] Buczyński P., Iwański M.: *Fatigue Life Comparison of Recycled Cold Mixes with Foamed Bitumen and with Bitumen Emulsion*. Procedia Eng 2017;172:135–42. <https://doi.org/10.1016/j.proeng.2017.02.035>.
- [22] Łukowski P.: *Material modification in concrete* [in Polish]. Ass. Of Concrete Producers, Cracow 2016.
- [23] Krasowski J., Buczyński P., Iwański M.: *The Effect of Polymer Powder on the Cracking of the Subbase Layer Composed of Cold Recycled Bitumen Emulsion Mixtures*. Materials 2021;14:5867. <https://doi.org/10.3390/ma14195867>.
- [24] EN 13286-41. Unbound and hydraulically bound mixtures. Test method for determination of the compressive strength of hydraulically bound mixtures n.d.
- [25] Buczyński P., Iwański M.: *Rheological properties of mineral-cement mix with foamed bitumen with the addition of redispersible polymer powder*. IOP Conf Ser Mater Sci Eng 2019;471:032013. <https://doi.org/10.1088/1757-899X/471/3/032013>.
- [26] PN-EN 12697-8:2019-01 Mieszanki mineralno-asfaltowe – Metody badań – Część 8: Oznaczanie zawartości wolnej przestrzeni próbek mineralno-asfaltowych.
- [27] EN 12697-23. Bituminous mixtures. Test methods. Determination of the indirect tensile strength of bituminous specimens n.d.
- [28] EN 12697-26. Bituminous mixtures. Test methods. Stiffness 2018.
- [29] Dołżycki B.: *Instrukcja projektowania i wbudowania mieszanek mineralno-cementowo-emulsyjnych (MCE)*, 2019.
- [30] WT-5. Mieszanki związane spoiwem hydraulicznym do dróg krajowych 2010.
- [31] Błażejowski K., Wójcik-Wiśniewska M., Baranowska W., Ostrowski P.: *Poradnik asfaltowy*. ORLEN Asfalt Sp. z o.o., Płock 2021.
- [32] WT-2. Nawierzchnie asfaltowe na drogach krajowych. Mieszanki mineralno-asfaltowe 2014.



NUMERICAL ANALYSIS OF STRESS AND TEMPERATURE IN THE FRICTION STIR WELDING (FSW) PROCESS OF STEEL

NUMERYCZNA ANALIZA ROZKŁADU NAPRĘŻEŃ I TEMPERATURY W PROCESIE ZGRZEWANIA TARCIOWEGO Z PRZEMIESZANIEM DLA STALI

MICHAŁ SZCZECINA*
Kielce University of Technology, Poland

Abstract

Friction stir welding (FSW) is a modern technology for joining various metals, which has already undergone many laboratory tests, but still requires the development of numerical models. Author of the paper decided to summarize the current state of scientific knowledge regarding the modelling of the FSW process using the finite element method (FEM) and showed the main directions of development of numerical research on this process. Very advanced models are a combination of solid mechanics and fluid dynamics, but they often require expanding the computing environment with its own subroutines, as well as calibration and validation of some material parameter and constants occurring e.g. in the heat generation and heat flow laws. The Author of the paper proposed his own, simplified model, based on the computational solid mechanics and Lagrangian formulation. The model turned out to be an effective tool to reproduce stress and temperature fields during the FSW process.

Keywords: friction stir welding, numerical modelling, Abaqus, FEMs

Streszczenie

Zgrzewanie tarciove z przemieszaniem (FSW) jest nowoczesną technologią łączenia różnych metali, posiadającą wiele zalet w porównaniu z tradycyjnym spawaniem. Zgrzewanie tarciove zostało do tej pory poddane licznym badaniom laboratoryjnym, natomiast wymaga ciągłego rozwoju modeli numerycznych do symulacji tego procesu metodą elementów skończonych (MES). Autor artykułu postanowił dokonać podsumowania aktualnego stanu wiedzy dotyczącej modelowania zgrzewania tarciowego przy użyciu MES oraz wskazać główne kierunki rozwoju symulacji numerycznych tego procesu. Zaawansowane modele numeryczne zgrzewania tarciowego są kombinacją mechaniki ciała stałego z dynamiką płynów, a więc często wymagają rozbudowania środowiska obliczeniowego za pomocą własnych podprogramów, jak również kalibracji i walidacji wielu parametrów i stałych wymaganych do zdefiniowania np. prawa wytwarzania ciepła i prawa przepływu strumienia ciepła. Autor zaproponował swój własny uproszczony model bazujący na mechanice ciała stałego i opisie Lagrange'a. Model okazał się efektywnym narzędziem do odtworzenia naprężeń i pola temperatury w procesie zgrzewania tarciowego z przemieszaniem.

Słowa kluczowe: zgrzewanie tarciove z przemieszaniem, modelowanie numeryczne, Abaqus, MES

1. INTRODUCTION

Friction stir welding (FSW) was invented by Thomas et al. [1] in 1991, so one can say that it is a relatively young and innovative technology. For over 30 years FWS has been used in many high technology applications, e.g. aerospace [2], and has also been a subject of numerous scientific research. There are a few advantages of the FSW process, and namely: lower temperatures in comparison with traditional welding, no melting, a FSW tool is unconsumable [3]. A development of computational methods, especially finite element method (FEM), allowed for advanced numerical modelling of the stir welding process. The modelling covers not only mechanical, but also thermal and coupled thermal-mechanical behaviour of welded parts. Some important phenomena can also be taken into account, i.e. heat generation and dissipation, metal flow, sticking and sliding. Author of the paper summarized the current state of the research field, indicate some issues of the numerical modelling of the SFW and propose their

own, simplified numerical approach of the process. Additionally, author demonstrate how the FSW can be modelled using Abaqus [4] software to reproduce stress and temperature fields during the process.

1.1. General description of the process

The FSW process can be divided into three phases: plunging, dwelling and welding. An operating tool consists of a conical shoulder and a pin, which is shaped in a few various ways, e.g. cylindrical, threaded, square or tapered (Fig. 1). In the first stage the rotating pin is lowered down into a joint line, which is determined by two surfaces (workpieces) prepared to be welded. Then the rotating tool is held steady to produce heat, which dissipates into the neighbouring material. In this stage temperature of the welded parts increases which causes material softening. Finally, the welding operation is performed by the relative displacement of the tool along the joint line (Fig. 2). The material transported from the front to the back of the welding tool forms a joint between two workpieces.

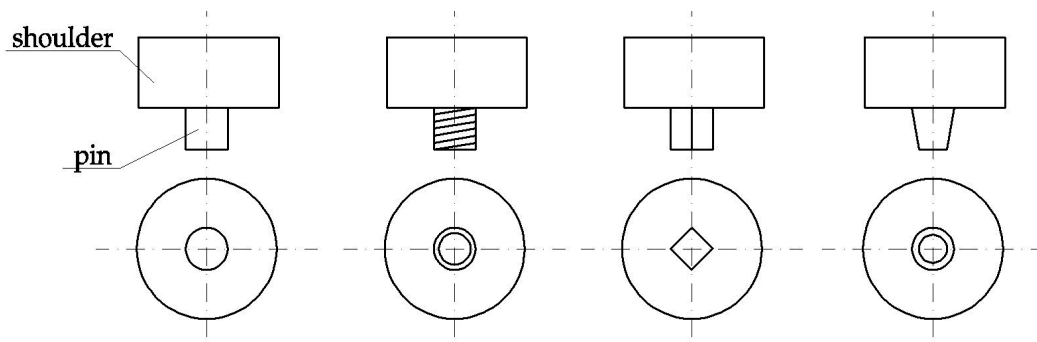


Fig. 1. Sample shapes of the operating tool used in the FSW process

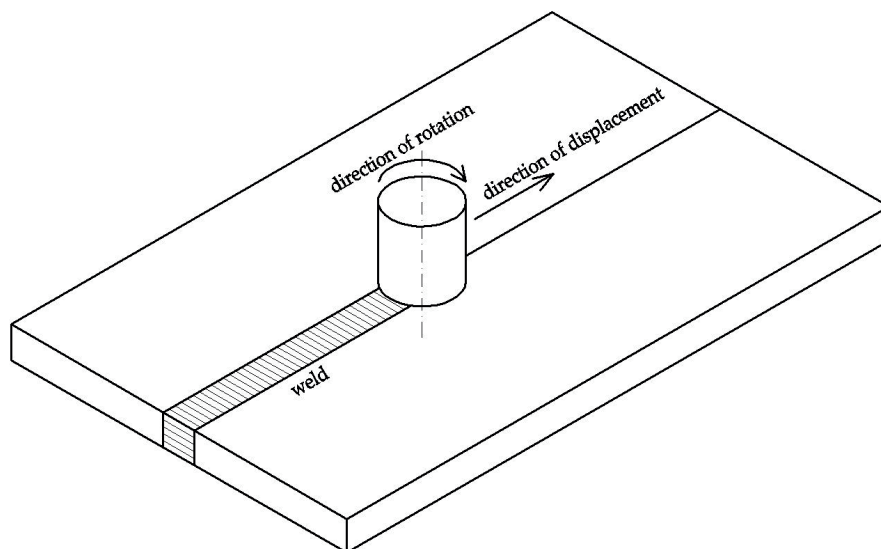


Fig. 2. General view of the FSW process

There are many important parameters that affect the whole welding process, first of all:

- geometry of the whole operating tool, discussed inter alia by Mishra&Ma [5], Sun et al. [6] and Nandan et al. [7];
- geometry of the operating tool shoulder [8];
- tilt of the operating tool and target depth [5];
- speed (transverse and rotational) of the operating tool [5, 6, 9];
- downward force;
- metallurgical and microstructural aspects, grain size and microhardness [6, 10];
- welding configuration of workpieces made of dissimilar metals [6];
- preheating or cooling of workpieces [5];
- joint design, especially when the joint is more complicated than a simple butt or lap joint [5].

A few important phenomena which occur in the whole FSW process and a few properties of welded materials have also been described in the subject literature [5]:

- metal flow, visualized in laboratory tests with the use of tracer technique by marker, welding of dissimilar materials, microstructural observations or particle tracing [11];
- heat generation, heat transfer [12];
- microstructural evolution in a nugget zone [13], a thermo-mechanically affected zone and a heat-affected zone [14];
- change in hardness of alloys [15];
- residual stress [16];
- change in postweld mechanical properties, especially strength, ductility, fracture toughness and fatigue [5];
- corrosion behaviour [17];
- interfacial sticking and slipping [18].

Kossakowski et al. [19] performed a macrostructural analysis of FSW joints, taking into consideration weld structure, rotation speed, tool travel and showing joint defects as a result of process parameters. The same authors [20] analysed effect of tool rotation and travel speed on joint parameters. Static and dynamic performance of FSW butt joint, including fatigue crack growth, was presented by Richards [21].

According to Mishra [5], the FSW process has many benefits, some of them in comparison to a traditional welding. The benefits can be divided into metallurgical (no cracking of a weld, no loss of material, low distortion of workpieces etc.), environmental (no grinding waste, no use of shielding gas, surface cleaning or solvents for degreasing) and energy benefits.

1.2. Numerical modeling of the FSW process

A finite element method approach to the FSW process has already been applied in many scientific research. A literature review on the topic was presented by Neto&Neto [3] and a comparative study of different FEM approaches can be found in a work of Meyghani et al. [22]. A critical review of the FSW numerical modelling was given by Lorrain et al. [23]. Some important introduction to FEM simulation of the FSW was presented in a few PhD and master theses [24-26]. There are few current studies and literature reviews concerning current progress in numerical modelling; one can refer to works of Bhattacharjee&Biswas [27] and Sen&Murugesan [28]. Author of this paper decided to complete and summarize the current state of the research field.

The first issue of a proper numerical simulation of the FSW process is a choice of theory that describes the material flow and thermo-mechanical behaviour. There are two main theories chosen for this purpose: computational fluid dynamics (CFD) and computational solid mechanics (CSM). A detailed study of both approaches was given by Bhattacharjee&Biswas [27]. Pros and cons of the above mentioned theories were described by Meyghani et al. [29].

The CFD is based on the Eulerian description with a fixed mesh and material is assumed as a non-Newtonian fluid. This approach allows to avoid numerical problems in case of large strains and element distortions, but it does not allow the separation of the element. Thanks to the flow boundary conditions only a small region around the welding tool can be modelled, which leads to a significant reduction of finite elements number and calculation time. Colegrove&Shercliff [30, 31] demonstrated the use of the CFD package FLUENT and modelled the 3D metal flow. The modelled recreated the FSW process quite well, but over-predicted the weld temperature and poorly predicted the welding forces. A viscosity relationship, including material softening, was proposed to overcome those problems. Jacquin et al. [32] presented a simple 3D thermo-mechanical model with velocity fields in a steady-state, solved using Abaqus/CAE software with extra procedures written in Fortran.

The CSM approach is based on the Lagrangian formulation, where the finite element mesh is attached to the material and follows its deformation [29]. Using an explicit time integration one can avoid numerical problems with convergence, but still large

distortions can lead to a significant reduction of a time step size. A detailed description and discussion on a global and local level modelling is described in a monograph written by Dialami et al. [33]. The same authors [34] demonstrated the finite volume method to model the FSW process. The technique of tracer particles in the FEM model based on CSM was presented by Gao and co-workers [35] in Abaqus environment.

The geometrical interpretation of the main difference between the Lagrangian and Eulerian formulation is presented in Figure 3. An excessive distortion of the FE mesh can appear in the Lagrangian description while in the Eulerian element boundaries do not have to coincide with the mesh.

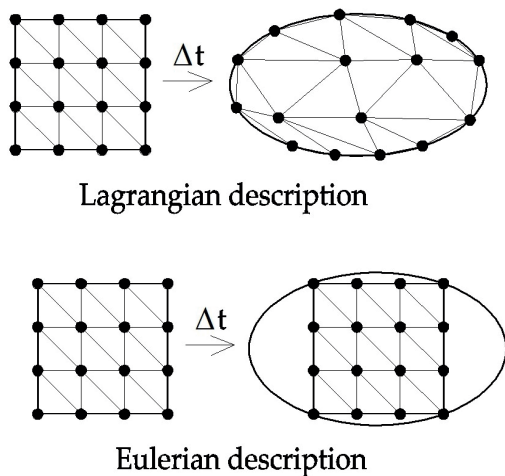


Fig. 3. Different mesh behavior in the Lagrangian and Eulerian formulation

In the research field there are also known and developed mixed methods, which are combinations of both Lagrangian and Eulerian formulations, and namely the so-called Arbitrary Lagrangian-Eulerian (ALE) and Coupled Eulerian-Lagrangian (CEL). The first approach assumes splitting into subsequent Eulerian and Lagrangian steps, computing the mesh velocity and remapping [25, 36]. The CEL method allows to define the workpiece as an Eulerian body while the welding tool is modelled as a rigid Lagrangian body [37]. This approach can bring promising results, as shown in the works [38, 39].

Another problem related to the FEM simulation of the FSW is a proper definition of the thermal and thermo-mechanical model. An early work of Chen&Kovacevic [40] presents the use of the ANSYS software to reproduce the influence of thermal fluctuations on the stress tensor components. One year later, Schmidt&Hattel

[41] proposed a fully coupled thermomechanical 3D model using Abaqus software and the ALE formulation. The same authors [42] described basics of the thermal modelling in the FSW process, including the heat conduction equation and the total heat generation equation and presented a new thermal-pseudomechanical model. Hamilton and co-workers [43] presented a thermal model introducing a slip factor, determined according to energy per unit length of weld. Mehta et al. [44] defined subroutines in Abaqus environment called DFLUX, FILM, USDFLD and UMASFL to capture the non-uniform heat flux, convective heat transfer, tool properties and mass velocity. Their work concerned the welding tools with polygonal pins.

Coupled thermo-mechanical models are nowadays widely used in the FSW simulations. Chiumenti et al. [45] presented a fully coupled model, where the local form of the FSW problem is stated in the form of coupled mechanical and transient heat transfer equations. It is also possible to apply a thermo-mechanically coupled viscoplastic flow model. A sample formulation is shown in a work of Santiago et al. [46], inspired with an early work of Ulysse [47].

Another important issue of the FSW simulation is a formulation of contact conditions, including sliding and sticking. Usually researchers define a classical Coulomb friction law, which can be expressed in the form:

$$\tau = \mu P \tag{1}$$

where: τ – indicates the friction stress (in [Pa]), μ – friction coefficient (unitless), P – contact force (in [N]).

Zhang [48] compared the classical and modified Coulomb laws and stated, that the classical law is limited to lower angular velocity of the welding tool. In case of higher velocity, the modified Coulomb law should be applied. More complex contact states were categorized and presented by Schmidt et al. [49] and contact conditions can be defined separately for sticking and sliding [3].

Finally, a constitutive material model for plastic or viscoplastic behaviour and behaviour for flow modelling of metal is also required as an input. Ulysse [47] and Santiago et al. [46] modelled the FSW process using 3D viscoplastic modelling. The other approach was presented by Zhu&Chao [50], which applied the von Mises yield criterion and the associated flow rule. As regards materials behaviour for flow modelling, the Sellars-Tegart and John-Cook models are the most common approach [3].

The finite element method is the most common technique used in numerical modelling of the FSW process. Sen&Murugesan [28] presented a comparative study of three FEM software packages, and namely ANSYS, ABAQUS and FLUENT. A very interesting approach to the FSW modelling is a use of artificial neural networks (ANN). Abdullah et al. [51] showed how to use ANN to model surface roughness of aluminium alloy. Okuyucu et al. [52] analysed a correlation between the FSW parameters and mechanical properties of aluminium using ANN.

One of the most important issues in welding is a phase transition in material. The phenomenon was not yet taken into consideration by the author of the paper because of its complexity. Nevertheless, a few publications [53-55] on the issue show that FEM simulation of the effect is possible, among other using SYSWELD software.

To sum up, all the above presented approaches are based on very robust, advanced numerical models. The models demand on a precise calibration and validation of input data and can take into account various physical phenomena, accompanying the FSW process. Numerical modelling of the FSW is developing still and reported results of FEM calculations are still closer to laboratory tests results. On the other hand, structural engineers need also simple numerical models which can give quick information about stress and temperature fields during the FSW process. Author of the paper made an attempt to create such a model, presented in the following sections.

2. INPUT DATA

The author of the paper would like to demonstrate a use of a simple numerical model of the FSW process, defined in the Abaqus environment [4]. The main goal of the research is a numerical reproduction of residual stress after the FSW process. Geometry and material properties of specimens were taken from the laboratory experiment of Hashemzadeh et al. [56]. All materials were defined as isotropic. Two steel plates, each 2000x150x12 mm of dimensions, were modelled. Mechanical and thermal properties of ASTM A36 carbon steel applied in the model are listed in the Table 1. Temperature dependency of the properties were taken from the paper of Chang&Teng [57]. Ultimate strength of steel was assumed as 450 MPa [58] and Poisson’s ratio was temperature-independent and equal to 0.3. The author’s choice fell on steel, because the author of the paper recognized that laboratory tests on steel [56] were documented in the most detailed way among all the results of laboratory tests that were collected for the purpose of performing numerical analyses in this paper.

The FSW tool was assumed as hybrid W-Re/pcBN [51]; geometry of the tool was defined according to [59] and shown in Figure 4. Main properties of the FSW process are as listed: rotation speed of the tool: 150 rpm, transverse speed of the tool: 0.1 ms⁻¹, vertical force acting on the shoulder of the tool: 90 kN [56]. Friction coefficient was assumed as equal to 0.3.

Table 1. Mechanical and thermal properties of ASTM A36 carbon steel

Temperature [°C]	Young’s modulus [GPa]	Yield stress [MPa]	Specific heat [Jkg ⁻¹ K ⁻¹]	Conductivity [Wm ⁻¹ K ⁻¹]	Expansion [10 ⁻⁶ K ⁻¹]
20	210	380	450	51	11.2
100	195	340	475	50	11.8
210	195	320	530	49	12.4
330	185	262	560	46	13.1
420	168	190	630	41	13.6
540	118	145	720	38	14.1
660	52	75	830	34	14.6
780	12	40	910	28	14.6
985	11.8	38	1055	25	14.6
1320	10.4	28	2000	32	14.6
1420	10.2	25	2100	42	14.6
1500	10	20	2150	42	14.6

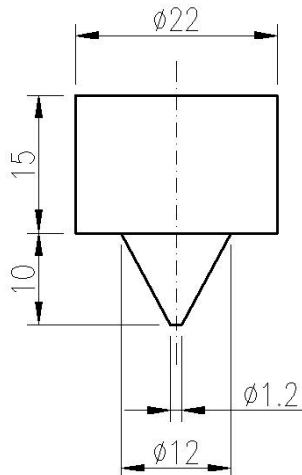


Fig. 4. Geometry of the welding tool (dimensions in [mm])

3. FEM MODEL

Numerical analysis was performed using the finite element method in Abaqus environment [4]. Author decided to apply the Lagrangian approach and the explicit dynamic step with the fully coupled thermal-stress analysis (the so-called temperature-displacement

in the Abaqus code). The plates were meshed with C3D8T brick finite elements, 12x12x3 mm each and the welding tool was discretized with C3D4T tetrahedrons and the average mesh size was assumed as 3 mm. The meshed assembly is presented in Figure 5 while, for the sake of visibility, the magnified welding tool with the plates were shown in Figure 6.

All mechanical and thermal properties were defined as shown in the section 2. Moreover, the classical von Mises yield criterion (input variable PLASTICITY in Abaqus code) was taken into account. The stress-strain relationship was defined as bi-linear with the following values of the yield strain (Eq. 2) and ultimate strain (Eq. 3) in the initial temperature, equal to 20°C:

$$\epsilon_y = \frac{\sigma_y}{E} = \frac{380 \text{ MPa}}{210 \text{ GPa}} = 0.00181 \quad (2)$$

$$\epsilon_u = \frac{\sigma_u}{E} = \frac{450 \text{ MPa}}{210 \text{ GPa}} = 0.00214 \quad (3)$$

and the relationship of a uniaxial behaviour is presented in Figure 7.

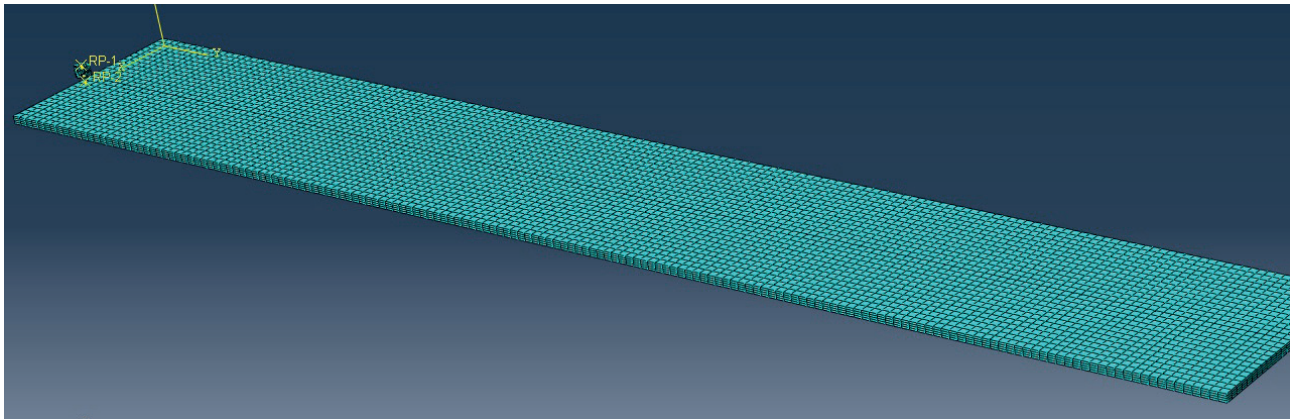


Fig. 5. Meshing of the plates and the welding tool

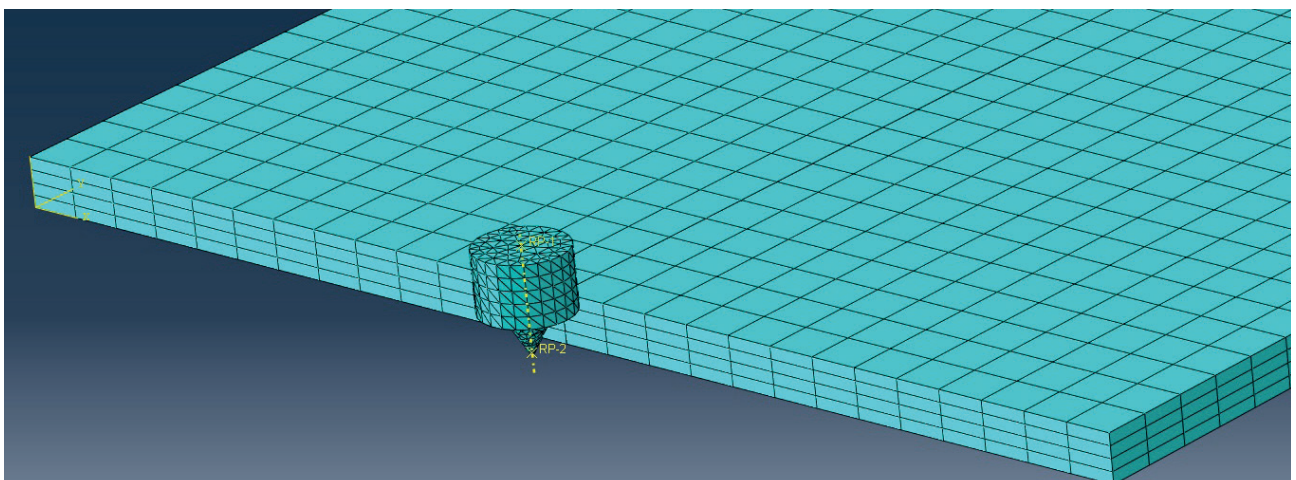


Fig. 6. The magnified welding tool with the edges of the plates

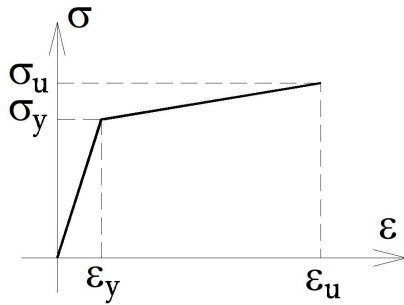


Fig. 7. Stress-strain curve defined in the numerical model

The welding tool was defined as a rigid body rotating with a constant angular velocity and the plates – as deformable elements moving with a constant transverse velocity. Boundary conditions were defined as follows:

- transverse velocity of the plates, shown in Figure 8;
- angular velocity of the welding tool and force acting on the shoulder, shown in Figure 9.

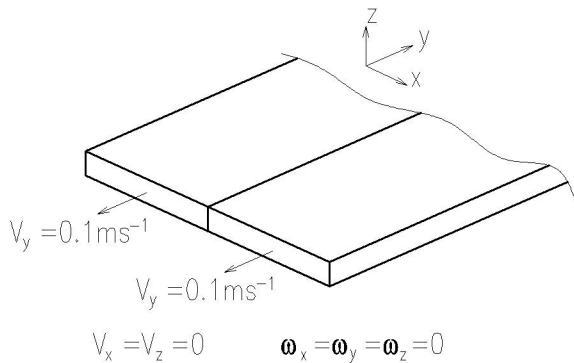


Fig. 8. Boundary conditions – transverse velocity of the welded plate

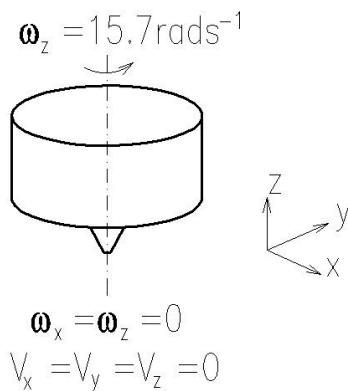


Fig. 9. Boundary conditions – angular velocity of the welding tool

Ambient temperature was set as 20°C, using the “predefined fields” option in the initial step in all nodes of the meshed model. A surface-to-surface contact between the welding tool and the plates was defined as follows:

- tangential behaviour – friction coefficient 0.3 (called “penalty” in Abaqus code);
- normal behaviour – “hard contact”;
- heat generation with default 0.5 fraction of converted heat distributed to slave surface.

A time period was set as 22 s, which is enough for the welding tool to make a full weld joining the plates and to come out of them. A type of incrementation was assumed as fixed with the user-defined time increment equal to 0.001.

4. ANALYSIS OF TEMPERATURE AND STRESS IN PLATES

In order to visualize the whole welding process and stress during the welding process, the author decided to present maximal principal stress and nodal temperatures. Maximal principal stress on the upper surface of the welded plates after time $t = 22 \text{ s}$ is presented in Figure 10 (please note, that the results are presented in [Pa] using a native notation in Abaqus code, e.g. e+08 means 10 to the power of 8). We can see how the stress field is propagating on the surface of the plates while the welding tool is moving along the Y axis. Moreover, the stress field expands also in the X axis, transverse to the welding direction. Figures 11 and 12 present the maximal principal stress in a transverse cross section and nodal temperature in a longitudinal cross section of the weld. Temperatures obtained under the welding tool are above the steel melting point and stress exceeds the yield stress in three columns (in each plate) of finite elements, which proves a limited range of material deformation caused by the process. Moreover, one can see that the stress and temperature distribution in the left-hand side and right-hand side plates (looking from viewport adopted in Fig. 11) are different. This fact can be explained by rotational motion of the welding tool. Because of the motion, in one of the plates metal particles are displaced in front of the leading edge of the tool shoulder while in the other plate they are moved to the trailing edge, so the whole model is not symmetrical.

Variation of temperature and principal stress depending on the distance z from the top of the right-hand side (see Fig. 11) plate in the section under the welding tool are presented in Figures 13 and 14. High values of temperature (in some nodes above the melting point) and stress indicate large yielding of steel in the weld zone during the process, which is necessary to stir metal particles of both welded plates.

Total strains and plastic strains (maximal principal) are shown in Figures 15 and 16. The values of the strains are lower than ultimate strains presented in the previous chapter.

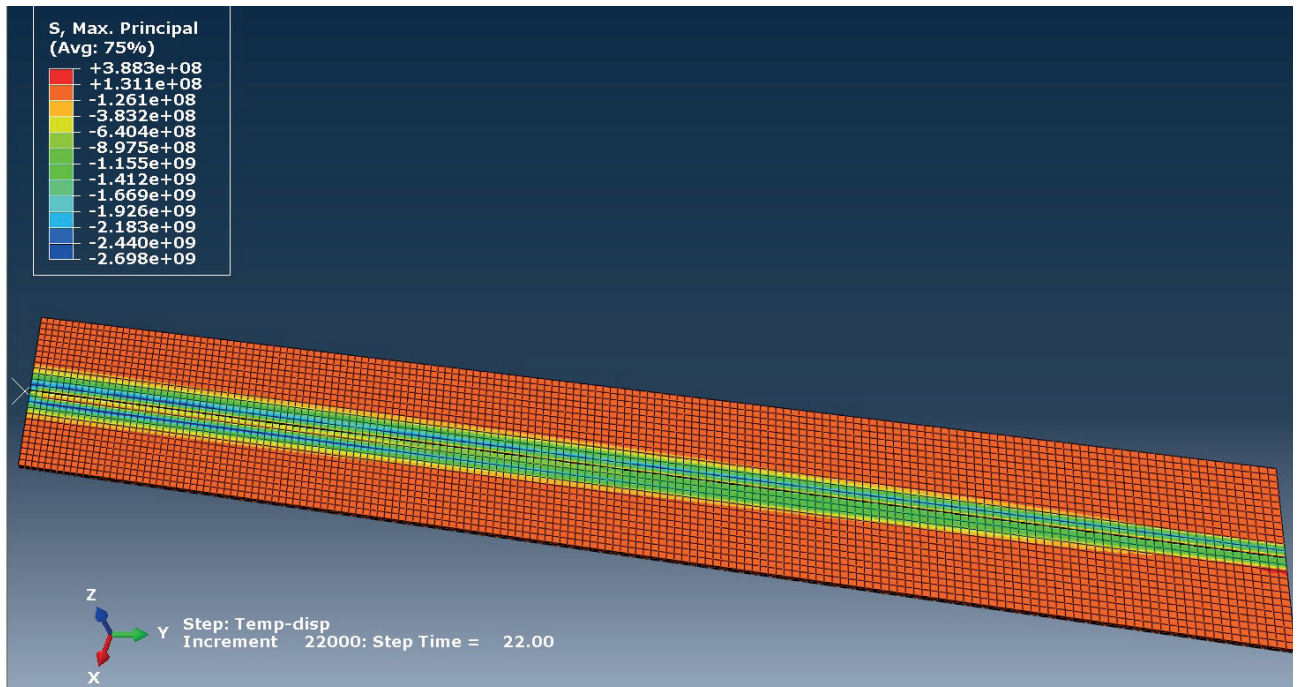


Fig. 10. Maximal principal stress after time $t = 22.0$ s; all results expressed in Pa

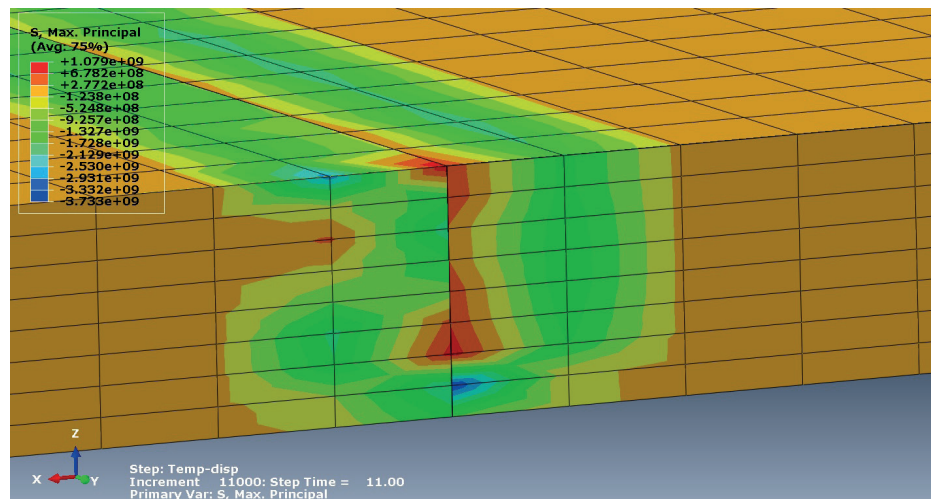


Fig. 11. Maximal principal stress in a transverse cross section of the plates, $t = 11.0$ s

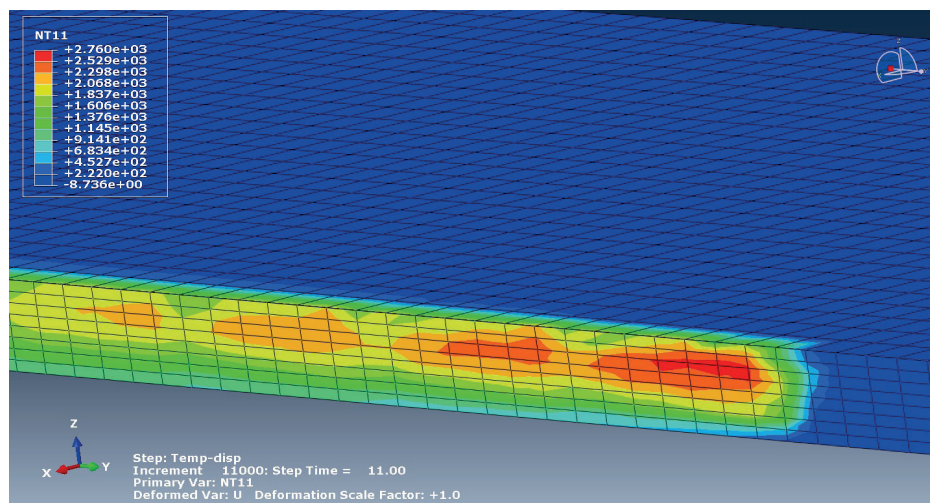


Fig. 12. Nodal temperatures (in $^{\circ}\text{C}$) in a longitudinal cross section of the weld, $t = 11.0$ s

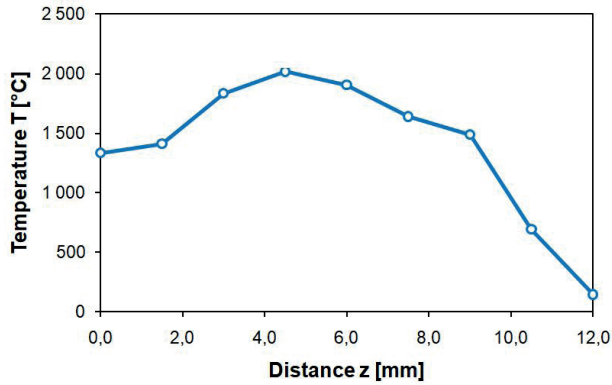


Fig. 13. Nodal temperature in a transverse section of the right-hand side plate vs distance z from the top of the plate, $t = 11.0$ s

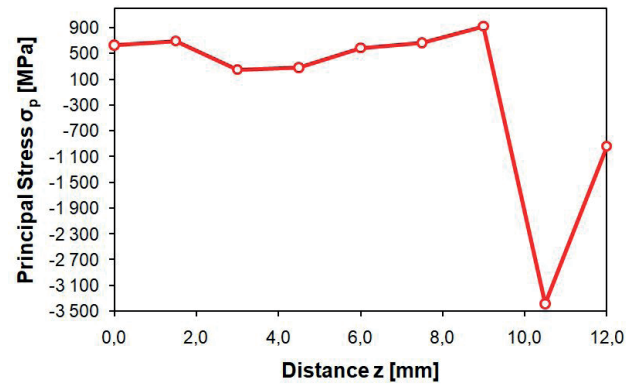


Fig. 14. Principal stress in a transverse section of the right-hand side plate vs distance z from the top of the plate, $t = 11.0$ s

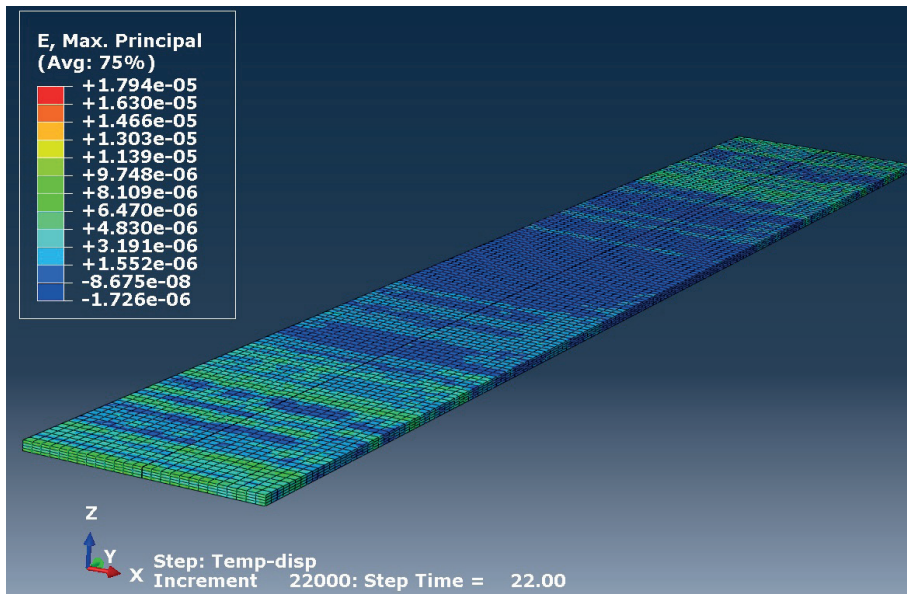


Fig. 15. Maximal principal total strains after time $t = 22.0$ s

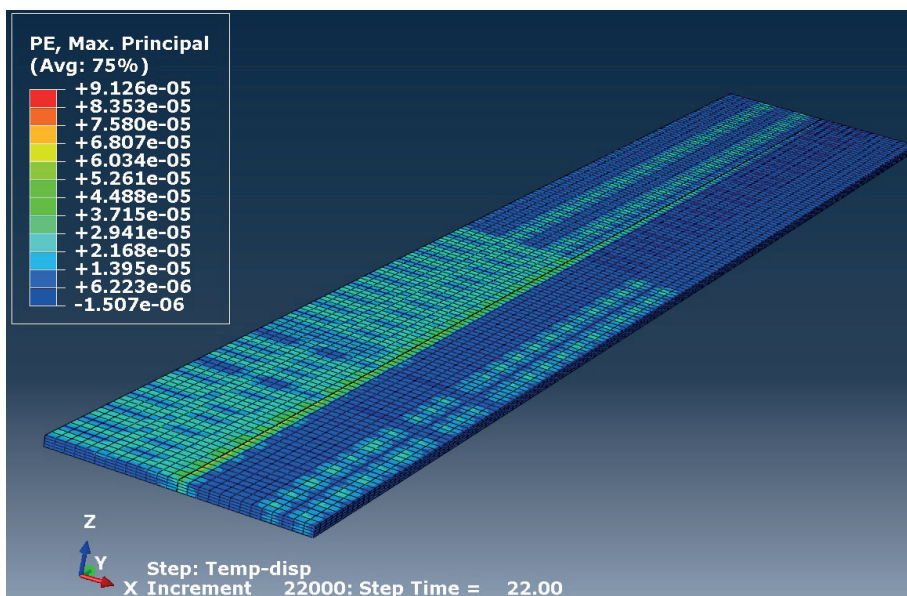


Fig. 16. Maximal principal plastic strains after time $t = 22.0$ s

5. DISCUSSION AND CONCLUSIONS

According to Neto&Neto [3], experimental investigations of the FSW process focused mainly on adjusting parameters such as angular and transverse speed of the welding tool, geometry of the tool, depth of penetration in welded parts. On the other hand, numerical simulation can be used to visualize some phenomena and results easier than in experimental investigations, e.g. material flow, heat generation and transfer, residual stress field and so on. Ten years after Neto&Neto [3] publication, the need for a new review and summary of progress in the numerical simulation of the FSW arose. This paper is an attempt to fill the gap. Author of this paper presented also a simple FEM simulation based on the Lagrangian approach and showed how to estimate stress in welded parts. The simple model can be useful in a practical use, e.g. for a structural engineer when designing a welded joint to make sure how large temperature and stress can be during welding.

The numerical model can be an effective tool in optimization and controlling of the FSW process. For a thorough scientific analysis, especially when

laboratory tests are compared with FEM simulations, more robust and complex numerical models are necessary. The most promising approaches are the Coupled Eulerian-Lagrangian (CEL) and Arbitrary Lagrangian-Eulerian (ALE) approach. Both methods are still being developed and while using them it is also possible to take into account the thermo-mechanical model of the FSW process. Researchers have already recognized the capabilities of advanced FEM codes and also try to incorporate their own subroutines. Some new opportunities are created by the use of artificial neural networks (ANN). At the moment ANN are rather applied to model some particular parameters of the FSW process or to find correlation between the parameters. The next step can be the so-called hybrid FEM and ANN modelling.

In this paper only one particular type of carbon steel was examined. As it was shown in works of Kossakowski et al. [60, 61], aluminium alloys and stainless steel are also in the scope of interest of contemporary construction industry. The author of this paper plans also to investigate the FSW process of these materials.

References

- [1] Thomas W.M., Murch M.G., Nicholas E.D., Temple-Smith P., Needham J.Ch., Dawes Ch.J.: *Improvements relating to friction welding. European patent application*, EP0653265A2, European Patent Office, 27.11.1992.
- [2] Thomas W.M., Nicholas E.D.: *Friction stir welding for the transportation industries*, Materials&Design, vol. 18, pp. 269-73, 1997, doi:10.1016/S0261-3069(97)00062-9.
- [3] Neto D.M., Neto P.: *Numerical modeling of friction stir welding process: a literature review*. The International Journal of Advanced Manufacturing Technology, vol. 65, pp. 115-126, 2013, doi:10.1007/s00170-012-4154-8.
- [4] Abaqus/CAE 2017. Simulia User Assistance. Johnston, RI, USA: Dassault Systemes Simulia Corp., 2017.
- [5] Mishra R.S., Ma Z.Y.: *Friction stir welding and processing*, Material Science and Engineering, vol. 50, pp. 1-78, 2005, doi:10.1016/j.msere.2005.07.001.
- [6] Sun Y., Gong W., Feng J., Lu G., Zhu R., Li Y.: *A Review of the Friction Stir Welding of Dissimilar Materials between Aluminum Alloys and Copper*. Metals, vol. 12, pp. 675, 2022, doi:10.3390/met12040675.
- [7] Nandan R., DebRoy T., Bhadeshia H.K.D.H.: *Recent advances in friction-stir welding – Process, weldment structure and properties*, Progress in Material Science, vol. 53, pp. 980-1023, 2008, doi:10.1016/j.pmatsci.2008.05.001.
- [8] Fabregas Villegas J., Martinez Guarin A., Unfried-Silgado J.: *A Coupled Rigid-viscoplastic Numerical Modeling for Evaluating Effects of Shoulder Geometry on Friction Stir-welded Aluminum Alloys*, International Journal of Engineering, vol. 32, pp. 313-321, 2019.
- [9] Gao S., Zhou L., Sun G., Zhao H., Chu X., Li G., Zhao H.: *Influence of Welding Speed on Microstructure and Mechanical Properties of 5251 Aluminum Alloy Joints Fabricated by Self-Reacting Friction Stir Welding*, Materials, vol. 14, pp. 6178, 2021, doi:10.3390/ma14206178.
- [10] Dialami N., Cervera M., Chiumenti M.: *Numerical Modelling of Microstructure Evolution in Friction Stir Welding (FSW)*, Metals, vol. 8, pp. 183, 2018, doi:10.3390/met8030183.
- [11] Dialami N., Chiumenti M., Cervera M.: *Material flow visualization in Friction Stir Welding via particle tracing*, International Journal of Material Forming, vol. 8, pp. 167-181, 2015, doi:10.1007/s12289-013-1157-4.
- [12] Chao Y.J., Qi X., Tang W.: *Heat Transfer in Friction Stir Welding – Experimental and Numerical Studies*, Journal of Manufacturing Science and Engineering, vol. 125, pp. 138-145, 2003, doi:10.1115/1.1537741.
- [13] Xie G.M., Ma Z.Y., Geng L.: *Partial recrystallization in the nugget zone of friction stir welded dual-phase Cu–Zn alloy*, Philosophical Magazine, vol. 89, pp. 1505-1516, 2009, doi:10.1080/14786430903019040.
- [14] Fonda R.W., Bingert J.F.: *Microstructural Evolution in the Heat-Affected Zone of a Friction Stir Weld*, Metallurgical and Materials Transactions A, vol. 35, pp. 1487-1499, 2004, doi:10.1007/s11661-004-0257-7.

- [15] Richmire S., Hall K., Hagsnehmas M.: *Design of experiment study on hardness variations in friction stir welding of AM60 Mg alloy*, Journal of Magnesium and Alloys, vol. 6, pp. 215-228, 2018, doi:10.1016/j.jma.2018.07.002.
- [16] Liu X., Xie P., Wimpory R., Li W., Lai R., Li M., Chen D., Liu Y., Zhao H.: *Residual Stress, Microstructure and Mechanical Properties in Thick 6005A-T6 Aluminium Alloy Friction Stir Welds*, Metals, vol. 9, pp. 803, 2019, doi:10.3390/met9070803.
- [17] Shyamlal Ch., Shanmugavel R., Winowlin Jappes J.T., Nair A., Ravichandran M., Abuthakeer S.S., Prakash Ch., Dixit S., Vatin N.I.: *Corrosion Behavior of Friction Stir Welded AA8090-T87 Aluminum Alloy*, Materials, vol. 15, pp. 5165, 2022, doi:10.3390/ma15155165.
- [18] Schenider J., Beshears R., Nunes Jr. A.C.: *Interfacial sticking and slipping in the friction stir welding process*, Materials Science and Engineering A, vol. 435-436, pp. 297-304, 2006, doi:10.1016/j.msea.2006.07.082.
- [19] Kossakowski P.G., Wciślik W., Bakalarz M.: *Macrostructural Analysis Of Friction Stir Welding (FSW) Joints*, Journal of Mechanical Engineering Research, vol. 1, pp. 28-33, 2018, doi:10.30564/jmer.v1i1.486.
- [20] Kossakowski P.G., Wciślik W., Bakalarz M.: *Effect of selected friction stir welding parameters on mechanical properties of joints*, Archives of Civil Engineering, vol. 65, pp. 51-62, 2019, doi:10.2478/ace-2019-0046.
- [21] Richards B.: *Microstructure-Property Correlations in Friction Stir Welded Al6061-T6 Alloys*. BSc thesis, Worcester Polytechnic Institute, Worcester, Massachusetts, USA, 2010.
- [22] Meyghani B., Awang M.B., Emamian S.S., Nor M.K.B.M., Pedapati S.R.: *A Comparison of Different Finite Element Methods in the Thermal Analysis of Friction Stir Welding (FSW)*. Metals, vol. 7(10), pp. 450, 2017, doi:10.3390/met7100450.
- [23] Lorrain O., Serri J., Favier V., Zahrouni H., El Hadrouz M.: *A contribution to a critical review of friction stir welding numerical simulation*, Journal of Mechanics of Materials and Structures, vol. 4(2), pp. 351-369, 2009, doi:10.2140/jomms.2009.4.351.
- [24] Oliphant A.H.: *Numerical Modeling of Friction Stir Welding: A Comparison of Alegra and Forge3*, MSc thesis, Brigham Young University, Provo, Utah, USA, 2004.
- [25] Guerdoux S.: *Numerical simulation of the friction stir welding process*, PhD thesis, l'Ecole des Mines de Paris, Paris, France, 2007.
- [26] Arakere A.P.: *Computational modeling of the friction stir welding (FSW) process and of the performance of FSW joints*, MSc thesis, Clemson University, Clemson, South Carolina, USA, 2013.
- [27] Bhattacharjee R., Biswas P.: *Review on thermo-mechanical and material flow analysis of dissimilar friction stir welding*, Welding International, vol. 35, pp. 295-332, 2021, doi:10.1080/09507116.2021.1992256.
- [28] Sen S., Murugesan J.: *Experimental and numerical analysis of friction stir welding: a review*. Eng Res Express 2022, 4, 032004. <https://doi.org/10.1088/2631-8695/ac7f1e>.
- [29] Meyghani B., Awang M.B., Momeni M., Rynkovskaya M.: *Development of a Finite Element Model for Thermal Analysis of Friction Stir Welding (FSW)*, IOP Conference Series: Materials Science and Engineering, vol. 495, pp. 012101, 2019, doi:10.1088/1757-899X/495/1/012101.
- [30] Colegrove P.A., Shercliff H.R.: *Experimental and numerical analysis of aluminium alloy 7075-T7351 friction stir weld*, Science and Technology of Welding and Joining, vol. 8:5, pp. 360-368, 2003, doi:10.1179/136217103225005534.
- [31] Colegrove P.A., Shercliff H.R.: *3-Dimensional CFD modelling of flow round a threaded friction stir welding tool profile*, Journal of Materials Processing Technology, vol. 169, pp. 320-327, 2005, doi:10.1016/j.jmatprotec.2005.03.015.
- [32] Jacquin D., de Meester B., Simar A., Deloison D., Montheillet F., Desrayaud C.: *A simple Eulerian thermomechanical modeling of friction stir welding*, Journal of Materials Processing Technology, vol. 211, pp. 57-65, 2011, doi:10.1016/j.jmatprotec.2010.08.016.
- [33] Dialami N., Chiumenti M., Cervera M., de Saracibar C.A.: *Local and global approaches to Friction Stir Welding*. Barcelona, Spain: International Center for Numerical Methods in Engineering, 2016.
- [34] Dialami N., Chiumenti M., Cervera M., de Saracibar C.A.: *Challenges in Thermo-mechanical Analysis of Friction Stir Welding Processes*, Archives of Computational Methods in Engineering, vol. 24, pp. 189-225, 2017, doi:10.1007/s11831-015-9163-y.
- [35] Gao E., Zhang X., Liu C., Ma Z.: *Numerical simulations on material flow behaviors in whole process of friction stir welding*, Transactions of Nonferrous Metals Society of China, vol. 28, pp. 2324-2334, 2018, doi:10.1016/S1003-6326(18)64877-0.
- [36] Zhao H.: *Friction stir welding (FSW) simulation using an arbitrary Lagrangian – Eulerian (ALE) moving mesh approach*, PhD thesis, West Virginia University, Morgantown, West Virginia, USA, 2005.
- [37] Chauhan P., Jain R., Pal S.K., Singh S.B.: *Modeling of defects in friction stir welding using coupled Eulerian and Lagrangian method*, Journal of Manufacturing Processes, vol. 34, pp. 158-166, 2018, doi:10.1016/j.jmapro.2018.05.022.
- [38] Kishta E.E., Abed F.H., Darras B.M.: *Nonlinear Finite Element Simulation of Friction Stir Processing of Marine Grade 5083 Aluminum Alloy*, Engineering Transactions, vol. 62, pp. 313-328, 2014.
- [39] Li K., Jarrar F., Sheikh-Ahmad J., Ozturk F.: *Using coupled Eulerian Lagrangian formulation for accurate modeling of the friction stir welding process*, Procedia Engineering, 207, 574-579, 2017, doi:10.1016/j.proeng.2017.10.1023.

- [40] Chen C.M., Kovacevic R.: *Finite element modeling of friction stir welding – thermal and thermomechanical analysis*, International Journal of Machine Tools and Manufacture, vol. 43, pp. 1319-1326, 2003, doi: 10.1016/S0890-6955(03)00158-5.
- [41] Schmidt H., Hattel J.: *A local model for the thermomechanical conditions in friction stir welding*, Modelling and Simulation in Materials Science and Engineering, vol. 13, pp. 77-93, 2004, doi:10.1088/0965-0393/13/1/006.
- [42] Schmidt H., Hattel J.: *Thermal modelling of friction stir welding*, Scripta Materialia, vol. 58, pp. 332-337, 2008, doi:10.1016/j.scriptamat.2007.10.008.
- [43] Hamilton C., Dymek S., Sommers A.: *A thermal model of friction stir welding in aluminum alloys*, International Journal of Machine Tools and Manufacture, vol. 48, pp. 1120-1130, 2008, doi:10.1016/j.ijmactools.2008.02.001.
- [44] Mehta M., Reddy G.M., Rao A.V., De A.: *Numerical modeling of friction stir welding using the tools with polygonal pins*, Defence Technology, vol. 11, pp. 229-236, 2015, doi:10.1016/j.dt.2015.05.001.
- [45] Chiumenti M., Cervera M., de Saracibar C.A., Dialami N.: *Numerical modeling of friction stir welding processes*, Computer Methods in Applied Mechanics and Engineering, vol. 254, pp. 353-369, 2013, doi:10.1016/j.cma.2012.09.013.
- [46] Santiago D.H., Lombera G., Urquiza S., Cassanelli A., de Vedia L.A.: *Numerical Modeling of Welded Joints by the “Fric-tion Stir Welding” Process*, Materials Research, vol. 7, pp. 569-574, 2004, doi:10.1590/S1516-14392004000400010.
- [47] Ulysse P.: *Three-dimensional modeling of the friction stir-welding process*, International Journal of Machine Tools and Manufacture, vol. 42, pp. 1549-1557, 2002, doi:10.1016/S0890-6955(02)00114-1.
- [48] Zhang Z.: *Comparison of two contact models in the simulation of friction stir welding process*, Journal of Material Science, vol. 43, pp. 5867-5877, 2008, doi:10.1007/s10853-008-2865-x.
- [49] Schmidt H., Hattel J., Wert J.: *An analytical model for the heat generation in friction stir welding*, Modelling and Simulation in Material Science and Engineering, vol. 12, pp. 143-157, 2003, doi:10.1088/0965-0393/12/1/013.
- [50] Zhu X.K., Chao Y.J.: *Numerical simulation of transient temperature and residual stresses in friction stir welding of 304L stainless steel*, Journal of Materials Processing Technology, vol. 146, pp. 263-272, 2004, doi:10.1016/j.jmatprotec.2003.10.025.
- [51] Abdullah I., Mohammed S.S., Abdallah S.A.: *Artificial neural network modelling of the surface roughness of friction stir welded AA7020-T6 aluminum alloy*, Engineering Research Journal, vol. 1, pp. 1-5, 2020, doi:10.21608/erjsh.2020.228168.
- [52] Okuyucu H., Kurt A., Arcaklioglu E.: *Artificial neural network application to the friction stir welding of aluminum plates*, Materials&Design, vol. 28, pp. 78-84, 2007, doi:10.1016/j.matdes.2005.06.003.
- [53] Jemioło S., Gajewski M.: *Symulacja MES obróbki cieplnej wyrobów stalowych z uwzględnieniem zjawisk termometalurgicznych. Część 1. Nieustalony przepływ ciepła z uwzględnieniem przejść fazowych* (Thermo-metallurgical phenomena in FE simulation of heat treatment for steel. Part 1: Unsteady heat transfer and phase change phenomena). Zeszyty Naukowe, Budownictwo, vol. 143, Oficyna Wydawnicza Politechniki Warszawskiej, Warszawa 2005.
- [54] Jemioło S., Gajewski M.: *Symulacja MES obróbki cieplnej wyrobów stalowych z uwzględnieniem zjawisk termometalurgicznych. Część 2. Przykłady numeryczne z zastosowaniem programu SYSWELD* (Thermo-metallurgical phenomena in FE simulation of heat treatment for steel. Part 2: Numerical examples using SYSWELD program). Zeszyty Naukowe, Budownictwo, vol. 143, Oficyna Wydawnicza Politechniki Warszawskiej, Warszawa 2005.
- [55] Jemioło S., Gajewski M.: *Zastosowanie programu SYSWELD w modelowaniu resztkowych naprężeń pospawalniczych* (SYSWELD program application in modelling of residual postwelding stresses). Zeszyty Naukowe, Budownictwo, z.143, Oficyna Wydawnicza Politechniki Warszawskiej, Warszawa 2005.
- [56] Hashemzadeh M., Garbatov Y., Guedes Soares C., O'Connor A.: *Friction stir welding induced residual stresses in thick steel plates from experimental and numerical analysis*, Ships and Offshore Structures, vol. 17, pp. 1053-1061, 2021, doi:10.1080/17445302.2021.1893531.
- [57] Chang P.H., Teng T.L.: *Numerical and experimental investigations on the residual stresses of the butt-welded joints*, Computational Materials Science, vol. 29, pp. 511-522, 2004, doi:10.1016/j.commatsci.2003.12.005.
- [58] Jeyakumar M., Christopher T., *Influence of residual stresses on failure pressure of cylindrical pressure vessels*, Chinese Journal of Aeronautics, vol. 26, pp. 1415-1421, 2013, doi:10.1016/j.cja.2013.07.025.
- [59] Giorjão R.A.R., Avila J.A., Escobar J.D., Ferrinho Pereira V., Marinho R.R., Torres Piza Paes M., Fonseca E.B., Costa A.M.S., Terada M.: *The study of volumetric wearing of PCBN/W-Re composite tool during friction stir processing of pipeline steels (X70) plates*, The International Journal of Advanced Manufacturing Technology, vol. 114, pp. 1555-1564, 2021, doi:10.1007/s00170-021-06932-8.
- [60] Kossakowski P., Wciślik W., Bakalarz M.: *Selected aspects of application of aluminium alloys in building structures*, Structure and Environment, vol. 9(4), pp. 256-263, 2017, https://sae.tu.kielce.pl/33/S&E_nr_33_Art_4.pdf.
- [61] Wciślik W., Kossakowski P., Sokołowski P.: *Stainless steel in building structures - advantages and examples of application*, Structure and Environment, vol. 9(3), pp. 191-198, 2017, https://sae.tu.kielce.pl/32/S&E_NR_32_Art_4.pdf.



CFD AND EXPERIMENTAL INVESTIGATION OF THE IMPACT OF DIMENSIONAL MODIFICATIONS ON WIND PRESSURE COEFFICIENT DISTRIBUTION

ANALIZA CFD ORAZ METODY EKSPERYMENTALNE W BADANIACH WPŁYWU MODYFIKACJI WYMIARÓW NA ROZKŁAD WSPÓŁCZYNNIKA PARCIA WIATRU

RAMJAN ALI*

European University of Bangladesh, Bangladesh

IFTEKHAR ANAM

University of Asia Pacific, Bangladesh

SHIGEO YOSHIDA

Kyushu University, Japan

Abstract

The sway of tall buildings in the wind is a fascinating and crucial consideration for professionals in the structural, environmental, and architectural fields. Previous research has related wind pressure to building load and natural ventilation, but few studies have looked at how building dimensions impact wind pressure. This study examined wind pressure coefficient distributions within and around several rectangular-shaped high-rise buildings using experimental and computational fluid dynamics approaches. The height-to-width ratio and height-to-thickness (length) ratio significantly affected the wind characteristics of buildings. The windward side with a narrower width experienced higher wind pressure, while the larger leeward side experienced a more negative wind effect. Wind pressure coefficient distribution varies with decrease in the side ratio. However, the side ratio of the building had little influence on positive wind pressure at wind incidence angle of 0° , which was a surprising finding. Pressure coefficients were evaluated and compared with standards by measuring fluctuating wind pressures at pressure points on all surfaces of models, and then calculating the mean, maximum, minimum, and r.m.s. values of these coefficients.

Keywords: Computational Fluid Dynamics, Wind pressure coefficient, Building dimensions, Windward, Leeward, Side Ratio

Streszczenie

Kołysanie się wysokich budynków pod wpływem wiatru jest fascynującym i kluczowym zagadnieniem dla specjalistów w dziedzinie konstrukcji, ochrony środowiska i architektury. W niniejszym artykule zbadano rozkłady współczynnika parcia wiatru wewnątrz i wokół kilku budynków wysokich o kształcie prostokąta, stosując metody eksperymentalne i numeryczne (obliczeniowa dynamika płynów). Stosunek wysokości budynku do jego szerokości oraz stosunek wysokości budynku do jego grubości (długości) miały znaczący wpływ na charakterystykę oddziaływania wiatru. Większe ciśnienie wiatru odnotowano po stronie zewnętrznej o mniejszej szerokości, podczas gdy na większej ścianie od strony zewnętrznej

oddziaływanie wiatru było bardziej negatywne. Rozkład współczynnika parcia wiatru zmienia się wraz ze spadkiem stosunku boków. Jednak stosunek ten miał niewielki wpływ na dodatnie ciśnienie wiatru przy kierunku wiatru 0°, co było zaskakującym odkryciem. Współczynniki ciśnienia zostały ocenione i porównane z podejściem normowym poprzez pomiar zmiennego ciśnienia wiatru w punktach parcia na wszystkich powierzchniach modeli, a następnie obliczenie średnich, maksymalnych, minimalnych i średnich kwadratowych wartości tych współczynników.

Słowa kluczowe: obliczeniowa dynamika płynów, współczynnik ciśnienia wiatru, strona nawietrzna, strona zawietrzna, proporcje boków

1. INTRODUCTION

In building science, wind impacts are directly linked to building loads and natural ventilation. Building designs, wind features, and site factors contribute to the complex and changeable nature of air flows around structures, as established by various studies (Blocken, 2014). Despite differences in parameter values between international wind regulations and codes, regression methods such as the logarithmic law, exponential law, and modified logarithmic law have been used to develop wind profiles (Kwon & Kareem, 2013). These profiles play an essential part in turbulence models and the use of computational fluid dynamics (CFD) methods, determining the dependability of numerical simulations. Scholars have deployed simulations to examine the usefulness of turbulent models, including extensive eddy simulation and the conventional k- turbulent model, demonstrating strong agreement with experimental results (Murakami & Mochida, 1988; Murakami, Mochida, & Hibi, 1987). However, the latter strategy proved superior in capturing unstable fields. Wind velocity, as well as pressure variations within and around structures, have been comprehensively explored using various k- models, enabling substantial progress in understanding wind features (Baskaran & Stathopoulos, 1989, 1993; Stathopoulos & Baskaran, 1996). Designing lateral systems and claddings for high-rise structures involves careful consideration of wind-induced vibrations. Standards such as ASCE Standard No. 7-05, Bangladesh National Building Code (2020), and Standards Australia/Standards New Zealand (2011) give instructions for analyzing wind force coefficients as well as wind pressure coefficients (Kwon & Kareem, 2013). While these rules include coefficients for rectangular and square structures with varying aspect ratios and heights at defined wind exposure angles, they lack suggestions for greatly expanded rectangular plan-shaped buildings or oblique wind incidence angles. Extensive research has been conducted on the wind pressure distributions of rectangular models, focusing on factors such as side ratios, boundary layer conditions, and wind

orientations. Kareem and Cermak (1984) conducted studies to examine the pressure distribution along the sidewalls of square models under various boundary layer flow conditions. In a complementary study, Kareem (1990) investigated the influence of turbulent boundary layer flows on the temporal and spatial characteristics of pressure fields observed on the surfaces of prismatic structures. In wind tunnel experiments conducted on an 11-story building, Józwiak et al. (1995) observed that on the sheltered side, specifically in the area between buildings, there were significantly higher negative pressures compared to those recorded for a stand-alone building, reaching up to 1.8 times the magnitude. However, the interference effect diminishes greatly when the building is strategically positioned. Additionally, Saathoff and Melbourne (1989) employed rectangular prisms and extended plates that were flat with square edge shapes to acquire insights into specific components of the two-dimensional detachment and restoration process, as well as the development of maximal suction forces. Investigations by Miyata and Miyazaki (1980), Lee (1975), and Vickery (1966) involved the measurement of the surface forces and relationships between dimensions in a 2-dimensional flow. According to Lee's study, an increase in perpendicular turbulence around the cube led to a decrease in base pressure and a reversal of pressure on the side faces. To examine how side ratios and wind direction affect the distribution of wind pressure, this research integrates experimental investigation with computational fluid dynamics (CFD) analysis.

2. NUMERICAL MODEL VALIDATION

The present study selected the model of the Commonwealth Advisory Aeronautical Council (CAARC) building for the numerical model validation. The CAARC model is shaped like a rectangular prism and measures 100 feet (x), 150 feet (y), and 600 feet (z) in height, as shown in Figure 1. The current study employed a wind velocity profile for an open exposure, the power law exponent of which was 0.16, which could be seen in Figure 2. A system of Cartesian

coordinates (x, y, z) was used to represent the flow, the x -axis represents the direction of the stream, the y -axis is stacked vertically, and the z -axis is in the opposite direction of the stream. Information about the CFD mesh is as follows: (1) mesh density 35%, (2) number of mesh 1871820, and (3) minimum grid size 1.37 feet.

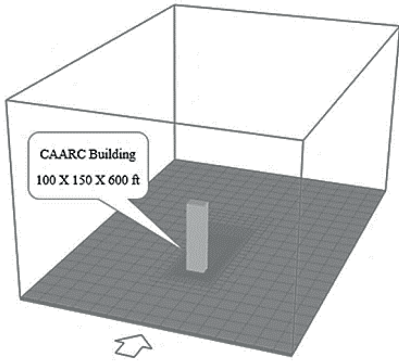


Fig. 1. Computational wind tunnel setup

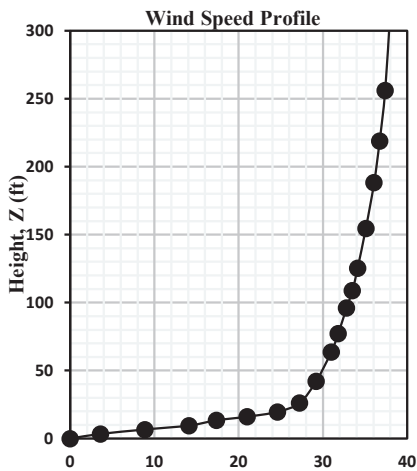


Fig. 2. Wind Speed Profile (Dagnew et al. 2009)

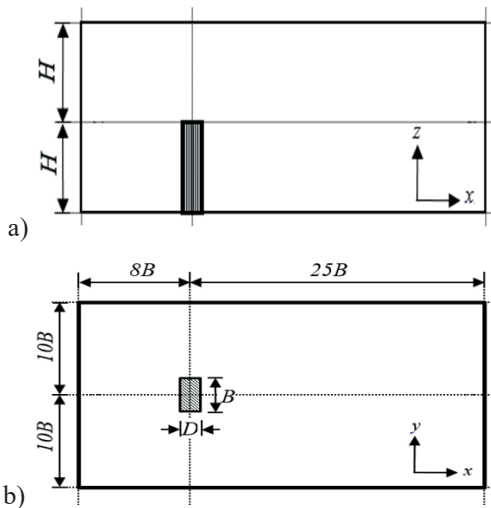


Fig. 3. Side (a) and top (b) view of the boundary conditions and computational domain

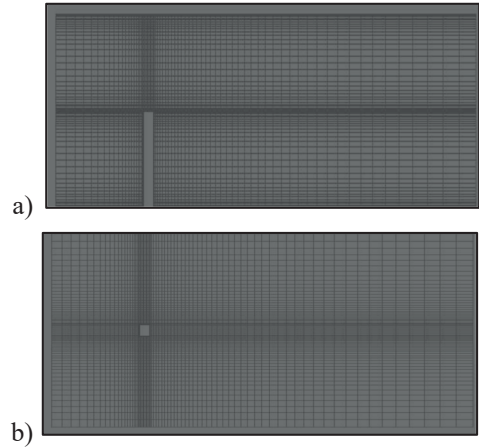


Fig. 4. Side (a) and top (b) view of the typical grid used for the study

The FLUENT code provides four choices for Subgrid-Scale (SGS) approach for LES. These are: Smagorinsky–Lilly model, Dynamic Smagorinsky–Lilly model, Wall-adapting local eddy-viscosity model, and Dynamic SGS kinetic energy model. The dynamic SGS kinetic energy model is used in this study as it accounts for the transport of the SGS turbulence kinetic energy, which was found to be better than an algebraic expression based on local equilibrium assumptions given by the Smagorinsky series. The Smagorinsky series assumes that equilibrium exists between the transferred energy through the grid-filter scale and the dissipation of kinetic energy at small subgrid scales. However, for high Reynolds number bluff body flows, the local equilibrium assumption is questionable. The SGS kinetic energy of the dynamic SGS kinetic energy

model is defined as $K_{sgs} = \frac{1}{2}(\overline{U_k^2} - \overline{U_k}^2)$ which is obtained by contracting the subgrid-scale stress in $\tau_{ij} = \rho \overline{U_i U_j} - \rho \overline{U_i} \overline{U_j}$. The SGS eddy viscosity, μ_t , is computed using K_{sgs} as, $\mu_t = C_k K_{sgs}^{1/2} \Delta f$, where Δf is the filter size computed from $\Delta f = \nu^{1/3}$. The subgrid-scale stress can then be written as $\tau_{ij} = \frac{2}{3} k_{sgs} \delta_{i,j} - 2 \mu_t \overline{S_{i,j}}$, while K_{sgs} is obtained by solving its transport equation:

$$\frac{\partial k_{sgs}}{\partial t} + \frac{\partial \overline{U_j} \cdot k_{sgs}}{\partial x_j} = -\tau_{ij} \frac{\partial \overline{U_j}}{\partial x_j} - C_\varepsilon \frac{K_{sgs}^3}{\Delta f} + \frac{\partial}{\partial x_j} \left(\frac{\mu_t}{\sigma_k} \frac{\partial k_{sgs}}{\partial x_j} \right)$$

The model constants, C_k and C_ϵ , are determined dynamically (Kim & Menon, 1997) and σ_k is 1.0 in the above equations.

The wind speed profile shown in Figure 2 was collected from Dagnev et al. (2009) since the result of the current study required reliable data with whom it could be compared and come to a conclusive decision if the current study was accurate enough. In their 2009 study, Dagnev et al. presented wind tunnel test results along with those from Tong Ji University and CFD analysis using numerical models, specifically Large Eddy Simulation and K-epsilon. This study aimed to compare its results with those of Dagnev et al., as shown in Figure 5.

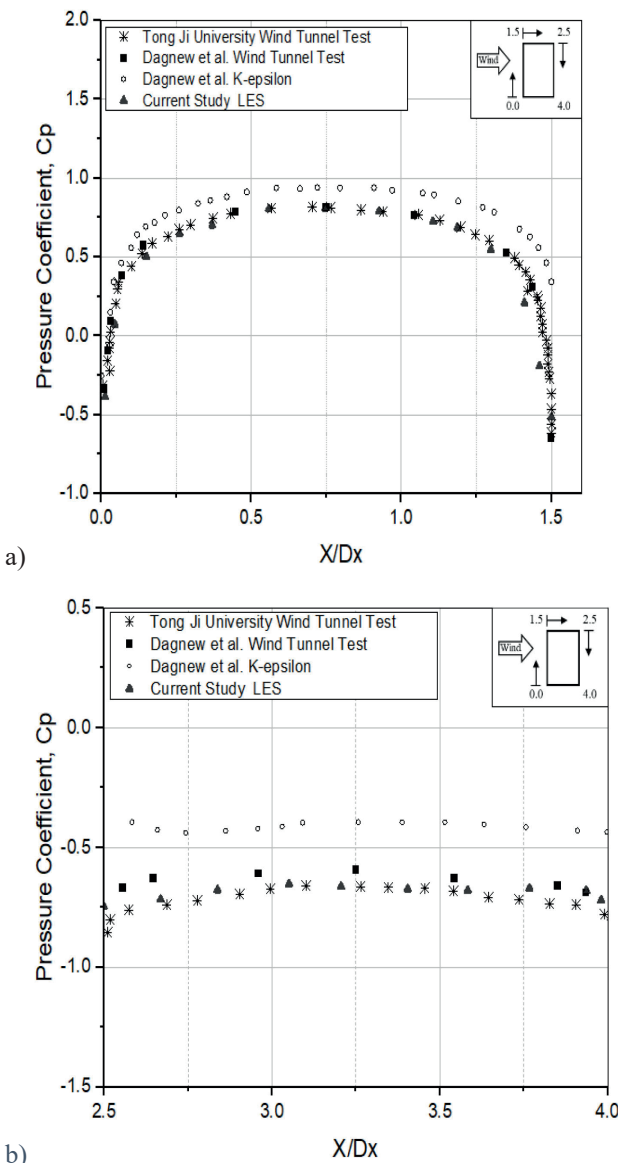


Fig. 5. Comparisons of wind pressure coefficient between current and previous studies on the CAARC building model (a) Windward (b) Leeward

The study found that in the windward face (X/D_x 0.0-1.5), the LES numerical model used in this study demonstrated greater accuracy than the K-epsilon model used by Dagnev et al., while both models agreed in the leeward face (X/D_x 2.5-4.0), and agreed with wind tunnels. The reference wind speed was 12.7 m/s. Wind pressure coefficients (C_p) were computed at $2/3H$ of the building on the leeward, sidewall, and windward sides for the inflow boundary conditions shown in Figures 3a and 3b.

3. WIND TUNNEL SETUP

The test portion of the wind tunnel is 27 feet long and 3.94 feet (width) by 2.80 feet in cross-section (height). The experimental flow is reproduced at a length scale of 1: 300 to replicate the features of an open rural area.

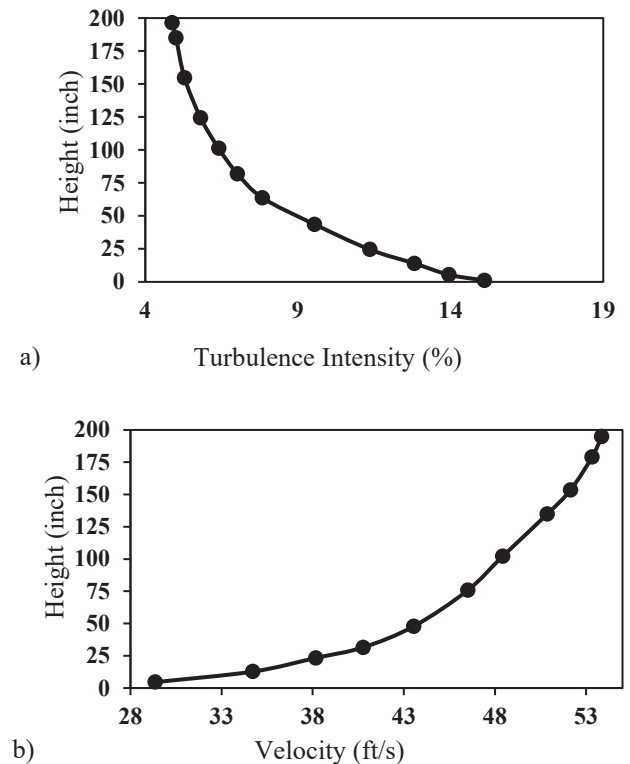


Fig. 6. Turbulence intensity (a) and Velocity profile (b)

Wind tunnel setup used in the study of (Amin & Ahuja, 2013) was followed with little adjustment for this study. The model is positioned 20 feet from the test section's upstream edge. In order to quantify the free stream velocity during experiments, a reference inlet and outlet tube is placed 20 inches above the wind tunnel floor and 11.5 feet away from the grid. Figures 6a and 6b, respectively, show the intensity of the turbulence and the non-dimensional mean

velocity. The reference wind speed used in this research has been kept constant at 40 ft/sec at the model's roof height. The power-law index (n) of the velocity profile within the tunnel is 0.162.

3.1. Information about models

The experiments utilized models made of translucent plastic, with a thickness of 0.25 inches. These models were created at a geometrical scale of 1:300, matching the scale used for the wind simulation. To ensure meaningful comparisons, the height and surface area of each model were kept constant at 15.5 square inches

and 12 inches, respectively. To accurately measure pressure distribution on the building models' surfaces, approximately 175 pressure taps were installed at seven different height levels: 1, 3, 5, 7, 9, 10, and 11 inches from the floor. These pressure taps were strategically positioned near the faces of the models to capture fluctuations in high pressure along the edges. For further details on the classification and dimensions of the building models, refer to Table 1. Figure 7 illustrates the locations of the pressure taps around the perimeters of the building models, with measurements provided in inches.

Table 1. Features of the models

Model	Building Dimension (L x W x H)	Side Ratio	Computational Domain (X x Y x Z)	Blockage Ratio	
				0°	90°
M-1	4" x 4" x 12" [100 mm x 100 mm x 300 mm]	1.0	90" x 90" x 33" [2250 mm x 2250 mm x 825 mm]	1.61%	1.61%
M-2	3.2" x 5" x 12" [80 mm x 125 mm x 300 mm]	1.56		1.30%	2.02%
M-3	2.67" x 6" x 12" [75 mm x 150 mm x 300 mm]	2.25		1.08%	2.42%
M-4	2.24" x 7.15" x 12" [55 mm x 175 mm x 300 mm]	3.2		0.90%	2.89%

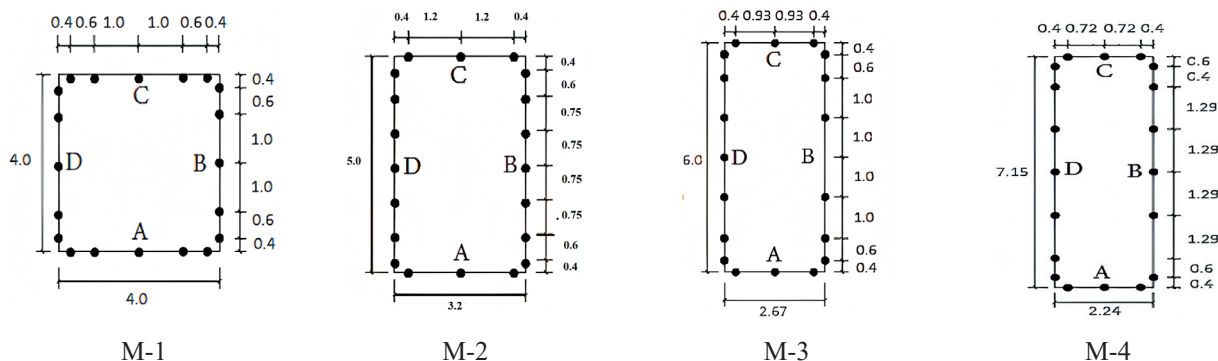


Fig. 7. The locations where pressure tapping was conducted along the perimeter and plan view of the models

4. RESULTS AND DISCUSSION

The varied wind pressure data were used to re-evaluate the pressure coefficients on every surface of building model throughout a range of wind angles of incidence from 0° to 90° at 15° intervals. The average (mean), root mean square (r.m.s.), and highest and lowest wind pressure coefficients were calculated during this reevaluation. The wind pressure coefficient contours of models M-1, M-2, M-3, and M-4 at a wind incidence angle of 0° are depicted in Figures 8, 10, 12, and 14 from the experimental while Figures 9, 11, 13, and 15 represent the wind pressure coefficient

from the CFD analysis, respectively. These figures visually represent how the wind pressure varies across the surface of the models under study. By examining these contours, we can better understand the aerodynamic forces at play and how they affect the performance of the models.

The wind pressure coefficient distribution was relatively similar for models M1, M2, and M3 based on both experimental and CFD results. However, for model M4, the CFD results showed fewer wind pressure coefficient values, which can be observed in Figures 14 and 15.

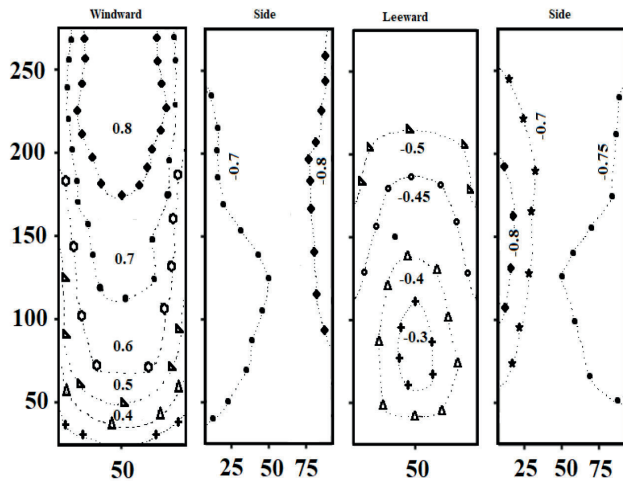


Fig. 8. Experimental wind pressure coefficient distribution for Model M-1

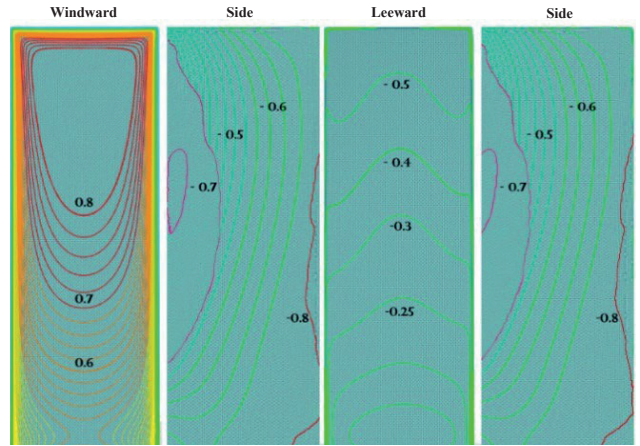


Fig. 9. CFD Analyzed wind pressure coefficient distribution for Model M-1

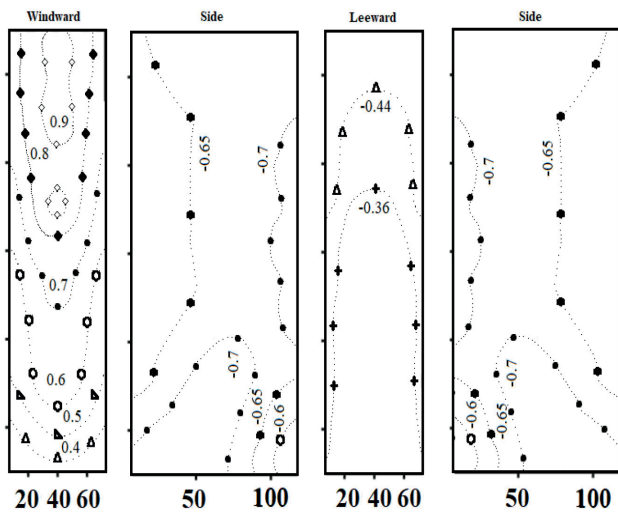


Fig. 10. Experimental wind pressure coefficient distribution for Model M-2

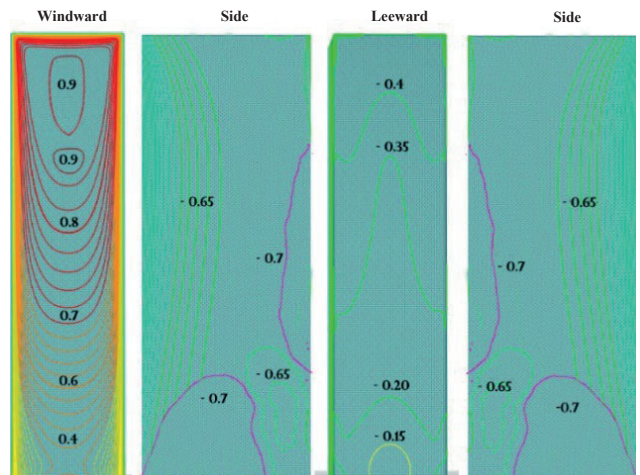


Fig. 11. CFD Analyzed wind pressure coefficient distribution for Model M-2

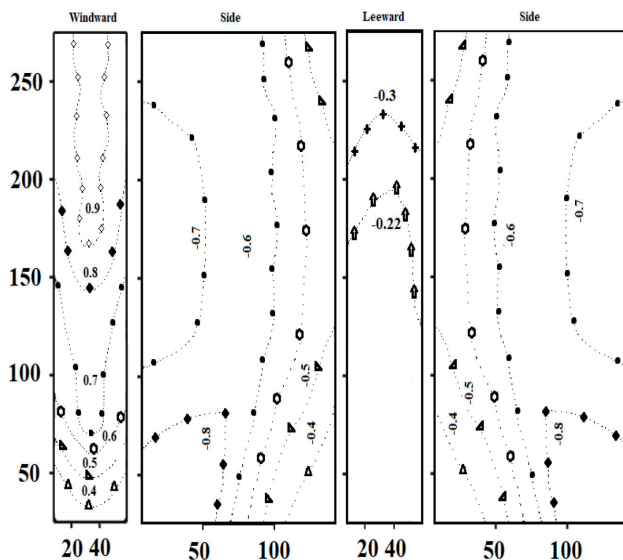


Fig. 12. Experimental wind pressure coefficient distribution for Model M-3

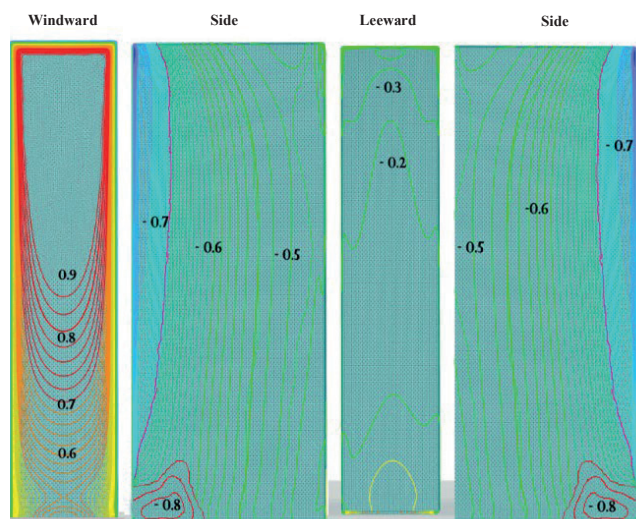


Fig. 13. CFD Analyzed wind pressure coefficient distribution for Model M-3

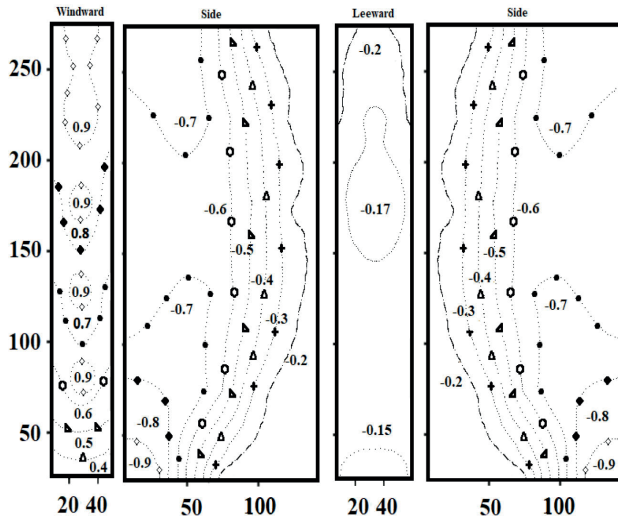


Fig. 14. Experimental wind pressure coefficient distribution for Model M-4

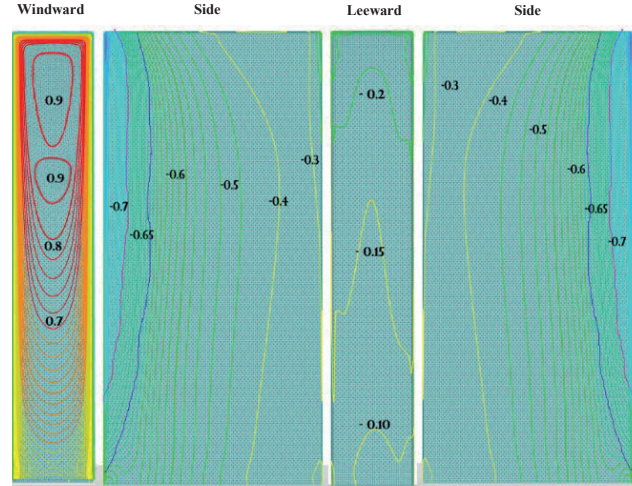


Fig. 15. CFD Analyzed wind pressure coefficient distribution for Model M-4

Experimental and CFD results have shown that the wind pressure distribution on models with different aspect ratios is significantly affected by both the height-to-width and height-to-length ratios. Upon analyzing the wind pressure coefficient values and distribution depicted in Figures 8 to 15, a few observations could be made. For instance, the positive pressure on model surfaces varied little (gentle), but higher positive wind pressures were observed on narrower windward sides. In contrast, larger windward side corresponded to more severe negative wind effects in the leeward side (Opposite side). Model M-3, and M-4 having a relatively narrower windward area compared with other models, showed a high positive pressure coefficient. On the other hand, M-1 having a relatively large windward surface showed higher negative pressure coefficient in the leeward side. The length of the side walls played little role in altering the positive wind pressure. Significant variations were observed in the pressure distribution on leeward surfaces, indicating intensified wind effects on leeward surfaces. Observing all the model's result it was found that the side wall peak wind pressure coefficient values remain almost same but the distribution varies with decrease in the windward width (surface). Furthermore, wider widths amplified both positive and negative effects in the vicinity of the models, while the negative effects diminished as the windward length of the models increased. The CFD analysis results agree with the remarks made by the experimental results.

Based on the results, it can be concluded that the size and shape of rectangular models have minimal impact

on the distribution of pressure coefficients on the windward side. However, observations revealed that the root mean square and average pressure coefficients on the leeward side exhibit an increase up to a specific threshold, specifically at a side ratio of 0.6. Beyond this threshold, as the side ratio increases, both the mean and r.m.s. pressure coefficients decrease. This trend is visually depicted in Figure 16. These observations suggest the presence of an optimal side ratio for rectangular models in terms of wind resistance. Further research endeavors could delve into this concept and potentially contribute to the development of more efficient and effective designs for structures that require resilience in windy conditions.

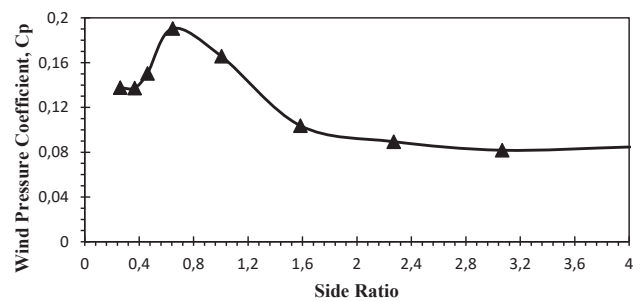


Fig. 16. The root mean square (R.M.S) wind pressure coefficient on the leeward side for various side ratios

Table 2 presents a comparison of wind pressure coefficients derived from experimental data and Computational Fluid Dynamic (CFD) analysis of building models at a wind incidence angle of 0°, alongside prominent wind standards and codes. Notably, all codes discussed in this study propose a pressure coefficient (Cp) of 0.8 for the

Table 2. Mean wind pressure coefficient comparison with CFD and different codes

Model	Side Ratio	Windward					Leeward					Side				
		Exp.	CFD	BNBC 2020	ASCE 7-05	AS/NZS 1170.2	Exp.	CFD	BNBC 2020	ASCE 7-05	AS/NZS 1170.2	Exp.	CFD	BNBC 2020	ASCE 7-05	AS/NZS 1170.2
M-1	1.00	0.74	0.76	0.8		-0,5	-0,5	-0.5	-0.5	-0.5	-0.69	-0.56	-0.7	-0.7	-0.65	
M-2	1.56	0.74	0.77	0.8		-0,41	-0,41	-0.4	-0.4	-0.4	-0.66	-0.53	-0.7	-0.7	-0.65	
M-3	2.25	0.75	0.78	0.8		-0,3	-0,28	-0.3	-0.3	-0.3	-0.62	-0.55	-0.7	-0.7	-0.65	
M-4	3.20	0.75	0.79	0.8		-0,2	-0,18	-0.25	-0.25	-0.25	-0.59	-0.46	-0.7	-0.7	-0.65	

windward side. Interestingly, the investigated models consistently exhibited mean C_p values lower than 0.8 on the windward face, indicating that the values recommended by the codes are reliable for rectangular-shaped buildings. Moreover, the mean C_p values obtained from both the experiment and CFD analysis for the leeward and side faces also matched or were lower than the values suggested by the codes. This suggests that despite significant fluctuations in C_p values along the side and leeward side, the engineering community can confidently rely on the values prescribed by the codes for rectangular-shaped buildings. Additionally, Table 2 provides insights into the influence of the side ratio on the pressure coefficient, a topic previously discussed.

5. CONCLUSION

The process of conducting wind pressure measurements on building models enables researchers to understand how side ratios and wind orientations affect wind pressure distribution and pressure coefficients on rectangular building models. According to the findings, the height-to-width and height-to-length ratios considerably impact the wind pressure distribution in models. When it comes to the positive pressure on model surfaces, smaller windward sides tend to have higher wind pressures than bigger windward sides, which are linked to more intense

negative wind impacts. In contrast to previous models, Model M-3, and M-4 has a shorter windward area, but it nevertheless displays a high positive pressure coefficient over a sizable portion of the windward surface, suggesting stronger wind pressure at the windward face. On the other hand, the amount of positive wind pressure is not significantly affected by the length of the side walls. The wind's impacts are more pronounced on both sides, and leeward surfaces, and the pressure distribution on leeward surfaces exhibits significant changes.

The depth or side ratio of rectangular structures has no effect on the intensity or pattern of distribution of the amount of pressure coefficients on the windward side for the wind direction of 0° . The mean and r.m.s. pressure coefficients, however, increase in absolute value to an aspect ratio of 0.6 on the leeward side. Both the root mean square and average pressure coefficients on the side that faces leeward subsequently fall in absolute value as the side ratio continues to rise. When the aspect ratio exceeds 3.0, a consistent negative pressure coefficient is observed on the leeward side, suggesting that the object achieves a minimal width. This study highlights the necessity for more investigation into the connection between different planar forms and wind impacts. Future studies will explore additional planar shapes like ovals and crosses whereas this article only concentrates on rectangular shapes.

References

- [1] ASCE:7-05, Minimum Design Loads for Buildings and other Structures, Structural Engineering Institute of the American Society of Civil Engineers, Reston, VA, USA, 2002.
- [2] Amin J.A., Ahuja A.K. (2013): *Effects of side ratio on wind-induced pressure distribution on rectangular buildings*. Journal of Structures.
- [3] Bangladesh National Building Code. (2020): Dhaka, Bangladesh: Housing and Building Research Institute.
- [4] Baskaran A., Stathopoulos T. (1993): *Numerical computation of wind pressures on buildings*. Computers & structures, 46(6), 1029-1039; doi.org/10.1016/0045-7949(93)90089-V.
- [5] Baskaran A., Stathopoulos T. (1989): *Computational evaluation of wind effects on buildings*. Building and Environment, 24(4), 325-333; doi.org/10.1016/0360-1323(89)90027-9.

- [6] Blocken B. (2014): *50 years of computational wind engineering: past, present and future*. Journal of Wind Engineering and Industrial Aerodynamics, 129, 69-102; doi.org/10.1016/j.jweia.2014.03.008.
- [7] Franke J., Hirsch C., Jensen A., Krüs H., Schatzmann M., Westbury P., Wright, N.G. (2004): *Recommendations on the use of CFD in wind engineering*, COST Action C14: Impact of Wind and Storm on City Life and Built Environment, von Karman Institute for Fluid Dynamics.
- [8] Józwiak R., Kacprzyk J., Zurański J.A. (1995): *Wind tunnel investigations of interference effects on pressure distribution on a building*. Journal of wind engineering and industrial aerodynamics, 57(2-3), 159-166; doi.org/10.1016/0167-6105(95)00004-B.
- [9] Kareem A. (1990): *Measurements of pressure and force fields on building models in simulated atmospheric flows*. Journal of Wind Engineering and Industrial Aerodynamics, 36, 589-599; doi.org/10.1016/0167-6105(90)90341-9.
- [10] Kareem A., Cermak J.E. (1984): *Pressure fluctuations on a square building model in boundary-layer flows*. Journal of Wind Engineering and Industrial Aerodynamics, 16(1), 17-41; doi.org/10.1016/0167-6105(84)90047-3.
- [11] Kwon D.K., Kareem A. (2013): *Comparative study of major international wind codes and standards for wind effects on tall buildings*. Engineering Structures, 51, 23-35; doi.org/10.1016/j.engstruct.2013.01.008.
- [12] Kim W.W., Menon S. (1997): *Application of the localized dynamic subgrid-scale model to turbulent wall-bounded flows*. Technical report AIAA-97-0210. Reno (NV): American Institute of Aeronautics and Astronautics, 35th Aerospace Sciences Meeting.
- [13] Lee B.E. (1975): *The effect of turbulence on the surface pressure field of a square prism*. Journal of Fluid Mechanics, 69(2), 263-282; doi.org/10.1017/S0022112075001437.
- [14] Miyata T., Miyazaki M. (1980): *Turbulence effects on aerodynamic response of rectangular bluff cylinders*. In Wind Engineering (pp. 631-642). Pergamon.
- [15] Murakami S., Mochida A., Hibi K. (1987): *Three-dimensional numerical simulation of air flow around a cubic model by means of large eddy simulation*. Journal of Wind Engineering and Industrial Aerodynamics, 25(3), 291-305; doi.org/10.1016/0167-6105(87)90023-7.
- [16] Murakami S., Mochida A. (1988): *3-D numerical simulation of airflow around a cubic model by means of the k-ε model*. Journal of Wind Engineering and Industrial Aerodynamics, 31(2-3), 283-303.
- [17] Standards Australia. (2011). AS/NZS 1170.2 Structural Design Actions, Part 2 Wind Actions; doi.org/10.1016/0167-6105(88)90009-8.
- [18] Saathoff P.J., Melbourne W.H. (1989): *The generation of peak pressures in separated/reattaching flows*. Journal of Wind Engineering and Industrial Aerodynamics, 32(1-2), 121-134; doi.org/10.1016/0167-6105(89)90023-8.
- [19] Stathopoulos T., Baskaran B.A. (1996): *Computer simulation of wind environmental conditions around buildings*. Engineering structures, 18(11), 876-885; doi.org/10.1016/0141-0296(95)00155-7.
- [20] Vickery B.J. (1966): *Fluctuating lift and drag on a long cylinder of square cross-section in a smooth and in a turbulent stream*. Journal of Fluid Mechanics, 25(3), 481-494; doi.org/10.1017/S002211206600020X.



RHEOLOGICAL PROPERTIES OF CEMENT PASTES MODIFIED WITH PUMICE, TRASS AND CHALCEDONITE POWDER

WŁAŚCIWOŚCI REOLOGICZNE ZACZYNÓW CEMENTOWYCH MODYFIKOWANYCH PUMEKSEM, TRASEM I MĄCZKĄ CHALCEDONITOWĄ

EDYTA SPYCHAŁ*

Kielce University of Technology, Poland

MARTIN VYŠVAŘIL

Brno University of Technology, Czechia

Abstract

The article presents the influence of pumice, trass and chalcedonite powder on rheological properties of cement pastes. Cement was being replaced both of additions 10% or 20% by mass and combination of pumice or trass and chalcedonite powder in the amount 5% or 10% of each of them. The main purpose of the publication was to assess the effects of chalcedonite powder with selected mineral additions in terms of rheological properties and compare them with the results obtained for pastes modified with only one of the additions. In each case, the additive or combination of additives introduced into the paste reduced the flow, compared to the result of paste without additive(s). Rheological properties varied depending on type and amount of additive(s).

Keywords: cement paste, pumice, trass, chalcedonite powder, consistency, yield stress, consistency index

Streszczenie

W artykule przedstawiono badania wpływu pumeksu, trasu oraz mączki chalcedonitowej na właściwości reologiczne zaczynów cementowych. Cement zastępowano każdym z dodatków w ilości 10% lub 20% oraz kombinacją pumeksu lub trasu z mączką chalcedonitową w ilości po 5% i 10% każdym z nich. Głównym celem pracy była ocena współdziałania mączki chalcedonitowej z wybranymi dodatkami mineralnymi w zakresie właściwości reologicznych oraz porównanie rezultatów badań z wynikami uzyskanymi dla zaczynów modyfikowanych tylko jednym z dodatków. W każdym z przypadków dodatek lub kombinacja dodatków wprowadzone do zaczynu wpłynęły na zmniejszenie rozplywu, w porównaniu do wyników uzyskanych dla zaczynu bez dodatku(ów). Właściwości reologiczne były zróżnicowane w zależności od rodzaju i ilości dodatku(ów).

Słowa kluczowe: zaczyn cementowy, pumeks, tras, mączka chalcedonitowa, konsystencja, granica płynięcia, wskaźnik konsystencji

1. INTRODUCTION

Building mortars and concrete are commonly used in civil engineering. Main ingredient used in their production is cement. However, one should note

that the production of this binder involves large energy inputs and emission of dust and gases such as nitrogen oxides, sulfur dioxide, carbon oxides, etc. to the atmosphere, what has direct impact on the

*Corresponding Author: e-mail: espychal@tu.kielce.pl

increase in the greenhouse effect. Estimated annual production of cement in Poland is over 19 million tons, and the production of 1 ton of cement clinker causes carbon dioxide emissions about 800 kg [1-6]. Because of the ideas of sustainable development and rational waste management, the type of solutions that would allow meeting the requirements imposed on the industry cement are sought in various ways. The use of mineral additions, including waste materials, allows a significant reduction in the emission of harmful gases into the atmosphere and also has a positive effect on the idea of a closed economy [1, 6-9]. Commonly used in cement production are: fly ash, granulated blast furnace slag and limestone flour [1, 10]. The PN-EN 197-1 standard also allows the use of other natural or artificial pozzolans. This is particularly important due to the limited resources of fly ash or due to the decarbonization of steel production processes and, therefore, the availability of blast furnace slag [1]. In many countries, one can find the technology of producing pozzolanic cements, containing natural pozzolans of volcanic or organic origin [11]. The optimal solution would be to use raw materials with a low carbon footprint that do not require additional thermal or chemical treatment. There are publications in the literature on the use of two- or three-component binders in which the cement is partially replaced by, among others: metakaolin [12, 13], zeolite [14-16], spongiolite [17], stone powders [1, 7-9, 18-20], simultaneously: zeolite and silica fume, fly ash and granulated blast furnace slag, limestone flour and zeolite, granite powder and fly ash [10, 14, 21, 22]. This is a current topic, especially due to the widespread use of Portland cements with additions and the popularization of low-clinker cements. Solutions are being sought that will be profitable from an ecological and economic point of view, bearing in mind the assumption that the properties of newly created binders must comply with standard requirements, ensuring the durability of the structure. Analyzing the literature, it can be concluded that researchers focus mainly on determining the impact of additions on mechanical properties, binding and hardening processes, corrosion resistance, microstructure of materials based on cement binder [7, 8, 10, 11, 13-15, 20-21, 23-25]. Only in a few publications rheological issues were analyzed [9, 12, 17, 26, 27].

Pumice, trass and chalcedonite powder were used as a partial replacement for cement. In this study, the authors focused on determining the rheological

properties of cement pastes modified with varying amounts of one of the additions or their combination. The main aim of the research was to assess the impact of chalcedonite powder in the context of the properties of three-component binders. Additionally, the effect of each of the additions used was determined separately as a partial substitute for cement. Consistency testing was performed and rheological properties were determined, such as consistency coefficient, yield stress, and thixotropy.

2. MATERIALS AND METHODS

The industrial ordinary Portland cement CEM I 42.5R was used in the research. Three materials were selected as additions: pumice, trass and chalcedonite powder. Pumice and trass are volcanic rocks. They were used in the work in the form of finely ground powder. They belong to the group of natural pozzolanas. Chalcedonite powder is a waste material generated during aggregate production through appropriate (contamination-free) grinding and air classification. The chemical composition of cement, pumice, trass and chalcedonite powder was presented in Table 1. It was measured by XRF method by Axios X-ray Fluorescence XRF spectrometer (Malvern Panalytical Ltd.).

The grain size distribution was measured with laser granulometer HELOS KR (Sympatec GmbH). Basing on the Table 2 it was established that the smallest grain size had chalcedonite powder. This material contained much more fine particles than other additions – about 79% of the particles in range 0-5 mm and about 98% of the particle in range 0-10 mm. Cement and trass contained about 33%, but pumice about 23% of the particles in range 0-5 mm. On the other hand content of particles in range 0-10 mm for cement and trass was about 48%, for pumice – about 39%. Cement, trass and pumice contained about 83% of the particles in range 0-35 mm.

Eleven type of pastes were prepared, in which Portland cement was substituted with pumice, trass and chalcedonite powder in the amounts of 10% (T10, P10, CH10) or 20% (T20, P20, CH20) and combination pumice with chalcedonite powder or trass with chalcedonite powder in the amount of 5% (T5CH5, P5CH5) or 10% (T10CH10, P10CH10) of each of them and the last kind of samples was the reference material – paste without mineral additions (C). Water/binder ratio was constant for all pastes and equal 0.5. The pastes mix proportion were detailed in Table 3.

Table 1. Chemical composition of cement and mineral additions [%]

Material	SiO ₂	Al ₂ O ₃	Fe ₂ O ₃	CaO	MgO	Na ₂ O	K ₂ O	SO ₃	TiO ₂	MnO	P ₂ O ₅	L.O.I.
Cement	18.33	4.71	4.25	64.13	1.65	0.05	0.59	2.68	0.26	0.19	0.16	2.99
Pumice	54.27	20.50	2.07	0.65	0.11	9.20	5.62	0.07	0.21	0.42	0.07	6.38
Trass	50.08	17.61	5.46	4.16	1.70	3.61	4.67	0.05	0.81	0.21	0.34	10.05
Chalcedonite powder	99.01	0.84	0.04	0.05	0.03	0.05	0.04	–	0.02	0.01	0.03	0.07

Table 2. Grain size distribution of cement and additions

Material	x ₁₀ mm	x ₅₀ mm	x ₉₀ mm	Content of particles, %			
				≤5 mm	≤10 mm	≤20 mm	≤35 mm
Cement	0.78	11.07	45.31	32.67	47.92	68.27	83.66
Pumice	1.36	13.88	47.26	23.55	39.69	65.13	82.56
Trass	0.94	10.55	47.48	33.05	49.14	69.13	83.21
Chalcedonite powder	0.43	1.80	7.31	78.76	97.75	100.00	100.00

Table 3. Composition of tested pastes [g]

Symbol of paste	Cement	Pumice	Trass	Chalcedonite powder	Water
C	70.0	0.0	0.0	0.0	35.0
P10	63.0	7.0	0.0	0.0	35.0
P20	56.0	14.0	0.0	0.0	35.0
T10	63.0	0.0	7.0	0.0	35.0
T20	56.0	0.0	14.0	0.0	35.0
CH10	63.0	0.0	0.0	7.0	35.0
CH20	56.0	0.0	0.0	14.0	35.0
P5CH5	63.0	3.5	0.0	3.5	35.0
P10CH10	56.0	7.0	0.0	7.0	35.0
T5CH5	63.0	0.0	3.5	3.5	35.0
T10CH10	56.0	0.0	7.0	7.0	35.0

The research of consistency was done by mini-slump cone test [28]. Every time, paste was prepared and filled into the cone with few layers to avoid the air bubbles. The cone was lifted with care and the sample was allowed to spread on the glass table flow. The flow diameter (mini-slump flow) and height sample (H) after flow were measured. The arithmetic mean of four measurements was given the final mini-slump cone.

The rheological measurements were carried out using Discovery HR-1 hybrid rheometer (TA Instruments) in a Peltier Concentric Cylinder system with a DIN rotor according to [29]. The standard gap for the DIN cylinder system (5.917 mm) was employed. The same procedure was maintained for the preparation and testing of all samples. After manual mixing of

the dry ingredients with water (1 min), the sample was immediately located into the cylinder for testing. The measurement was started by a 60 s preshear at 50 s⁻¹ followed by 60 s of resting time in order to re-homogenize the sample and to eliminate its shear history. The preshear started 3 minutes after the start of mixing. Then the shear rate increased and decreased in a range from 0 to 100 s⁻¹ through 30 steps with 15 s of measuring time at each shear rate. Flow curves were measured after 5 and 30 minutes from the start of mixing the materials. Yield stress (τ_0), consistency coefficient (K) and fluidity index (n) were calculated from the decreasing branch of the flow curve using the Herschel-Bulkley model [30]:

$$\tau = \tau_0 + K \cdot \dot{\gamma}^n \quad (1)$$

where: τ – shear stress [Pa]; τ_0 – yield stress [Pa]; K – consistency coefficient (comparable to plastic viscosity) [Pa·s]; $\dot{\gamma}$ – share rate [s⁻¹]; n – fluidity index.

Thixotropy of the pastes was determined by the TRIOS software as a hysteresis area between the flow curves. During preparation and during consistency and rheological tests, the temperature in the laboratory was kept at 20°C ±2°C. The water/binder ratio was constant for all pastes in both research.

3. TEST RESULTS AND DISCUSSION

The results of consistency measurements for all pastes are shown in Table 4 and in Figure 1.

Table 4. Consistency results of the tested pastes

Symbol of paste	Consistency		
	Mini-slump cone [mm]	Standard deviation [mm]	H [mm]
C	61.3	1.3	14.5
P10	41.7	1.0	22.4
P20	40.5	0.5	26.8
T10	43.5	0.4	20.1
T20	43.1	0.2	21.4
CH10	46.1	0.5	18.2
CH20	42.2	0.5	22.1
P5CH5	41.4	0.3	22.2
P10CH10	42.0	0.4	21.6
T5CH5	40.1	0.3	27.7
T10CH10	41.2	0.5	22.1

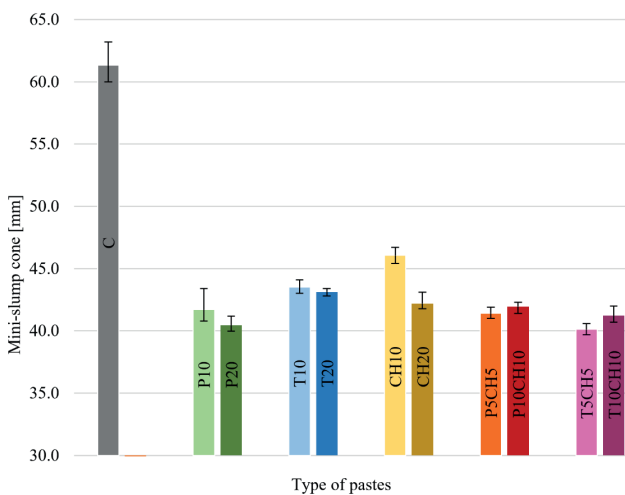


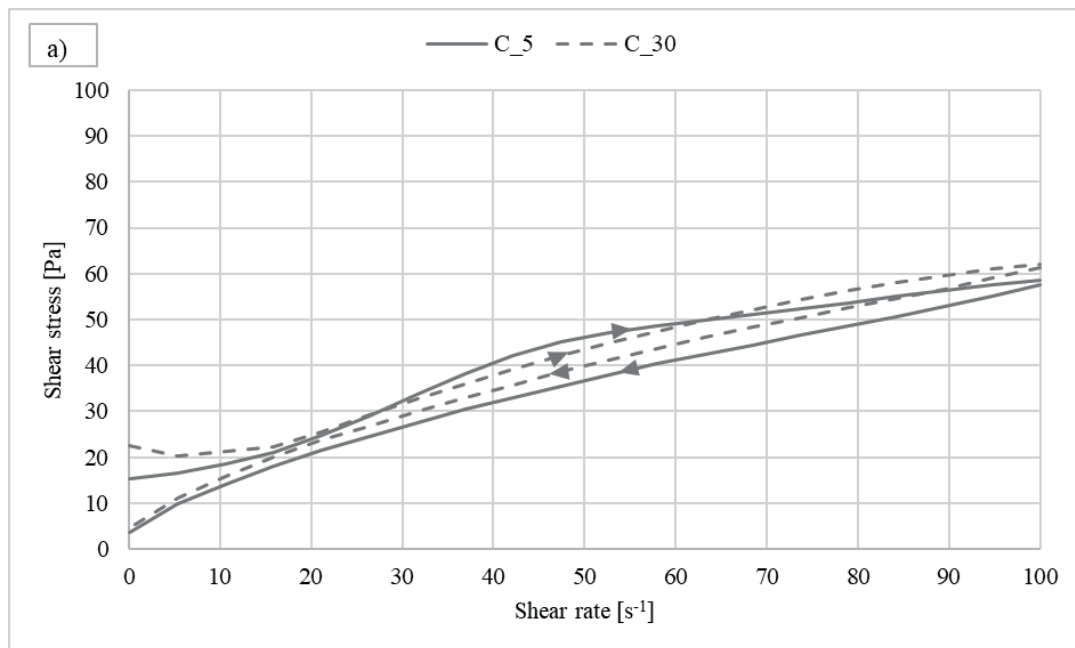
Fig. 1. Mini-slump flow of pastes

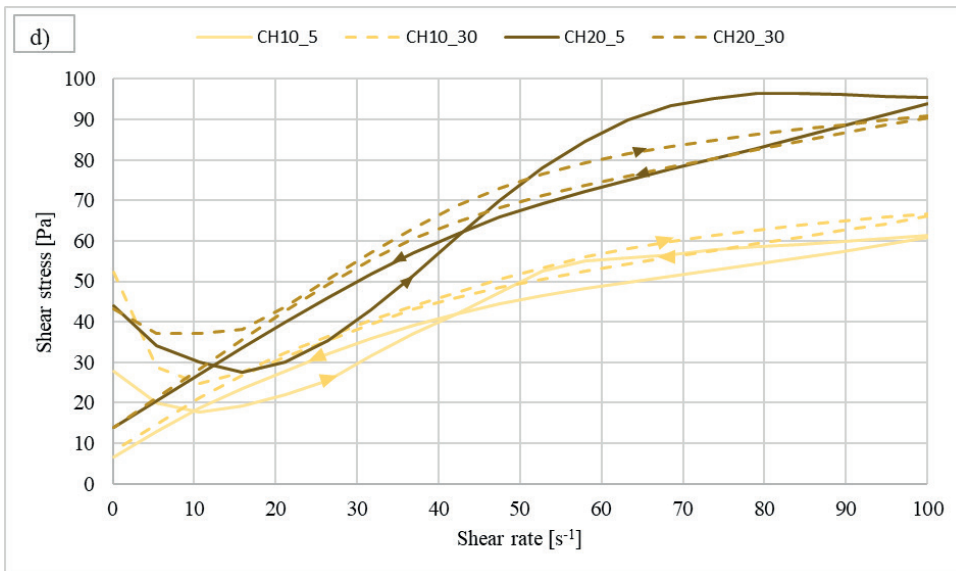
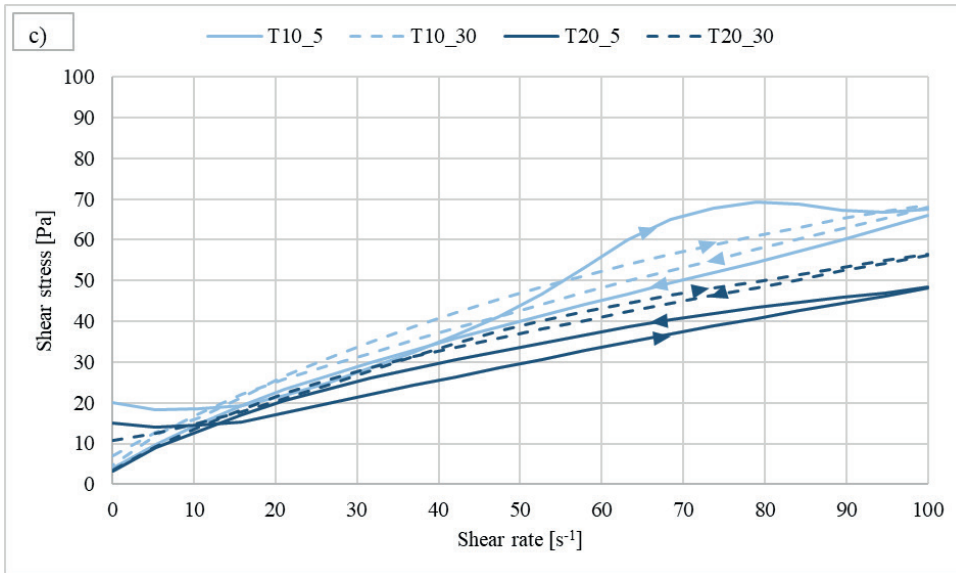
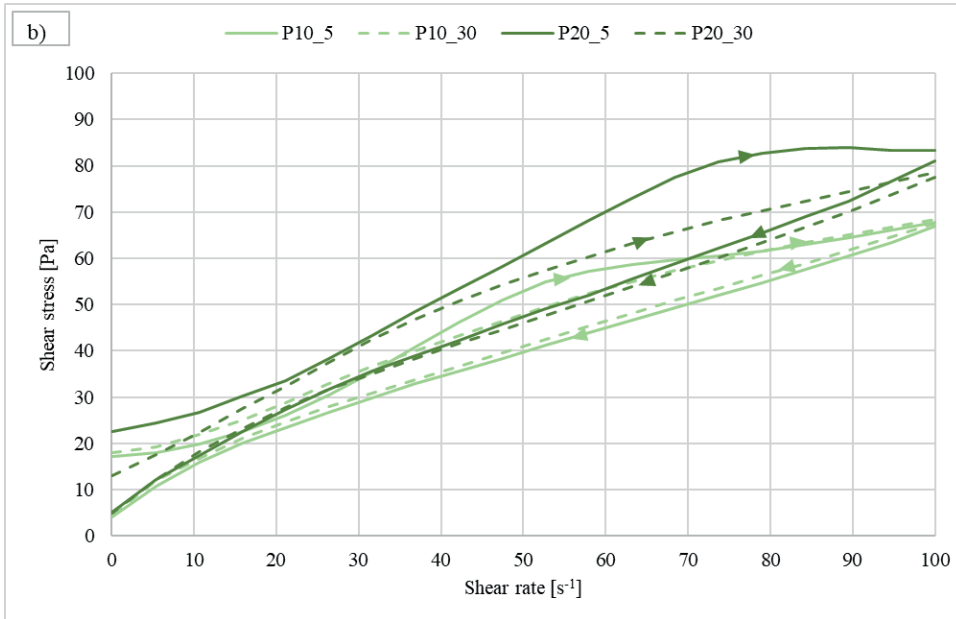
The biggest mini-slump flow was achieved for paste without additions (C) and it was equal 61.3 mm. All modified pastes had smallest consistency compared to reference sample, about 25-35% smaller flow than C paste. Paste contained combination of trass and chalcedonite powder in the amount of 5% of each of them (T5CH5) had the smallest flow (40.1 mm). In the case of replacing cement with one of the additions, the greater its amount, the smaller the flow was recorded. The greatest change in consistency was observed in pastes containing chalcedonite powder, which was related to the smallest grain size of this additive (especially the content of particles ≤5 mm). Increasing its share from 10% to 20% resulted in a reduction in flow by 39 mm (comparing the flow of CH10 and CH20 pastes). The influence of the amount of trass on paste flow was negligible. A different effect was noted when a combination of two additions was used. Increasing the total amount of additions from 10% to 20% resulted in even a slight plasticization of the pastes (wider spread). The height of samples (H) in consistency research was bigger for all pastes compared to C sample. The increase in the amount of additive resulted in an increase in the H parameter. The increase in the amount of combine additives resulted in a decrease in the H parameter (comparing pastes P5CHP with P10CH10 and T5CH5 with T10CH10). It can be concluded that the effect of one additive was thickening, but replacing part of the pumice or trass with chalcedonite powder gave a liquefying effect.

The results of determining rheological parameters of pastes are presented in Table 5. The flow curves of cement pastes without additions and the flow curves of cement pastes with additions are shown in Figure 2 (measurements done after 5 and 30 minutes). As can be seen from the values of the determination of R^2 (Table 5), the results of rheological parameters described by the Herschel-Bulkley model characterized by a high fit (R^2 close to 1 value). In this model, the highest values of yield stress (τ_0) was obtained for the pastes modified with 20% of chalcedonite powder. The consistency coefficient (K), which is a measure of the viscosity of pastes had the highest values for the samples with chalcedonite powder, which means that these pastes had relatively the highest viscosity. Pastes containing both pumice and trass were characterized by a lower K parameter than pastes without the additive. As the date presented in Table 5 show that replacement cement by chalcedonite powder caused increase in pseudoplasticity (decrease of n parameter), opposite

Table 5. Rheological measurements of pastes

Series of paste	Time of measurements after mixing [min]	τ_0 [Pa]	K [Pa·s]	n [-]	R^2 [-]	Thixotropy [Pa·s ⁻¹]
C	5	2.94	2.26	0.69	0.9997	592
	30	3.71	2.51	0.68	0.9998	390
P10	5	4.50	1.74	0.77	0.9989	739
	30	4.90	1.91	0.75	0.9993	564
P20	5	5.38	1.85	0.80	0.9987	1199
	30	5.22	2.07	0.77	0.9984	679
T10	5	3.66	1.93	0.75	0.9994	606
	30	4.33	2.41	0.71	0.9998	244
T20	5	1.36	3.20	0.59	0.9979	-198
	30	1.85	2.91	0.64	0.9989	112
CH10	5	3.04	5.11	0.53	0.9922	200
	30	4.18	5.58	0.53	0.9929	33
CH20	5	9.48	4.71	0.63	0.9936	515
	30	7.82	7.03	0.54	0.9863	495
P5CH5	5	2.11	3.46	0.56	0.9988	-259
	30	2.77	3.42	0.58	0.9990	102
P10CH10	5	4.78	2.06	0.84	0.9995	-1638
	30	4.49	3.45	0.69	0.9994	463
T5CH5	5	4.05	1.77	0.80	0.9995	-1025
	30	3.14	3.22	0.64	0.9991	310
T10CH10	5	4.44	3.20	0.67	0.9990	-1021
	30	2.54	4.61	0.59	0.9958	182





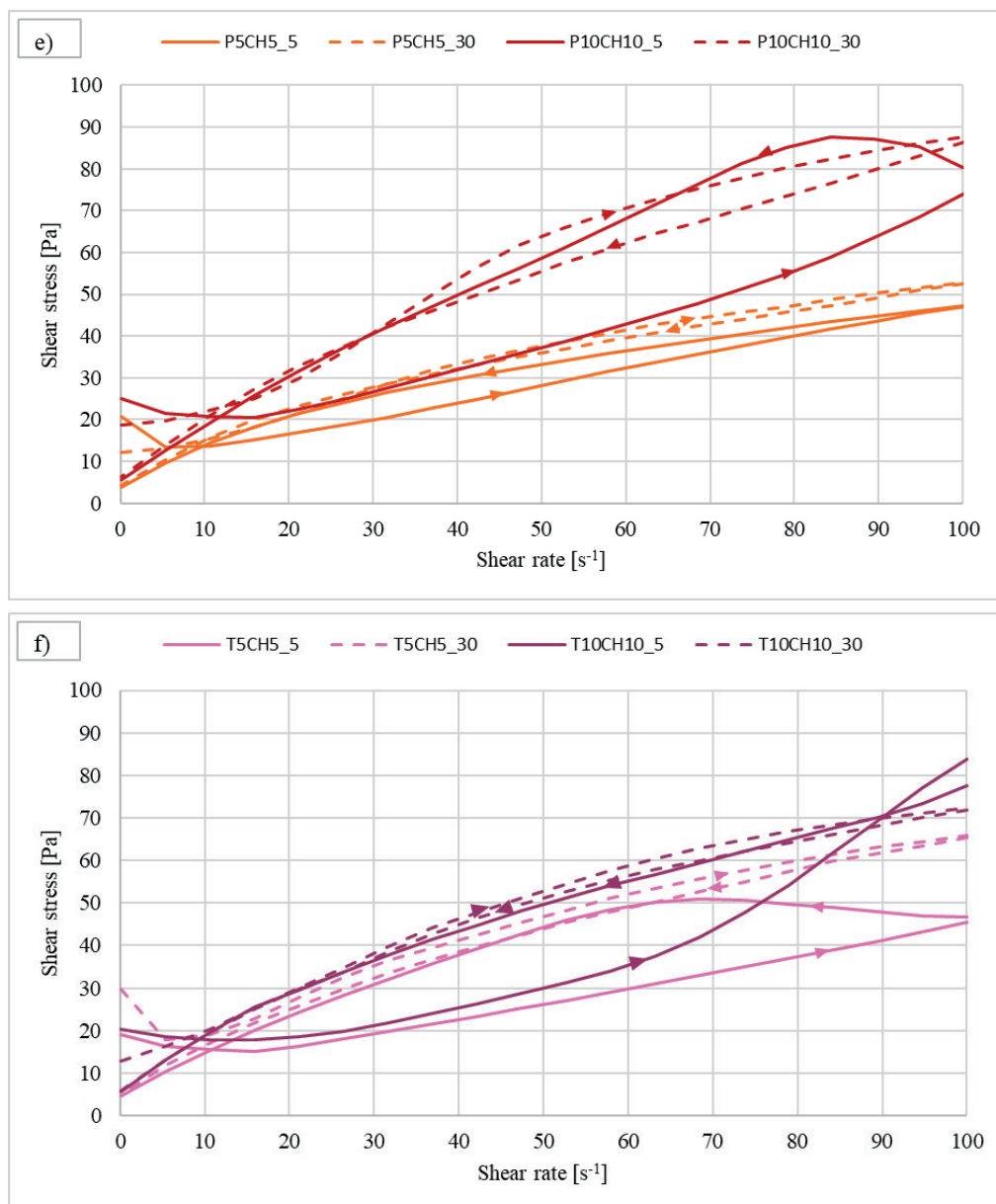


Fig. 2. Flow curves for all tested pastes

to an action of pumice (decrease in pseudoplasticity). This phenomenon was visible regardless of the amount of additive used. In other cases, the effect was varied. For cement pastes with one type of addition, a deterioration of thixotropic behavior over time (decrease in thixotropy values) was observed, which is due to ongoing hydration and pozzolanic reactions of the binder forming denser paste structures. The opposite trend was evident for pastes with combined additives when there was a change in behavior from rheopectic to thixotropic over time (an increase in thixotropy values from negative to positive). Apparently, in the initial phase of hydration of pastes with a combination of the addition of chalcedonite with pumice or trass,

cohesive forces between these particles are formed, which are broken over time by hydration and pozzolanic reactions. This idea can also be supported by the opposite trend of yield stress development over time for pastes with a combined addition (a decrease in yield stress due to the interruption of cohesive forces) in contrast to an increase in yield stress for pastes with one type of addition due to the increasing density of ongoing reactions.

The changing of yield stress and consistency coefficient (comparable to plastic viscosity) over time are shown in Table 5 and Figures 3 and 4. Analysis of rheological research results of cement pastes with pumice, trass and chalcedonite powder showed varied

impact of additions on yield stress and consistency coefficient compared to values of these parameters for cement pastes without additions. The addition of pumice to cement resulted in an increase in yield stress and a decrease in paste viscosity (regardless of the amount of addition and time of measurement). It is probably due to the internal structure of this material. On the other hand, cement pastes with chalcedonite powder had higher yield stress and consistency coefficient than reference cement paste due to the very fine particles (with a larger specific surface area) and pseudocrystalline composition of chalcedonite. Suspensions of crystalline substances flow more poorly (have a higher viscosity) compared to suspensions of amorphous substances. Trass in the addition of 10% had a similar effect to pumice; in the addition of 20% there was a decrease in yield stress and an increase in viscosity of pastes. The interaction of the addition of

chalcedonite powder with pumice and chalcedonite powder with trass were varied. Although individual additions of pumice and chalcedonite powder in the amount of 10% increased the yield stress, the combination of 5% pumice and 5% chalcedonite decreased the yield stress of the cement paste. For the other combinations, there was usually an increase in the yield stress of the pastes. The viscosities of pastes with combined additives also varied greatly. The time trend of the viscosity development was, with minor exceptions, increasing. On the basis of the presented curves (Fig. 2) and the results presented on Figures 3 and 4, it was found that the type and the amount of additive(s) influenced not only yield stress and viscosity of pastes prepared from them, but also their rheological stability. Pastes containing 10% pumice and combination of 5% pumice and 5% chalcedonite powder achieved the most stable viscosity over time.

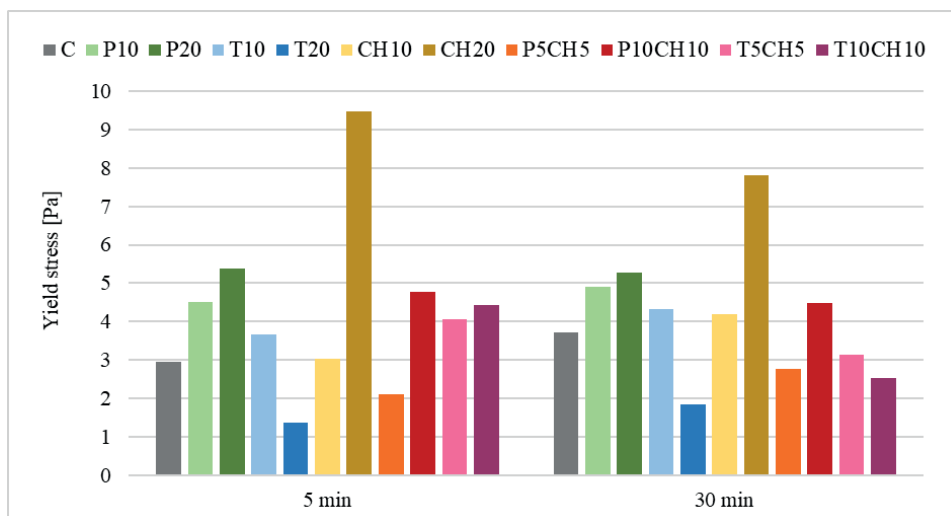


Fig. 3. Yield stress of pastes

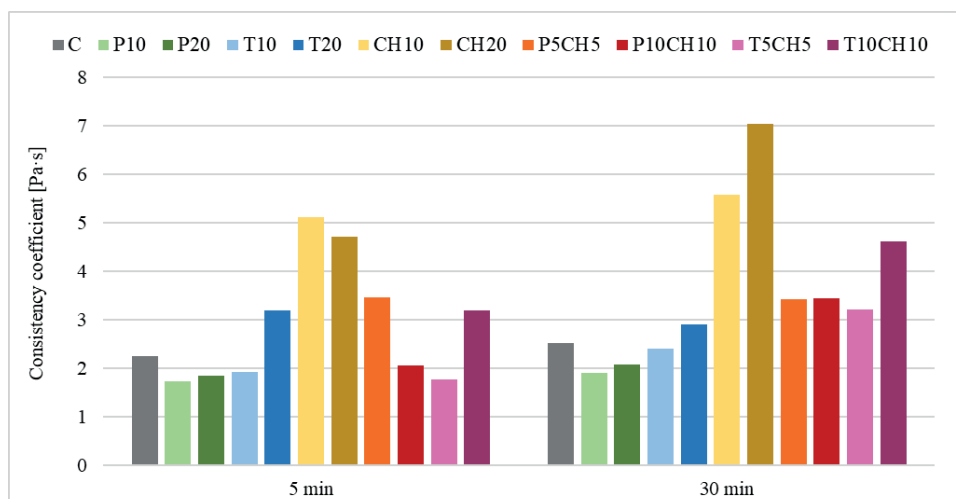


Fig. 4. Consistency coefficient of pastes

4. CONCLUSIONS

All modified pastes were characterized by lower flow than cement paste without the addition(s). The pumice, trass and chalcedonite (added one by one) acted as thickeners.

The influence of the type(s) of additions used and their amounts on the rheological properties of cement pastes is varied.

The rheological properties of two- or three-component pastes depend, among others, on the grain size of the addition(s) used.

Partial replacement of pumice or trass with chalcedonite powder had a differential impact on the consistency and rheological properties of the pastes (depending on the amount of additive). In most cases, chalcedonite powder reduced consistency of

pastes (compared pastes with only pumice or trass), except paste with combination 5% pumice and 5% chalcedonite powder. On the other hand, when comparing the properties of pastes with 10% and 20% of two additives – the increase in the amount of chalcedonite powder has a plasticizing effect, compared to the properties of pastes containing only pumice or trass. Chalcedonite powder reduced yield stress, but increased consistency of pastes with pumice, what was not so noticeable in pastes modified with chalcedonite powder and trass. The use of chalcedonite powder in combination with pumice or trass changes the thixotropic behavior of the cement slurry in the initial phase of hydration to rheopectic. However, over time, these cement slurries become thixotropic.

References

- [1] Baran T.: *The use of waste and industrial by-products and possibilities of reducing CO₂ emission in the cement industry-industrial trials*. Cement Wapno Beton, 25(3), 2021, pp. 169-184, doi: 10.32047/CWB.2021.26.3.1.
- [2] Siemieniuk J., Szatyłowicz E.: *Zmniejszenie emisji CO₂ w procesie produkcji cementu*. Civil and Environmental Engineering, 9, 2018, pp. 81-87, in Polish.
- [3] Środa B.: *Dekarbonizacja w przemyśle cementowym – nowe podejście*, Budownictwo Technologie Architektura, 2, 2019, pp. 70-73, in Polish.
- [4] Lewandowski M., Kądziałowski G.: *Green competencies of cement industry employees in the context of the assumptions of the European Green Deal*, Cement Wapno Beton, 27(4), 2022, pp. 265-274, doi: <https://doi.org/10.32047/CWB.2022.27.4.3>.
- [5] Wiśniewska K.: *Przemysł cementowy – wyzwania na 2022 rok*, Materiały Budowlane, 5, 2022, pp. 74, in Polish.
- [6] Baran T., Ostrowski M., Francuz P.: *Zmniejszenie emisji CO₂ związane z wykorzystaniem ubocznych produktów w przemyśle cementowym*, Konferencja Dni Betonu, Wisła 11-13 październik 2021, in Polish.
- [7] Spychał E., Kotwa A.: *Assessment of the possibility of using chalcedonite powder as a component of mortars*. Structure and Environment, Vol. 14, Nr 4, 2022, pp. 119-125, doi: 10.30540/sae-2022-014.
- [8] Chajec A.: *Granite powder vs. fly ash for the sustainable production of air-cured cementitious mortars*. Materials, 14(5), 1208, 2021, doi: 10.3390/ma14051208.
- [9] Karakurt C., Dumangöz M.: *Rheological and durability properties of self-compacting concrete produced using marble dust and blast furnace slag*. Materials, 15(5):1795, 2022, doi:10.3390/ma15051795.
- [10] Wieczorek M., Pichniarczyk P.: *Properties of cement with the low Portland clinker and the different content of silica fly ash as well granulated blast furnace slag*. Cement Wapno Beton, 27(4), 2022, pp. 285-299, doi: <https://doi.org/10.32047/CWB.2022.27.4.5>.
- [11] Kurdowski W., Baran T.: *Calcined marl as a potential main component of cement*. Cement Wapno Beton, 27(5), 2022, pp. 346-354, doi: <https://doi.org/10.32047/CWB.2022.27.5.4>.
- [12] Mansour M.S., Abadlia M.T., Afalfiz A., Ladaoui W.: *Reologia zapraw i betonów z dodatkami mineralnymi*. Cement Wapno Beton, 5, 2013, pp. 264-270.
- [13] Małaszkiwicz D., Świdorski M.: *Wpływ dodatku metakaolinitu na wybrane właściwości kompozytów cementowych*. Materiały Budowlane, 10, 2016, pp. 25-27, doi: 10.15199/33.2016.10.08, in Polish.
- [14] Czapik P., Cebulski M.: *The properties of cement mortar with natural zeolite and silica fume additions*. Structure and Environment, Vol. 10, No. 2, 2018, pp. 105-113, doi: 10.30540/sae-2018-010.
- [15] Czapik P., Czechowicz M.: *Effects of natural zeolite particle size on the cement paste properties*, Structure and Environment, 9(3), 2017, pp. 180-190.
- [16] Vejmelková E., Keppert M., Ondráček M., Černý R.: *Effect of natural zeolite on the properties of high performance concrete*. Cement Wapno Beton, 3, 2013, pp. 150-159.
- [17] Vyšvařil M., Žižlavský T., Rovnaníková P.: *Fresh state properties of spongilite blended cement pastes*. 17th International Conference: Special Concrete and Composites 2020, doi: 10.1063/5.0041605.

- [18] Abdelaziz M.A., El-Aleem S.A., Menshawy W.M.: *Effect of fine materials in local quarry dusts of limestone and basalt on the properties of Portland cement pastes and mortars*. International Journal of Engineering Research, 3,6, 2014, 1038-1056.
- [19] Szaj P.: *Effect of some mineral supplements on rheological properties of cement slurries*. Prace Naukowe Instytutu Górnictwa Politechniki Warszawskiej, Studia i Materiały, Vol. 134, Nr 41, 2012, pp. 285-294, in Polish.
- [20] Prokopski G., Marchuk V., Huts A.: *Granite dust as a mineral component of a dry cement mortar mixtures*. Archives of Civil Engineering, Vol. 63, Nr 3, 2020, pp. 81-96, doi: 10.24425/ace.2020.134385.
- [21] Sanytsky M., Usherov-Marshak A., Kropyvnytska T., Heviuk I.: *Performance of multicomponent Portland cements containing granulated blast furnace slag, zeolite, and limestone*. Cement Wapno Beton, 25(5), 2020, pp. 416-427, doi: <https://doi.org/10.32047/CWB.2020.25.5.7>.
- [22] Czarnecki S., Chajec A., Malazdrewicz S., Sadowski Ł.: *The prediction of abrasion resistance of mortars modified with granite powder and fly ash using artificial neural networks*, Applied Sciences, 13(6): 4011, 2023, doi: 10.3390/app13064011.
- [23] Kılıç A., Sertabipoğlu Z.: *Effect of heat treatment on pozzolanic activity of volcanic pumice used as cementitious material*. Cement and Concrete Composites, 57, 2015, pp. 128-132, doi: <http://dx.doi.org/10.1016/j.cemconcomp.2014.12.006>.
- [24] Kabay N., Tufekci M.M., Kizilkanat B., Oktay D.: *Properties of concrete with pumice powder and fly ash as cement replacement materials*. Construction and Building Materials, 85, 2015, pp. 1-8, doi: <http://dx.doi.org/10.1016/j.conbuildmat.2015.03.026>.
- [25] Joshaghani A.: *The effect of trass and fly ash in minimizing alkali-carbonate reaction in concrete*. Construction and Building Materials, 150, 2017, pp. 583-590, doi: <http://dx.doi.org/10.1016/j.conbuildmat.2017.06.034>.
- [26] Li J., Che D., Liu Z., Yu L., Ouyang X.: *Effect of basalt powder on hydration, rheology, and strength development of cement paste*. Materials, 15, 8632, doi: <https://doi.org/10.3390/ma15238632>.
- [27] Gołaszewski J., Kostrzanowska A., Ponikiewski T.: *Rheological properties of multicomponent portland cements with addition of calcium fly ashes*. Materiały Budowlane, 5, 2012, pp. 40-43, in Polish.
- [28] Tan Z., Bernal S.A., Provis J.L.: *Reproducible mini-slump test procedure for measuring the yield stress of cementitious pastes*, Materials and Structures, 50, 235, 2017, doi: <https://doi.org/10.1617/s11527-017-1103-x>.
- [29] ASTM D2196-20 Standard of Test Methods for Rheological Properties Non-Newtonian Materials by Rotational Viscometer, Annual Book of ASTM Standards, West Conshohocken, PA, USA, 2020.
- [30] Žižlavský T., Vyšvařil M.: *Effect of natural lightweight aggregate on fresh state properties of lime mortars*. AIP Conference Proceedings 2322, 020018, 2021, doi: 10.1063/5.0041828.

Acknowledgement

The research was financially supported by the program of the Minister of Science and Higher Education under the name: "Regional Initiative of Excellence" in 2019-2022 project number 025/RID/2018/19 financing amount PLN 12.000.000.



THE COMPARATIVE STUDIES OF THE PROPERTIES OF JOINT SEALANTS PRODUCED BY MANUFACTURERS AND IN LABORATORY CONDITIONS WITH THE USE OF HIGHLY MODIFIED BITUMEN

BADANIA PORÓWNAWCZE WŁAŚCIWOŚCI MAS ZALEWOWYCH WYTWARZANYCH PRZEZ PRODUCENTÓW I W WARUNKACH LABORATORYJNYCH Z WYKORZYSTANIEM ASFALTU WYSOKOMODYFIKOWANEGO

JUSTYNA STĘPIEŃ*, MATEUSZ M. IWAŃSKI
Kielce University of Technology, Poland

EVA REMIŠOVÁ, MARTIN DECKÝ, DUŠAN BRILIAK
University of Žilina, Slovakia

Abstract

Joint sealants produced on the basis of modified bitumen are an effective mean for protection of expansion joints on bridges and for repair of cracks in various road surfaces. A comparative study was performed to evaluate seven hot-applied joint sealants obtained commercially and three joint sealants produced in laboratory conditions with different contents of highly modified asphalt binder (40 to 100%). The basic properties of the joint sealants and asphalt binders were evaluated, including penetration, softening point, breaking point and elastic recovery. Additionally, Fourier infrared spectroscopy (FTIR) method was used to evaluate the chemical composition of the asphalt binders. The variability of the basic properties of joint sealants was estimated in the range from -77.1% to 43.6% in relation to the base asphalt binder. It has been established that the addition of crumb rubber, hydrated lime and rapeseed oil may be viable in controlling the parameters of the joint sealants.

Keywords: hot-applied joint sealant, highly modified bitumen, expansion joint, hydrated lime, crumb rubber

Streszczenie

Zalewy szczelin produkowane na bazie asfaltów modyfikowanych są skutecznym rodzajem zabezpieczenia przerw dylatacyjnych na obiektach mostowych oraz naprawy uszkodzeń różnych typów nawierzchni drogowych. Badaniami porównawczymi objęto siedem mas zalewowych stosowanych na gorąco, wytworzonych przez krajowych i zagranicznych producentów, oraz trzy masy zalewowe wytworzone w warunkach laboratoryjnych o różnej zawartości wysokomodyfikowanego lepiszcza asfaltowego (40 do 100%). Ocenie poddano podstawowe cechy lepiszczy asfaltowych oraz parametry wyprodukowanych na ich bazie mas zalewowych, obejmujące: penetrację w 25°C, temperaturę mięknięcia, temperaturę łamliwości Fraassa i nawrót

sprężysty. Dodatkowo, do porównania składu chemicznego lepiszczu asfaltowych wykorzystano metodę spektroskopii fourierowskiej w podczerwieni (FTIR). Oszacowano procentowy zakres zmienności podstawowych właściwości mas zalewowych w relacji do bazowego lepiszczu asfaltowego w granicach od -77,1% do 43,6% w relacji do bazowego lepiszczu asfaltowego. Ustalono, że istotnym regulatorem parametrów mas zalewowych mogą być dodatki odpadów gumowych, wapna hydratyzowanego oraz oleju rzepakowego.

Słowa kluczowe: zalewa szczelin na gorąco, asfalt wysokomodyfikowany, szczelina dylatacyjna, wapno hydratyzowane, odpady gumowe

1. INTRODUCTION

One of the basic requirements for sealing expansion joints is the use of a highly flexible sealant made on the basis of petroleum based bitumen with the addition of elastomeric polymers (such as SBS, crumb rubber), fillers and surface-active substances [1-6]. Cold and hot-applied sealants are a commonly used type of protection of expansion joints on structures with reinforced concrete and steel structures, as well as in asphalt concrete, concrete or epoxy surfaces. Joint sealants are responsible for the transfer of deformations between the expansion joints due to its deformability over a wide range of temperatures. The dimensions of the expansion joint are selected individually for each structure. The bituminous expansion joint is a surface element that not only transmits the load of heavy vehicles' wheels, but also compensates vertical and horizontal deformations caused by the expansion joint's edge movement in the construction e.g. a road bridges [7-9].

The paper concerns a selection of the properties of hot-applied joint sealants, classified as the high-extension type N1 (elastic) or low-extension type N2 (normal), in accordance with the standard EN 14188-1 [10]. The selection of the joint sealant type, in terms of its viscoelastic properties, as well as the method of application should result from the role and function that it will perform during the service life of the road or bridge surface. As construction materials, joint sealants must meet the requirements of the applicable standards and guidelines [2, 10, 11]. The current standard [10] does not introduce material restrictions on the composition of the joint sealants, but it provides a specific set of requirements that should be met by the final product.

Crack sealing with hot-applied sealants based on modified bitumen is also a widely used technology for the surface repairs of the upper layers of road surfaces, made of either asphalt mixtures or cement concrete. Preventing the degradation of road structures requires the immediate and permanent maintenance of their discontinuities, which occur during pavement

service [12]. The properties of applied joint sealants must be adapted to the nature of the job, the location where they will be used in the surface structure, and the effects of external factors [13-15].

Phenomena such as aging, fatigue and thermal stability of joint sealants based on bitumen can cause failures or even secondary cracking. The use of non-modified asphalt binders in crack sealants provides a cheap solution for the maintenance of cracking pavements; however, such formulations are prone to debonding and poor low- or high-temperature performance. Therefore, it is necessary to prepare joint and crack sealants with adequate performance.

Highly modified bitumens are characterized by a large amount (typically 7 to 8 percent) of specialized styrene-butadiene-styrene block copolymers, ensuring their compatibility with the base bitumen. In pavement engineering, various technological solutions are used in the field of asphalt modification, and the use of additives for mineral and asphalt mixtures depends on their purpose in the road surface construction, the environmental conditions, and the pro-ecological requirements [16-20]. Therefore, modified asphalt binders are used to produce and investigate joint and crack sealant [1, 3, 21-25]. Styrene-butadiene-styrene (SBS) and crumb rubber (CR, 10, 15, 20%) have been utilized by Gong et al. [26] to modify sealants with bitumen to overcome the disadvantages of the poor high-temperature and rheological properties of sealants. It has been shown that the SBS/CR-modified asphalt sealant has a greater viscosity and higher temperature deformation resistance.

Gnatenko et al. [27] in their study confirmed that to reduce brittleness and increase the flexibility of joint sealants and mastics at low temperatures, it was necessary to use a plasticizer. On the other hand, improving their performance at high temperatures required the use of thermoplastic elastomers made of SBS, latexes, mineral fillers (5, 10 and 15%), or fine crumb rubbers (3, 5, 15 and 20%), which are similar to those used in road paving asphalt binders [19, 20].

As shown above, joint sealants are complex preparations and given the broad range of base asphalt binders, modifiers, fillers, and other non-soluble additives. So far, no clear guidelines have been developed regarding the material composition and detailed requirements for the properties of individual components of joint sealants.

Joint and crack sealants may be produced in very diverse combinations of components:

- one-component, exclusively of modified or highly modified bitumen;
- two-component with the use of virgin components, produced from asphalt binders and mineral fillers in various proportions;
- multi-component with the use of virgin components (asphalt binders and mineral fillers) and waste materials (crumb rubber, aggregate dusts) in various proportions.

Due to the observed failure modes in asphalt expansion joints [3, 9, 30] and road surface repairs after sealing [12, 24] it is necessary to conduct further research on the properties and composition of joint sealants in terms of their applicability in various climatic conditions and traffic loads.

The lack of conclusive requirements for the components of asphalt-based sealant indicates the need to conduct investigation in this area and to search for additives that are an important regulator of their properties.

The aim of the planned research and analyses was:

- Verification of the possibility of reducing the content of asphalt binder in multi-component hot-applied joint sealant in relation to used in industry products up to 40%.
- Evaluation of the influence of hydrated lime and rapeseed oil as regulators on the variability of the properties of joint sealants.

- Comparison of the basic characteristics of joint sealants produced by manufacturers and in laboratory conditions in relation to the same properties of base bitumen.
- Estimation of the percentage range of variability of the properties of joint sealants in relation to the base asphalt binder.

It has been established that it is possible to regulate selected properties of the joint sealants by changing the chemical composition and proportions of its components (fillers, hydrated lime, rapeseed oil, crumb rubber). It was found that it was difficult to ensure the required standard parameters of joint sealants for the content of asphalt binder below 50%, even when using highly modified bitumen.

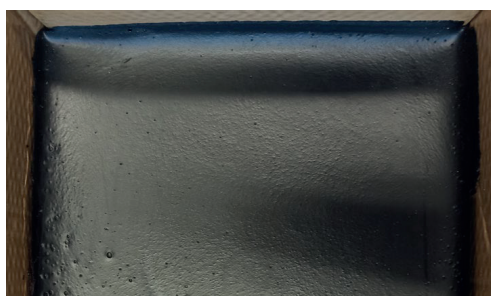
2. MATERIALS AND METHODS

2.1. Materials

2.1.1. Origin of materials

The investigations covered hot-applied joint sealant of various characteristics, obtained commercially (Fig. 1a), as well as produced in laboratory conditions (Figs. 1b, 1c). The sealants produced by commercial manufacturers, were marked with MS symbols (MS1 – MS7), while those produced in laboratory conditions were marked as LS (LS1 – LS3). Seven hot-applied asphalt-based joint sealants were used, obtained from 4 selected domestic and foreign manufacturers. According to the manufacturers, the intended use of the sealants included: sealing cracks, horizontal gaps, expansion joints and technological joints in road surfaces of all traffic load categories. Three joint sealants LS1 – LS3 were produced with the use of new components (bitumen and fillers).

a)



b)



c)



Fig. 1. Photographs of investigated hot-applied joint sealant: a) produced by manufacturer (MS3); b) during manufacturing with homogenizer Unidrive X100 under laboratory conditions [31]; c) in laboratory utensil after homogenization (LS1)

2.1.2. Joint Sealants Produced by Manufacturers

According to the manufacturers' declarations, the joint sealants selected for the investigation complied with the requirements of EN 14188-1 [10] standard for the following types:

- Flexible (high-extension) – type N1 (MS1, MS2, MS4);
- Normal (low-extension) – type N2 (MS3, MS5, MS6, MS7).

Selected declared properties are presented in Table 1.

On the basis of the solvent extraction of the MS1 – MS7 sealants and subsequent EDX spectroscopy (Quanta Feg 250 SEM and EDS spectrum), their material and chemical composition was identified [36]. It was found that among the investigated sealants there are various compositions:

- one-component, exclusively of highly modified bitumen (MS1);
- two-component, constituting a composition of asphalt binders and mineral fillers (MS7);
- multi-component with the use of new components (asphalt binders, mineral fillers) and waste materials (rubber crumbs) in various proportions (MS2 – MS6).

The occurrence of rubber particles of different size, origin and method of production (cryogenic and mechanical method) in investigated joint sealants (MS2 – MS6) with different content percentages (8.7-19.3%) was found. Selected images of the crumb rubber used in MS3, MS5 and MS6 are presented in Figure 2.

Table 1. Selected characteristics of joint sealant declared by manufacturers

Material Properties	Characteristics of Investigated Joint Sealant and Declaration by Manufacturers							Testing Method
	MS1	MS2	MS3	MS4	MS5	MS6	MS7	
Type of hot-applied joint sealant	N1	N1	N2	N1	N2	N2	N2	EN 14188-1 [10]
Density at +25°C, in Mg/m ³	No dec.*	1.15 ±0.05	1.12	1.15 ±0.05	1.2	No dec.	1.2 ±0.1	EN 13880-1 [32]
Softening point, ring and ball, in °C	No dec.	98 ±8	≥85	98 ±8	102	No dec.	≥85	EN 1427 [33]
Cone penetration at 25°C, in 0.1 mm	40 to 130	60 ±10	40 to 100	60 ±10	54	40 to 100	40 to 100	EN 13880-2 [34]
Penetration and recovery at +25°C, in%	≥60	65 ±5	<60	65 ±5	59	≤60	≤60	EN 13880-3 [35]

* No dec. — No declaration by manufacturer

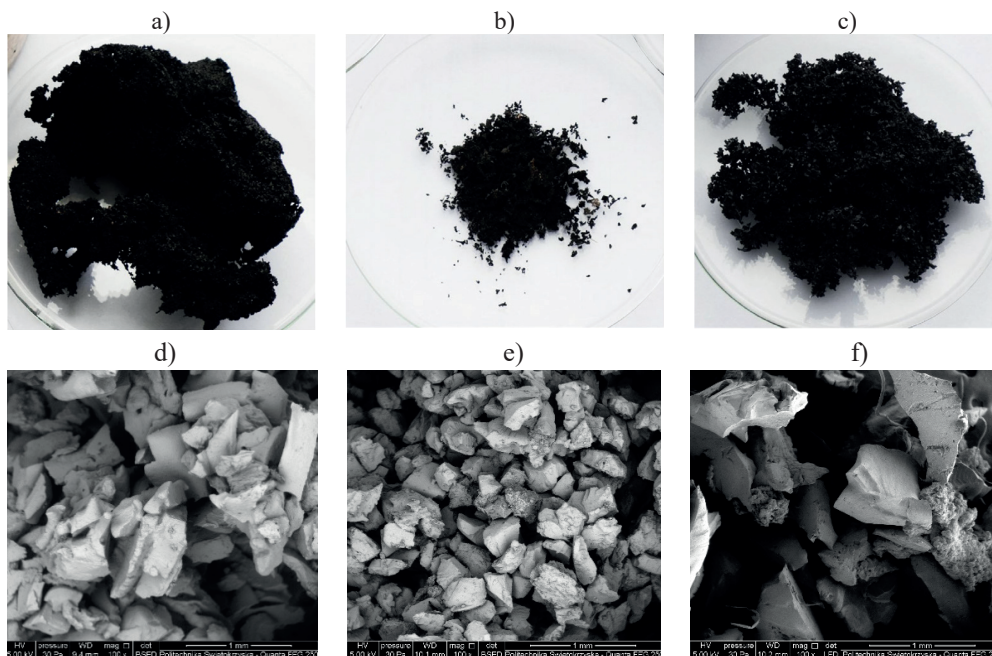


Fig. 2. Images of the rubber crumbs recovered from the selected joint sealants: a), b), c) MS3, MS5, MS6 – without magnification; d), e), f) MS3, MS5, MS6 – magnification × 100 by scanning electron microscope

The variation in the content of the rubber waste components, as well as the method of producing crumb rubber, significantly affects the physicochemical properties of rubber–asphalt binders [37]. Rubber crumbs were utilized for modifying the asphalt-based sealants in order to obtain greater viscosity and higher temperature deformation resistance. The use of rubber also increases the material's resistance to low temperatures. Therefore, it should be assumed that it is an important regulator of the properties of joint sealant.

Mineral filler that passed through a 0.063 mm sieve has been identified in different contents (10.6 to 50.2%) in the joint sealants from manufacturers (MS2 –MS7). The analysis of the chemical composition with the use of EDX spectroscopy showed the presence of calcium or silicon with the highest percentage in the investigated materials.

2.1.3. Joint Sealants Produced under Laboratory Conditions

The following materials were used in the production of the joint sealants LS1 – LS3 under laboratory conditions:

- highly modified bitumen 65/105-80 according to PN-EN 14023:2011/Ap1:2014-04 (National Annex) [38];
- lime filler;
- hydrated lime (calcium hydroxide).

The highly modified bitumen 65/105-80 is characterized by a high content of SBS polymer in the amount of about 7.0-7.5% m/m. Such significant amount of this component results in the formation of a continuous polymer network in the binder structure, which is not present in typical polymer bitumen. This improves the properties of the asphalt at high and low temperatures. Its main advantages include increased resistance to cracking, permanent deformations and fatigue. These features contribute to the applicability of the 65/105-80 bitumen as the basic component for flexible hot-applied joint sealants.

The most important properties of 65/105-80 asphalt binder, declared by its manufacturer, are presented in Table 2.

In order to ensure the high quality of the joint sealant, a mixed filler was used in the study, which contained hydrated lime (calcium hydroxide) in the amounts of 10, 20 and 30% interchangeably with lime filler.

Three types of joint sealant were produced, differing in the content of mineral filler used in the amounts of 20, 40 and 60%.

Table 2. Selected characteristics of the highly modified asphalt binder (65/105-80) declared by manufacturer

Property of asphalt binder	Needle penetration at 25°C	Softening point, ring, and ball	Fraass breaking point	Elastic recovery at 25°C
Unit	0.1 mm	°C	°C	%
Test method	EN 1426 [39]	EN 1427 [33]	EN 12593 [40]	EN 13398 [41]
Declared value	65 to 105	≥ 80	< -18	≥ 80

2.2. Research Methodology

The comparative analyses covered the properties of ten joint sealants produced by commercial manufacturers (MS) and produced in laboratory conditions (LS) with varying content of asphalt binder (40 to 100%) and other components. Previous investigation in this area [36, 39] has been compared, verified and extended.

The testing methodologies included the solvent extraction of the investigated joint sealant MS1 – MS7 with the use of tetrachloroethylene as a solvent:

- The determination of the soluble binder content (EN 12697-1).
- The recovery of soluble bitumen with the use of a rotary evaporator (EN 12697-3+A1).

Distillation conditions used in the testing methodologies for recovery of soluble bitumen were as follows:

- Solvent: Tetrachloroethylene,
- Boiling Point: 121°C,
- Temperature (First Phase): 110°C,
- Pressure (First Phase): 40 kPa,
- Temperature (Second Phase): 110°C,
- Pressure (Second Phase): 40 kPa,
- Extra Temperature: 180°C.

Samples of LS1 – LS3 were prepared in laboratory conditions. The mineral sample filler was dried at 105°C for 24 h in order to eliminate the moisture it contained. The filler was then dosed in the required proportion into the asphalt binder and mixed at 500 rpm for 30 minutes at a constant temperature of 160°C.

Table 3 presents the basic compositions of the analysed joint sealants.

Each of the LS sealants was produced in laboratory conditions in three variants with different content of hydrated lime in the mineral filler, i.e.:

- 0% (LS1/0, LS2/0, LS3/0),
- 10% (LS1/10, LS2/10, LS3/10),
- 20% (LS1/20, LS2/20, LS3/20),
- 30% (LS1/30, LS2/30, LS3/30).

Table 3. Compositions of the investigated joint sealants

Component materials of joint sealant	Mass share of components in sealant (%)									
	MS1	MS2	MS3	MS4	MS5	MS6	MS7	LS1	LS2	LS3
Soluble asphalt binder (MS sealant)/ Asphalt binder (LS sealant)	100	71.3	59.0	69.8	70.7	72.8	49.8	80.0	60.0	40.0
Mineral filler (≤ 0.063 mm)	0	14.2	21.7	15.6	10.6	18.5	50.2	20.0	40.0	60.0
Mineral and rubber dust (> 0.063 mm; ≤ 0.19 mm)	0	5.5	12.4	4.1	3.9	0	0	0	0	0
Rubber powder/crumbs (> 0.19 mm)	0	9.0	6.9	10.5	14.8	8.7	0	0	0	0
Total	100	100	100	100	100	100	100	100	100	100

The testing methodologies included:

- Fourier transform infrared spectroscopy (FTIR) using the attenuated total reflectance (ATR-FTIR) method for comparative analyses of asphalt binders used for the production of joint sealants;
- Basic properties of the joint sealant and (soluble) asphalt binder:
 - Needle penetration at 25°C acc. EN 1426 [39],
 - Softening point, ring, and ball acc. EN 1427 [33],
 - Fraass breaking point acc. EN 12593 [40],
 - Elastic recovery at 25°C acc. EN 13398 [41].

In order to determine the range of variability of the basic properties of joint sealants in relation to the base asphalt binder, the percentage differences in the values of individual parameters were determined.

3. RESULTS AND DISCUSSION

3.1. Comparative analyses of asphalt binders used in joint sealants

3.1.1. Conventional properties of asphalt binder used in joint sealants

The comparative evaluations of the penetration at 25°C, the softening point, the Fraass breaking point, and the elastic recovery were performed. Table 4 shows the test results of the asphalt binders used in investigated joint sealants.

The analysis of the results in Table 4 shows that the asphalt binders extracted from the MS1 – MS7 joint sealants did not relate clearly to the types provided in the national annexes (PL) of EN 12591 [42] and EN 14023 [38], which are used for paving asphalt binders. This result may have been affected by the influence of the modification of the varying content of crumb rubber or other substances.

The results of the elastic recovery test at 25°C in the case of sealants MS1, MS2 and MS3 – MS7 indicated a very high rate of elastomeric modification similar to that seen in the highly modified bitumens produced in Poland according to the national annex of the PN-EN 14023 standard [38]. The MS3 sample failed before the end of the test but showed an almost immediate return to its original shape. The needle penetration tests indicated significant variability in the consistency of the asphalt binders (58.6 to 136.3 × 0.1 mm). All the analysed binders are characterized by high resistance to low-temperature cracking, expressed by the Fraass breaking point parameter (approx. -25°C). Asphalt binders used in MS1, MS2, MS3 – MS6 sealants had similar average values of softening point, ranging from 95.3°C to 101.4°C. Slightly lower values were found in binders recovered from the MS3 sealants (81.3°C) and those used in LS1 – LS3 (89.0°C). The lowest average softening point was obtained for the MS7 joint sealant (63.1°C).

On the basis of the analysis of the properties of highly modified bitumen 65/105-80, used in LS1 – LS3 joint sealants, it can be concluded that it is characterized by very favorable parameters, which recommend its use as a basic component for flexible hot-applied joint sealant. The high elasticity of the binder ensures the proper operation of the elastic joint sealants, allowing for the transmission of the significant deformations and strains caused by both vehicle traffic and climatic factors. Excellent low-temperature and high-temperature properties will ensure the required durability of the joint sealant, which is very important in the case of making expansion joints and sealing gaps in the surface.

Table 4. Test results of asphalt binders used in investigated joint and crack sealants

Joint sealant	Property of asphalt binders (mean value ± standard deviation)			
	Needle penetration at 25°C	Softening point, ring, and ball	Fraass breaking point	Elastic recovery at 25°C
Unit	0.1 mm	°C	°C	%
Test method	EN 1426 [39]	EN 1427 [33]	EN 12593 [40]	EN 13398 [41]
Valid N	5	4	3	2
MS1	58.6 ±3.1	95.3 ±0.7	<−25.0	99.0 ±0.5
MS2	136.3 ±3.7	96.8 ±0.7	−24.7 ±0.6	100.0 ±0.0
MS3	79.6 ±2.2	81.3 ±0.4	<−25.0	133 mm; 179 mm*
MS4	134.2 ±2.8	98.5 ±1.0	<−25.0	100.0 ±0.7
MS5	63.0 ±1.9	101.4 ±1.8	−24.7 ±0.6	96.0 ±0.0
MS6	102.2 ±4.1	96.2 ±3.3	<−25.0	97.0 ±1.4
MS7	93.7 ±0.9	63.1 ±0.3	<−25.0	98.0 ±2.8
LS1 – LS3	73.0 ±2.1	89.0 ±0.5	−25.0 ±0.6	95.0 ±0.0

* The sample failed before the end of test.

3.1.2. The chemical analyses of the asphalt binder used in joint sealants with the use of FTIR method

The extracted soluble asphalt binders from MS2 – MS7 sealants and highly modified bitumens used in MS1 and LS1 – LS3 sealants were evaluated using FTIR spectra.

Figure 3 presents the 1900 cm⁻¹ to 500 cm⁻¹ absorption bands of the overlaid spectra of the extracted asphalt binder (MS2 – MS7) and modified bitumen (MS1, LS1 – LS3).

The FTIR spectrum for highly modified bitumen 65/105-80 used in LS1 – LS3 sealants is most similar to the asphalt binders used in sealants: MS1, MS2, MS4 and MS5. This indicates the presence of similar chemical compounds in them. Three of these materials (MS1, MS2, MS4) were extracted from the hot-applied joint sealants, classified as high-extension type N1 (flexible), in accordance with the standard [10].

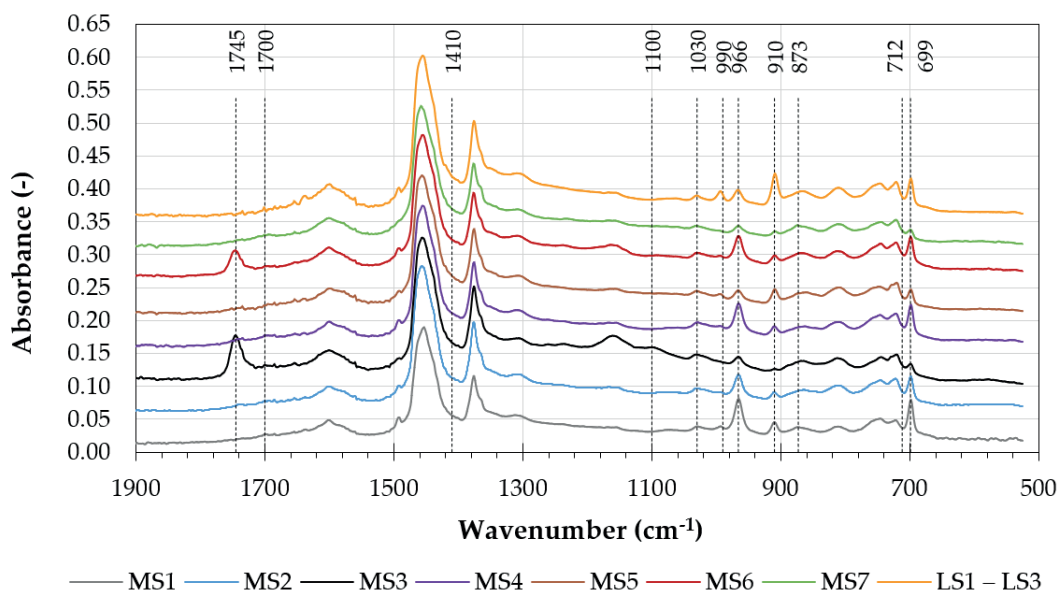


Fig. 3. FTIR spectra of the asphalt binders used in investigated joint sealants

All the FTIR spectra of the extracted asphalt binders and new highly modified bitumen show low, comparable peak heights in the 1700 cm⁻¹ and 1030 cm⁻¹ wavenumber regions associated with carbonyl and sulfoxide compounds, indicating that they were not exposed to a significant amount of oxidation.

All of the bitumen binders exhibited significant peaks at 966 cm⁻¹, indicating the presence of butadiene structures. Clear peaks at 990 cm⁻¹ and 910 cm⁻¹, which are characteristic of vinyl groups, and at 699 cm⁻¹, which is characteristic of styrene structures, have been identified in most binders (except MS7). These responses indicate the presence of styrene-butadiene rubber in the samples of the tested soluble material. Additionally, the asphalt binder extracted from the MS3 and MS6 joint sealants registered prominent peaks at the 1745 cm⁻¹ wavenumber, which is typically seen in bio-oil derivatives (e.g., fatty acid methyl esters) and may correspond to the stretching of the -C=O in ester

functional groups. The MS3 and MS6 bitumens were used in hot-applied joint sealants, classified as low-extension type N2 (normal), in accordance with the standard EN 14188-1 [10].

The above confirms the correct choice of 65/105-80 bitumen for the production of joint sealant with the same properties and application as for the N1 type with high-extension (flexible).

3.2. Comparative analyses of basic properties of joint sealants in relations to the base asphalt binder

3.2.1. The results of basic properties of joint sealants in relations to the base asphalt binder

The evaluations of the penetration at 25°C, the softening point, the Fraass breaking point, and the elastic recovery were performed to measure the effects of different types and compositions of joint sealants on their basic properties. Table 5 presents the results obtained for the investigated joint sealants.

Table 5. Test results of investigated joint sealants

Joint and crack sealant	Property of joint sealant (mean value ± standard deviation)			
	Needle penetration at 25°C	Softening point, ring, and ball	Fraass breaking point	Elastic recovery at 25°C
Unit	0.1 mm	°C	°C	%
Test method	EN 1426 [39]	EN 1427 [33]	EN 12593 [40]	EN 13398 [41]
Valid N	5	4	3	2
MS1	58.6 ± 3.1	95.3 ± 0.7	< -25.0	99.0 ± 0.5
MS2	69.5 ± 1.6	100.3 ± 0.4	< -25.0	96.0 ± 0.7
MS3	36.2 ± 2.5	108.9 ± 0.7	-24.3 ± 0.6	62.0 mm; 48.0 mm*
MS4	65.5 ± 0.9	109.1 ± 0.6	< -25.0	98.0 ± 0.0
MS5	46.3 ± 1.8	104.8 ± 0.4	-21.3 ± 1.5	94.0 ± 0.0
MS6	56.9 ± 5.7	103.2 ± 3.8	< -25.0	97.0 ± 0.0
MS7	78.3 ± 1.6	86.4 ± 1.1	< -25.0	91.0 ± 0.0
LS1/0	66.5 ± 3.0	85.75 ± 0.9	-22 ± 1.3	-
LS1/10	64.86 ± 2.9	87.02 ± 1.0	-21 ± 1.2	94.0 ± 0.5
LS1/10_oil	104.80 ± 1.2	84.82 ± 1.1	-23 ± 1.1	97.5 ± 0.0
LS1/20	63.33 ± 3.0	87.45 ± 1.1	-19 ± 0.6	-
LS1/30	62.0 ± 3.1	88.85 ± 1.2	-18 ± 0.8	-
LS2/0	47.5 ± 1.2	85.9 ± 1.1	-20 ± 1.1	-
LS2/10	46.0 ± 1.5	87.49 ± 1.2	-20 ± 1.4	-
LS2/20	43.25 ± 1.4	88.58 ± 0.9	-18 ± 0.7	-
LS2/30	40.0 ± 1.3	90.46 ± 0.7	-18 ± 0.6	-
LS3/0	21.0 ± 1.1	92.98 ± 1	-19 ± 1.0	-
LS3/10	19.5 ± 0.9	95.26 ± 1.1	-18 ± 0.7	-
LS3/20	17.67 ± 1.2	96.65 ± 0.9	-17 ± 0.4	-
LS3/30	16.75 ± 1.2	97.99 ± 1.1	-17 ± 0.3	-

* The sample failed before the end of test

According to standard [10], the minimum softening point for joint sealants is 85°C.

In the study, needle penetration and elastic recovery were used to assess the characteristics of joint sealant. The applicable standard [10] does not specify the requirements for these tests, but this characteristic was relied on because the purpose of the tests was to compare the same properties of the base bitumen and the joint sealants. For sealants, the required standard test is cone penetration, which should be 40 to 130 × 0.1 mm for the N1 type of sealant and 40 to 100 × 0.1 mm for the N2 sealant type. Elastic recovery is an important parameter that determines the elastic properties of the tested asphalt binder.

The Fraass breaking point parameter is not required according to standard [10], but it is still valuable for the assessment of the elasticity of the tested material at low temperature. Conventional asphalt bridge expansion joints used in low-temperature regions generally show precocious cracking (within the first 2 years) [3]. The manufacturer of sealant MS7 declared compliance with the requirements of the EN 12593 [40] standard with regard to the Fraass breaking point by providing a value of $\leq -30^{\circ}\text{C}$.

On the basis of the analysis of the test results for the LS1 – LS3 joint sealant (Table 5), it can be concluded that the amount of limestone filler has a significant impact on the quality of the sealant, apart from the content of highly modified bitumen 65/105-80.

The use of 60% limestone filler in LS1 – LS3 joint sealants results in an adversely large increase in its brittleness temperature according to Fraass, a significant decrease in needle penetration and an increase in the softening point. The addition of hydrated lime has also a significant impact on the analyzed parameters of the sealants. As its content in the filler increases, the sealant stiffens and is characterized by a decrease in penetration at 25°C and an increase in the softening point. However, with an increase in the concentration of hydrated lime, there is an increase in the brittleness temperature according to Fraass, which is an unfavorable phenomenon, especially with its content of 30%. This type of joint sealants will be very stiff in the pavement working conditions, which in turn will cause its cracking and loss of durability. Lower content of lime filler in the joint sealants has a positive effect on its test parameters. Analyzing the results of the research, it can be concluded that hydrated lime can act as a regulator of the properties of the joint sealants, with its content up to 20% in the filler. The results of the

determinations for the LS1 – LS3 sealants also show that the binder content should not be less than 60% during the production of the sealant. A lower binder content has been used in the MS7 sealant produced by the commercial manufacturer, however, it is a hot-applied sealant, classified as low-extension type N2 (normal), in accordance with the standard EN 14188-1 [10], for which lower requirements are imposed.

The joint sealant containing 80% of highly modified bitumen and 20% mixed filler containing 90% limestone powder and 10% hydrated lime (LS1/10) was qualified for the next stage of the investigating. The sealant with such a composition is characterized by the best parameters among all those performed in the first stage of testing. In order to better understand its properties, an elastic recovery test was also performed.

An attempt was also made to reduce the cracking temperature according to Fraass breaking point with the addition of rapeseed oil in the amount of 3% in relation to the total weight. In this way, a new mixture was obtained, which was subjected to the same tests as the LS1/10 joint sealant without additives, namely penetration, softening point, Fraass breaking point, and elastic recovery. The new sealant was marked with the symbol LS1/10_oil.

The properties of joint sealants in relation to the parameters of the base asphalt binder were presented in Figures 4-7.

For the majority of sealants produced in laboratory conditions (LS1 – LS2) worse low-temperature properties were obtained (higher temperatures according to Fraass) than sealants from manufacturers (MS1 – MS7). The differences were up to 8°C. Unfavorable penetration properties (mean values in the range from 16.8 to 21.0 × 0.1 mm) were obtained for the LS3 sealant.

The penetration and softening point tests indicated that the MS3 sealant was the hardest in consistency from sealants produced by manufacturers, while MS7 was the most susceptible to high temperatures. Among the joint sealants developed in the laboratory, LS3 had the hardest consistency for all 4 variants of hydrated lime content.

For MS3 and LS3, the observed needle penetration results were less than 40 × 0.1 mm, indicating that the cone penetration required by standard [10] was also not guaranteed.

The obtained joint sealants were characterized by high elasticity, as evidenced by the elastic recovery of almost 100% (Fig. 7, Table 5). This means that they

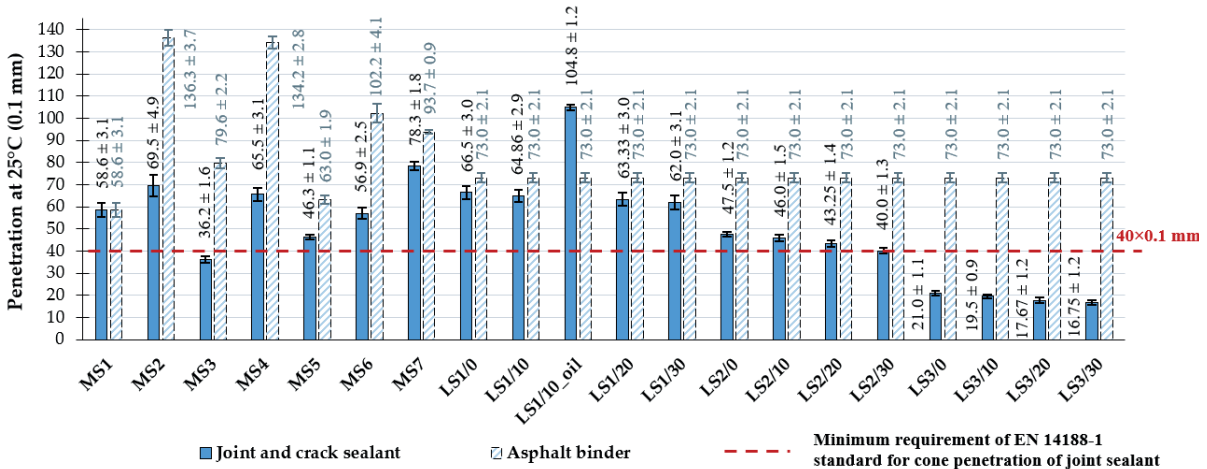


Fig. 4. Results of needle penetration at 25°C of the investigated joint sealants and asphalt binders used in sealants (mean value ± standard deviation)

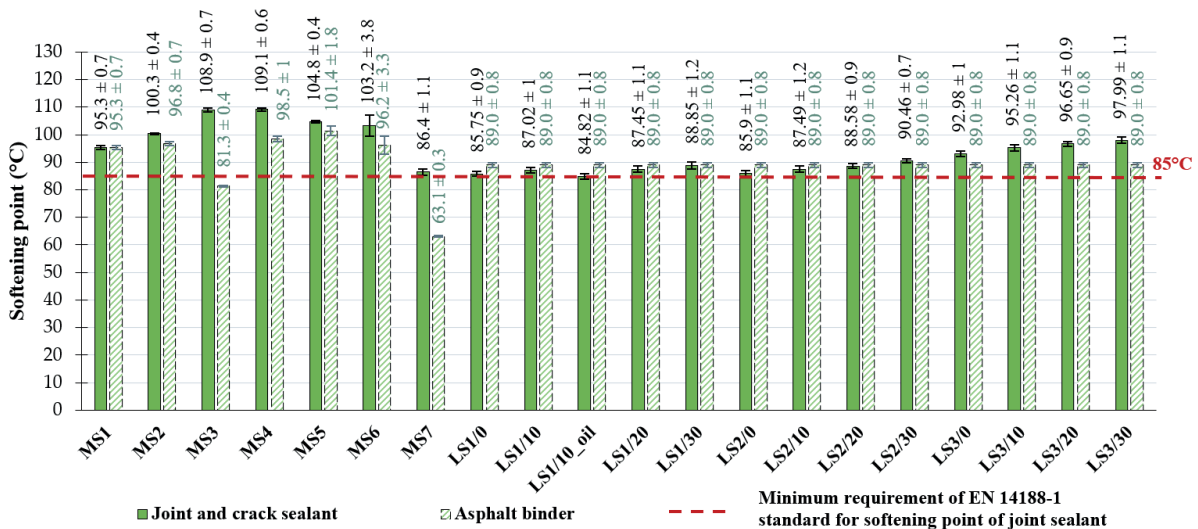


Fig. 5. Results of softening point of the investigated joint sealants and asphalt binders used in sealants (mean value ± standard deviation)

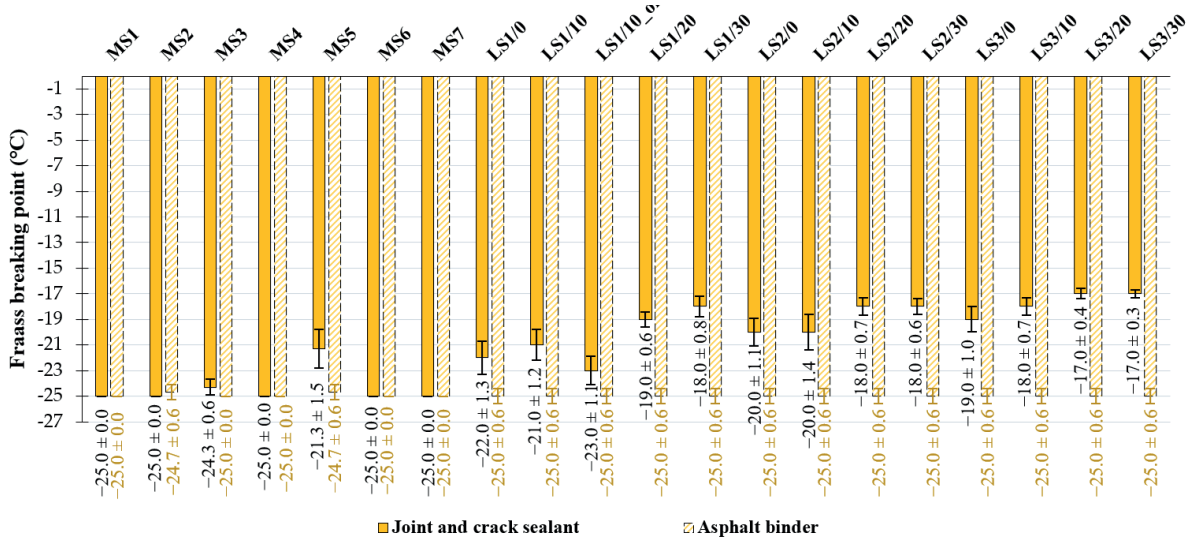


Fig. 6. Results of Fraass breaking point of the investigated joint sealants and asphalt binders used in sealants (mean value ± standard deviation)

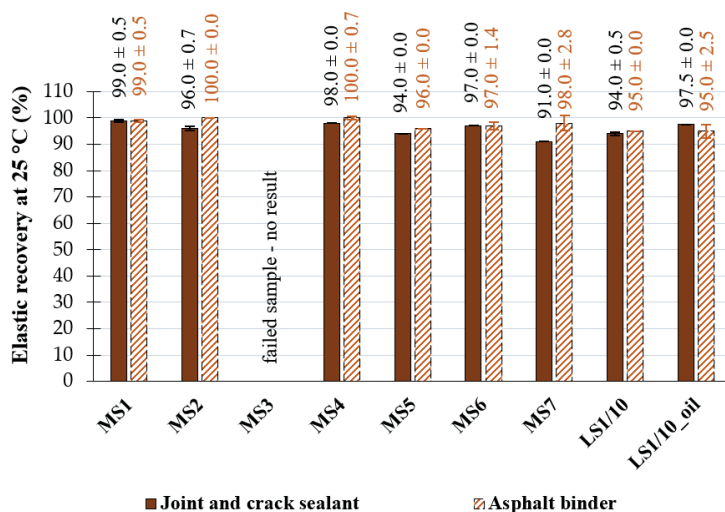


Fig. 7. Results of elastic recovery at 25°C of the investigated joint sealants and asphalt binders used in sealants (mean value ± standard deviation)

can undergo very large deformations without failure, and after reducing (or disappearing) of the stresses transmitted by the structure – they will return to their original shape. In relation to the base bitumen, no significant decrease in this parameter was observed, regardless of the composition of the joint sealant.

The addition of 3% rapeseed oil (in relation to the total weight) results in a favourable reduction of its Fraass temperature by about 2°C (Fig. 6, Table 5). At the same time, a reduction in the softening point was achieved.

A decrease in the average softening point (84.8°C) for the LS1/10_oil sealant was slightly below the parameter required by standard [10]. This indicates the need to extend the scope of investigating for joint sealants with the addition of rapeseed oil taking into account the service life.

3.3. The range of variability of the properties of joint sealants in relation to the base asphalt binder

In order to determine the range of variability of the basic properties of joint sealants in relation to the base asphalt binder, the differences in the values of individual parameters were determined (Table 6). The percentage changes in the values shown in Figures 8 and 9 were also estimated.

The largest range of variability of the investigated parameters was characterized by needle penetration, the differences in relation to the base bitumen ranged from -66.8×0.1 mm (MS2) to 31.8×0.1 mm (LS1/10_oil). Joint sealant with rapeseed oil was the only joint sealant for which an increase in penetration relative to the asphalt binder was recorded.

For the softening point, the largest change in values was recorded for the MS3 sealant (increase

by 27.6°C). For Fraass breaking point, the maximum difference in average values was 8°C for the LS3/20 and LS3/30 sealants.

No significant differences were found between elastic recovery of sealants and base bitumen. The maximum reduction of this parameter concerned the MS7 sealant with a high content of mineral filler of approx. 50%.

In terms of penetration, the highest percentage decrease in value in relation to the asphalt binder was obtained for the MS3 joint sealant (54.5%) among the sealants obtained from manufacturers. In the case of sealants produced in laboratory conditions, the percentage changes in penetration values reached 77.1% for the LS3/30 sealant with the highest content of mineral filler. Smaller percentage differences concerned the softening point and ranged from 0% to 36.9% for MS1 – MS7 and from -13.2% to 10.1% for LS1 – LS3 sealants.

Figure 10 presents the dispersion and nature of changes in the percentage values of the studied parameters depending on the content of asphalt binder in the joint sealants.

With the lowest content of asphalt binder (40%) in the joint sealant, the percentage differences in the properties of the tested sealants in relation to the asphalt binder ranged from -71.2% to -77.1% for needle penetration, 4.5% to 10.1% for softening point and from -24% to 32% for Fraass breaking point. For comparison, with a higher content of asphalt binder in the mass (approx. 60-70%), these differences were characterized by values in the range of -54.5% to -26.5% for penetration, -3.6% to 33.9% for softening point and from -28.0% to 1.2% for Fraass breaking point.

Table 6. Test results of differences in properties of the sealant in relation to the asphalt binder

Joint and crack sealant	Content of asphalt binder	Differences in mean properties in relation to the asphalt binder			
		Needle penetration at 25°C	Softening point, ring, and ball	Fraass breaking point	Elastic recovery at 25°C
Unit	%	0.1 mm	°C	°C	%
Test method	–	EN 1426	EN 1427	EN 12593	EN 13398
Valid N	–	5	4	3	2
MS1	100.0	0.00	0.00	0.0	0.0
MS2	71.3	-66.80	3.50	-0.3	-4.0
MS3	59.0	-43.40	27.60	0.7	0.0
MS4	69.8	-68.70	10.60	0.0	-2.0
MS5	70.7	-16.70	3.40	3.4	-2.0
MS6	72.8	-45.30	7.00	0.0	0.0
MS7	49.8	-15.40	23.30	0.0	-7.0
LS1/0	80.0	-6.50	-3.25	3.0	–
LS1/10	80.0	-8.14	-1.98	4.0	-1.0
LS1/10_oil	80.0	31.80	-4.18	2.0	2.5
LS1/20	80.0	-9.67	-1.55	6.0	–
LS1/30	80.0	-11.00	-0.15	7.0	–
LS2/0	60.0	-25.50	-3.10	5.0	–
LS2/10	60.0	-27.00	-1.51	5.0	–
LS2/20	60.0	-29.75	-0.42	7.0	–
LS2/30	60.0	-33.00	1.46	7.0	–
LS3/0	40.0	-52.00	3.98	6.0	–
LS3/10	40.0	-53.50	6.26	7.0	–
LS3/20	40.0	-55.33	7.65	8.0	–
LS3/30	40.0	-56.25	8.99	8.0	–

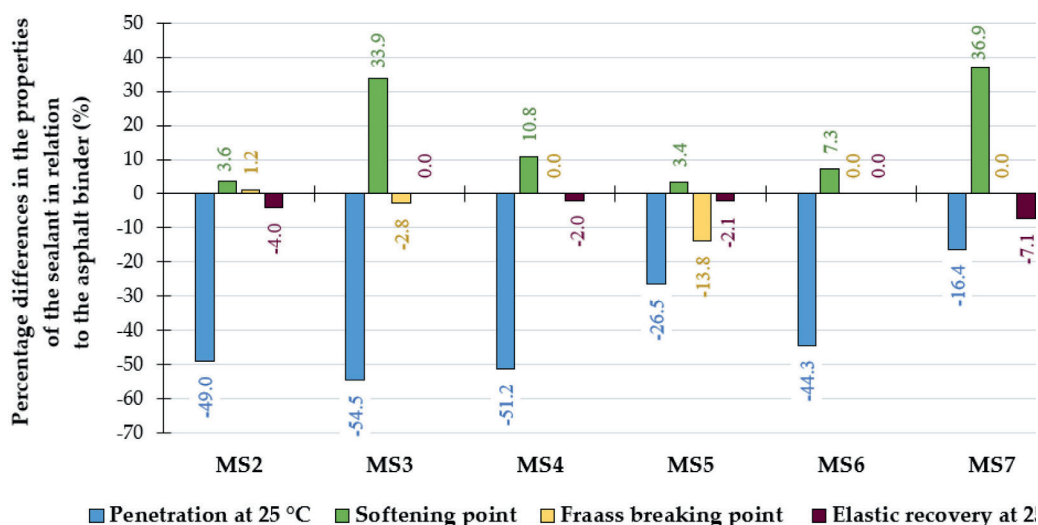


Fig. 8. Results of percentage differences in properties of the MS2 – MS7 sealants in relation to the asphalt binder

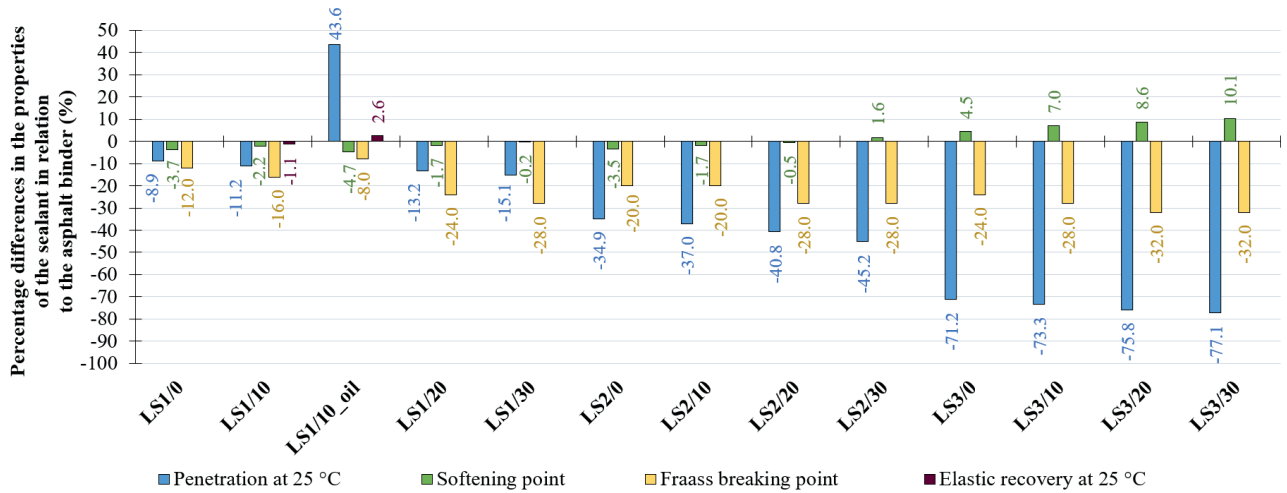


Fig. 9. Results of percentage differences in properties of the LS1 – LS3 in relation to the asphalt binder

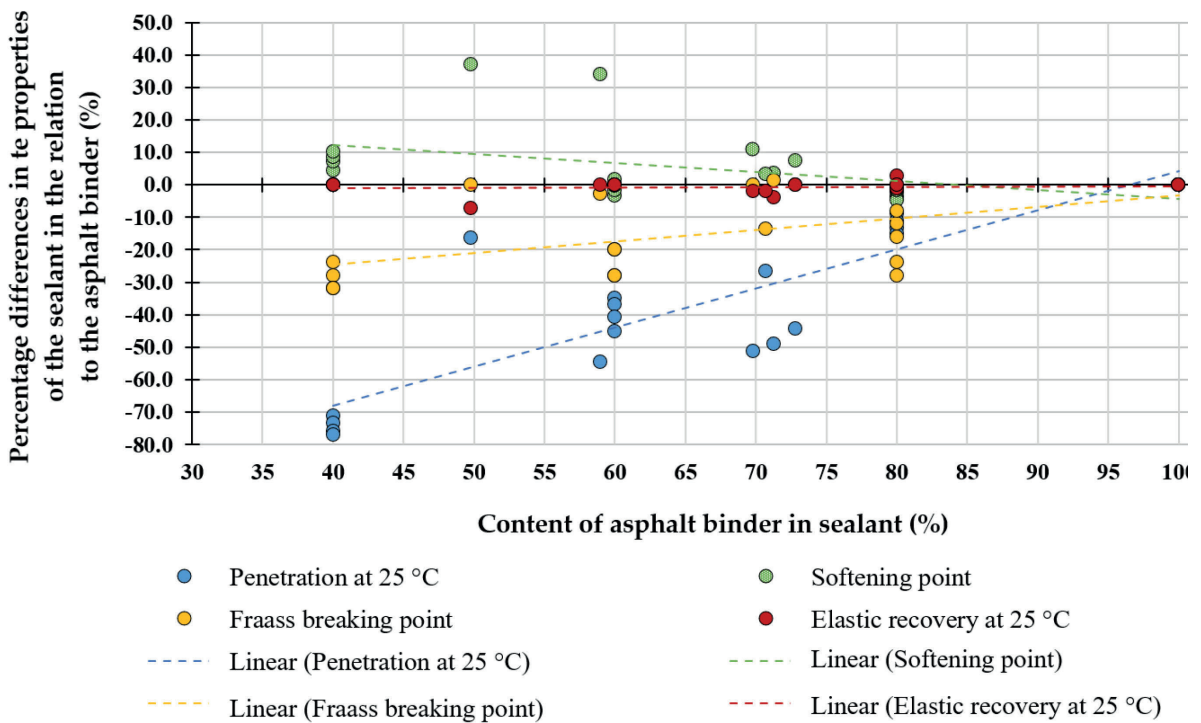


Fig. 10. Results of percentage differences in properties of the sealant in relation to the asphalt binder depending on the content of the asphalt binder

With the increase in the content of asphalt binder in the sealants, smaller percentage differences in the properties of the joint sealant in relation to the asphalt binder were observed. It was found that the greatest influence of asphalt binder content on percentage differences in the properties of the joint sealants in relation to the asphalt binder concerns penetration, while the smallest – elastic recovery, despite the different properties of the other components of the sealant.

3.4. Discussion

Joint sealants are complex formulations and, given a broad range of base asphalt binders, modifiers, fillers, and other non-soluble additives, their composition may vary widely, while still fulfilling the performance specifications. It is possible to regulate the selected properties of the joint sealant by changing the chemical composition and the proportion of its components (fillers, hydrated lime, rapeseed oil, rubber crumb). It is also possible to search for

further material and technological solutions in order to improve the quality and durability of joint sealants used for extension joints and crack repairs.

The tests showed similar properties of the MS and LS sealants in terms of elastic recovery at 25°C (91 to 99%), despite the different contents and chemical compositions of their individual components, the results indicated a very high degree of elastomeric modification of the bitumens used in the sealants and/or the effect of rubber modification, regardless of the sealant type (normal or elastic). The positive effects of the use of polymer SBS and/or crumb rubber in joint sealants were also indicated in other studies [6, 27, 43].

The determined values of the softening point corresponded with the European standard [10] requirements for most investigated hot-applied joint sealants ($\geq 85^\circ\text{C}$). The lowest softening points were determined for the joint sealant in which 3% rapeseed oil was used (84.8°C) and were slightly below the value required by the standard [10].

The needle penetration tests indicated significant variability in the consistency of the joint sealants (16.75 to 104.8×0.1 mm). It should be noted that cone penetration for joint sealants is characterized by lower values than needle penetration, ranging from a few to a dozen or so percent in relations to the needle penetration of the same sealant, as shown by previous studies [36]. The MS3 and LS3 sealants met neither the requirements of the applicable European standard [10] nor the manufacturer's declaration for minimum cone penetration (40 to 100×0.1 mm). Thus, they will not meet the standard requirements [10] in this area.

In the case of LS3 sealant, this is due to the high content of mineral filler (60%).

The percentage range of variability of the basic properties of joint sealants was estimated in the range from -77.1% to 43.6% in relation to the base asphalt binder, differentiated by their composition and the analyzed property.

On the basis of the tests performed, it can be concluded that it is advisable to use highly modified bitumen 65/105-80 as a binder for the joint sealants intended for filling gaps in the pavement or for asphalt expansion joints. It is characterized by parameters comparable to the requirements for the joint sealants currently used in industry and the standard [10], while attention should be paid to the content of filler and other components.

The analysis of the test results showed that, depending on the needs, it is possible to regulate the properties of the sealant by changing the proportions of its components

– binder and filler. Increasing the filler content in the composition of the sealants causes a decrease in penetration (the sealant is more rigid), an increase in the softening point and a slight increase in the Fraass breaking point. Hydrated lime also plays an important role in the composition of the filler, with the help of which the stiffness of the sealant can be adjusted. On the other hand, by increasing or decreasing the binder content of the sealant, its consistency and thus its intended use can be controlled. If it is to fill narrow gaps in the pavement, it should have a more liquid consistency, and therefore a higher binder content, and in the case of using expansion joints to cover expansion joints, its amount should be lower. Hydrated lime used in these investigated sealants may act as an active filler that has antioxidant and other effects, as other studies show [22-24].

On the basis of highly modified asphalt 65/105-80 and lime filler, the flexible joint sealants were made, which can be used for:

- execution of bituminous expansion joints on bridge structures;
- filling expansion joints in asphalt and concrete pavements, also in concrete floors with large spans;
- filling gaps between concrete or stone elements and mineral and asphalt mixture;
- sealing joints between the pavement and devices built into it, such as manhole covers, drain grates, etc.;
- filling and sealing linear cracks and damaged technological joints in asphalt pavements.

A visible discrepancy was observed between the Fraass breaking point performance of the asphalt binders extracted from the MS and LS joint sealants. The differences between the Fraass breaking points of the MS joint sealants and the asphalt binders extracted from them were in most cases indistinguishable. On the other hand, these differences in LS joint sealants were significant and amounted to 8°C increase in this property. Similar difference was observed in case of the MS5 sealant. In case of the LS joint sealants, this result could be attributed to the extraction process and its effect on the polymer network contributing to the performance of the highly modified asphalt binder used in these formulations. Based on this observation, a additional study into the effects of extraction process on the properties of different highly modified asphalt binders should be carried out.

Sealants developed in laboratory conditions (LS) had less favorable properties in terms of resistance to low temperatures (higher Fraass temperature values) than those produced by commercial manufacturers, which indicates the need to expand the scope of

further research in this area. The lack of conclusive requirements for the components of hot-applied joint sealant indicates the need to conduct investigation in this area and to search for additives that are an important regulator of their properties.

4. CONCLUSIONS

The present study considered the basic performance parameters of seven hot-applied sealants produced by domestic and foreign manufacturers and three sealants obtained in laboratory conditions with different contents of highly modified asphalt binder (40 to 100%) and other components. Based on the study, the conclusions were as follows:

- The percentage content and properties of the base bitumen have a decisive influence on the properties of the joint sealants. In order to obtain favorable performance parameters of the joint sealant type N1 (flexible) acc. to European standard [10] it is recommended to use highly modified bitumens with polymers and/or with the use of other substances, e.g. crumb rubber, in order to achieve greater viscosity and higher temperature deformation resistance.
- It was found that it was difficult to ensure the required standard parameters of joint sealants for the content of asphalt binder below 50%, even when using highly modified bitumen. In this case, it is advisable to consider replacing part of the mineral filler with rubber waste, however, this requires verification on the basis of further laboratory tests.
- The addition of hydrated lime and rapeseed oil may be an important regulator of the parameters of joint sealants, in addition to the content and properties of modified bitumen.
- On the basis of the test results for the joint sealant produced in laboratory (LS1 – LS3), it can be concluded that the amount of limestone filler has a significant impact on the quality of the sealant, apart from the content of highly modified bitumen 65/105-80. The joint sealant containing 80% highly modified bitumen and 20% mixed filler containing 90% limestone powder and 10% hydrated lime (LS1/10) was characterized by the best parameters.
- An attempt was also made to reduce the Fraass breaking point with the addition of rapeseed oil in the amount of 3% in relation to the total weight. Due to the fact that the softening point was too low in relation to the requirements of the standard [10] and the needle penetration was significantly increased in relation to the base bitumen, the possibility of reducing the oil content in subsequent laboratory tests should be considered.
- With the increase in the content of asphalt binder in the sealants, smaller percentage differences in the properties of the joint sealant in relation to the asphalt binder were observed. It was found that the greatest influence of asphalt binder content on percentage differences in the properties of the joint sealants in relation to the asphalt binder concerns penetration, while the smallest – elastic recovery, despite the different properties of the other components of the sealant.
- In terms of penetration, the highest percentage decrease in value in relation to the asphalt binder was obtained for the MS3 joint sealant (54.5%) with the highest rubber content among the sealants obtained from commercial manufacturers. In the case of sealants produced under laboratory conditions, the percentage changes in penetration values reached 77.1% for the LS3/30 sealant with the highest content of mineral filler. Smaller percentage differences concerned the softening point and ranged from 0% to 36.9% for MS1 – MS7 and from -13.2% to 10.1% for LS1 – LS3 sealants.

The analysis of the test results showed that, depending on the needs, it is possible to regulate the properties of the sealant by changing the proportions of its components – binder and filler. The lack of conclusive requirements for the components of asphalt-based sealant indicates the need to conduct further research on the properties and composition of joint sealants in terms of their applicability in various climatic conditions and traffic loads. In further studies it would be advisable to extend the analyses with additional [10] standard tests for sealants, e.g. related to cone penetration, penetration and recovery (resilience) and adhesion to the surface.

References

- [1] Liu S., Mo L., Wang K., Xie Y., Woldekidan M.F.: *Preparation, Microstructure and Rheological Properties of Asphalt Sealants for Bridge Expansion Joints*. Constr. Build. Mater. 2016, 105, 1-13, doi:10.1016/j.conbuildmat.2015.12.017.
- [2] Flexible Asphaltic Plug Expansion Joints for Road Bridges; EAD 120093; European assessment documents and European technical assessments, 2019.

- [3] Yu T., Li C., Wu S.: *Performance of Polymer Modified Asphalt Bridge Expansion Joints in Low-Temperature Regions*. J. Perform. Constr. Facil. 2009, 23, 227-233, doi:10.1061/(ASCE)0887-3828(2009)23:4(227).
- [4] Tan X., Zhang J., Guo D., Sun G., Zhou Y., Zhang W., Guan Y.: *Preparation, Characterization and Repeated Repair Ability Evaluation of Asphalt-Based Crack Sealant Containing Microencapsulated Epoxy Resin and Curing Agent*. Constr. Build. Mater. 2020, 256, 119433, doi:10.1016/j.conbuildmat.2020.119433.
- [5] Masson J.-F., Collins P., Bundalo-Perc S., Woods J.R., Al-Qadi I.: *Variations in Composition and Rheology of Bituminous Crack Sealants for Pavement Maintenance*. Transp. Res. Rec. J. Transp. Res. Board 2005, 1933, 107-112, doi:10.1177/0361198105193300112.
- [6] Ghabchi R., Arshadi A., Zaman M., March F.: *Technical Challenges of Utilizing Ground Tire Rubber in Asphalt Pavements in the United States*. Materials (Basel). 2021, 14, 4482, doi:10.3390/ma14164482.
- [7] Flexible Asphaltic Plug Expansion Joints for Road Bridges; EAD 120093; European assessment documents and European technical assessments, 2019.
- [8] Di Mascio P., Loprencipe G., Moretti L., Puzzo L., Zoccali P.: *Bridge Expansion Joint in Road Transition Curve: Effects Assessment on Heavy Vehicles*. Appl. Sci. 2017, 7, 599, doi:10.3390/app7060599.
- [9] Lima J.M., Brito J.: *Inspection Survey of 150 Expansion Joints in Road Bridges*. Eng. Struct. 2009, 31, 1077-1084, doi:https://doi.org/10.1016/j.engstruct.2009.01.011.
- [10] EN 14188-1; Joint Fillers and Sealants – Part 1: Specifications for Hot Applied Sealants. In: Comité Européen de Normalisation (CEN): Brussels, Belgium, 2004.
- [11] ASTM D6690. Standard Specification for Joint and Crack Sealants, Hot Applied, for Concrete and Asphalt Pavements, 2001.
- [12] Wang S., Xu Y., Liu M., Gao Y., Jia Y., Li Y., Chen Z., Wei Z.: *Dynamic Behavior of Crack Sealant Bonding Interface in the Asphalt Pavement Crack Repair Structure under Moving Vehicle Load*. Case Stud. Constr. Mater. 2023, 18, e01821, doi:10.1016/j.cscm.2022.e01821.
- [13] Cao L., Yang C., Dong Z., Nonde L.: *Evaluation of Crack Sealant Adhesion Properties under Complex Service Ambient Conditions Based on the Weak Boundary Layer (WBL) Theory*. Constr. Build. Mater. 2019, 200, 293-300, doi:10.1016/j.conbuildmat.2018.12.159.
- [14] Cao L., Yang C., Dong Z., Wang W., Yin H.: *Aging Mechanism of Hot-Poured Sealants for Asphalt Pavement under Natural Environmental Exposure*. Int. J. Pavement Eng. 2022, 23, 197-206, doi:10.1080/10298436.2020.1736296.
- [15] Lamarre A., Fini E.H., Abu-Lebdeh T.M.: *Investigating Effects of Water Conditioning on the Adhesion Properties of Crack Sealant*. Am. J. Eng. Appl. Sci. 2016, 9, 178-186, doi:10.3844/ajeassp.2016.178.186.
- [16] Iwanski M.M., Chomicz-Kowalska A., Maciejewski K.: *Impact of Additives on the Foamability of a Road Paving Bitumen*. In: Proceedings of the IOP Conference Series: Materials Science and Engineering; 2019; Vol. 603.
- [17] Iwański M., Mazurek G., Buczyński P., Iwański M.M.: *Effects of Hydraulic Binder Composition on the Rheological Characteristics of Recycled Mixtures with Foamed Bitumen for Full Depth Reclamation*. Constr. Build. Mater. 2022, 330, 127274, doi:10.1016/j.conbuildmat.2022.127274.
- [18] Iwański M., Chomicz-Kowalska A., Mazurek G., Buczyński P., Cholewińska M., Iwański M.M., Maciejewski K., Ramiączek P.: *Effects of the Water-Based Foaming Process on the Basic and Rheological Properties of Bitumen 70/100*. Materials (Basel). 2021, 14, 2803, doi:10.3390/ma14112803.
- [19] Stepień J., Maciejewski K.: *Using Reclaimed Cement Concrete in Pavement Base Mixes with Foamed Bitumen Produced in Cold Recycling Technology*. Materials (Basel). 2022, 15, 5175, doi:10.3390/ma15155175.
- [20] Chomicz-Kowalska A., Bartos J., Maciejewski K., Remisova E., Komacka J., Holy M.: *The Effect of WMA Additive on Basic Properties of 35/50 and 50/70 Foamed Road Bitumen*. Struct. Environ. 2019, 11, 126-138.
- [21] Gong Y., Pang Y., He F., Bi H.: *Investigation on Preparation and Properties of Crack Sealants Based on CNTs/SBS Composite-Modified Asphalt*. Materials (Basel). 2021, 14, 4569, doi:10.3390/ma14164569.
- [22] Smith K.L., Romine R.A.: *Materials and Procedures for Sealing and Filling Cracks in Asphalt-Surfaced Pavements*. FHWA-RD-99-147. 2001, 85 p.
- [23] Wang X.L., Yu J.Y., Cheng S.B., Kuang D.L.: *Preparation and Properties of MAH-g-SBS Modified Asphalt Crack Filling Material*. Wuhan Ligong Daxue Xuebao/Journal Wuhan Univ. Technol. 2007, 29, 59-61.
- [24] Zhang H., Sheng X., Wang S., Xu T.: *Effects of Different Modifiers on Thermal Stability, Constituents and Microstructures of Asphalt-based Sealant*. J. Therm. Anal. Calorim. 2020, 142, 1183-1192.
- [25] Maciejewski K., Ramiączek P., Chomicz-Kowalska A.: *The Impact of EBA and ECB Polymer Modification of 50/70 Bitumen*. Struct. Environ. 2013, 5, 15-20.
- [26] Gong Y., Wu S., Zhang Y., Pang Y., Ma Y.: *Investigation of the High-Temperature and Rheological Properties for Asphalt Sealant Modified by SBS and Rubber Crumb*. Polymers (Basel). 2022, 14, 2558, doi:10.3390/polym14132558.
- [27] Gnatenko R., Tsyrukunova K., Zhdanyuk V.: *Technological Sides of Crack Sealing in Asphalt Pavements*. Transp. Res. Procedia 2016, 14, 804-810, doi:10.1016/j.trpro.2016.05.028.

- [28] Holý M., Remišová E.: *Analysis of Influence of Bitumen Composition on the Properties Represented by Empirical and Viscosity Test*. Transp. Res. Procedia 2019, 40, 34-41, doi:10.1016/j.trpro.2019.07.007.
- [29] Remisova E., Briliak D., Holy M.: *Evaluation of Thermo-Viscous Properties of Bitumen Concerning the Chemical Composition*. Materials (Basel). 2023, 16, 1379, doi:10.3390/ma16041379.
- [30] Di Mascio P., Loprencipe G., Moretti L., Puzzo L., Zoccali P.: *Bridge Expansion Joint in Road Transition Curve: Effects Assessment on Heavy Vehicles*. Appl. Sci. 2017, 7, 599, doi:10.3390/app7060599.
- [31] <https://danlab.pl/> (access: 29 November, 2023).
- [32] EN 13880-1: Hot Applied Joint Sealants Test Method for the Determination of Density at 25°C; Comité Européen de Normalisation (CEN): Brussels, Belgium.
- [33] EN 1427: Bitumen and Bituminous Binders – Determination of the Softening Point – Ring and Ball Method; Comité Européen de Normalisation (CEN): Brussels, Belgium.
- [34] EN 13880-2: Hot Applied Joint Sealants – Part 2: Test Method for the Determination of Cone Penetration at 25°C; Comité Européen de Normalisation (CEN): Brussels, Belgium.
- [35] EN 13880-3: Hot Applied Joint Sealants Test Method for the Determination of Penetration and Recovery (Resilience); Comité Européen de Normalisation (CEN): Brussels, Belgium.
- [36] Stępień J., Remišová E.: *Characterization of Hot-Applied Joint Sealants and Their Components in Terms of Their Chemical Composition and Basic Performance Properties*. Materials (Basel). 2023, 16, 1-23, doi:<https://doi.org/10.3390/ma16196490>.
- [37] Putman B.J., Amirkhani S.N.: *Characterization of the Interaction Effect of Crumb Rubber Modified Binders Using HP-GPC*. J. Mater. Civ. Eng. 2010, 22, 153-159, doi:10.1061/(ASCE)0899-1561(2010)22:2(153).
- [38] PN-EN 14023:2011/Ap1:2014-04: Asfalty i lepiszcza asfaltowe. Zasady klasyfikacji asfaltów modyfikowanych polimerami; PKN, P.K.N., Ed.; Warsaw, Poland.
- [39] EN 1426: Bitumen and Bituminous Binders – Determination of Needle Penetration; Comité Européen de Normalisation (CEN): Brussels, Belgium.
- [40] EN 12593: Bitumen and Bituminous Binders – Determination of the Fraass Breaking Point; Comité Européen de Normalisation (CEN): Brussels, Belgium.
- [41] EN 13398: Bitumen and Bituminous Binders – Determination of the Elastic Recovery of Modified Bitumen; Comité Européen de Normalisation (CEN): Brussels, Belgium.
- [42] EN 12591: Bitumen and Bituminous Binders – Specifications for Paving Grade Bitumens; Comité Européen de Normalisation (CEN): Brussels, Belgium.
- [43] Gong Y., Wu S., Zhang Y., Pang Y., Ma Y.: *Investigation of the High-Temperature and Rheological Properties for Asphalt Sealant Modified by SBS and Rubber Crumb*. Polymers (Basel). 2022, 14, 2558, doi:10.3390/polym14132558.
- [44] Alfaqawi R.M., Fareed A., Zaidi S.B.A., Airey G.D., Rahim A.: *Effect of Hydrated Lime and Other Mineral Fillers on Stiffening and Oxidative Ageing in Bitumen Mastic*. Constr. Build. Mater. 2022, 315, 125789, doi:10.1016/j.conbuildmat.2021.125789.
- [45] Iwański M., Chomicz-Kowalska A., Iwański M.M.: *Influence of Hydrated Lime on Durability of SMA Asphalt Pavement with Quartzite Aggregate*. Struct. Environ. 2013, 5, 5-11.

Acknowledgements

The work is supported by the program of the Minister of Science and Higher Education under the following name: Regional Initiative of Excellence in 2019–2023 project number 025/RID/2018/19 financing amount PLN 12.000.000.



LOCAL BUCKLING OF ONE-SIDE ELASTICALLY RESTRAINED THIN-WALLED CROSS-SECTION WALL UNDER LONGITUDINAL STRESS VARIATION

WYBOCZENIE LOKALNE JEDNOSTRONNIE SPRĘŻYŚCIE ZAMOCOWANEJ ŚCIANKI PRZEKROJU CIENKOŚCIENNEGO PRZY WZDŁUŻNEJ ZMIENNOŚCI NAPRĘŻEŃ

ANDRZEJ SZYCHOWSKI*
Kielce University of Technology, Poland

Abstract

In cold-formed thin-walled cross-sections, complex phenomena, related to local and distortional buckling of slender walls containing edge fold stiffeners, occur. In order to determine the design resistance of such a cross-section in the post-buckling range, it is necessary to determine the critical stress of local buckling for individual walls. On this basis, the corresponding effective widths are determined. Subsequently, the distortional buckling effect is taken into account, typically by reducing the thickness of the substitute cross-section of the stiffener.

The paper presents approximation formulas of plate buckling coefficients (k^) that are used to calculate critical local buckling stress for technically crucial stress distributions. The full range of variation of the index of elastic fixity of the longitudinal edge of the thin-walled cross-section was considered. The coefficients were determined for a more accurate, relative to Eurocode 3, computational model. Both the effect of reciprocal elastic restraint of component walls of the cross-section and the effect of longitudinal stress variation, which occurs in transversely bent beams, were taken into account.*

Keywords: thin-walled member, critical stress of local buckling, elastic restraint, longitudinal stress variation, approximation formulas

Streszczenie

W profilowanych na zimno przekrojach cienkościennych występują złożone zjawiska związane z wyoboczeniem lokalnym i dystorsyjnym smukłych ścianek zawierających krawędziowe odgięcia usztywniające. W celu wyznaczenia nośności obliczeniowej takiego przekroju w zakresie nadkrytycznym należy wyznaczyć naprężenia krytyczne wyoboczenia lokalnego dla poszczególnych ścianek. Na tej podstawie wyznacza się odpowiednie szerokości efektywne. W kolejnym kroku uwzględnia się efekt wyoboczenia dystorsyjnego, najczęściej poprzez redukcję grubości tzw. zastępczego przekroju usztywnienia.

W pracy przedstawiono wzory aproksymacyjne płytowych współczynników wyoboczeniowych (k^) służące do obliczania naprężeń krytycznych wyoboczenia lokalnego dla technicznie ważnych rozkładów naprężeń. Uwzględniono pełny zakres zmienności wskaźnika sprężystego utwierdzenia krawędzi podłużnej półki przekroju cienkościennego. Współczynniki*

wyznaczono dla dokładniejszego, w stosunku do Eurokodu 3, modelu obliczeniowego. Uwzględniono zarówno efekt wzajemnego sprężystego zamocowania ścianek składowych przekroju, jak również występujący w poprzecznie zginanych belkach efekt wzdłużnej zmienności naprężeń.

Słowa kluczowe: element cienkościenny, naprężenie krytyczne wybożenia lokalnego, sprężyste zamocowanie, wzdłużna zmienność naprężeń, wzory aproksymacyjne

1. INTRODUCTION

In thin-walled steel members with cold-formed open cross-sections containing edge fold stiffeners, there are cases of loading in which the flange (internal wall) is subjected to compression, and simultaneously, there is a longitudinal stress variation along its length. In the case of Class 4 cross-sections, local and distortional stability loss can occur, leading to a reduction in the design resistance of the cross-section in the post-buckling state. In the analysis of local buckling, these walls can be treated as thin plates loaded with normal stresses in their plane.

The most highly stressed plate elements of a bent thin-walled cross-section are usually those either two-side or one-side elastically restrained in the other plates (Fig. 1).

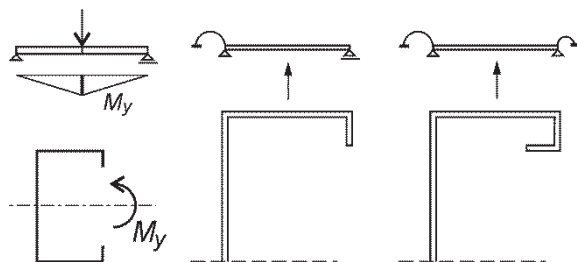


Fig. 1. Static scheme of a cold-formed thin-walled section's compressed plate (flange)

Two-side (symmetrical) restraint is found, for example, in the flanges of box sections (closed sections), where these flanges rest on webs bent in their planes. On the other hand, one-side elastic restraint against rotation is generally found in the flanges of open cold-formed cross-sections, with one side supported on the web, and the other side on the edge fold stiffeners. Depending on the type of edge fold stiffeners, either simple support of the plate (single edge fold) or elastic restraint against rotation (in the case of double or triple edge fold) can be found. From a technological point of view, single edge fold is the simplest and most cost-effective to produce, and they are quite commonly used in practice. Complex phenomena associated with local buckling and distortional buckling of slender walls and their edge fold stiffeners occur in this type of thin-walled cross-sections.

In the case of bending members with a cold-formed cross-section, the compressed flange is generally elastically restrained against rotation in the web and is also flexibly supported against deflection on the compressed edge fold. In the computational model according to [1], the wall with edge fold is treated as an internal plate rigidly supported against deflection also on this edge fold until the distortional buckling stress is reached in the cross-section. It is further assumed that the plate so separated from the cross-section is simply supported on all edges, and critical local buckling stress $\sigma_{cr,L}$ is determined for this static scheme. However, such simplification, for many technically significant geometric proportions of the cross-section, e.g., C-section or Z-section, does not correspond to the actual behavior of the thin-walled cross-section under load.

Naturally, while the assumption of simple support of the plate resting on the single edge fold (due to its low torsional stiffness further reduced by compressive stresses) should be considered appropriate, the assumption of the same simple support scheme on the web may lead to an underestimation of the critical stress $\sigma_{cr,L}$.

The correctly calculated critical stress $\sigma_{cr,L}$ (which can be determined as the product of the plate buckling coefficient k and the Euler stress σ_E) is used to determine the so-called relative plate slenderness λ_p , which is then used to determine the effective width of the compressed flange [2]. It also indirectly affects the correct determination of critical distortional buckling stress $\sigma_{cr,D}$ according to [1]. In the standard computational model, the effective width of the flange from the edge fold side is a component of the equivalent section directly affecting the value of the stress $\sigma_{cr,D}$. Once the relative slenderness λ_d (which is a function of $\sigma_{cr,D}$ and indirectly a function of $\sigma_{cr,L}$) is determined, the reduced thickness of the edge stiffener and, ultimately, the design resistance of the effective cross-section can be determined.

Therefore, the correct determination of $\sigma_{cr,L}$ according to a more accurate computational model affects both the effective widths of the compressed flange as well as indirectly the reduced thickness of the edge stiffener section and ultimately the design resistance of the entire cross-section.

The paper [3] presents the Critical Plate Method (CPM) for determining the local critical resistance (determined from the local buckling condition) and the design ultimate resistance of a thin-walled cross-section according to a more accurate, compared to Eurocode 3 standards, computational model. The local critical resistance limits in the elastic range (i.e., for $\sigma_{cr,L} < f_y$, where f_y is the design yield strength of steel) the interval of pre-buckling behavior of the cross-section, in which the assumptions of the theory of thin-walled bars by Vlasov [4] are satisfied. To effectively apply CPM, it is necessary to determine the critical stress of the weakest plate of the thin-walled cross-section, the so-called critical plate, taking into account both the effect of reciprocal elastic restraint of the walls and the effect of the longitudinal stress variation.

The purpose of this paper is to provide approximation formulas for determining the plate buckling coefficient k^* and, ultimately, the critical stress $\sigma_{cr,L}$ of an internal plate that is one side elastically restrained against rotation with the simultaneous occurrence of longitudinal stress variation. Such a plate model can be used to approximate the behavior of a compressed flange with a single edge fold (Fig. 1) of a cold-formed section under local buckling. This approach allows for a much more accurate determination of $\sigma_{cr,L}$ compared to the computational model according to [2], which ignores the influence of the elastic restraint of the walls and the longitudinal stress variation. Therefore, in case of an internal wall, the plate buckling coefficient according to [2] is $k = 4$ regardless of the degree of its elastic restraint and the longitudinal stress variation.

Approximation formulas for k^* were derived for: 1) the full range of the edge index of fixity (from hinge support through elastic restraint to complete restraint), and 2) for longitudinal stress distribution according to a linear or nonlinear function, according to a second-degree parabola.

According to the author's knowledge, such formulas are not found in technical literature.

2. CRITICAL BUCKLING STRESS

The computational model presented in the design standards for Class 4 thin-walled members [1, 2, 5] assumes that the analysis of local buckling in the cross-section can be carried out based on the concept of separating simply supported plate elements. Buckling stresses are then determined for plates separated in such a manner. In the case of the compressed internal plate considered in this paper, the buckling coefficient

according to [2] is $k = 4$. After determining the relative slenderness of the individual plates (walls), the corresponding effective widths are determined, which are then combined to form the effective cross-section of the thin-walled member.

However, experimental studies of entire cross-sections e.g. [6-8], computations with the Finite Strip Method (FSM), e.g. [9, 10] or the Finite Element Method (FEM), e.g. [11], as well as theoretical analyses, e.g. [12-14], have shown that during local buckling, there is an effect of elastic interaction between rigidly connected adjacent plates (section walls). According to the author's previous papers [3, 11, 15], this effect can be considered in the engineering computational model.

The Critical Plate Method (CPM), presented in the paper [3] enables a more precise consideration of the real behavior of the thin-walled member compared to Eurocode 3. The study in [3] demonstrated that in many technically important cases, the local loss of stability is determined by the weakest plate ("critical plate" or "CP"), which is elastically restrained against rotation in the stronger plate ("restraining plate" or "RP").

The index of fixity along the longitudinal edge of the critical plate can be determined using formula (1):

$$\kappa = 1 / \left[\left(1 + 2D_s / (b_s C_\theta) \right) \right] \quad (1)$$

where: D_s – plate (wall s) flexural rigidity; C_θ – rotational spring stiffness of the supported edge; b_s – width of the plate.

The method of determining individual design parameters, including the procedure for iteratively determining the rotational spring stiffness C_θ , is described in detail in the paper [3].

Of course, there are cases of geometric cross-section proportions and stress distributions where the effect of elastic restraint of the component walls does not occur or is negligible and can be omitted from a technical point of view. Such cross sections were defined in the paper [3] as "zero cross-sections", along with criteria for their classification. Calculations of such cross-sections following the procedure of separating simply supported plates according to Eurocode 3 does not lead to underestimation of cross-section resistance.

In the paper [16], the issue of the loss of local stability of the compressed flange of a cold-formed cross-section (Fig. 2) was reduced to the buckling analysis of a one-side elastically restrained internal plate in the most stressed segment of the thin-walled member. The spacing of transverse stiffeners (e.g.,

ribs, diaphragms, or supports) was assumed as the length of i -th bar segment l_{si} , regardless of the spontaneously formed local buckling nodal lines [14]. Such a definition of the segment results from observations of the form of local buckling in the presence of longitudinal stress variations [8, 14]. In this case, buckling half-waves of varying length and decreasing amplitude are formed along the length of the critical plate.

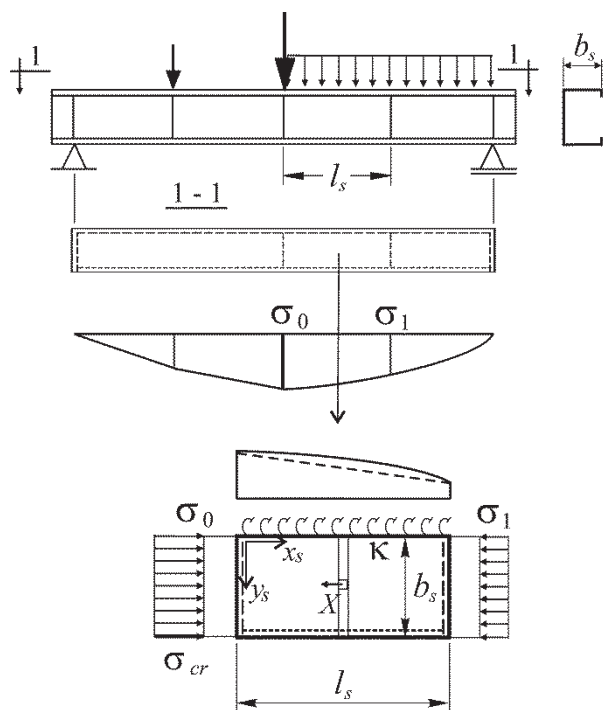


Fig. 2. Example of a compressed plate separated from a bent thin-walled member

In the case of members with cold-formed sections, the influence of the corner rounding geometry on the relevant width of the flange (wall) b_s should be taken into account. The method of determining b_s is presented in [1]. However, the influence of the corner rounding radius on the degree of elastic restraint of the wall for the most commonly used r/t_s ratios is insignificant and can be neglected. More detailed information on this subject is provided in [3].

The longitudinal variation of stresses according to a linear function or a second-degree parabola can be described using the following formulas, respectively:

$$\sigma_x = \sigma_o \left(1 - m \frac{x_s}{l_s} \right) \quad (2)$$

$$\sigma_x = \sigma_o \left(1 - m \frac{x_s^2}{l_s^2} \right) \quad (3)$$

where:

$$m = 1 - \sigma_1 / \sigma_0 \quad (4)$$

Local buckling stress ($\sigma_{cr,L}$) is referred to the most compressed edge (cf. Fig. 2) and is expressed in the form of the classical formula:

$$\sigma_{cr} = k \sigma_E \quad (5)$$

where: k – plate buckling coefficient; σ_E – Euler stress according to formula (6):

$$\sigma_E = \frac{\pi^2 E}{12(1-\nu^2)} \left(\frac{t_s}{b_s} \right)^2 \quad (6)$$

In the paper [16], the plate buckling problem was solved using the energy method. The deflection function was expressed as a polynomial-sinusoidal series. Stress variation along the length of the plate was obtained by introducing longitudinal body forces (X) according to the concept first presented in papers [17, 18]. Elastic strain energy of the plate bending and the energy of elastic restraint of the longitudinal edge ($y_s = 0$) were taken into account. The function of the work done by external forces when the plate is loaded according to equations (2) and (3) was determined from a sequence of formulas derived in the paper [19]. Based on the obtained relationships, a computer program “Ncr-plate-span-elastic(2).nb” was developed in the *Mathematica*® environment, which is used, among other things, to determine and tabulate the coefficients k . Graphs of k for elastically restrained internal plates were presented, at $\gamma_s = l_s/b_s = 1 \div 8$, for the following cases: 1) linear stress distribution for $m = 0.5$; and 2) nonlinear stress distribution for $m = 0.5$ [16].

To significantly facilitate the calculation of critical stresses for technically important combinations of parameters: $3 \leq \gamma_s \leq 20$; $0 \leq m \leq 1$; and $0 \leq \kappa \leq 1$, approximate formulas for plate buckling coefficients were presented in this paper, denoted by the symbol k^* for differentiation.

3. APPROXIMATION FORMULAS FOR THE COEFFICIENT k^*

The approximation formulas were derived from numerical analysis of a large set of coefficient arrays obtained using the program “Ncr-plate-span-elastic(2).nb” for the following parameters: $\kappa = 0$; 0.2; 0.333; 0.429; 0.5; 0.6; 0.714; 0.8; 0.882; 0.937; 0.972; 1.0; $m = 0$; 0.25; 0.5; 0.75; 1; and $2 \leq \gamma_s \leq 20$ with a step of 0.1 (a total of 60 arrays containing

more than 10,800 coefficients). In order to increase the degree of fit of the function of plate deflection to the non-symmetric (in the longitudinal direction) form of buckling occurring with longitudinal stress variation, the parameter i_0 determining the number of half-waves of the sinus function was increased from the value of 16 (for $\gamma_s \leq 8$ according to [16]) to 35 (for $\gamma_s \leq 20$).

The general form of the approximation formula for the coefficient k^* , similarly to the paper [20], is expressed by equation (7):

$$k^*(\kappa, m, \gamma) = k_\infty(\kappa) + \frac{f_q(\kappa, m)}{\gamma_s^{w_q(m)}} \quad (7)$$

where: $k_\infty(\kappa)$ – the buckling coefficient for an infinitely long and one-side elastically restrained internal plate at constant stress intensity (i.e. for $m = 0$); $w_q(m)$ – power exponent; $f_q(\kappa, m)$ – expression taking into account the longitudinal stress variation and the index of fixity according to equation (8):

$$f_q(\kappa, m) = \sum_{n=0}^{n_0} \left(\sum_{j=0}^{j_0} c_{nj} m^j \right) \kappa^n \quad (8)$$

where: c_{nj} – coefficients matrix elements determined using the least-squares method.

The buckling coefficient $k_\infty(\kappa)$ was determined as:

$$k_\infty(\kappa) = 4 + 0.452\kappa + 0.95\kappa^3 \quad (9)$$

For a linear stress distribution, the power exponent was determined as $w_q(m) = 0.68 + 0.04m$, and the calculated coefficient matrix was recorded in Table 1.

For a nonlinear stress distribution (according to a second-degree parabola), the power exponent was determined as $w_q(m) = 1.01 + 0.04m$, and the calculated coefficients matrix was recorded in Table 2.

Explicit formulas for the coefficients k^* for linear and nonlinear stress distributions were written as formulas (10) and (11), respectively, and are included in the Appendix.

Table 1. Matrix of coefficients c_{nj} for a linear stress distribution

$n \setminus j$	1	2	3
0	3.689	-2.692	1.26
1	0.348	-0.343	0.18
2	0	0	0
3	0.521	-0.406	0.181

Table 2. Matrix of coefficients c_{nj} for a nonlinear stress distribution

$n \setminus j$	1	2	3	4
0	3.863	-6.653	6.836	-2.603
1	0	0	0	0
2	1.135	-3.311	3.964	-1.621
3	-0.429	1.819	-2.355	0.995

In Figure 3 solid lines show the coefficient k of a one-side elastically restrained and axially compressed internal plate determined by the program according to [16], while red dashed lines show the graphs of the coefficient k^* obtained from formula (9) in the $\gamma_s = 3 \div 8$ range. The graphs were generated for a linear stress distribution according to (2) for $m = 1$ and different values of the index of fixity ($\kappa = 0 \div 1$) of the longitudinal edge ($\nu_s = 0$). The assignment of numbers to individual curves corresponding to the index κ is given in Table 3. Dotted lines represent the classic graph of the coefficient k (the so-called garland shaped curve) for uniformly compressed and simply supported plates according to [12].

Similarly, Figure 4 compares k graphs determined according to [16] and k^* graphs calculated from formula (10) for nonlinear stress distribution according to (3) for $m = 1$.

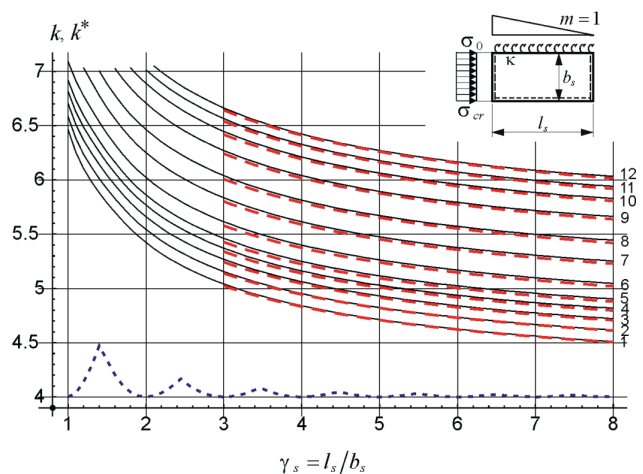


Fig. 3. Comparison of plate buckling coefficients (k, k^*) for linear stress distribution

Table 3. Assignment of curve numbers in Figures 3 and 4 to the index κ

No	1	2	3	4	5	6	7	8	9	10	11	12
κ	0	0.2	0.333	0.429	0.5	0.6	0.714	0.8	0.882	0.937	0.972	1

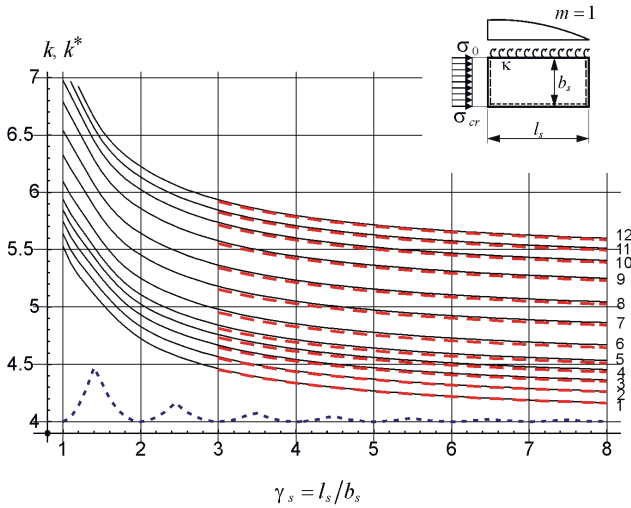


Fig. 4. Comparison of plate buckling coefficients (k, k^*) for nonlinear (according to the second-degree parabola) stress distribution

A comparison of the graphs (Figs. 3 and 4) shows very good agreement between the values of the coefficients k^* according to the approximation formulas compared to the k determined by the computer program [16].

Table 4 lists the coefficients k^* for a one-side elastically restrained internal plate (for $l_s/b_s = 4, 8, 12, 16$) as a function of the index of fixity ($\kappa = 0, 0.2, 0.4, 0.6, 0.8$ and 1) for constant ($m = 0$) and linear stress distribution ($m = 0.5$ and 1).

From the comparison of the k^* coefficient values presented in Table 4 with the value of $k = 4$ according

to the standard [2] it follows that: 1) taking into account only the effect of elastic restraint (i.e. for constant stress distribution, $m = 0$) increases k^* by a maximum of 35% (for $\kappa = 1$); 2) taking into account only the effect of longitudinal stress distribution for $m = 1$ (in the absence of elastic restraint, i.e. for $\kappa = 0$) causes an increase in k^* from 20.8% for $l_s/b_s = 4$ to 7.8% for $l_s/b_s = 16$; 3) taking into account the total impact of the above-mentioned effects increases k^* from 60.3% for $l_s/b_s = 4, \kappa = 1$ and $m = 1$ to 44.3% for $l_s/b_s = 16, \kappa = 1$ and $m = 1$.

Similarly, Table 5 provides the coefficients k^* for the nonlinear (according to the second-degree parabola) stress distribution ($m = 0.5$ and 1). Note: to facilitate comparisons, Table 5 also includes values for $m = 0$ (i.e. a constant stress distribution along the entire length).

From the comparison of the k^* coefficient values presented in Table 5 with the value of $k = 4$ according to the standard [2] it follows that: 1) taking into account only the effect of elastic restraint (i.e. for constant stress distribution, $m = 0$) increases k^* (similarly to Table 4) by a maximum of 35% (for $\kappa = 1$); 2) taking into account only the effect of longitudinal stress distribution for $m = 1$ (in the absence of elastic restraint, i.e. for $\kappa = 0$) causes an increase in k^* from 8.5% for $l_s/b_s = 4$ to 2% for $l_s/b_s = 16$; 3) taking into account the total impact of the above-mentioned effects increases k^* from 44.5% for $l_s/b_s = 4, \kappa = 1$ and $m = 1$ to 37.3% for $l_s/b_s = 16, \kappa = 1$ and $m = 1$.

A comparison of the graphs shown in Figure 3 and Figure 4 and a comparison of the values in Table 4 and

Table 4. Coefficients k^* for the linear stress distribution as a function of index κ

l_s/b_s	m	κ					
		0	0.2	0.4	0.6	0.8	1
4	0	4	4.10	4.24	4.48	4.85	5.40
	0.5	4.50	4.61	4.77	5.02	5.42	6.01
	1	4.83	4.94	5.11	5.37	5.79	6.41
8	0	4	4.10	4.24	4.48	4.85	5.40
	0.5	4.31	4.41	4.56	4.81	5.20	5.78
	1	4.51	4.61	4.77	5.02	5.42	6.01
12	0	4	4.10	4.24	4.48	4.85	5.40
	0.5	4.23	4.34	4.48	4.73	5.11	5.69
	1	4.38	4.48	4.63	4.88	5.28	5.86
16	0	4	4.10	4.24	4.48	4.85	5.40
	0.5	4.19	4.29	4.44	4.68	5.06	5.63
	1	4.31	4.41	4.56	4.81	5.20	5.77

Table 5. Coefficients k^* for the nonlinear (according to the second-degree parabola) stress distribution as a function of index κ

l_s/b_s	m	κ					
		0	0.2	0.4	0.6	0.8	1
4	0	4	4.10	4.24	4.48	4.85	5.40
	0.5	4.23	4.33	4.48	4.72	5.10	5.67
	1	4.34	4.44	5.58	4.83	5.21	5.78
8	0	4	4.10	4.24	4.48	4.85	5.40
	0.5	4.11	4.21	4.36	4.60	4.97	5.53
	1	4.16	4.26	4.41	4.65	5.02	5.59
12	0	4	4.10	4.24	4.48	4.85	5.40
	0.5	4.07	4.17	4.32	4.55	4.93	5.49
	1	4.11	4.20	4.35	4.59	4.96	5.52
16	0	4	4.10	4.24	4.48	4.85	5.40
	0.5	4.05	4.15	4.30	4.53	4.91	5.47
	1	4.08	4.18	4.32	4.56	4.93	5.49

Table 5 show that: 1) with an increase in the index κ and the parameter m , the values of the plate buckling coefficients (k, k^*) increase, 2) with an increase in plate length, the favorable effect of longitudinal stress variation decreases, but the favorable effect of elastic restraint remains, 3) smaller values of k and k^* for the same values of parameters (κ, m, γ_s) were obtained for nonlinear stress distribution.

Based on numerous computational tests (performed also for intermediate values of parameters m and κ), it was found that a safe (slightly conservative) estimate of the coefficient k^* can be obtained from formulas (9) and (10) in the following ranges: $3 \leq \gamma_s \leq 20$; $0 \leq m \leq 1$; $0 \leq \kappa \leq 1$. For very long plates ($\gamma_s > 20$), for $0 \leq \kappa \leq 1$, a conservative estimate of the coefficient k^* can be obtained directly from formula (9).

4. SUMMARY

Enhancing the accuracy of representing the behavior of thin-walled members, such as cold-formed ones, in engineering computational models is a natural direction in the development of modern design methods. Currently, there is an increased interest in approximation formulas which would take into account more advanced computational models of steel elements, e.g. [21, 22].

Taking into account both the index of fixity ($0 \leq \kappa \leq 1$) and longitudinal stress variation ($0 \leq m \leq 1$) in calculations of thin-walled members leads to a more accurate assessment of critical stress in relation to the computational model according to [2]. The standard model ignores the above-mentioned effects, which in many technically important cases leads to underestimation of σ_{crL} .

The approximation formulas for the plate buckling coefficient k^* provided in this paper allow for a relatively straightforward determination of critical stress in compressed and one-side elastically restrained internal walls with longitudinal stress variation. Such a plate-load system can model the behavior of the compression flange of a thin-walled section subjected to bending.

Correct determination of the elastic critical stress of local buckling under loading that induces longitudinal stress variation determines the interval of pre-buckling behavior of a thin-walled member [8, 14] and limits the validity interval of Vlasov's theory [4] in the elastic range ($\sigma_{crL} \leq f_y$). Critical stress determined in this way serve for a more precise calculation of the relative slenderness of the critical plate and the assessment of the design resistance of the cross-section based on the CPM [3].

APPENDIX

Approximation formulas for plate buckling coefficients k^* :

1) linear stress distribution:

$$k^*(\kappa, m, \gamma) = 4 + 0.452\kappa + 0.95\kappa^3 + \left[3.689m - 2.692m^2 + 1.26m^3 + (0.348m - 0.343m^2 + 0.18m^3)\kappa + (0.521m - 0.406m^2 + 0.181m^3)\kappa^3 \right] / \gamma_s^{(0.68+0.04m)} \quad (10)$$

2) non-linear stress distribution (according to the second-degree parabola):

$$\begin{aligned}
 k^*(\kappa, m, \gamma) = & 4 + 0.452\kappa + 0.95\kappa^3 + \left[3.863m - 6.653m^2 + 6.836m^3 - 2.603m^4 + \right. \\
 & + \left(1.135m - 3.311m^2 + 3.964m^3 - 1.621m^4 \right) \kappa^2 + \\
 & \left. + \left(-0.429m + 1.819m^2 - 2.355m^3 + 0.995m^4 \right) \kappa^3 \right] / \gamma_s^{(1.01+0.04m)}
 \end{aligned} \quad (11)$$

References

- [1] EN 1993-1-3:2006 Eurocode 3 – Design of steel structures – Part 1-3: General rules – Supplementary rules for cold-formed members and sheeting.
- [2] EN 1993-1-5:2006 Eurocode 3 – Design of steel structures – Part 1-5: Plated structural elements.
- [3] Szychowski A.: *Computation of thin-walled cross-section resistance to local buckling with the use of the Critical Plate Method*. Archives of Civil Engineering, 2016, Vol. 62, Issue 2, 229-264; doi:10.1515/ace-2015-0077.
- [4] Vlasov V.Z.: *Thin-Walled Elastic Beams*. Israel Program for Scientific Translations, Jerusalem, 1961.
- [5] EN 1993-1-1:2006 Eurocode 3 – Design of steel structures – Part 1-1: General rules and rules for buildings.
- [6] Beale R.G., Godley M.H.R, Enjily V.: *A theoretical and experimental investigation into cold-formed channel sections in bending with the unstiffened flanges in compression*. Computer & Structures 79, 2001, 2403-2411, doi.org/10.1016/S0045-7949(01)00073-6.
- [7] Kotelko M., Lim T.H., Rhodes J.: *Post – failure behaviour of box section beams under pure bending (an experimental study)*. Thin-Walled Structures 38, (2000), 179-194, doi.org/10.1016/S0263-8231(00)00032-X.
- [8] Kowal Z., Szychowski A.: *Experimental determination of critical loads in thin-walled bars with Z-section subjected to warping torsion*. Thin-Walled Structures 75, 2014, 87-102, doi.org/10.1016/j.tws.2013.10.020.
- [9] Papangelis J.P., Hancock G.J.: *Computer analysis of thin-walled structural members*, Computer & Structures Vol. 56. No. 1. 1995, 157-176, doi.org/10.1016/0045-7949(94)00545-E.
- [10] Schafer B.W., Ádány S.: *Buckling analysis of cold-formed steel members using CUFSM: conventional and constrained finite strip methods*. Proceedings of the Eighteenth International Specialty Conference on Cold-Formed Steel Structures, Orlando, FL. October 2006.
- [11] Szychowski A., Brzezińska K.: *Local buckling and resistance of continuous steel beams with thin-walled I-shaped cross-sections*. Applied Sciences, 2020, 10(13), 4461, doi:10.3390/app10134461.
- [12] Bulson P.S.: *The Stability of Flat Plates*, Chatto and Windus, London 1970.
- [13] Jakubowski S.: *Buckling of thin-walled girders under compound load*. Thin-Walled Structures 1988, 6, 129-150, doi.org/10.1016/0263-8231(88)90004-3.
- [14] Szychowski A.: *A theoretical analysis of the local buckling in thin-walled bars with open cross-section subjected to warping torsion*. Thin-Walled Structures 76 (2014) 42-55, doi.org/10.1016/j.tws.2013.11.002.
- [15] Brzezińska K., Szychowski A.: *Stability and resistance of steel continuous beams with thin-walled box sections*. Archives of Civil Engineering, 2018, Vol. 64, Issue 4, 123-143; doi.org/10.2478/ace-2018-0048.
- [16] Szychowski A.: *Local stability of the compressed flange of a cold-formed thin-walled section* (in Polish). Zeszyty Naukowe Politechniki Rzeszowskiej Nr 276, Seria: Budownictwo i Inżynieria Środowiska, Zeszyt 58, Nr 3/2011/II, 307-314.
- [17] Kowal Z.: *The stability of compressed flange of plate girder with a box section* (in Polish). Zeszyty Naukowe Politechniki Wrocławskiej, Budownictwo 1965, 122, 73-85.
- [18] Kowal Z.: *The stability top metal plate of pontoon foundation* (in Polish). Węgiel Brunatny 1966; 4: 331-333.
- [19] Szychowski A.: *The stability of eccentrically compressed thin plates with a longitudinal free edge and with stress variation in the longitudinal direction*. Thin-Walled Structures 2008; 46 (5): 494-505, doi.org/10.1016/j.tws.2007.10.009.
- [20] Szychowski A.: *Stability of cantilever walls of steel thin-walled bars with open cross-section*. Thin-Walled Structures 94 (2015), 348-358, doi.org/10.1016/j.tws. 2015.04.029.
- [21] Gardner L., Fieber A., Macorini L.: *Formulae for calculating elastic local buckling stresses of full structural cross-sections*. Structures 17 (2019): 2-20, doi.org/10.1016/j.istruc.2019.01.012.

- [22] Piotrowski R., Szychowski A.: *Impact of support closed section ribs on the critical moment for lateral torsional buckling of steel beams*. Structure and Environment, vol. 10, no. 1, pp. 5-18, 2018, doi: 10.30540/sae-2018-001.

Acknowledgements

Internal scientific research financed from the research subsidy entitled: “Stability and resistance of steel compression and bending members under local and overall (internode) buckling”, No. 02.0.18.00/1.02.001, SUBB. BKWK. 23.002.



environment
environment



ASSESSMENT OF THE SUITABILITY OF SPECTRAL INDICES FOR DETECTING AREAS OF INCREASED STRESS AMONG PLANTS – A CASE STUDY OF THE BOTANICAL GARDEN IN KIELCE

OCENA PRZYDATNOŚCI WSKAŹNIKÓW SPEKTRALNYCH DO WYKRYWANIA OBSZARÓW WZMOŻONEGO STRESU WŚRÓD ROŚLIN – STUDIUM PRZYPADKU OGRODU BOTANICZNEGO W KIELCACH

SZYMON SYLWESTER SOBURA*
Kielce University of Technology, Poland

Abstract

An important factor threatening global security is climate change and its impact on changing rainfall patterns and seasonal temperature variability. For this reason, farmers and crop scientists are striving to detect plant stress as soon as possible and introduce preventive measures so that key decisions in maintaining plant health are made in a timely way. Currently, multispectral images acquired from UAVs (Unmanned Aerial Vehicles) make it possible to provide objective and reliable information related to the state of agro-ecosystems, the dynamics of changes occurring on them and the monitoring of natural resources in a rapid and non-contact method. In the present study, the suitability of low-altitude multispectral imaging for proper stress detection in plants was assessed. The botanical garden in Kielce, a site with a high biodiversity of plant specimens, was chosen as the testing ground. In this study, four spectral indexes maps were analysed in the form of: NDVI (Normalized Difference Vegetation Index), NDRE (Normalized Difference Red-Edge Index), GNDVI (Green Normalized Difference Vegetation Index) and the less frequently used PSRI (Plant Senescence Reflectance Index) for the assessment of plant health. PSRI values > 0.50 clearly identified areas of high stress, in contrast to the other spectral indices analysed in this study. The study confirmed the suitability of the PSRI for conducting monitoring activities in areas with varying crop characteristics in an efficient and rapid approach.

Keywords: Remote Sensing (RS), botanical garden, crop monitoring, stress detection, Plant Senescence Reflectance Index (PSRI), Unmanned Aerial Vehicle (UAV), Precision Agriculture (PA)

Streszczenie

Ważnym czynnikiem zagrażającym globalnemu bezpieczeństwu są zmiany klimatyczne i ich wpływ na zmiany wzorców opadowych oraz zmienność sezonowych temperatur. Z tego powodu osoby zajmujące się ochroną walorów przyrodniczych oraz upraw dążą do jak najszybszej detekcji stresu roślin i wprowadzeniu działań profilaktycznych, aby kluczowe decyzje w utrzymaniu zdrowia roślin zostały podjęte w odpowiednim czasie. Obecnie zdjęcia multispektralne pozyskane z UAV (ang. Unmanned Aerial Vehicles) umożliwiają dostarczenie obiektywnej i wiarygodnej informacji związanej ze

stanem agrosystemów, dynamiki zmian na nich zachodzących oraz monitorowania zasobów przyrodniczych w sposób szybki i bezkontaktowy. W niniejszej pracy oceniono przydatność zobrazowań multispektralnych z niskiego pułapu do prawidłowej detekcji stresu u roślin. Jako poligon doświadczalny wybrano ogród botaniczny w Kielcach, będący obiektem o dużej bioróżnorodności okazów roślin. W pracy przeanalizowano cztery mapy wskaźników spektralnych w postaci: NDVI (ang. Normalized Difference Vegetation Index), NDRE (ang. Normalized Difference Red-Edge Index), GNDVI (ang. Green Normalized Difference Vegetation Index) oraz rzadziej stosowany wskaźnik PSRI (ang. Plant Senescence Reflectance Index) pod kątem oceny kondycji zdrowotnej roślin. Wartości wskaźnika PSRI > 0,50 w sposób jednoznaczny zidentyfikowały obszary wysokiego stresu w odróżnieniu od pozostałych analizowanych w pracy wskaźników spektralnych. Badania potwierdziły przydatność wskaźnika PSRI do prowadzenia działań monitoringowych na obszarach o zróżnicowanej charakterystyce uprawianych roślin w sposób efektywny i szybki.

Słowa kluczowe: teledetekcja, ogród botaniczny, monitoring upraw, detekcja stresu, wskaźnik spektralny PSRI, bezzałogowy statek powietrzny (BSP), rolnictwo precyzyjne

1. INTRODUCTION

Historically, plant diseases were monitored visually by people who had expertise in this area of science. Observations of plant phenology carried out in this way were subject to bias and observer error, which contributed to the search for an alternative technique for monitoring plant health [1]. Currently, multispectral imagery acquired from UAVs makes it possible to provide objective and reliable information related to the condition of the agro-ecosystem, the dynamics of changes occurring on them and the monitoring of natural resources in a rapid and non-contact manner [2-4]. Conducting monitoring activities in botanical garden areas through the implementation of unmanned aerial vehicle technology, allows not only a rapid response to local anomalies (e.g. in the form of waterlogging, drought, increased pest activity) but also the estimation of yield capacity and maintenance of plants in good health [5]. Unfortunately, many scientific papers focus on the use of multispectral UAV imagery for specific crops and thus fail to test the versatility of this technology for a wider range of plant species.

Monitoring activities to assess plant growth and condition have been carried out for many years using imagery that captures infrared radiation [6]. Remote sensing provides objective documentation, and the scale, resolution and nature of the imaging can be tailored to the specifications of the task at hand [7]. Thanks to the miniaturisation of aerial cameras and thus their increased availability, remote sensing methods for environmental monitoring have found a number of applications in the life sciences. Unmanned aerial vehicles enable the adaptation of compact sensors (e.g. multi- and hyperspectral cameras), making it possible to carry out cyclic low-altitude flights with greater safety than manned aircraft, thereby increasing the spatial resolution of

the images [1, 6, 8]. Satellite platforms with mounted remote sensing sensors can be an alternative. However, they have some limitations for monitoring plant physiology. The main limitations are the large Ground Sampling Distance (GSD), insufficient revisit time during the growing season and sensitivity to meteorological conditions (cloud cover). In addition, the low spatial resolution of satellite imagery (e.g. MODIS satellite, Landsat 7 and 8) translates into the 'mixed pixels' phenomenon and degrades the spectral purity of the samples under study, which in turn affects the outcome of the quantitative and qualitative analyses. For this reason, images acquired by UAVs appear to be the right direction for the acquisition of spatial information on plant vegetation in a rapid and less weather-dependent manner.

The main objective of the research presented in this paper was to assess the suitability of low-altitude multispectral imaging acquired with the Micasense Red-Edge MX camera for the successful detection of stress in plants. The indirect aim of the experiments carried out was to determine the potential of the NDVI, NDRE, GNDVI spectral indices, and in particular the PSRI index, for the rapid identification of anomalies within the analysed experimental facility, which was the botanical garden in Kielce (Poland).

2. LITERATURE REVIEW

Many European gardens were established as facilities for growing medicinal plants and are often an integral part of Europe's cultural heritage. The current purpose of botanical gardens is most often to protect plant diversity. According to data presented in the paper [9], at least 20% of currently existing plant species are threatened with extinction. This can have implications for human innovation when trying to meet challenges such as food security and biodiversity conservation. Rational land management requires

reliable information on land cover, land use and changes occurring [10]. Information provided from a number of sources [3, 11-13] highlights that photogrammetry and low-altitude remote sensing data can be useful for a better understanding of soil processes and plant assimilation apparatuses, which in turn can translate into more effective crop management.

A significant factor threatening global security on many levels is climate change and its impact on changes in precipitation patterns and seasonal temperature variability. For this reason, conservationists aim to detect plant stress as soon as possible and introduce preventive measures so that key decisions in maintaining plant health are made in a timely manner [14]. Phenological observations are classically carried out for specific plant species in botanical gardens, small research areas or agricultural fields around the world and date back to the 19th century [15]. Although these observations are of interest for studying trends in phenology over time and their causal factors, they are often spotty and therefore provide only little information on spatial variability. In this context, low-altitude remote sensing data can provide valuable information on phenology and enable dynamic mapping of vegetation development and monitoring of their stress conditions, i.e. the response of plants to unfavourable environmental conditions. UAV imagery – and in particular multispectral imagery and the spectral indices calculated from it – has been used repeatedly by other researchers to detect symptoms of plant impairment due to biotic and abiotic factors [1, 5]. Spectral indices are a set of ratios and mathematical transformations of the reflectance intensity recorded by a detector in different spectral channels. Many spectral indices are calculated from spectral channels registering the red and infrared bands because of the high correlation between the contrast in absorption of these bands and the health of the plant group analysed. This approach, thanks to its efficiency, has found wide application in the natural sciences, relating the values of spectral indices to the physical phenomena or physico-chemical parameters with which they correlate [16, 17].

A literature review [5, 14, 16, 18, 19] repeatedly highlighted the usefulness of remote sensing techniques for conducting effective monitoring of plant health and locating pest sites in growing areas. The authors' results [20] indicated an increase in pest abundance with a decrease in the NDVI index in both variants of the analyses conducted, i.e. using data from an aircraft and CIR composition and a

satellite recording spectral reflectance in multiple channels. Thus, the relationship between Hessian fly occurrence and the normalised difference vegetation index (NDVI) in winter wheat fields in Kansas (USA) was confirmed. This means that only the cooperation of remote-sensing specialists with biologists, allows the values of the obtained spectral indices to be correctly interpreted and the cause determining the reduced plant health to be known.

According to [17], remote sensing data can be used to detect and monitor plant species diversity. In their study, the authors highlighted that plant diversity (mono-cultural and multi-species) has a close relationship with remote sensing metrics and their productivity. Thus, the monitoring of flora-diverse areas should be considered individually for the plant species under study.

The development trend of plants depends on many conditions, including the occurrence of biotic and abiotic factors that negatively affect vegetation. Capturing the timing of groups of such factors based on in situ ground measurements is dependent on the plantation area. According to [11, 21], more and more plant care professionals are using drones to provide preventive measures in the aforementioned area. In this way, it is possible to reduce the potential risk of stressors among plants in areas with a large surface area and, as a result, to ensure the correct course of vegetation of plants at the most important moments of their development stage [3, 5].

The main role of UAVs in monitoring plant phenology is to acquire multispectral images that, when processed, enable the identification of hotspots (e.g. the presence of pests or insects) and regions at increased risk of drought or waterlogging. Furthermore, spatial and multitemporal maps of spectral indices allow observations of the effects of applied nitrogen fertilisers and pesticides on vegetation development [16]. It is worth mentioning that in some scientific papers [1, 17], the authors identify low-altitude remote sensing as an information acquisition technique for the construction of predictive models of plant condition based on artificial intelligence. This approach makes it possible to increase the precision of plant disease identification and monitoring at an early stage, which seems a good research direction.

Digital documentation of botanical gardens is important not only for maintenance work, but also for the proper management of the site and the provision of tourist and educational services. The diverse landscape forms and variety of nurtured plants within

a botanic garden, translate into the uniqueness of such creations on a national scale [22, 23]. Given the complex layout of botanic gardens and the diverse flora, modern surveying technologies may prove to be an appropriate form of recording and then processing and sharing the information available in botanic gardens through GIS [18, 24].

All the monitoring activities and examples presented earlier, create UAV technology as a rich support tool during the management of a botanic garden, thus influencing relevant decisions and policies for the management of the site.

3. METHODOLOGY

The work involved in the measurement experiment was divided into four main stages:

1. Selection of a representative testing area.
2. Establishment of a photogrammetric network and acquisition of UAV images with an adapted optical and multispectral camera, at two different vegetation periods.
3. Performing optical and multispectral orthomosaics for two time periods and calculating NDVI, NDRE, GNDVI and PSRI spectral indexes maps on their basis.
4. Field verification of the results obtained and assessment of the suitability of the selected spectral indices for the study.

The workflow adopted was to evaluate low-altitude remote sensing technology for conducting analyses based on spectral indices for a wide range of plants. Compared to thematically similar studies in the field of remote sensing environmental monitoring, an innovation in the presented methodology is the implementation of the rarely used spectral index PSRI to assess the condition of a wide range of plant species. The following chapters describe in detail the stages of the experimental fieldwork and computational work.

3.1. Selection of the test object

The object of the research was a botanical garden with an area of approximately 11 hectares and located in the city of Kielce, the capital of the Świętokrzyskie Voivodeship in Poland. The detailed location of the study object is shown in Figure 1.

The garden is located on the slopes of the Karczówka mountain from where one can observe the panorama of the city of Kielce and the nearby ranges of the Świętokrzyskie Mountains (Geonatura Kielce – Botanical Garden Website, access: 20.11.2022). The area of the botanical garden is diverse in terms of

biodiversity and topography. The height differences within the garden reach 20 metres, while the terrain slopes towards the south.

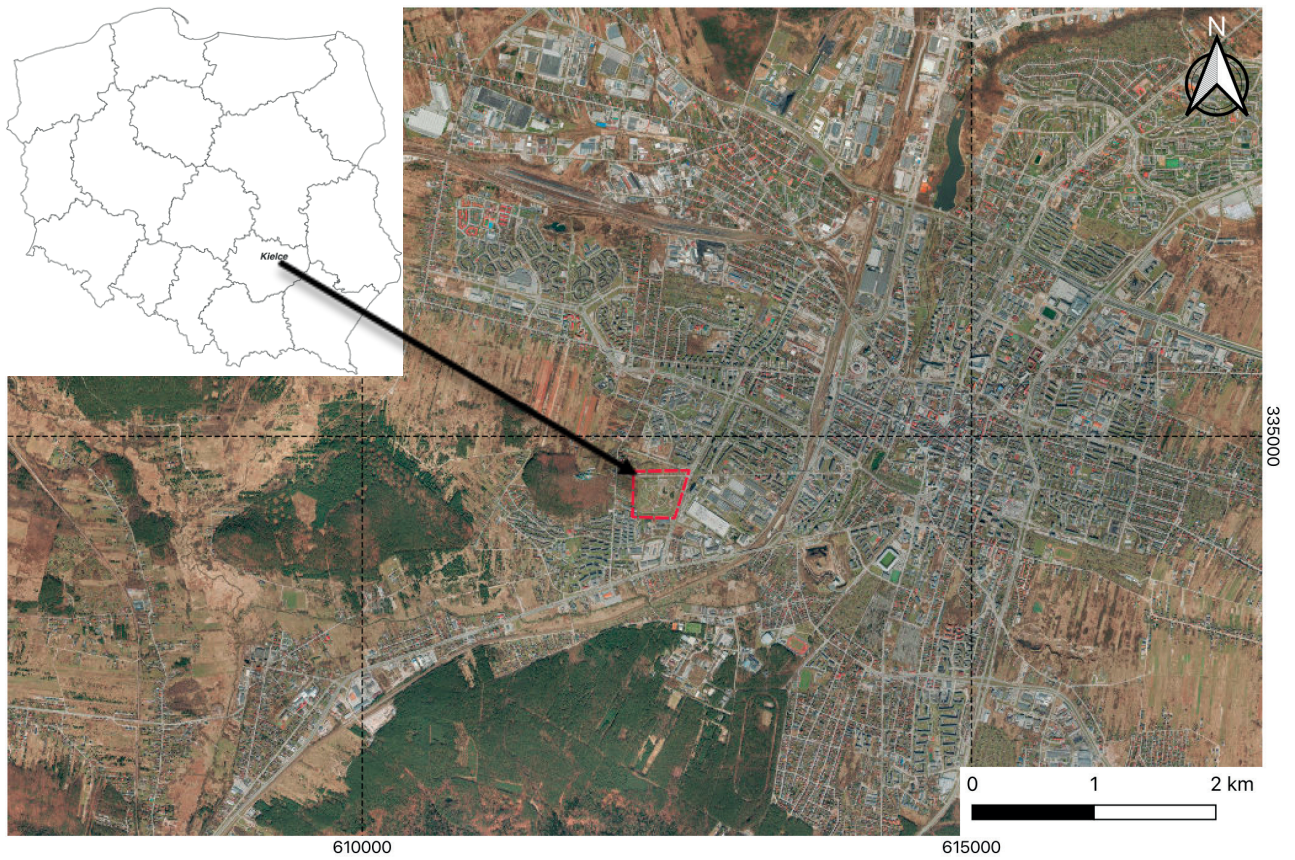
The botanical garden complex in Kielce comprises eight main sectors, with further plant collections including:

- Ornamental plants section – peonies, lilies, hydrangeas, roses, ornamental grasses;
- Section of useful plants – medicinal and spice plants, orchard plants, vineyard, flower meadow;
- Native flora section – upland mixed fir woodland, sub-continental oak-hornbeam, light oak, heathland;
- Water and marsh flora section – water lilies, native water and marsh plants, water scythes;
- Demonstration garden section – French, country, oriental and Japanese gardens.

There were two main reasons for choosing the site presented for the study. Firstly, the botanical garden was considered to be a representative example of a large diversity of plant species contained within a small area. The second reason was that there was a history of repeated disease of some of the plant specimens, including: the roses and azaleas collection (over 15 acres), the heathland (approximately 20 acres) and the East Asian woodland collection (approximately 10 acres). The advice of the garden personnel on how to verify the observations made was an added advantage of the chosen research site. Thus, the research discussed in the publication was practical and the results obtained could be implemented to improve the functioning of the site presented in the paper and to better understand the phenology of the existing plants in the garden.

3.2. Description of study

The measurement experiment was planned during the vegetation period of plants located on the grounds of the botanical garden in Kielce. Two flights by unmanned aerial vehicle were carried out on 24.05.2022 and 13.07.2022, with variable weather conditions (variable cloud cover and wind direction) during each measurement day. In each measurement series, an X5S optical camera (15 mm focal length) and a Micasense Red-Edge MX multispectral camera were attached to the drone. The execution of the two UAV flights at different times was intended to assess the trend of plant development and to select a more favourable period of plant phenology for subsequent studies using flying measurement platforms and analyses based on spectral indices. A detailed diagram of the work carried out for the two UAV flights carried out is presented in Figure 2.



a)



b)



c)

Fig. 1. Location of the botanic garden in Kielce: a) location of the research object in Poland (coordinates in the Polish small-scale development system, EPSG: 2180), b) top view of the botanic garden, c) view of the garden in the north-western direction

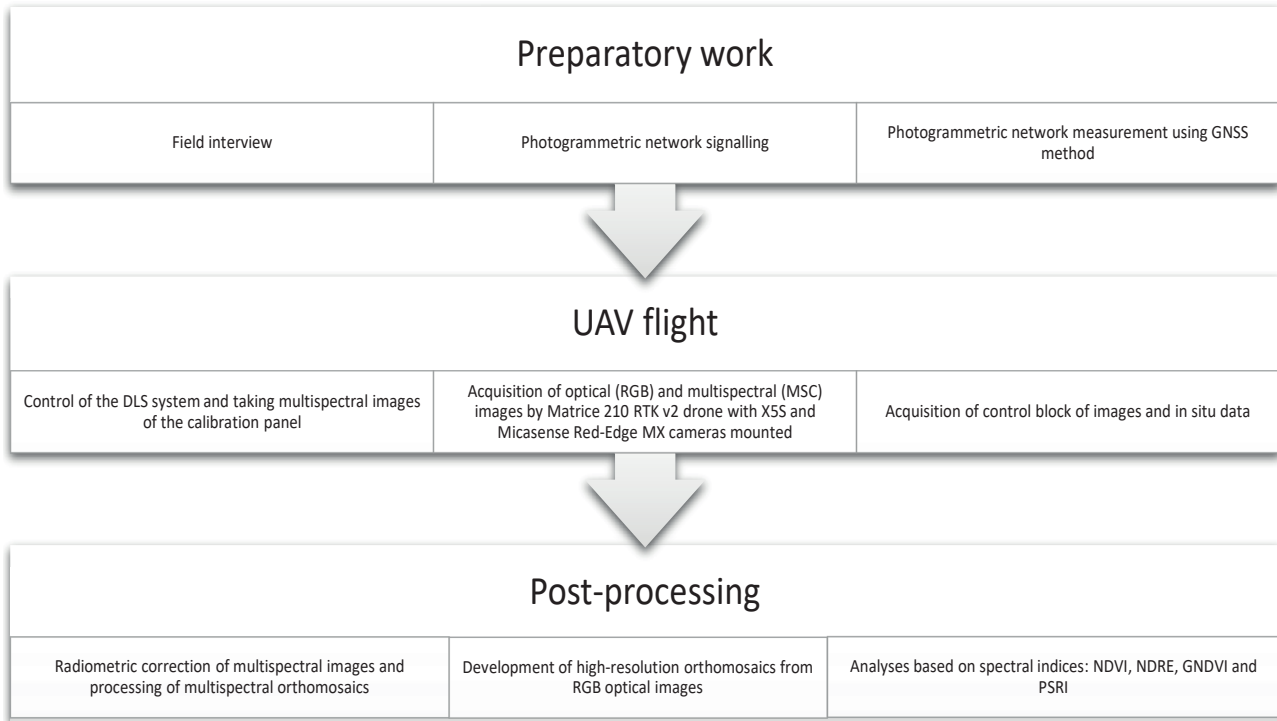


Fig. 2. The workflow used in the study

3.3. Field work

The work began with a field interview to identify field details that act as a natural photogrammetric network for the absolute orientation of the images. The survey network was necessary to ensure high geometric accuracy of the final products of the image processing and, as a result, to enable reliable comparative analyses from the two measurement periods. The terrain details, which are usually kerbstones or manhole covers, were measured using GNSS (Global Navigation Satellite System) technology. For this purpose, a Topcon HiPer HR satellite receiver was used, operating with reference to the TPI NETpro reference station network. A total of 16 points were measured as ground control points and check points. The accuracy of the spatial coordinates of the measured points was $mp_{XYZ} < 3$ cm.

The aerial missions were carried out using a Matrice 210 RTK v2 unmanned aircraft (Fig. 3), which allows adaptation and operation with two optical sensors simultaneously. The a priori parameters of the photogrammetric flight were the same for both time periods analysed (May and July). The projected field pixel was 1.8 cm/pix for the X5S optical camera and 5.7 cm/pix for the multispectral camera. The overlap and cross-sectional coverage images were 70%, respectively, which is in line with the experience

of other researchers carrying out UAV missions for surface mapping [6, 26]. In addition, the flight of the UAV was signalled to the spatial information services through the teleinformation system recommended by the Polish Air Navigation Services Agency (PANSNA).



Fig. 3. Matrice 210 RTK v2 unmanned aerial vehicle used in the study, with the Micasense multispectral camera (left side) and X5S optical camera (right side) and DLS sensor (top of the drone) mounted

Table 1 presents the specifications of the Micasense Red-Edge MX five-channel multispectral camera used in the study. Before the UAV flight and after the UAV mission, images of the calibration panel were acquired. Due to variable cloud cover during both survey days (24.05.2022 and 13.07.2022), ambient irradiance information was additionally recorded via the Downwelling Light Sensor (DLS) so that the results from the radiometric correction performed would be more accurate.

Table 1. Micasense Red-Edge MX multispectral camera specifications

Weight	231.9 g	
Spectral Bands	Blue, Green, Red, Red edge, Near-IR, 12-bit RAW for each	
Dimensions	8.7 cm x 5.9 cm x 4.5 cm	
Wavelength (nm)	Band 1	Blue – 475 nm center, 32 nm bandwidth
	Band 2	Green – 560 nm center, 27 nm bandwidth
	Band 3	Red – 668 nm center, 14 nm bandwidth
	Band 4	Red edge – 717 nm center, 12 nm bandwidth
	Band 5	Near-IR – 842 nm center, 57 nm bandwidth
Ground Sample Distance (GSD)	8 cm per pixel (per band) at 120 m AGL	

Source: Micasense Producer Website, access: 20.11.2022.

3.4. Control measurements

In order to control the results obtained from the analyses based on spectral indices, an additional block of multispectral images was acquired for each time period. In total, four blocks of multispectral images were acquired. For the analyses, the most favourable blocks of photos were adopted in terms of the recorded change in cloudiness, i.e. those blocks of photos with the smallest change in cloudiness. In addition, the moisture content of plants and soil in the botanic garden was controlled in a point-based manner, using moisture sensors. This allowed the values of the vegetation indices to be additionally related to the environmental factor of water deficiency.

3.5. Image post-processing and spectral indices

The acquired UAV image blocks, were processed in Agisoft Metashape software. Radiometric calibration was carried out for multispectral imagery to convert the raw Digital Number (DN) into a physical radiance value. Due to the variable illumination of the botanical garden at the time of aerial data acquisition, a calibration panel with known reflectance for the different ranges

of recorded electromagnetic waves and parameters from the light sensor regarding ambient irradiance were used for the radiometric calibration. In order to carry out aerotriangulation of blocks of acquired images combined with simultaneous self-calibration of the UAV camera during its operation, natural terrain details were used as ground control points with known spatial coordinates. The results of the in-camera work were five-channel multispectral orthomosaics for two time periods and high-resolution RGB orthomosaics with a geometric resolution of 2 cm/pix. The mean squared error of the model fit on the 10 check points did not exceed $mp_{xyz} < 20$ cm in any case. Multichannel multispectral orthomosaics were used to calculate the values of the characteristic spectral indices. High-resolution RGB orthomosaics, on the other hand, were used to support the interpretation of indicator values. In the present study, four spectral indices, computable from Micasense Red-Edge MX camera images, were determined as: NDVI, NDRE, GNDVI and PSRI.

The NDVI described by equation (1) is the most widely recognised and used spectral index for assessing plant development. Through its strong correlation with chlorophyll content, it allows the assessment of photosynthesis and monitoring activities during the plant growing season [28]:

$$NDVI = \frac{\rho_{NIR} - \rho_{RED}}{\rho_{NIR} + \rho_{RED}} \quad (1)$$

where ρ_{NIR} are DN values which are a measure of the reflectivity of electromagnetic radiation in the near-infrared ($\sim 0.84 \mu\text{m}$), and ρ_{RED} values of the reflectivity of the red band of the optical radiation spectrum ($\sim 0.68 \mu\text{m}$).

The NDRE spectral index has a similar application to the NDVI index cited earlier. The domain of both functions is also identical, being in the range $<-1.0; 1.0>$. It is often used to assess the condition of plants for which the NDVI index quickly reaches high values [16]. It also allows the stress of the lower part of tall plants, rather than the top layer of crop crowns, to be assessed and is described by equation (2):

$$NDRE = \frac{\rho_{NIR} - \rho_{RED-EDGE}}{\rho_{NIR} + \rho_{RED-EDGE}} \quad (2)$$

where $\rho_{RED-EDGE}$ is the DN (Digital Number) values which is a measure of electromagnetic reflectivity at the red edge ($\sim 0.72 \mu\text{m}$).

The GNDVI index is calculated based on equation (3). It has found general application in precision

agriculture for monitoring plant water stress and photosynthesis [14, 17]. It is correlated with soil and plant nitrogen content and is therefore used to assess the quality of fertilisation of plant care areas and the uptake of nitrogen itself by crops:

$$GNDVI = \frac{\rho_{NIR} - \rho_{GREEN}}{\rho_{NIR} + \rho_{GREEN}} \quad (3)$$

where ρ_{GREEN} is the spectral channel with the recorded electromagnetic reflection in the green range ($\sim 0.56 \mu\text{m}$).

The PSRI is sensitive to the ratio of carotenoids to chlorophyll. For Micasense Red-Edge MX camera images, calculated as in formula (4). An increased PSRI indicates increased stress in plants [28]:

$$PSRI = \frac{(\rho_{RED} - \rho_{BLUE})}{\rho_{RED-EDGE}} \quad (4)$$

where ρ_{BLUE} is the spectral channel with the recorded reflection of electromagnetic radiation in the blue range ($\sim 0.47 \mu\text{m}$).

The raster algebra was carried out in the free software Qgis, in which the spatial maps of the previously mentioned spectral indices were also created. For all map compositions, the same region was chosen to enhance the significant features by using linear histogram stretching [29]. This made it possible to reliably compare the resulting maps of spectral indices between each other. The choice of spectral indices selected for the study was mainly dictated by the low spectral resolution of the Micasense Red-Edge MX camera. Initial data mining and statistical tests were performed in RStudio software, using the dplyr and sqldf libraries.

4. RESULTS

4.1. Maps of spectral indices

Processing of the acquired UAV images resulted in a high-resolution orthomosaic for each time period, followed by four maps of the spatial distribution of spectral indices. Due to the variable cloud cover during both measurement days, analyses on the reflectance maps were abandoned. By focusing only on the spectral indices, the influence of two factors on the results of the quantitative analyses, i.e., the variable illumination of the scene and the ground denivelations, was minimised. Figure 4 presents the resulting orthomosaics and maps of the calculated spectral indices from the first measurement series, conducted on 24.05.2022.

The correct progress of the vegetation process in the southern part of the botanical garden was confirmed on the maps of NDVI (Fig. 4b) and NDRE (Fig. 4c) indicators. This is evidenced by increased values of spectral indices (tones of blue color) relative to areas of poorer health (colors from orange to red). The lush vegetation in the southern complex is also confirmed by the high-resolution orthomosaic (Fig. 4a). The northeastern part of the botanical garden was being prepared for lily planting, hence the exposed soil and underestimated values of all spectral indices are evident. Increased PSRI values (Fig. 4e) indicative of additional plant stress, are mainly found among areas with exposed soil, which is justified by the increased temperature of these areas and thus increased vulnerability to drought. In contrast, the highest PSRI values ($PSRI > 0.50$) were recorded only for plants occurring in the azalea and heathland section. The thresholding of PSRI values was done by interpreting the PSRI map histogram and cutting off extreme outliers from the set. Subsequent batches of plants were analysed in detail. No anomalies were observed among the tall trees, confirming that the development of the trees is consistent with their phenology.

The values of the NDVI and NDRE indices in the central part of the botanical garden, in the complex of roses and azaleas (inside the marked red outline in Fig. 4a, right side) show underestimated values relative to nearby planted areas. The weakness of the plants in the garden section in question is also confirmed by the GNDVI index (Fig. 4d). This may indicate incorrect nitrogen uptake by the plants or washing away of applied fertilisers during rain, which is likely due to the high slope of the site. A similar trend was observed in the heathland section (inside the marked red outline in Fig. 4a, left side). Thus, both plant complexes were singled out as areas with a higher risk of plant stress and were subjected to detailed analyses in the remainder of the study. The results obtained confirm the problems already signalled by the Botanic Garden staff with the plant complexes mentioned. No disturbances were observed in the health condition of the plants located in the area of the 'East Asian Forest' section, which may mean that the preventive activities introduced have had a positive effect.

The localised anomalies shown in Figure 5a are characterised by a large contrast in the values of the spectral indices relative to other plants of the same type.

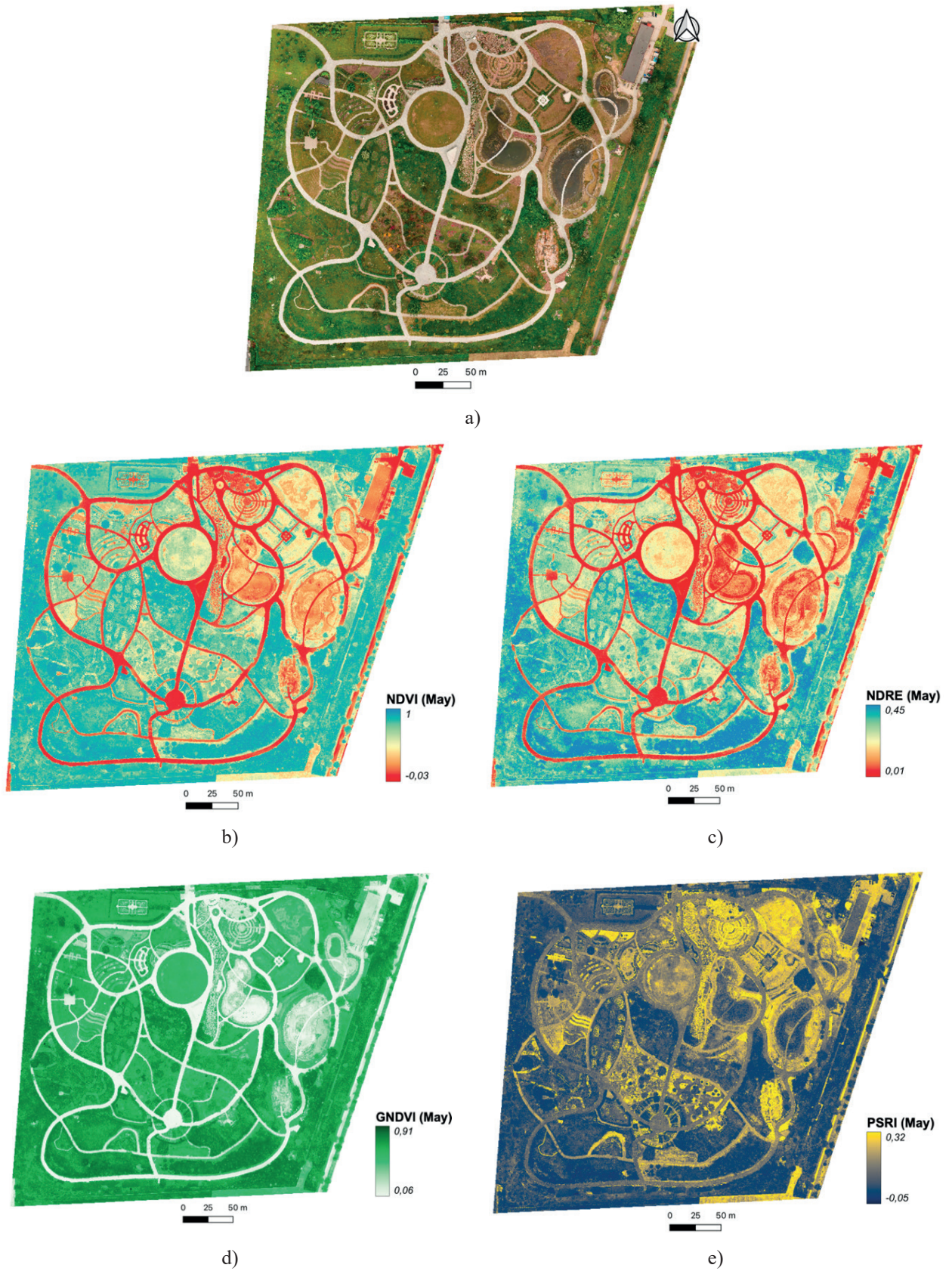


Fig. 4. Botanical Garden in Kielce for the first measurement series (May), presented as: a) orthomosaic, b) NDVI, c) NDRE, d) GNDVI, e) PSRI

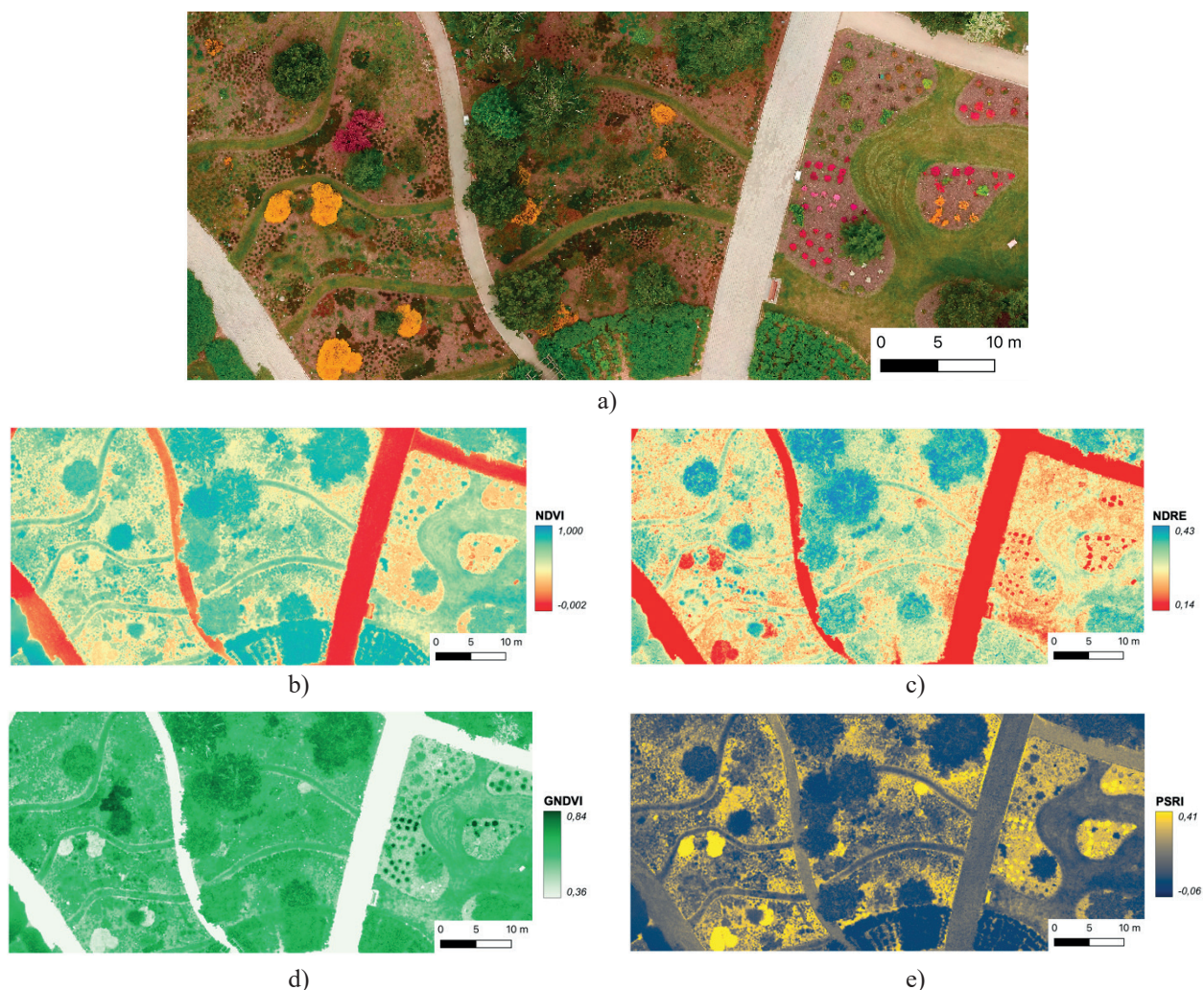


Fig. 5. Localized anomalies within the heathland (left side) and roses and azaleas (right side) sections of the botanical garden against: a) orthomosaic, b) NDVI, c) NDRE, d) GNDVI, e) PSRI

These anomalies may be due to the sensitivity of the two plant complexes presented earlier to changes in biochemical parameters in the form of chlorophyll and nitrogen concentrations. The chosen time period, i.e. the end of May, was advantageous for conducting environmental analyses due to favourable and stable atmospheric conditions preceding the UAV flight carried out – low rains, temperatures oscillating in the range of 16-20°C. On the basis of in situ measurements, the factors of waterlogging and drought were additionally excluded as factors that could negatively affect the development of plants during their growing season. The NDVI (Fig. 5b) and NDRE (Fig. 5c) indices confirm that plant development abnormalities affect not only the upper plant layer, but also the flowers located under the upper crown. Neither the NDRE and GNDVI index (Fig. 5d) can clearly determine whether the reason for the disturbance is a problem with the absorption of

organic compounds by the plants or a reduced alpha/beta chlorophyll content. Noteworthy is the PSRI index (Fig. 5e), which, after threshold reclassification, is the only one that directly typifies the plants presented for detailed analysis. This means that the PSRI can help improve monitoring activities to ensure the correct health of the plants in the Kielce Botanic Garden.

4.2. Temporal variation of spectral indices

The analysis of the variability of the values of the spectral indices was intended to find additional anomalies occurring inside the study object and to assess the prevention activities carried out in terms of localised disturbances in Figure 5. The second measurement series was carried out on 13.07.2022 (the results are included in Appendix 1). Figure 6 shows maps of the differences in the spectral indices NDVI, NDRE, GNDVI and PSRI between the two time periods analysed in the study.

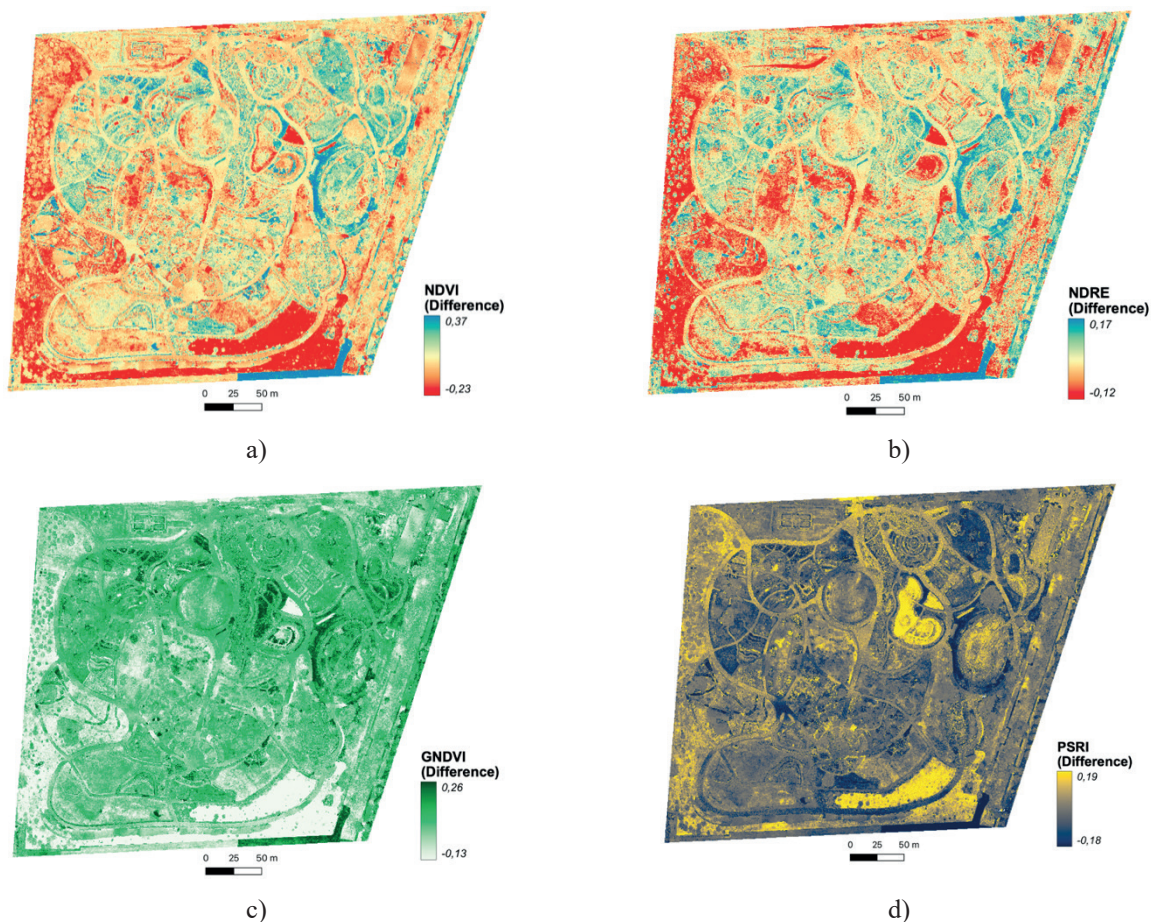


Fig. 6. Maps of differences in the values of spectral indices for the period May-July 2022: a) NDVI, b) NDRE, c) GNDVI, d) PSRI

The values of NDVI (Fig. 6a) and NDRE (Fig. 6b) differ significantly in the analysed period May-July. One of the reasons for this phenomenon, may be the weather conditions. The second UAV flight with the multispectral camera, was made after a prolonged period of sustained high temperatures and low rainfall. The drought factor was confirmed by in situ surveys. The soil moisture of the upper parts of the plants (north-facing) was only slightly lower than the soil moisture within the plant complex on the southern slope.

It should be noted that many of the plant genotypes present in the garden have different growing seasons. This in turn affected the values of the indices obtained from the different data acquisition periods. The values of NDVI and NDRE differences are also influenced by the soil background, which retouches the purity of the untreated spectral samples and affects the result of the quantitative analyses. This phenomenon is of particular importance in the context of the interpretation of all the indices presented in this paper for the north-eastern area of the garden, originally dominated by a large

part of the exposed soil. The decrease in the value of the GNDVI index (Fig. 6c) in the south-eastern part of the garden indicates a weaker vegetation pattern of the plants constituting the East Asian Forest section. This may indicate that the plants are past their peak growing season. The ratio of existing trees and shrubs in the East Asian woodland section to low vegetation (grasses) is low. The pruning of grasses prior to the period of increased heat may have led to increased vulnerability to grass infestation due to high temperatures and additional soil exposure – for which NDVI, NDRE and GNDVI values are generally lower. No grass withering was observed on the eastern side of the botanical garden, which is probably due to the large number of tall trees on this side of the garden, which provided shade for the surrounding plants. The PSRI difference map (Fig. 6d) did not identify areas of increased stress on the grown plants in this case with the exception of the previously mentioned grasses.

A preliminary comparison of the processed control images from the Micasense Red-Edge MX

multispectral camera for both time periods analysed, confirmed the observations made earlier. The areas presented in Figure 5 showed vegetation progression during the July period by increasing NDVI, NDRE and GNDVI values while decreasing PSRI. This means that the early diagnosis of the botanic garden's listed sections of roses and azaleas and the heathland as areas of abnormal plant growth enabled preventive treatments to be implemented effectively and correctly.

5. STATISTICAL ANALYSES

In order to perform a detailed analysis for the entire study site (Fig. 4) and areas with identified abnormalities with increased stress (Fig. 5), statistical parameters were calculated for the spectral indices used. Figure 7 shows their distribution along with their standard deviations for plants from the entire botanic garden. Only plant sections inside the botanic garden were considered for the calculation of the signatures. Areas of anthropogenic activity, artificial field details and shaded areas were excluded from the analysis. Nevertheless, during the initial data mining, outlier observations were noted from the entire data set. In order to eliminate their influence, the mean values of the spectral indices were calculated using a truncated average, trimming the minimum and maximum values with a threshold of 5%. The large values of individual standard deviations are due to the biodiversity of the cultivated plant specimens in the botanic garden.

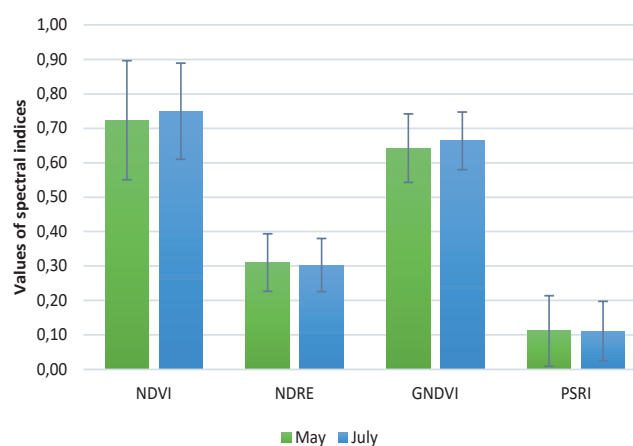


Fig. 7. Graph of the distribution of mean values of the analysed spectral indices for the period May-July, for the biologically active area of the botanic garden

The average NDVI values presented in Figure 7 increased in July, which in the present case means that the organic matter content increased. This is

also confirmed by the observed upward trend in the GNDVI index. During the first measuring series, there was a large amount of exposed soil prepared for the planting of further plant varieties. During the second measurement series, the area of exposed soil decreased due to the vegetation of later crop maturing. The mean value of the NDRE index decreased on 13 July compared to 24 May. This may indicate a better response of the NDRE index to plant water stress than the NDVI index. The reduction in plant and soil moisture during May-July was confirmed by in situ studies. The average values of the PSRI for the botanical garden plants in both analysed time periods, remained at a similarly low level. This result attests to the correct application of agrotechnical procedures and the high quality of plant care in the area of the entire botanic garden in Kielce.

The distribution of the scatter plots of spectral indices for the problematic plant complexes, which included heathland, azalea and roses (Fig. 5a), is presented in Figure 8. No extreme outlier observations were observed in any of the analysed cases. Figure 8a shows the quantiles of the distribution of spectral indices for the heathland. The largest scatter in the data occurred for the NDVI in July, for which half of the observations are in the range 0.45-0.80. The values of the PSRI in the heathland are significantly higher in May compared to the values of the PSRI in July – for which the observations in the second quantile are in the range 0.05-0.10. A similar trend in the values of the spectral indices for the analysed time periods occurs for the second problematic plant division (Fig. 8b). The conclusions obtained from the box plot analysis confirm the effectiveness of the applied preventive measures within the heathland, azalea and roses complex.

Due to the large ranges of the indicated index groups in Figure 8, it was decided to check the statistical significance of the obtained differences in spectral indexes for the analysed May-July time period. For this purpose, the student's t-test was used, assuming a normal distribution of the index values. The null hypothesis referred to the absence of significantly statistical differences between the NDVI, NDRE, GNDVI and PSRI index groups. The test results for the two problematic sections of the botanical garden are presented in Table 2.

The results of the student's t-test performed confirm the validity of the alternative hypothesis in each variant. The alternative hypothesis was that the obtained differences in the NDVI, NDRE, GNDVI and PSRI spectral index values are statistically significant.

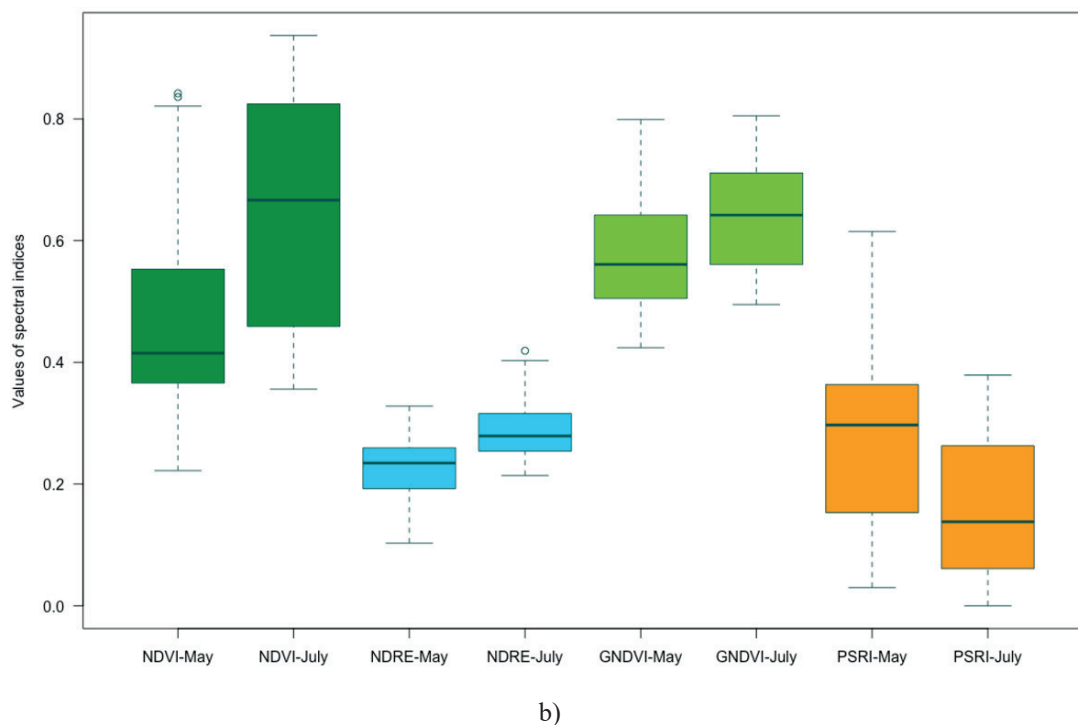
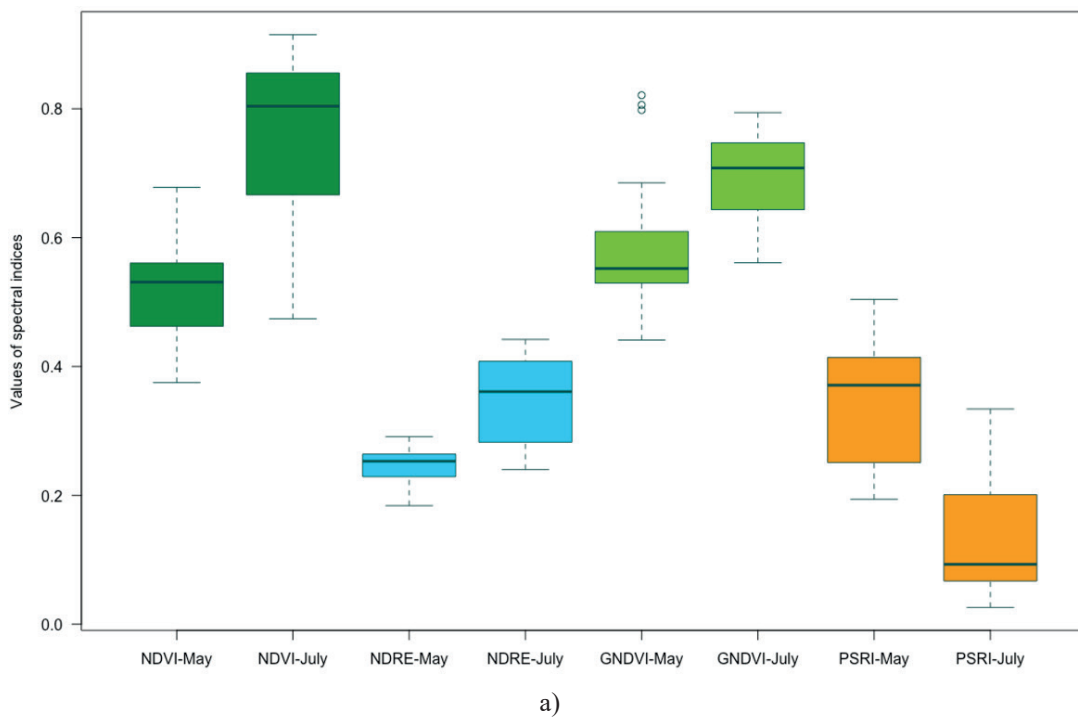


Fig. 8. Scatter plots of spectral indices for (a) heathland section, (b) azalea and roses section

Table 2. Summary of p-value results from Student's t-test ($\alpha = 0.05$)

Name of the plant section	Heathlands				Azaleas and roses			
	NDVI	NDRE	GNDVI	PSRI	NDVI	NDRE	GNDVI	PSRI
Comparable spectral indices for the period May - July								
p-value	< 0.001	< 0.001	0.002	< 0.001	< 0.001	< 0.001	< 0.001	< 0.001

6. SUMMARY AND CONCLUSIONS

This paper confirms that measurement methods involving low-altitude remote sensing techniques are useful for the correct detection of plant stress with unique flora and complex spatial characteristics. Remote sensing using unmanned aerial vehicles not only has the advantages of flexibility in terms of prevailing atmospheric conditions, high speed and high resolution of the acquired images, but also real-time advantages. Thus, the processing results of multispectral images from UAVs make it possible to effectively compensate for some of the disadvantages of ground-based measurements.

Failure to detect early stress in plants can result in stress extending beyond the recovery period of the nurtured flowers, causing vegetation dieback on a much larger scale. On the site of the botanical garden in Kielce, the vegetation problem of the heathland, azalea and roses complex was identified by mapping the NDVI, NDRE, GNDVI and PSRI spectral indices (Fig. 5). The PSRI index values, after thresholding $PSRI > 0.50$, clearly identified areas of high stress. This confirms the applicability of the PSRI index to conduct monitoring activities in botanical garden areas in an efficient and rapid method. The results obtained are identical to the predictions of the specialists working in the botanic garden presented.

Performing analyses on the processed remote-sensing images, for different vegetation periods, made it possible to identify the state of the greenery under study and to verify predictions of the vegetation course. The differences in the values of the spectral indices obtained for the May-July time period were found to be statistically significant (Table 2). Thus, the correct health condition of plants in the month of July and the effectiveness of preventive measures carried out in the botanic garden area were confirmed.

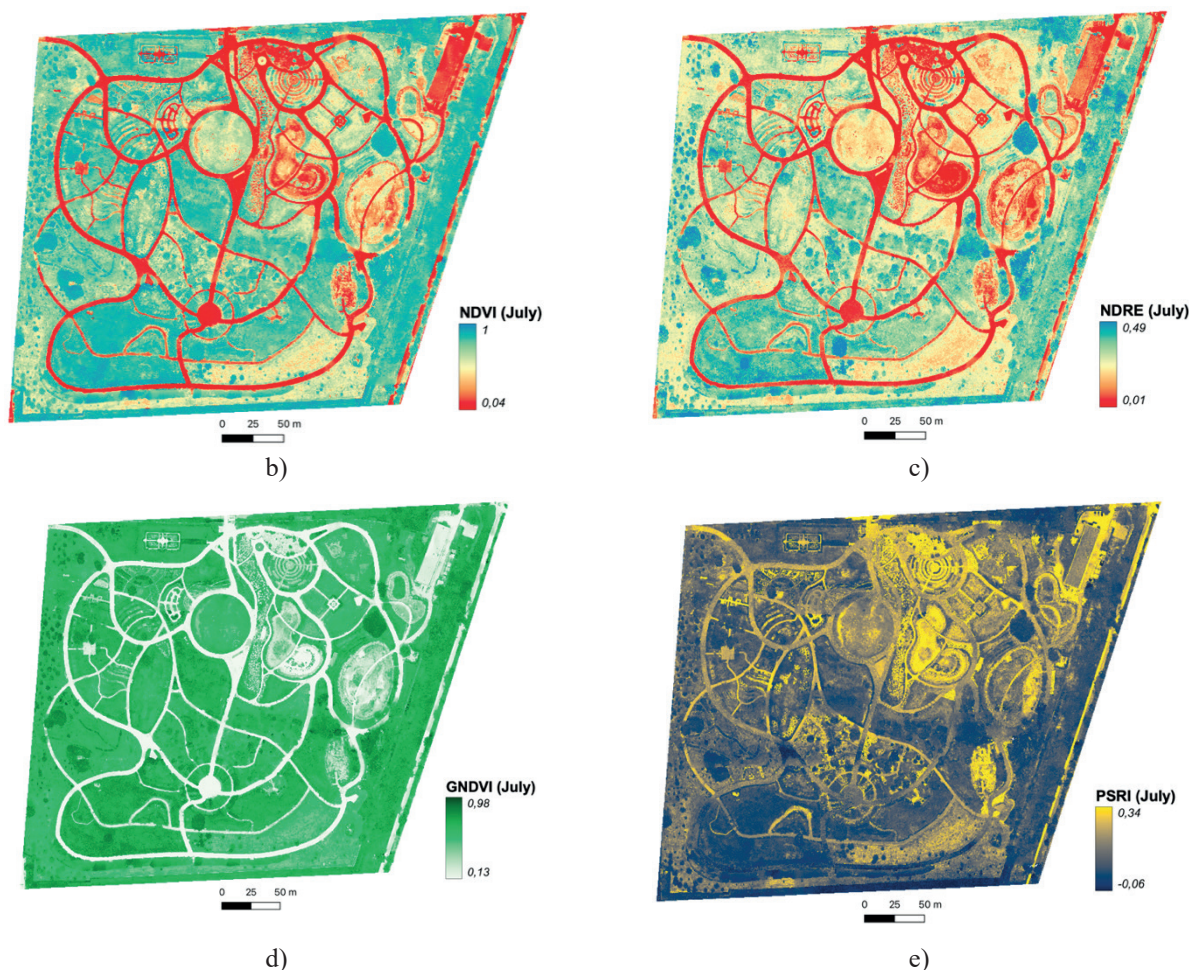
High-resolution satellite imagery remains expensive for many ecological applications – mainly due to the need to purchase the entire satellite scene, rather than the slice of area needed for analysis. In contrast, the cost of acquiring UAV imagery is rapidly decreasing, making it a potential tool for monitoring individual plants and local landscapes. Precision agriculture regularly uses high-resolution drone imagery, and the declining cost of low-altitude imagery is also making the technology accessible to ecologists.

UAV remote sensing is a critical tool to fill the time gap in satellite data for crop and plant monitoring. This paper demonstrates the usefulness of the Micasense Red-Edge MX camera to locate areas of high stress in advance, while enabling proactive management of plant complexes to improve the performance of the entire botanical garden.

APPENDIX



a)



Botanical Garden in Kielce for the second measurement series (July), presented as: a) orthomosaic, b) NDVI index, c) NDRE index, d) GNDVI index, e) PSRI index

References

- [1] Neupane K., Baysal-Gurel F.: *Automatic identification and monitoring of plant diseases using unmanned aerial vehicles: A review*, Remote Sens (Basel), vol. 13, no. 19, 2021, doi: 10.3390/rs13193841.
- [2] Stupen R., Ryzhok Z., Stupen N., Stupen O.: *The modeling of the yielding capacity of winter cereals due to satellite monitoring data of agricultural lands in Ukraine*, Geodesy and Cartography, vol. 47, no. 1, pp. 1-9, 2021, doi: 10.3846/gac.2021.11740.
- [3] Radoglou-Grammatikis P., Sarigiannidis P., Lagkas T., Moscholios I.: *A compilation of UAV applications for precision agriculture*, Computer Networks, vol. 172, 2020, doi: 10.1016/j.comnet.2020.107148.
- [4] Marzec P.: *Wykorzystanie wskaźników spektralnych do monitoringu stresu roślin na terenie ogrodu botanicznego w Kielcach*, Master Thesis, Kielce University of Technology, 2022.
- [5] Vanegas F., Bratanov D., Powell K., Weiss J., Gonzalez F.: *A novel methodology for improving plant pest surveillance in vineyards and crops using UAV-based hyperspectral and spatial data*, Sensors (Switzerland), vol. 18, no. 1, pp. 1-21, 2018, doi: 10.3390/s18010260.
- [6] Hunt E.R., Dean Hively W., Fujikawa S.J., Linden D.S., Daughtry C.S.T., McCarty G.W.: *Acquisition of NIR-green-blue digital photographs from unmanned aircraft for crop monitoring*, Remote Sens (Basel), vol. 2, no. 1, pp. 290-305, 2010, doi: 10.3390/rs2010290.
- [7] Mularz S., Drzewiecki W., Pirowski T.: *Teledetekcyjne metody rejestracji krajobrazu*, Roczniki Geomatyki, vol. V, no. 8, pp. 67-80, 2007.
- [8] Warchoń A.: *Analiza dokładności przestrzennej danych z lotniczego, naziemnego i mobilnego skaningu laserowego jako wstęp do ich integracji*, Archiwum Fotogrametrii, Kartografii i Teledetekcji, vol. 25, pp. 255-260, 2013.
- [9] Smith P.: *The challenge for botanic garden science*, Plants People Planet, vol. 1, no. 1, pp. 38-43, 2019, doi: 10.1002/ppp3.10.

- [10] Drzewiecki W.: Land-Use / Land Cover Monitoring Based on Multitemporal Remote Sensing Images, *Roczniki Geomatyki*, vol. VI, no. 3, pp. 132-142, 2008.
- [11] Velusamy P., Rajendran S., Mahendran R.K., Naseer S., Shafiq M., Choi J.-G.: Unmanned Aerial Vehicles (UAV) in Precision Agriculture: Applications and Challenges, *Energies (Basel)*, vol. 15, no. 217, pp. 1-19, 2022, doi: <https://doi.org/10.3390/en15010217>.
- [12] Balawejder M., Matkowska K., Colak H.E.: The Impact of Surveying Works on the Development of Smart City, *Geographic Information Systems Conference and Exhibition "GIS ODYSSEY 2018"*, no. 2623-5714, pp. 20-32, 2018.
- [13] Hejmanowska B., Twardowski M., Żądło A.: An application of the "traffic lights" idea to crop control in integrated administration control system, *Geomatics and Environmental Engineering*, vol. 15, no. 4, pp. 129-152, 2021, doi: [10.7494/geom.2021.15.4.129](https://doi.org/10.7494/geom.2021.15.4.129).
- [14] Sagan V. et al.: UAV/Satellite multiscale data fusion for crop monitoring and early stress detection, *International Archives of the Photogrammetry, Remote Sensing and Spatial Information Sciences*, vol. 42, no. 2/W13, pp. 715-722, 2019, doi: [10.5194/isprs-archives-XLII-2-W13-715-2019](https://doi.org/10.5194/isprs-archives-XLII-2-W13-715-2019).
- [15] Curnel Y., Oger R.: Agrophenology Indicators From Remote Sensing: State of the Art, *Isprs.Org*, pp. 31-38, 2007, [Online]. Available: http://www.isprs.org/proceedings/XXXVI/8-W48/31_XXXVI-8-W48.pdf.
- [16] Luo D. et al.: Using UAV image data to monitor the effects of different nitrogen application rates on tea quality, *J Sci Food Agric*, vol. 102, no. 4, pp. 1540-1549, 2022, doi: [10.1002/jsfa.11489](https://doi.org/10.1002/jsfa.11489).
- [17] Scher C.L. et al.: Application of remote sensing technology to estimate productivity and assess phylogenetic heritability, *Appl Plant Sci*, vol. 8, no. 11, pp. 1-14, 2020, doi: [10.1002/aps3.11401](https://doi.org/10.1002/aps3.11401).
- [18] Rafa N., Nuzhat S., Uddin S.M.N., Gupta M., Rakshit R.: Ecotourism as a forest conservation tool: An ndvi analysis of the sitakunda botanical garden and ecopark in chattogram, bangladesh, *Sustainability*, vol. 13, no. 21, 2021, doi: [10.3390/su132112190](https://doi.org/10.3390/su132112190).
- [19] Minh Chinh L.: Using Satellite Images To Retrieve the River Turbidity and Water Flow Velocity for Monitoring Their Influences on Bridge Substructures, *Structure and Environment*, vol. 15, no. 2, pp. 63-72, 2023, doi: [10.30540/sac-2023-006](https://doi.org/10.30540/sac-2023-006).
- [20] Backoulou F.G., Elliott N., Giles K., Alves T., Brewer M., Starek M.: Using multispectral imagery to map spatially variable sugarcane aphid infestations in sorghum, *Southwest. Entomol*, vol. 43, pp. 37-44, 2018, doi: <https://doi.org/10.3958/059.043.0122>.
- [21] Feng L., Chen S., Zhang C., Zhang Y., He Y.: A comprehensive review on recent applications of unmanned aerial vehicle remote sensing with various sensors for high-throughput plant phenotyping, *Comput Electron Agric*, vol. 182, 2021, doi: [10.1016/j.compag.2021.106033](https://doi.org/10.1016/j.compag.2021.106033).
- [22] Liang H., Li W., Lai S., Zhu L., Jiang W., Zhang Q.: The integration of terrestrial laser scanning and terrestrial and unmanned aerial vehicle digital photogrammetry for the documentation of Chinese classical gardens – A case study of Huanxiu Shanzhuang, Suzhou, China, *J Cult Herit*, vol. 33, pp. 222-230, 2018, doi: [10.1016/j.culher.2018.03.004](https://doi.org/10.1016/j.culher.2018.03.004).
- [23] Hajdukiewicz M., Romanyshyn I.: An accuracy assessment of spot heights on Digital Elevation Model (DEM) derived from ALS survey: case study of Łysica massif, *Structure and Environment*, vol. 9, no. 2, pp. 125-132, 2016.
- [24] Zhang Y., Song C., Sun G., Band L.E., Noormets A., Zhang Q.: Understanding moisture stress on light use efficiency across terrestrial ecosystems based on global flux and remote-sensing data, *J Geophys Res Biogeosci*, vol. 120, no. 10, pp. 2053-2066, 2015, doi: [10.1002/2015JG003023](https://doi.org/10.1002/2015JG003023).
- [25] Geonatura Kielce – Botanical Garden website. Accessed: Nov. 20, 2022. [Online]. Available: <https://geonatura-kielce.pl/ogrodbotaniczny/informacje-ogolne/>.
- [26] Sobura S.: Calibration of the Low-Cost Uav Camera on a Spatial Test Field, *Geodesy and Cartography*, vol. 48, no. 3, pp. 134-143, 2022, doi: [10.3846/gac.2022.16215](https://doi.org/10.3846/gac.2022.16215).
- [27] Micasense producer website. Accessed: Nov. 20, 2022. [Online]. Available: <https://support.micasense.com/hc/en-us>.
- [28] Sobura S., Hejmanowska B., Widłak M., Muszyńska J.: *The Application of Remote Sensing Techniques and Spectral Analyzes to Assess the Content of Heavy Metals in Soil – A Case Study of Barania Góra Reserve*, Poland, *Geomatics and Environmental Engineering*, vol. 16, no. 4, pp. 187-213, 2022, doi: [10.7494/geom.2022.16.4.187](https://doi.org/10.7494/geom.2022.16.4.187).
- [29] Pyka K.: *Wavelet-based local contrast enhancement for satellite, aerial and close range images*, *Remote Sens (Basel)*, vol. 9, no. 1, 2017, doi: [10.3390/rs9010025](https://doi.org/10.3390/rs9010025).

Acknowledgements

I would like to thank the entire employee team of Geonatura Kielce for making it possible to carry out research at the botanical garden, and Dr Agnieszka Pierścińska and Dr Bartosz Piwowarski, for their substantive input and valuable comments on the phenology of problematic fragments of the plant collection tended in the garden.



GROUNDWATER CONTAMINATION RISK ASSESSMENT IN THE FIRST EXPLOITABLE AQUIFER STRATUM WITHIN BODZENTYN MUNICIPALITY, ŚWIĘTOKRZYSKIE VOIVODESHIP

OCENA RYZYKA ZANIECZYSZCZENIA WÓD PODZIEMNYCH W PIERWSZEJ EKSPLOATOWANEJ WARSTWIE WODONOŚNEJ NA TERENIE GMINY BODZENTYN, WOJEWÓDZTWO ŚWIĘTOKRZYSKIE

EDYTA NARTOWSKA*
Kielce University of Technology, Poland

Abstract

The objective of this study is to assess the threat of contaminating groundwater originating from the first exploitative aquifer level in the municipality of Bodzentyn within the Świętokrzyskie Voivodship. The analysis included 23 representative groundwater intakes from MHP 816 Bodzentyn sheet. The various potential sources of groundwater contamination were identified. The intrinsic vulnerability of the first aquifer to contamination and the water recharge area were determined. In the results intakes potentially threatened by anthropogenic pollution were indicated. Providing information on the potential risks of groundwater contamination will help better plan environmental and decision-making activities in this area. The results can serve as a basis for policy development, land use and sustainable resource management in the municipality of Bodzentyn.

Keywords: groundwater intake, well, first aquifer, pollution, hazard, MHP-816

Streszczenie

Celem niniejszego opracowania jest ocena zagrożenia zanieczyszczeniem wód podziemnych pochodzących z pierwszego eksploatowanego poziomu wodonośnego w gminie Bodzentyn na terenie województwa świętokrzyskiego. Analizą objęto 23 reprezentatywne ujęcia wód podziemnych z arkusza MHP 816 Bodzentyn. Zidentyfikowano różne potencjalne źródła zanieczyszczenia wód podziemnych. Określono wewnętrzną podatność pierwszego poziomu wodonośnego na zanieczyszczenie oraz obszar zasilania. W wynikach wskazano ujęcia potencjalnie zagrożone zanieczyszczeniami antropogenicznymi. Dostarczenie informacji na temat potencjalnego ryzyka zanieczyszczenia wód podziemnych pomoże lepiej zaplanować działania środowiskowe i decyzyjne na tym obszarze. Wyniki mogą służyć jako podstawa do rozwoju polityki, zagospodarowania przestrzennego i zrównoważonego zarządzania zasobami w gminie Bodzentyn.

Słowa kluczowe: ujęcie wód podziemnych, studnia, pierwsza warstwa wodonośna, zanieczyszczenie, zagrożenie, MHP-816

1. INTRODUCTION

Groundwater serves as a crucial source of drinking water, irrigation, and industrial processes, playing a decisive role in maintaining the balance of various ecosystems. The chemical composition of water is closely related to the lithology of rocks and sediments covering mountain slopes [1, 2]. The preservation and quality of groundwater resources are essential to ensure the sustainable development of communities and ecosystems. Geological and hydrogeological conditions play a significant role in assessing the threat to groundwater quality. Giao et al. [2] confirmed that the quality of groundwater is associated with its geological location and potential sources of pollution. The increasing anthropogenic activities and urbanization have made the vulnerability of groundwater to contamination a matter of significant concern [3-6]. In Poland, the Water Law Act [7] imposes on owners, among other things, the obligation to carry out a risk analysis for groundwater intakes. The risk analysis is meant to justify the potential need for establishing an intermediate protection zone, the extent of which is determined based on hydrogeological conditions and prevailing circumstances within the area of groundwater inflow to the intakes.

An essential element of the risk analysis involves understanding the intrinsic vulnerability of groundwater to contamination, which is closely connected to the geological and hydrogeological conditions of the area, as well as the type of aquifer recharge [8]. The intrinsic vulnerability determines the potential for conservative pollutants (migrating according to the actual speed of groundwater flow) to migrate from the Earth's surface to the initial aquifer layer. Based on the seepage time of conservative contaminants into the first aquifer, it is possible to assess the risk of danger to the groundwater intake [9, 10]. In Poland, based on the data regarding the intrinsic vulnerability of groundwater, a Map of Groundwater Vulnerability to Contamination has been developed. However, due to the broad scale of 1:500,000, this document represents only the initial stage of groundwater threat recognition [9]. It's important to note that a 1 mm thick line on the map corresponds to a 500 m wide strip in actual terrain. Therefore, capturing the local variations in the susceptibility of shallow groundwater to contamination can be challenging, and undertaking actions toward detailed analyses appears justified.

According to the review of documents from the Polish Geological Institute, it is evident that groundwater in

the Bodzentyn municipality area may be susceptible to contamination due to the weak substrate isolation and the porous nature of carbonate rocks [11]. As per authors [12, 13], carbonate rocks exhibit significant variability in pore/crack dimensions, which affects the dynamics of groundwater. Considering the fractured rock nature of the local underground water reservoir 816 in Bodzentyn, characterized by spatial and temporal variability [14], there is a need to determine the intrinsic vulnerability of groundwater around the groundwater intakes. Subsequently, by identifying the area of water inflow to the intake and the existing sources of pollution within its vicinity, it is possible to assess the risk of endangerment to the intake [15]. This necessity is reinforced by the fact that the Bodzentyn municipality lies within the scope of protected areas, thereby industrial activities must not disrupt sustainable development.

The objective of this study is to comprehensively assess the threat of contaminating groundwater originating from the first aquifer level in the municipalities of Bodzentyn, Świętokrzyskie Voivodship. Through a detailed investigation of geological and hydrogeological conditions, land use practices, and potential sources of contamination, this research aims to achieve the following goals:

- To determine the intrinsic vulnerability of the first aquifer to contamination for 23 local deep wells.
- Identify and categorize the various potential sources of groundwater contamination within the study area.
- To calculate the radius of the water recharge area to the groundwater intake.

This study is likely the first research focusing on individual well intakes, considering local variations and taking existing sources of pollution into account. Studying the impact of anthropogenic activities on groundwater quality using the developed methodology allows for analyses under various geological and hydrogeological conditions. Therefore, it is not limited to regional actions but can be effectively applied in different geographic areas.

2. METHODS AND MATERIALS

2.1. Research methodology

The depth to the groundwater table and the physical properties of the overlying layer are crucial parameters that significantly influence the vulnerability of groundwater to contamination [16].

The intrinsic vulnerability of the first aquifer to contamination was calculated for 23 local deep

wells in the municipality of Bodzentyn. Each well was then categorized into classes of vulnerability to contamination depending on the expanding seepage duration (t_a) in years [10]:

- A1 – Signifying an aquifer with an exceptionally high risk where $t_a < 2$ years. Soil-water system susceptible to most pollutants.
- A2 – Representing an aquifer with a high risk where $2 \leq t_a < 5$ years. Soil-water system is susceptible to many types of pollutants, in addition to those highly sorptive (e.g., heavy metals).
- B – Designating an aquifer with a moderate risk where $5 \leq t_a < 25$ years. Soil-water system susceptible to some types of pollution, but only if introduced or washed out continuously.
- C – Denoting an aquifer with a low risk where $25 \leq t_a < 100$ years. Soil-water system is susceptible only to conservative pollution introduced or washed out continuously and over a large area.
- D – Indicating an aquifer that is virtually devoid of risk where $t_a > 100$ years. Isolation layers with minimal infiltration are present or a permanent natural hydraulic barrier exists.

The water exchange time (t_a) was calculated using the following equation (1) [9, 17]:

$$t_a = \sum_1^n \frac{m_{ai} \cdot w_{0i}}{P \cdot \omega_i} \quad (1)$$

where: m_{ai} – thickness of the vadose zone calculated for each layer of soil (i) [m]; w_{0i} – average volumetric water content of the strata in the vadose zone calculated for each layer of soil (i) [-]; P – mean annual precipitation [mm/a], 700 mm (1991-2020) was assumed; ω_i – effective infiltration coefficient [-].

This formula, despite the fact that it may overestimate the values of vertical seepage [18] can be a useful tool for determining protection zones of groundwater intakes.

Identification of potential sources of contamination for existing groundwater intakes was based on the Geolog database [19] and current (2023) Google Street View maps. Then, based on the hydrogeological map (MHP-816) [20], the direction of groundwater flow was determined. Finally, the radius of the area of water runoff to each intake was calculated to check the risk of the groundwater intake being threatened by a specific pollution source.

The radius of the water runoff for each groundwater intake was calculated using formula (2):

$$r = 2.764 \cdot \sqrt{\frac{Q \cdot t}{m \cdot n_e}} \quad (2)$$

where: Q – well capacity [m^3/h]; t – 9130 days \approx isochrone 25 years; m – thickness of the aquifer [m]; n_e – effective porosity (according to the graph of the relationship k to n_e , on page 110 – “General Hydrogeology”) [10].

The filtration coefficient was obtained from well cards provided by the National Geological Institute.

2.2. Characteristics of the study area

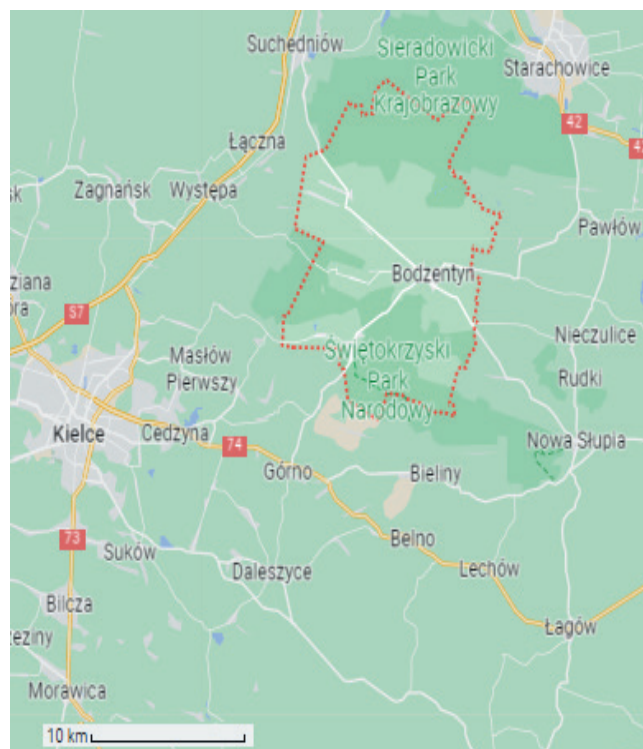
Bodzentyn Municipality is located in the Świętokrzyskie Voivodeship in southeastern Poland. Bodzentyn town is located about 30 kilometers from Kielce (Fig. 1a). It is situated within the Świętokrzyskie Mountains. There are nature reserves, national parks and protected areas in the municipality to protect local flora and fauna. These areas have restrictions on human activities to minimize disturbance to the ecosystem (Fig. 1b). The area is characterized by rolling hills, forests, and numerous streams and rivers. The city of Bodzentyn is surrounded on all sides by agricultural land. Their area in the municipality is 8185 hectares [21] (Fig. 1c).

2.2.1. Geological and hydrogeological conditions

Figure 2 depicts the geological diversity of Bodzentyn municipality.

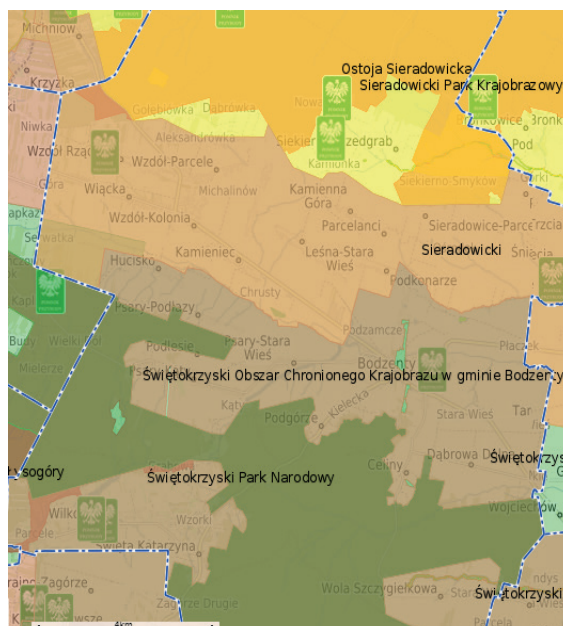
The water management of Bodzentyn municipality relies on groundwater originating from the Middle and Upper Devonian limestone formations (Fig. 3). Their water-bearing capacity varies greatly, depending on the degree of fracturing, karstification, and the occurrence of local lenses of sandstone and shale. The capacity can vary for individual wells from 0.5 m^3/h to 119 m^3/h [23]. The primary significance lies in the local underground water reservoir 816 in Bodzentyn. It is situated within the confines of groundwater body No. 102. According to the assessment for the period 2022-2027, the reservoir was deemed to be not at risk. In 2019, both the quantitative and qualitative statuses were appraised as good [11]. However, the same document notes a potential local hazard to groundwater intakes stemming from anthropogenic pollution of unknown origin. Rzonca [14] points out that the underground water reservoir is virtually inseparable from the surface terrain, thereby posing a substantial risk of groundwater contamination.

a)



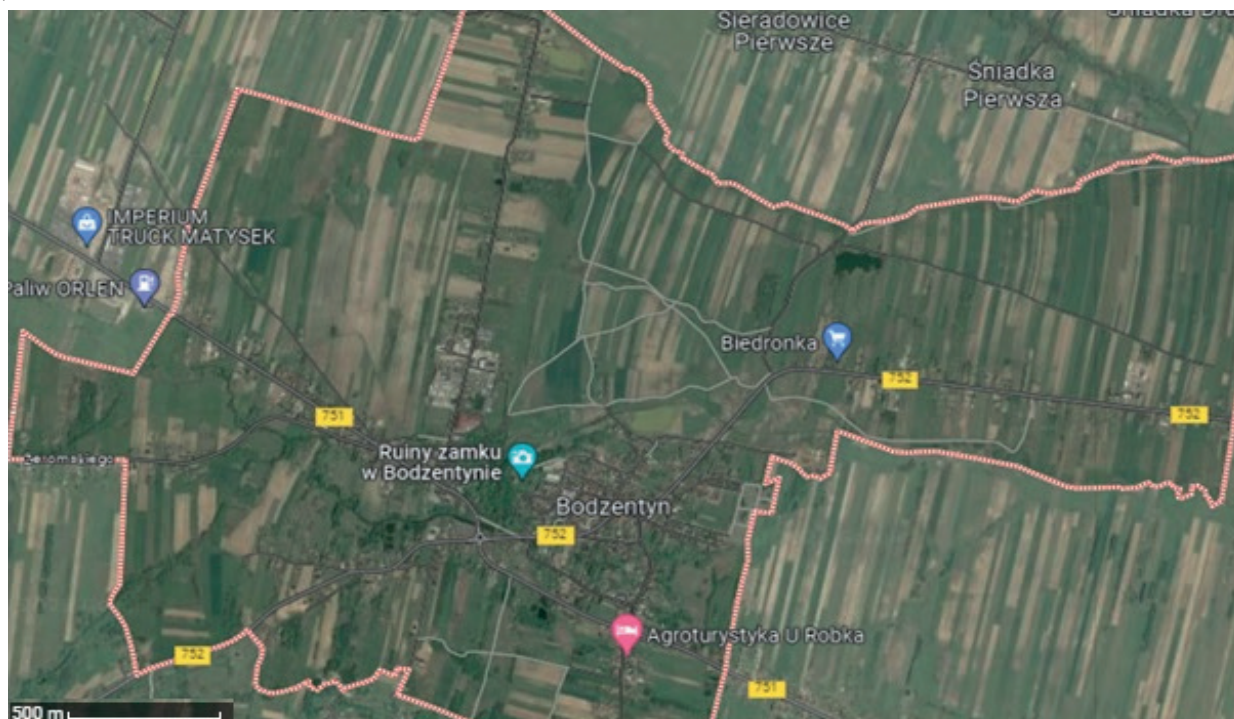
--- Bodzentyn municipality

b)



- Ostoja Sieradowicka Special Area of Conservation
- Sieradowicki Protected Landscape Area
- Sieradowicki Landscape Park
- Świętokrzyski Area of Protected Landscape
- Świętokrzyski National Park

c)



Agricultural land

Fig. 1. Bodzentyn municipality: a) against the background of the city of Kielce, Poland; b) on the background of protected areas; c) against the background of agricultural land [22]

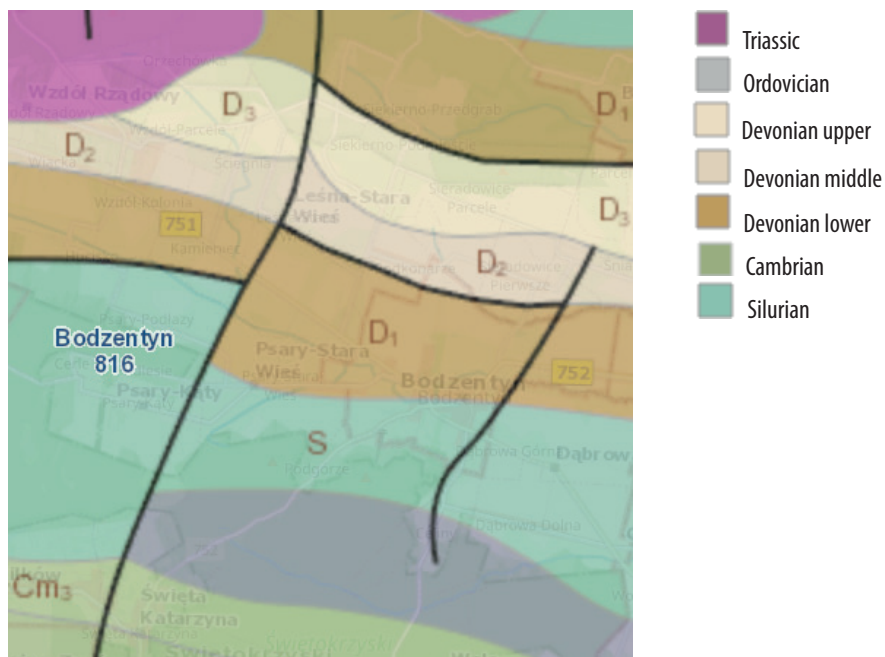


Fig. 2. Cartography of the depth of the study area (Bodzentyn municipality) [19]

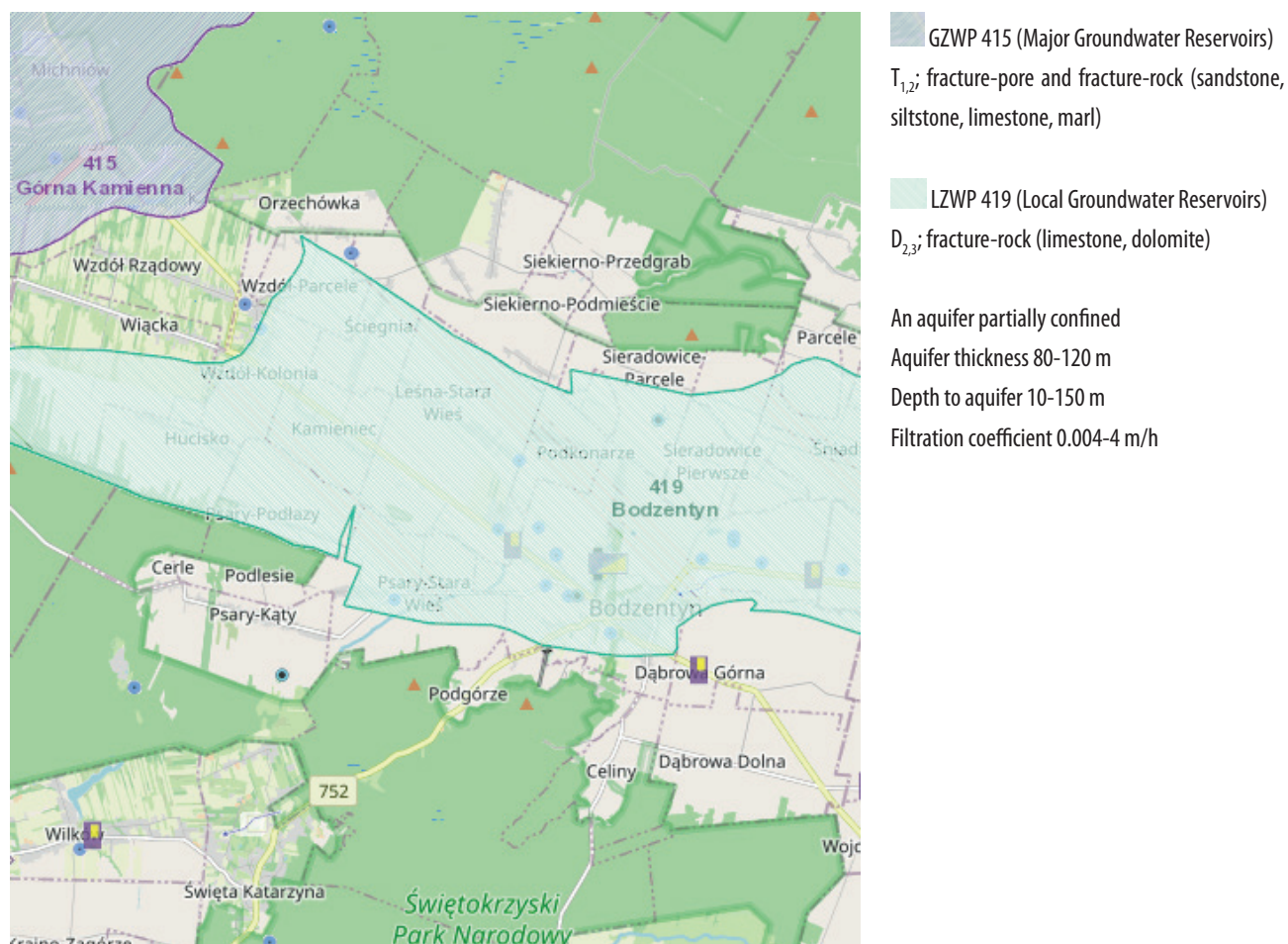


Fig. 3. The Underground Water Reservoirs for the municipality of Bodzentyn [11, 19]

3. RESULTS AND DISCUSSION

Table 1 provides a comprehensive overview of the outcomes associated with 23 local deep wells in Bodzentyn municipality. The groundwater intakes show different levels of vulnerability to contamination, ranging from exceptionally high risk to moderate risk.

In Figure 4, a geographical map has been constructed illustrating the precise positions of the well intakes along with the pre-existing contamination sources.

Figure 5 illustrates the results concerning the natural vulnerability of groundwater to contamination in relation to groundwater intakes within the reach of pollution sources.

In the catchment area of wells no. 816013, no. 8160067, no. 8160068, no. 8160069, no. 8160076, and 816108, agricultural fields are present (Fig. 1c). Due to the elevated risk of groundwater contamination at these extraction points, further risk analyses in this area are required, taking into account the pollutant load

Table 1. Hydrogeological characteristics and assessment of the class of intrinsic vulnerability of groundwater intakes to contamination in the municipality of Bodzentyn

No. of well ¹	Location	PPW ² [m]	t_a ³ [y]	Calc. risk class ⁴	Q ⁵ [m ³ /h]	OSW ⁶ [m]
8160001	Bodzentyn	55	5.3	B	8	N. D
8160002	Bodzentyn	5.8	0.9	A1	40	345
8160007	Sieradowice	32	2.8	A2	58	2021
8160008	Wilków	No aquifer was detected to a depth of 698 m				
8160009	Bodzentyn	9.8	0.8	A1	1.1	N. D
8160011	Bodzentyn	7	0.4	A1	63.8	475
8160013	Wzdół Rządowy	15.1	8.7	B	2.5	171
8160014	Leśna-Stara Wieś	27	5.9	B	4.2	157
8160028	Bodzentyn	32	17.9	B	1.2	78
8160054	Bodzentyn	23	13.9	B	2.8	N. D
8160056	Psary Kąty	5.4	1.6	A1	0.8	N. D
8160058	Bodzentyn	3	0.9	A1	26.2	199
8160067	Bodzentyn	6.2	1.0	A1	37.7	214
8160068	Psary-Stara Wieś	20.5	6.4	B	1.0	131
8160069	Wzdół Rządowy	13	4.0	A2	80	521
8160070	Bodzentyn	23.5	0.9	A1	64.6	391
8160073	Bodzentyn	31	2.8	A2	9	145
8160076	Wzdół Rządowy	21.5	4.1	A2	0.5	98
8160080	Bodzentyn	21	12.3	B	15	1054
8160092	Orzechówka	67	3.5	A2	1.3	171
8160103	Leśna-Stara Wieś	10	2.3	A2	7.4	254
8160108	Wzdół-Parcele	16	1.1	A1	60	377
8160157	Bodzentyn	6.5	0.4	A1	63.8	349

¹ Number according to the database of the National Geological Institute (geolog.pgi.gov.pl); ² Depth to the first exploitable aquifer (abbreviations in Polish 'PPW'); ³ Average water migration time from the ground surface to the first aquifer in years according to Eq. 1; ⁴ A1 – $t_a < 2$; A2 – $t_a < 2-5$; B – $t_a (5,25 >)$; C – $t_a (25,100 >)$; D – $t_a > 100$ [year] [6];

⁵ Exploitable capacity of wells; ⁶ Radius of the water runoff area acc. to Eq. 2; n.d. not available – no filtration coefficient

Source: own elaboration.

f. ex. nitrates. In the catchment area of water intake no. 8160028, which is characterized by a moderate pollution risk, there is a wastewater treatment plant. The gas station is located near the area of runoff to well nos. 8160058, 8160070 with high vulnerability to contamination. Within the range of influence of groundwater intakes number 816001, 816002, 8160073, there is a truck and tractor repair station and a building materials warehouse. The company has a hazardous waste permit of 13.29 Mg/year. The listed groundwater intakes have a very high vulnerability to contamination, so it is recommended that the quality of these aquifers be monitored or protective steps be taken. Particular attention should also be given to well number 8160028, which is located near the wastewater treatment plant area. The other groundwater intakes no anthropogenic hazards have been identified within them.

The results are difficult to compare because the map 'first aquifer sensitivity and quality' at a scale of 1:50,000 for MHP-816 sheet has not been developed

for the area [19]. In addition, the development of these maps operated on other assumptions [8]. Presented study is probably the first study for individual well intakes that shows local variation and takes into account existing sources of pollution.

Studies by other researchers confirm that groundwater management can be effectively carried out based on the assessment of groundwater vulnerability to contamination [24, 25]. Krogulec et al. [24] suggest considering various susceptibility assessment scenarios (variants dependent on average, maximum, and minimum groundwater levels). Reshma and Sidhu [25] also emphasize the importance of conducting comparative studies. Therefore, the presented results can serve as a basis for such analyses. In the future, this data could also be utilized as a significant component of a dataset for machine learning in predicting the degree of groundwater contamination risk. Similar analyses have been successfully conducted by Soriano et al. [26].

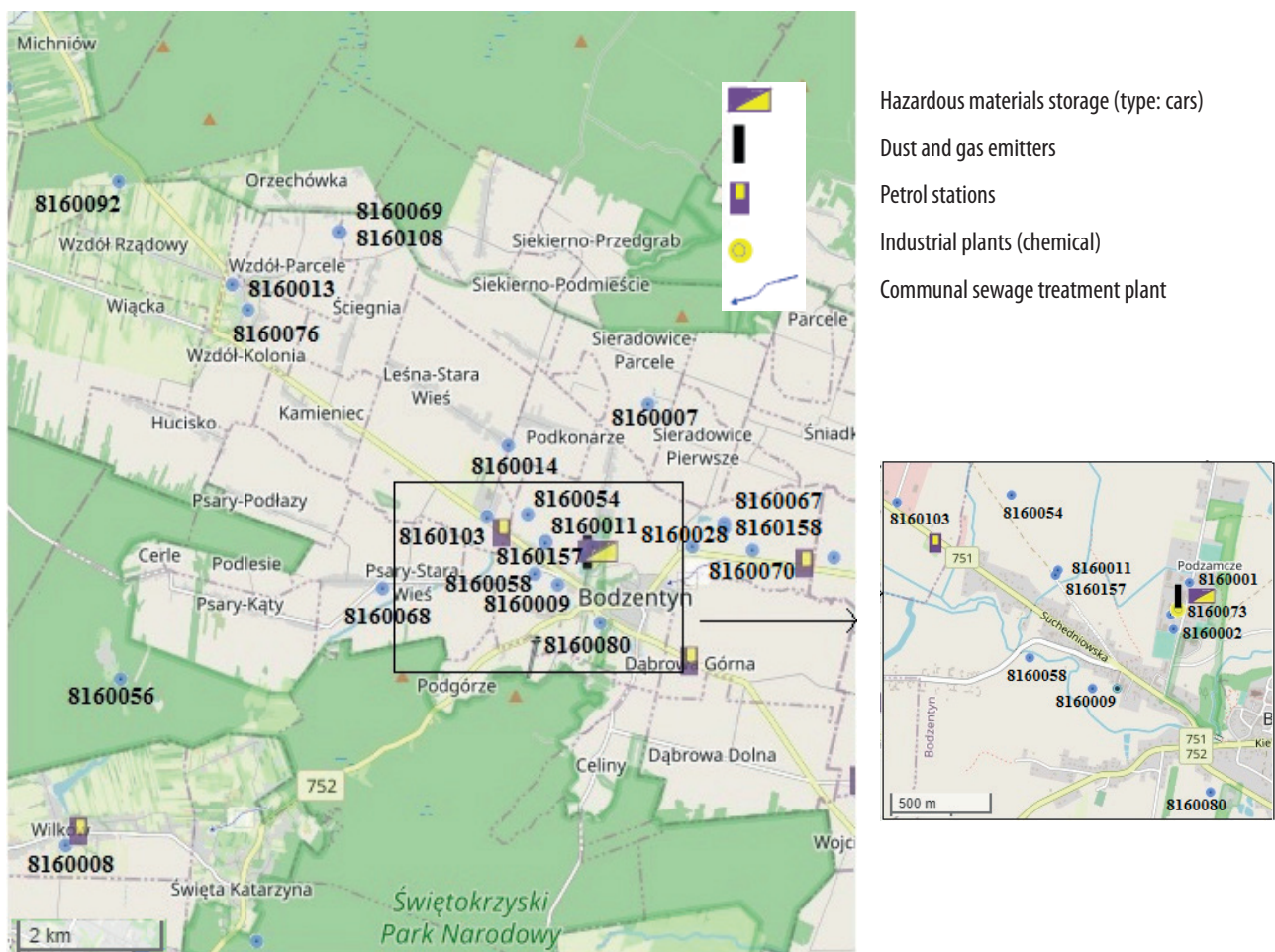


Fig. 4. Location of groundwater intakes with potential pollution sources for the municipality of Bodzentyn. Own elaboration based on [19]

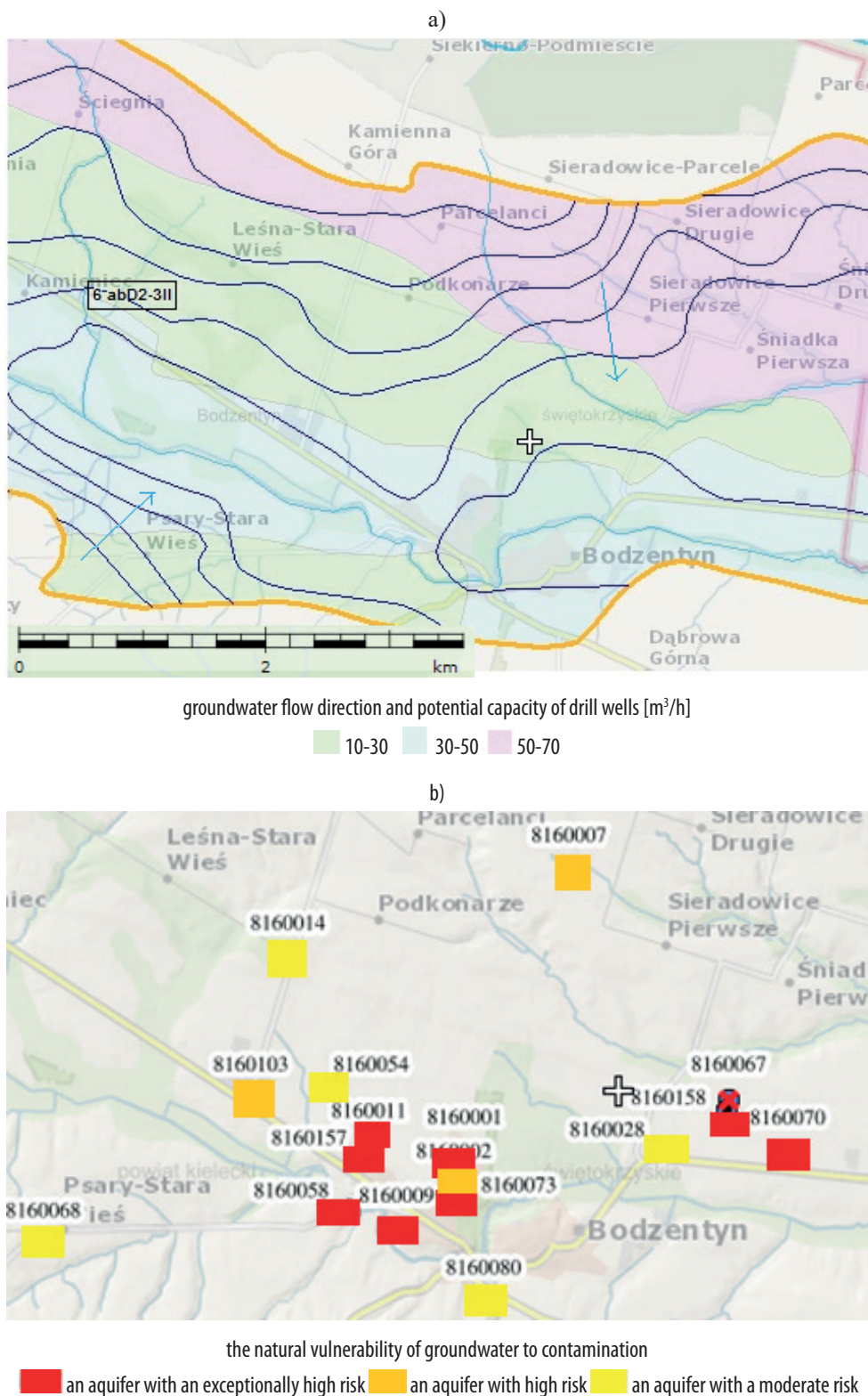


Fig. 5. The intrinsic vulnerability of groundwater to contamination in relation to groundwater intakes and the groundwater flow direction

4. CONCLUSIONS

The primary objective of this study was to evaluate the potential risk of groundwater contamination originating from the first exploitative aquifer level within the Bodzentyn municipality of the Świętokrzyskie Voivodship. Analysis of 23 representative groundwater intakes revealed potential contamination sources and assessed the aquifer's vulnerability. Specific wells near agricultural fields, gas stations, repair stations, and wastewater treatment plants are at

risk. Comprehensive risk analyses, particularly for agricultural wells, considering contaminants like nitrates, are recommended. Ongoing monitoring or protective measures are crucial due to the vulnerability of these intakes. The presented results can serve as a basis for further comparative analyses in this region. Understanding contamination risks informs better environmental planning, decision-making, and policy formulation, benefiting sustainable resource management in Bodzentyn.

References

- [1] Michalik A.: *The Use of Chemical and Cluster Analysis for Studying Spring Water Quality in Świętokrzyski National Park*. Polish J. of Environ. Stud., 17 (2008).
- [2] Metryka-Telka M., Styś-Maniara M., Dołęga-Śródka A.: *Activity of ²²²Rn in tap water in Kielce county*. Structure and Environment, 14 (2) (2022), el 007
- [3] Giao N.T., Nhien H.T.H., Anh P.K. et al.: *Groundwater quality assessment for drinking purposes: a case study in the Mekong Delta, Vietnam*. Sci Rep., 13 (2023), 4380.
- [4] Makanda K., Nzama S., Kanyerere T.: *Assessing the Role of Water Resources Protection Practice for Sustainable Water Resources Management: A Review*. Water, 14 (2022), 3153.
- [5] Link A., El-Hokayem L., Usman M., Conrad C., Reinecke R., Berger M., Wada Y., Coroama V., Finkbeiner M.: *Groundwater-dependent ecosystems at risk – global hotspot analysis and implications*. Environ. Res. Lett., 18 (2023), 094026.
- [6] Canora F., Sdao F.: *Groundwater Vulnerability to Pollution Assessment*. Water, 14 (2022), 2205.
- [7] Chakraborty M., Tejankar A., Coppola G. et al.: *Assessment of groundwater quality using statistical methods: a case study*. Arab J Geosci., 15 (2022), 1136.
- [8] Water Law Act of 20 July 2017, item 156. Published in the Polish Journal of Laws on 23 August 2017.
- [9] Czop M., Herbich P., Janica R., Lidzbarski M., Mulik B., Nikiel G., Prażak J., Rodzoch A., Staško S., Woźnicka M., Zimoch I.: *Protection zones of groundwater intakes- risk analysis and design Methodological guide* (in Polish), National Geological Institute, Warsaw 2022.
- [10] Duda R., Witeczak S., Żurek A.: *Map of Vulnerability of Poland's Groundwater to Pollution 1:50 000* (in Polish), AGH University of Science and Technology, Cracow 2011.
- [11] Pazdro Z.: *General Hydrogeology – Third Edition Supplemented. Practical aspects of assessing the susceptibility of groundwater to contamination by the DRASTIC method* [in Polish], Białystok 2013.
- [12] Documents of the National Geological Institute [online] 2023. Available from <https://www.pgi.gov.pl/docman-tree/psh/zadania-psh/jcwpd/jcwpd-100-119/4535-karta-informacyjna-jcwpd-nr-102/file.htm>.
- [13] Skowera K.: *Fusion of differential analysis of volumetric strain method (dilatometric thermoporometry) and mercury intrusion porosimetry method for pore space characterization in carbonate rocks*. Structure and Environment, 15(2) (2023), el 009.
- [14] Steiakakis E., Vavadakis D., Mourkakou O.: *Groundwater Vulnerability and Delineation of Protection Zones in the Discharge Area of a Karstic Aquifer – Application in Agvia's Karst System (Crete, Greece)*. Water, 15 (2023), 231.
- [15] Rzonca B.: *The hydrogeological properties of the Devonian carbonate rocks in the Holy Cross Region*. Geologia, 32(3) (2006), 235-343.
- [16] Nartowska E.: *The risk of contamination of the first aquifer in the central part of the Świętokrzyskie Voivodship (MHP-814 Piekoszów)*. Acta Sci. Pol. Architectura, 22 (1) (2023), 61-70.
- [17] Patel P., Mehta D., Sharma N.: *Assessment of groundwater vulnerability using the GIS approach-based GOD method in Surat district of Gujarat state, India*. Water Practice and Technology, 18 (2) (2023).
- [18] Witeczak S., Żurek A.: *Use of soil-agriculture maps in assessing the protective role of soils for groundwater* (In Polish). [w:] Kleczkowski A.S. (Ed.): *Methodological basis of groundwater protection*, AGH University of Science and Technology, Cracow 1994, 155-180.
- [19] Macioszczyk T.: *Vertical water seepage time as an indicator of the degree of aquifer shielding* (in Polish). Przegląd Geologiczny, 47(8) (1999).
- [20] Database of National Geological Institute [online] 2023. Available from: <https://geolog.pgi.gov.pl/>.

- [21] Database of National Geological Institute [online] 2023. Available from: <https://baza.pgi.gov.pl/resources.html?type=mhp&id=816>.
- [22] Podawca K., Pawłat-Zawrzykraj A.: *The Agriculture and Forestry Lands Level of Changes in Planning Process as a Sustainable Development Measure of Municipalities Located within National Parks Impact Areas*. J. Ecol. Eng., 20(8) (2019), 153-164.
- [23] Spatial Information System City and Municipality Office of Bodzentyn [online] 2023. Available from: <https://bodzentyn.e-mapa.net/>
- [24] Nartowska E., Budzianowski D., Styś-Maniara M.: *Assessment of the Thermal Power of Groundwater Intakes in the Kielce District*. Civil and Environmental Engineering Reports, 32(4) (2022), 3922.
- [25] Krogulec E., Zabłocki S., Zadrozna D.: *Variability of Intrinsic Groundwater Vulnerability to Pollution in River Valley due to Groundwater Depth and Recharge Changes*. Appl. Sci., 9 (1133) (2019).
- [26] Reshma R., Sindhu G.: *Assessment of groundwater vulnerability to contamination: a case study*. Environ Monit Assess., 191 (356) (2019).
- [27] Soriano Jr. M. et al. *Assessment of groundwater well vulnerability to contamination through physics-informed machine learning*.: Environ. Res. Lett. 16 (2021), 084013.

Acknowledgements

This research was funded by the Faculty of Environmental Engineering, Geomatics and Renewable Energy of the Kielce University of Technology. No SUBB.IKGT 05.0.12.00/1.02.001//SUBB.IKGT.23.002.

INFLUENCE OF THE BINDER ON THE PROPERTIES OF COLD MIXTURES WPŁYW ŚRODKA WIĄZĄCEGO NA WŁAŚCIWOŚCI MIESZANEK NA ZIMNO

MACIEJ KRASOWSKI, PRZEMYSŁAW BUCZYŃSKI
Kielce University of Technology, Poland
JURAJ MUŠUTA
University of Zilina, Slovakia

Structure and Environment vol. 15, No. 4/2023, p. 185

DOI: 10.30540/sae-2023-016

Abstract

The paper aims to present the basic properties of cold mixes in terms of the type of binding agent. In the theoretical part of the article, a description of the technology for producing cold recycled mixtures and the types of road binders used in cold mixtures was presented. The research part presents the experimental design, and gives an overview of the research methodology used to assess the impact of the type of binding agent. Mixes differing in type and binder content were designed. During the laboratory work, mixtures were prepared with cement binder (CBGM), cement-modified polymer binder (CBGM+P), mineral-cement-emulsion modified with polymer binder (BE-RCM+P), and mineral-cement mixtures with foamed bitumen modified with polymer binder (FB-RCM+P). The project aimed to produce cold mixtures with variations in the type and amount of binder used. The mixtures were prepared using cold mix technology. The effect of the binder on the cold mix properties was studied. During the research, the following properties were examined: void content (V_m), indirect tensile strength (ITS), resistance to water damage (TSR), stiffness modulus using the IT-CY method and an axial compressive strength. On the basis of the research carried out, an analysis was made. Among other things, the polymer modification was found to have a positive effect on the void content of the mix. The research carried out in this way made it possible to show the influence of the binder on the properties of cold mixes.

Streszczenie

Praca miała na celu przedstawienie podstawowych właściwości mieszanek na zimno w aspekcie rodzaju środka wiążącego. W części teoretycznej artykułu przedstawiono opis technologii wykonywania mieszanek metodą recyklingu głębokiego na zimno oraz rodzaje spoiw drogowych wykorzystywanych w mieszankach na zimno. W części badawczej przedstawiono plan eksperymentu oraz przybliżono metodykę badawczą wykorzystaną w ocenie wpływu rodzaju środka wiążącego. Zaprojektowano mieszanki związane cementem (CBGM), mieszanki związane cementem modyfikowane polimerem (CBGM+P), mieszanki mineralno-cementowo-emulsyjne modyfikowane polimerem (MCE+P) oraz mieszanki mineralno-cementowe z asfaltem spienionym modyfikowane polimerem (MCAS+P). Projekt zakładał wykonanie mieszanek w technologii na zimno, zróżnicowanych pod względem rodzaju oraz ilości zastosowanego spoiwa. W ramach badań sprawdzono zawartość wolnych przestrzeni V_m , wytrzymałość na rozciąganie pośrednie ITS, odporność na szkodliwe działanie wody TSR, moduł sztywności według metody IT-CY oraz przeprowadzono badanie wytrzymałości na ścislenie osiowe po 28 dniach pielęgnacji. Na podstawie wykonanych badań dokonano analizy. Tak przeprowadzone badania pozwoliły na ukazanie wpływu spoiwa na właściwości mieszanek na zimno.

**NUMERICAL ANALYSIS OF STRESS AND TEMPERATURE
IN THE FRICTION STIR WELDING (FSW) PROCESS OF STEEL**

**NUMERYCZNA ANALIZA ROZKŁADU NAPRĘŻEŃ I TEMPERATURY W PROCESIE
ZGRZEWANIA TARCIOWEGO Z PRZEMIESZANIEM DLA STALI**

MICHAŁ SZCZECINA
Kielce University of Technology, Poland

Structure and Environment vol. 15, No. 4/2023, p. 196

DOI: 10.30540/sae-2023-017

Abstract

Friction stir welding (FSW) is a modern technology for joining various metals, which has already undergone many laboratory tests, but still requires the development of numerical models. Author of the paper decided to summarize the current state of scientific knowledge regarding the modelling of the FSW process using the finite element method (FEM) and showed the main directions of development of numerical research on this process. Very advanced models are a combination of solid mechanics and fluid dynamics, but they often require expanding the computing environment with its own subroutines, as well as calibration and validation of some material parameter and constants occurring e.g. in the heat generation and heat flow laws. Author of the paper proposed his own, simplified model, based on the computational solid mechanics and Lagrangian formulation. The model turned out to be an effective tool to reproduce stress and temperature fields during the FSW process.

Streszczenie

Zgrzewanie tarciove z przemieszaniem (FSW) jest nowoczesną technologią łączenia różnych metali, posiadającą wiele zalet w porównaniu z tradycyjnym spawaniem. Zgrzewanie tarciove zostało do tej pory poddane licznym badaniom laboratoryjnym, natomiast wymaga ciągłego rozwoju modeli numerycznych do symulacji tego procesu metodą elementów skończonych (MES). Autor artykułu postanowił dokonać podsumowania aktualnego stanu wiedzy dotyczącej modelowania zgrzewania tarciovego przy użyciu MES oraz wskazać główne kierunki rozwoju symulacji numerycznych tego procesu. Zaawansowane modele numeryczne zgrzewania tarciovego są kombinacją mechaniki ciała stałego z dynamiką płynów, a więc często wymagają rozbudowania środowiska obliczeniowego za pomocą własnych podprogramów, jak również kalibracji i walidacji wielu parametrów i stałych wymaganych do zdefiniowania np. prawa wytwarzania ciepła i prawa przepływu strumienia ciepła. Autor zaproponował swój własny uproszczony model bazujący na mechanice ciała stałego i opisie Lagrange'a. Model okazał się efektywnym narzędziem do odtworzenia naprężeń i pola temperatury w procesie zgrzewania tarciovego z przemieszaniem.

CFD AND EXPERIMENTAL INVESTIGATION OF THE IMPACT OF DIMENSIONAL MODIFICATIONS ON WIND PRESSURE COEFFICIENT DISTRIBUTION**ANALIZA CFD ORAZ METODY EKSPERYMENTALNE W BADANIACH WPŁYWU MODYFIKACJI WYMIARÓW NA ROZKŁAD WSPÓŁCZYNNIKA PARCIA WIATRU**

RAMJAN ALI

European University of Bangladesh, Bangladesh

IFTEKHAR ANAM

University of Asia Pacific, Bangladesh

SHIGEO YOSHIDA

Kyushu University, Japan

Structure and Environment vol. 15, No. 4/2023, p. 208

DOI: 10.30540/sae-2023-018

Abstract

The sway of tall buildings in the wind is a fascinating and crucial consideration for professionals in the structural, environmental, and architectural fields. Previous research has related wind pressure to building load and natural ventilation, but few studies have looked at how building dimensions impact wind pressure. This study examined wind pressure coefficient distributions within and around several rectangular-shaped high-rise buildings using experimental and computational fluid dynamics approaches. The height-to-width ratio and height-to-thickness (length) ratio significantly affected the wind characteristics of buildings. The windward side with a narrower width experienced higher wind pressure, while the larger leeward side experienced a more negative wind effect. Wind pressure coefficient distribution varies with decrease in the side ratio. However, the side ratio of the building had little influence on positive wind pressure at wind incidence angle of 0° , which was a surprising finding. Pressure coefficients were evaluated and compared with standards by measuring fluctuating wind pressures at pressure points on all surfaces of models, and then calculating the mean, maximum, minimum, and r.m.s. values of these coefficients.

Streszczenie

Kołysanie się wysokich budynków pod wpływem wiatru jest fascynującym i kluczowym zagadnieniem dla specjalistów w dziedzinie konstrukcji, ochrony środowiska i architektury. W niniejszym artykule zbadano rozkłady współczynnika parcia wiatru wewnątrz i wokół kilku budynków wysokich o kształcie prostokąta, stosując metody eksperymentalne i numeryczne (obliczeniowa dynamika płynów). Stosunek wysokości budynku do jego szerokości oraz stosunek wysokości budynku do jego grubości (długości) miały znaczący wpływ na charakterystykę oddziaływania wiatru. Większe ciśnienie wiatru odnotowano po stronie nawietrznej o mniejszej szerokości, podczas gdy na większej ścianie od strony zawietrznej oddziaływanie wiatru było bardziej negatywne. Rozkład współczynnika parcia wiatru zmienia się wraz ze spadkiem stosunku boków. Jednak stosunek ten miał niewielki wpływ na dodatnie ciśnienie wiatru przy kierunku wiatru 0° , co było zaskakującym odkryciem. Współczynniki ciśnienia zostały ocenione i porównane z podejściem normowym poprzez pomiar zmiennego ciśnienia wiatru w punktach parcia na wszystkich powierzchniach modeli, a następnie obliczenie średnich, maksymalnych, minimalnych i średnich kwadratowych wartości tych współczynników.

**RHEOLOGICAL PROPERTIES OF CEMENT PASTES MODIFIED
WITH PUMICE, TRASS AND CHALCEDONITE POWDER**

**WŁAŚCIWOŚCI REOLOGICZNE ZACZYNÓW CEMENTOWYCH MODYFIKOWANYCH
PUMEKSEM, TRASEM I MĄCZKĄ CHALCEDONITOWĄ**

EDYTA SPYCHAŁ

Kielce University of Technology, Poland

MARTIN VYŠVAŘIL

Brno University of Technology, Czechia

Structure and Environment vol. 15, No. 4/2023, p. 217

DOI: 10.30540/sae-2023-019

Abstract

The article presents the influence of pumice, trass and chalcedonite powder on rheological properties of cement pastes. Cement was being replaced both of additions 10% or 20% by mass and combination of pumice or trass and chalcedonite powder in the amount 5% or 10% of each of them. The main purpose of the publication was to assess the effects of chalcedonite powder with selected mineral additions in terms of rheological properties and comparison their with the results obtained for pastes modified with only one of the additions. In each case, the additive or combination of additives introduced into the paste reduced the flow, compared to the result of paste without additive(s). Rheological properties varied depending on type and amount of additive(s).

Streszczenie

W artykule przedstawiono badania wpływu pumeksu, trasu oraz mączki chalcedonitowej na właściwości reologiczne zaczynów cementowych. Cement zastępowano każdym z dodatków w ilości 10% lub 20% oraz kombinacją pumeksu lub trasu z mączką chalcedonitową w ilości po 5% i 10% każdym z nich. Głównym celem pracy była ocena współdziałania mączki chalcedonitowej z wybranymi dodatkami mineralnymi w zakresie właściwości reologicznych oraz porównanie rezultatów badań z wynikami uzyskanymi dla zaczynów modyfikowanych tylko jednym z dodatków. W każdym z przypadków dodatek lub kombinacja dodatków wprowadzone do zaczynu wpłynęły na zmniejszenie rozplywu, w porównaniu do wyników uzyskanych dla zaczynu bez dodatku(ów). Właściwości reologiczne były zróżnicowane w zależności od rodzaju i ilości dodatku(ów).

**THE COMPARATIVE STUDIES OF THE PROPERTIES
OF JOINT SEALANTS PRODUCED BY MANUFACTURERS
AND IN LABORATORY CONDITIONS WITH THE USE OF HIGHLY MODIFIED BITUMEN**
**BADANIA PORÓWNAWCZE WŁAŚCIWOŚCI MAS ZALEWOWYCH WYTWARZANYCH
PRZEZ PRODUCENTÓW I W WARUNKACH LABORATORYJNYCH Z WYKORZYSTANIEM
ASFALTU WYSOKOMODYFIKOWANEGO**

JUSTYNA STĘPIEŃ, MATEUSZ M. IWAŃSKI
Kielce University of Technology, Poland

EVA REMIŠOVÁ, MARTIN DECKÝ, DUŠAN BRILIAK
University of Žilina, Slovakia

Structure and Environment vol. 15, No. 4/2023, p. 227

DOI: 10.30540/sae-2023-020

Abstract

Joint sealants produced on the basis of modified bitumen are an effective mean for protection of expansion joints on bridges and for repair of cracks in various road surfaces. A comparative study was performed to evaluate seven hot-applied joint sealants obtained commercially and three joint sealants produced in laboratory conditions with different contents of highly modified asphalt binder (40 to 100%). The basic properties of the joint sealants and asphalt binders were evaluated, including penetration, softening point, breaking point and elastic recovery. Additionally, Fourier infrared spectroscopy (FTIR) method was used to evaluate the chemical composition of the asphalt binders. The variability of the basic properties of joint sealants was estimated in the range from -77.1% to 43.6% in relation to the base asphalt binder. It has been established that the addition of crumb rubber, hydrated lime and rapeseed oil may be viable in controlling the parameters of the joint sealants.

Streszczenie

Zalewy szczelin produkowane na bazie asfaltów modyfikowanych są skutecznym rodzajem zabezpieczenia przerw dylatacyjnych na obiektach mostowych oraz naprawy uszkodzeń różnych typów nawierzchni drogowych. Badaniami porównawczymi objęto siedem mas zalewowych stosowanych na gorąco, wytworzonych przez krajowych i zagranicznych producentów, oraz trzy masy zalewowe wytworzone w warunkach laboratoryjnych o różnej zawartości wysokomodyfikowanego lepiszcza asfaltowego (40 do 100%). Ocenie poddano podstawowe cechy lepiszczy asfaltowych oraz parametry wyprodukowanych na ich bazie mas zalewowych, obejmujące: penetrację w 25°C, temperaturę mięknięcia, temperaturę lamlności Fraassa i nawrót sprężysty. Dodatkowo, do porównania składu chemicznego lepiszczy asfaltowych wykorzystano metodę spektroskopii fourierowskiej w podczerwieni (FTIR). Oszacowano procentowy zakres zmienności podstawowych właściwości mas zalewowych w relacji do bazowego lepiszcza asfaltowego w granicach od -77,1% do 43,6% w relacji do bazowego lepiszcza asfaltowego. Ustalono, że istotnym regulatorem parametrów mas zalewowych mogą być dodatki odpadów gumowych, wapna hydratyzowanego oraz oleju rzepakowego.

**LOCAL BUCKLING OF ONE-SIDE ELASTICALLY RESTRAINED
THIN-WALLED CROSS-SECTION WALL UNDER LONGITUDINAL STRESS VARIATION**
**WYBOCZENIE LOKALNE JEDNOSTRONNIE SPRĘŻYŚCIE ZAMOCOWANEJ ŚCIANKI
PRZEKROJU CIENKOŚCIENNEGO PRZY WZDŁUŻNEJ ZMIENNOŚCI NAPRĘŻEŃ**

ANDRZEJ SZYCHOWSKI
Kielce University of Technology, Poland

Structure and Environment vol. 15, No. 4/2023, p. 244

DOI: 10.30540/sae-2023-021

Abstract

In cold-formed thin-walled cross-sections, complex phenomena, related to local and distortional buckling of slender walls containing edge fold stiffeners, occur. In order to determine the design resistance of such a cross-section in the post-buckling range, it is necessary to determine the critical stress of local buckling for individual walls. On this basis, the corresponding effective widths are determined. Subsequently, the distortional buckling effect is taken into account, typically by reducing the thickness of the substitute cross-section of the stiffener.

The paper presents approximation formulas of plate buckling coefficients (k^) that are used to calculate critical local buckling stress for technically crucial stress distributions. The full range of variation of the index of elastic fixity of the longitudinal edge of the thin-walled cross-section was considered. The coefficients were determined for a more accurate, relative to Eurocode 3, computational model. Both the effect of reciprocal elastic restraint of component walls of the cross-section and the effect of longitudinal stress variation, which occurs in transversely bent beams, were taken into account.*

Streszczenie

W profilowanych na zimno przekrojach cienkościennych występują złożone zjawiska związane z wyboczeniem lokalnym i dystorsyjnym smukłych ścianek zawierających krawędziowe odgięcia usztywniające. W celu wyznaczenia nośności obliczeniowej takiego przekroju w zakresie nadkrytycznym należy wyznaczyć naprężenia krytyczne wyboczenia lokalnego dla poszczególnych ścianek. Na tej podstawie wyznacza się odpowiednie szerokości efektywne. W kolejnym kroku uwzględnia się efekt wyboczenia dystorsyjnego, najczęściej poprzez redukcję grubości tzw. zastępczego przekroju usztywnienia.

W pracy przedstawiono wzory aproksymacyjne płytowych współczynników wyboczeniowych (k^) służące do obliczania naprężeń krytycznych wyboczenia lokalnego dla technicznie ważnych rozkładów naprężeń. Uwzględniono pełny zakres zmienności wskaźnika sprężystego utwierdzenia krawędzi podłużnej półki przekroju cienkościennego. Współczynniki wyznaczono dla dokładniejszego, w stosunku do Eurokodu 3, modelu obliczeniowego. Uwzględniono zarówno efekt wzajemnego sprężystego zamocowania ścianek składowych przekroju, jak również występujący w poprzecznie zginanych belkach efekt wzdłużnej zmienności naprężeń.*

**ASSESSMENT OF THE SUITABILITY OF SPECTRAL INDICES
FOR DETECTING AREAS OF INCREASED STRESS AMONG PLANTS
– A CASE STUDY OF THE BOTANICAL GARDEN IN KIELCE**

**OCENA PRZYDATNOŚCI WSKAŹNIKÓW SPEKTRALNYCH DO WYKRYWANIA
OBSZARÓW WZMOŻONEGO STRESU WŚRÓD ROŚLIN – STUDIUM PRZYPADKU OGRODU
BOTANICZNEGO W KIELCACH**

SZYMON SYLWESTER SOBURA
Kielce University of Technology, Poland

Structure and Environment vol. 15, No. 4/2023, p. 253

DOI: 10.30540/sac-2023-022

Abstract

An important factor threatening global security is climate change and its impact on changing rainfall patterns and seasonal temperature variability. For this reason, farmers and crop scientists are striving to detect plant stress as soon as possible and introduce preventive measures so that key decisions in maintaining plant health are made in a timely way. Currently, multispectral images acquired from UAVs (Unmanned Aerial Vehicles) make it possible to provide objective and reliable information related to the state of agro-ecosystems, the dynamics of changes occurring on them and the monitoring of natural resources in a rapid and non-contact method. In the present study, the suitability of low-altitude multispectral imaging for proper stress detection in plants was assessed. The botanical garden in Kielce, a site with a high biodiversity of plant specimens, was chosen as the testing ground. In this study, four spectral indexes maps were analysed in the form of: NDVI (Normalized Difference Vegetation Index), NDRE (Normalized Difference Red-Edge Index), GNDVI (Green Normalized Difference Vegetation Index) and the less frequently used PSRI (Plant Senescence Reflectance Index) for the assessment of plant health. PSRI values > 0.50 clearly identified areas of high stress, in contrast to the other spectral indices analysed in this study. The study confirmed the suitability of the PSRI for conducting monitoring activities in areas with varying crop characteristics in an efficient and rapid approach.

Streszczenie

Ważnym czynnikiem zagrażającym globalnemu bezpieczeństwu są zmiany klimatyczne i ich wpływ na zmiany wzorców opadowych oraz zmienność sezonowych temperatur. Z tego powodu osoby zajmujące się ochroną walorów przyrodniczych oraz upraw dążą do jak najszybszej detekcji stresu roślin i wprowadzeniu działań profilaktycznych, aby kluczowe decyzje w utrzymaniu zdrowia roślin zostały podjęte w odpowiednim czasie. Obecnie zdjęcia multispektralne pozyskane z UAV (ang. Unmanned Aerial Vehicles) umożliwiają dostarczenie obiektywnej i wiarygodnej informacji związanej ze stanem agrosystemów, dynamiki zmian na nich zachodzących oraz monitorowania zasobów przyrodniczych w sposób szybki i bezkontaktowy. W niniejszej pracy oceniono przydatność zobrazowań multispektralnych z niskiego pułapu do prawidłowej detekcji stresu u roślin. Jako poligon doświadczalny wybrano ogród botaniczny w Kielcach, będący obiektem o dużej bioróżnorodności okazów roślin. W pracy przeanalizowano cztery mapy wskaźników spektralnych w postaci: NDVI (ang. Normalized Difference Vegetation Index), NDRE (ang. Normalized Difference Red-Edge Index), GNDVI (ang. Green Normalized Difference Vegetation Index) oraz rzadziej stosowany wskaźnik PSRI (ang. Plant Senescence Reflectance Index) pod kątem oceny kondycji zdrowotnej roślin. Wartości wskaźnika PSRI > 0,50 w sposób jednoznaczny zidentyfikowały obszary wysokiego stresu w odróżnieniu od pozostałych analizowanych w pracy wskaźników spektralnych. Badania potwierdziły przydatność wskaźnika PSRI do prowadzenia działań monitoringowych na obszarach o zróżnicowanej charakterystyce uprawianych roślin w sposób efektywny i szybki.

**GROUNDWATER CONTAMINATION RISK ASSESSMENT IN THE FIRST EXPLOITABLE
AQUIFER STRATUM WITHIN BODZENTYN MUNICIPALITY, ŚWIĘTOKRZYSKIE VOIVODESHIP**

**OCENA RYZYKA ZANIECZYSZCZENIA WÓD PODZIEMNYCH W PIERWSZEJ
EKSPLOATOWANEJ WARSTWIE WODONOŚNEJ NA TERENIE GMINY BODZENTYN,
WOJEWÓDZTWO ŚWIĘTOKRZYSKIE**

EDYTA NARTOWSKA
Kielce University of Technology, Poland

Structure and Environment vol. 15, No. 4/2023, p. 269

DOI: 10.30540/sac-2023-023

Abstract

The objective of this study is to assess the threat of contaminating groundwater originating from the first exploitative aquifer level in the municipality of Bodzentyn within the Świętokrzyskie Voivodship. The analysis included 23 representative groundwater intakes from MHP 816 Bodzentyn sheet. The various potential sources of groundwater contamination were identified. The intrinsic vulnerability of the first aquifer to contamination and the water recharge area were determined. In the results intakes potentially threatened by anthropogenic pollution were indicated. Providing information on the potential risks of groundwater contamination will help better plan environmental and decision-making activities in this area. The results can serve as a basis for policy development, land use and sustainable resource management in the municipality of Bodzentyn.

Streszczenie

Celem niniejszego opracowania jest ocena zagrożenia zanieczyszczeniem wód podziemnych pochodzących z pierwszego eksploatowanego poziomu wodonośnego w gminie Bodzentyn na terenie województwa świętokrzyskiego. Analizą objęto 23 reprezentatywne ujęcia wód podziemnych z arkusza MHP 816 Bodzentyn. Zidentyfikowano różne potencjalne źródła zanieczyszczenia wód podziemnych. Określono wewnętrzną podatność pierwszego poziomu wodonośnego na zanieczyszczenie oraz obszar zasilania. W wynikach wskazano ujęcia potencjalnie zagrożone zanieczyszczeniami antropogenicznymi. Dostarczenie informacji na temat potencjalnego ryzyka zanieczyszczenia wód podziemnych pomoże lepiej zaplanować działania środowiskowe i decyzyjne na tym obszarze. Wyniki mogą służyć jako podstawa do rozwoju polityki, zagospodarowania przestrzennego i zrównoważonego zarządzania zasobami w gminie Bodzentyn.

GUIDELINES FOR AUTHORS

Authors of reports of original research should provide a thorough description of their work and its results, followed by the objective discussion of the significance of the work. Underlying data should be represented accurately in the paper. A study should contain sufficient amount of details and references to allow others to replicate the research work. Fraudulent or knowingly inaccurate statements constitute unethical behaviour and are unacceptable. Reviews and professional publications should also be accurate and objective, and editorial opinions should be clearly identified as such.

Authors may be asked to provide the raw data in connection with a paper for editorial review, and should be prepared to provide public access to such data, if practicable, and should in any event be prepared to retain such data for a reasonable time after publication.

Authors should declare that they have created entirely original works. If the authors have used the work and/or words of others, that must be appropriately cited or quoted. Plagiarism takes many forms, from passing off another paper as the author own paper, to copying or paraphrasing substantial parts of another paper (without attribution), or to claiming results from research conducted by others. Plagiarism in all its forms constitutes unethical publishing behaviour and is unacceptable.

Generally, authors should not publish manuscripts describing essentially the same research in more than one journal, or primary publication. Submitting the same manuscript to more than one journal concurrently constitutes unethical publishing behaviour, and is unacceptable. In general, an author should not submit for consideration in another journal a previously published paper. Publication of some kinds of papers (e.g., clinical guidelines, translations) in more than one journal is sometimes justifiable, provided that certain conditions are met. The authors and editors of the journals concerned must agree to the secondary publication, which must reflect the same data and interpretation of the primary document. The primary reference must be cited in the secondary publication.

Proper acknowledgment of the work of others must always be given. Authors should cite publications that have been influential in determining the nature of the reported work. Information obtained privately, as in conversation, correspondence, or discussion with third parties, must not be used or reported without explicit, written permission from the source. Information obtained in the course of confidential services, such as reviewing manuscripts or grant applications, must not be used without the explicit written permission of the author of the work involved in these services.

Authorship should be limited to those who have made a significant contribution to the concept, design, execution, or interpretation of the reported study. All those who have made significant contributions should be listed as co-authors. Where there are others who have participated in certain substantive aspects of the research project, they should be acknowledged, or listed as contributors. The corresponding author should ensure that all appropriate co-authors and no inappropriate co-authors are included in the paper, and that all co-authors have seen and approved the final version of the paper, and have agreed to its submission for publication.

All authors should disclose in their manuscript any financial or other substantive conflict of interest that might be construed to influence the results or interpretation of their manuscript. All sources of financial support for the project should be disclosed. Examples of potential conflicts of interest which should be disclosed include employment, consultancies, stock ownership, honoraria, paid expert testimony, patent applications/registrations, and grants or other funding. Potential conflicts of interest should be disclosed at the earliest stage possible.

When an author discovers a significant error or inaccuracy in his/her own published paper, it is the author's obligation to promptly notify the journal editor or publisher, and cooperate with the editor to retract or correct the paper. If the editor or the publisher learns from a third party that a published paper contains a significant error, it is the obligation of the author to promptly retract or correct the paper, or provide evidence to the editor of the correctness of the original paper.

Paper submission to the Editorial Board is considered equivalent to a declaration that the content of the paper has not been previously published and has not been submitted to another editorial board.

The author's duties

Acceptance of a manuscript for publication in the journal carries with it an understanding that the author, when requested, will fulfil an obligation to contribute their expertise to the review of others' manuscripts. Authors are also requested to name three independent reviewers together with institutional email addresses. The named possible reviewers must not be located within the submitting organisation.

The author's rights

As an author, you (or your employer or institution) have certain rights to reuse your work.

After the paper acceptance

Upon acceptance of a paper, authors will be asked to complete a "***Licence Agreement***" form. The corresponding author will receive an email confirming acceptance of the manuscript, along with a Licence Agreement.

After reading the terms and conditions of the Agreement, the author will be asked to print, sign, and send a scanned copy of the document as an attachment via email to the following address: sae@tu.kielce.pl.

NEW SUBMISSIONS

Submission to this journal proceeds totally online, and you will be guided stepwise through the creation and uploading of your files. The system automatically converts your files to a single PDF file, which is used in the peer-review process.

Formatting requirements

All manuscripts must contain the essential elements needed to convey your manuscript, for example Abstract, Keywords, Introduction, Materials and Methods, Results, Conclusions, Artwork and Tables with Captions.

The text of the paper should be written in Times New Roman font, 12 points with single line spacing and paragraph indent 0.5 cm, the margin on both sides should be 2.5 cm. The paper should be limited to 7,500 words and should include: abstract, keywords, main text, references, tables and figures. The word equivalent for a table is 250 words. The contents of the paper should be appropriately divided into numbered sections and subsections.

Figures and tables in the text

Please ensure the figures and the tables included in the single file are placed next to the relevant text in the manuscript, rather than at the bottom or the top of the file. The corresponding caption should be placed directly below the figure or above the table.

Figures

Figures should be of high quality — resolution of at least 300 dpi, format: TIF (preferred), JPG, EPS or WMF. Do not use frames around figures. Any descriptions found in drawings, photos, and tables should be in English, in Times New Roman font. They should be easily legible when the figure is reduced to a width of 84 mm. The colours on the charts should be contrasting.

Ensure that each illustration has a caption. A caption should comprise a brief title (not on the figure itself) and a description of the illustration. Keep text in the illustrations themselves to a minimum, but explain all symbols and abbreviations used. In addition, a dot should be used as a decimal fraction separator in the drawings.

Tables

Drawings and tables should be numbered consecutively with Arabic numerals, and their titles should be given both in English and Polish. If the drawings or data for the tables have been taken from other papers, the source must be stated in the caption. In addition, a dot should be used as a decimal fraction separator in the tables.

Please submit tables as editable text and not as images. Tables can be placed either next to the relevant text in the article, or at the bottom, or the top of the file. Tables should be numbered consecutively in accordance with their appearance in the text. The table notes should be placed below the table body. Tables should be used sparingly, and it is needed to ensure that the data presented in them do not duplicate results described elsewhere in the paper. Vertical rules and shading in table cells should be avoided.

Mathematical formulas

Please submit maths equations as editable text, and not as images. Present simple formulas in line with normal text where possible, and use the solidus (/) instead of a horizontal line for small fractional terms, e.g., X/Y. In principle, variables are to be presented in italics. Powers of e are often more conveniently denoted by exp. Number consecutively any equations that have to be displayed separately from the text (if referred to explicitly in the text).

Peer Review

This journal operates a single blind review process. All contributions will be initially assessed by the editor with respect to their suitability for the journal. Papers deemed suitable are then typically sent to a minimum of two independent expert reviewers to assess the scientific quality of the paper. The Editor is responsible for the final decision on acceptance or rejection of papers. The Editor's decision is final. If your paper is rejected, please do not resubmit a modified version of this paper, as it will not be considered for publication.

ARTICLE STRUCTURE

Essential title page information

Title

The title of the paper should be concise.

Author names and affiliations

Please clearly indicate the first name(s) and surname(s) of each author, and check that all names are accurately spelled. You can add your name in parentheses in your own script behind the English transliteration. Present the authors' affiliation addresses (where the actual work was done) below the names. Indicate all affiliations with a lower-case superscript letter immediately after the author's name and in front of the appropriate address. Provide the full postal address of each affiliation, including the country name and, if available, the e-mail address of each author.

Corresponding author

Clearly indicate who will handle correspondence at all stages of reviewing and publication, also post-publication. This responsibility includes answering any future queries about Methodology and Materials. **Ensure that the e-mail address is given and that contact details are kept up to date by the corresponding author.**

Abstract

The abstract should consist of 120 to 150 words. It should briefly present the content of the paper, including information about the purpose and scope of the work, results and conclusions. The abstract should not refer to bibliography or equations, nor use unknown abbreviations.

Keywords

Immediately after the abstract, provide 3 to 7 keywords, and avoid general and plural terms and multiple concepts (avoid, for example, "and", "of"). Be sparing with abbreviations: only abbreviations firmly established in the field may be eligible. These keywords will be used for indexing purposes.

Abbreviations

Define abbreviations that are not standard in this field. They should be placed on the first page of the paper. Such abbreviations that are unavoidable in the abstract must be defined at their first mention there, as well as in the footnote. Ensure consistency of abbreviations throughout the article.

Introduction

The main part of the paper should be preceded by a short summary of the state of knowledge in the topics discussed.

State the objectives of the paper and provide an adequate background, avoiding a detailed literature survey, or a summary of the results.

The formulation of the problem should be presented in a clear and concise way.

Materials and methods

Provide sufficient details to allow the procedure to be reproduced by an independent researcher. Methods that are already published should be summarized, and indicated by a reference. If quoting directly from a previously published method, use quotation marks, and also cite the source. Any modifications to existing methods should also be described.

Results

Results should be clear and concise. The results of research should be presented in a synthetic manner, avoiding repetition, e.g., data presented in charts should not be given in a tabular form.

Discussion

This should explore the significance of the results, not repeat them. A combined Results and Discussion section is often appropriate. Avoid extensive citations and discussion of published literature.

Conclusions

The main conclusions of the study may be presented in a short Conclusions section, which may stand alone, or form a subsection of a Discussion or Conclusions. They should be based on the research carried out.

Acknowledgements

Collate acknowledgements in a separate section at the end of the paper before the references and do not, therefore, include them on the title page, as a footnote to the title or otherwise. List here those individuals who provided help during the research (e.g., providing language help, writing assistance or proof reading the article, etc.).

Formatting of funding sources

List funding sources in this standard way to facilitate compliance to funder's requirements:

Funding: This paper was supported by the National Science Centre [grant numbers xxxx, yyyy]; and the Ministry of Education and Science [grant number aaaa].

It is not necessary to include detailed descriptions of the program or type of grants and awards. When funding is from a block grant, or other resources available to a university, college, or other research institution, submit the name of the institute or organization that provided the funding.

If no funding has been provided for the research, it is recommended to include the following sentence:

This research did not receive any specific grant from funding agencies in the public, commercial, or not-for-profit sectors.

References

Citation in text

Please ensure that every reference cited in the text is also present in the reference list (and vice versa). Any references cited in the abstract must be given in full. Unpublished results and personal communications are not recommended in the reference list, but may be mentioned in the text. If these references are included in the reference list, they should follow the standard reference style of the journal and should include a substitution of the publication date with either 'Unpublished results' or 'Personal communication'. Citation of a reference as 'in press' implies that the item has been accepted for publication.

The publications quoted in the paper should be in English. Quoted publications should be numbered in square brackets in the order in which they appear in the text and listed in the references. No reference should be made to unpublished papers, internal reports, etc. The list of publications cited at the end of the article should contain all bibliographic data, that is in the case of:

- book: surname and initials of authors' first names, book title, publishing house, place and year of publication, e.g. Kurdowski W.: *Chemistry of cement and concrete*. PWN, Warsaw 2010;
- paper in a journal: surname and initials of authors' first names, paper title, title of the journal, volume, number, year of publication, number of the beginning and end page of the paper, DOI, e.g., Grzeszczyk S.: *The truth about the geopolymers*, Cement Wapno Beton, 26 (6) (2021), 101-108, DOI: <https://doi.org/10.32047/CWB.2021.26.6.1>;
- a chapter or article in a collective paper: surname and initials of first names of authors' of a chapter/article, the title of a chapter/article, title of a collective study preceded by the preposition [in:] (volume/number), publishing house, place and year of publication, page number of the beginning and end of the chapter/article, ISBN number, e.g. Kotwica Ł., Małolepszy J.: *The role and effect of chemical admixtures modifying the viscosity of cement slurries*, in: Rheology in concrete technology, Monograph, Publishing house of the Silesian University of Technology, Gliwice 2009, 57-62, ISBN 978-83-7335-609-2;
- papers published in conference materials: surname and initials of the authors' first names, paper title, title of conference materials, publisher, place and date of publication, pages, doi, e.g., Zapała-Sławeta J., Owsiak Z.: *The impact of lithium nitrate on the physical and mechanical properties of Portland cement*. MATBUD”2018th Scientific — Technical Conference on Material Problems in Civil Engineering, Kraków 2018, 1-8, DOI 10.1051/mateconf/201816304002;
- electronic publications: surname and initials of authors' names, paper title, (place), year of publication, internet address, date of access.